Trinity College Dublin
Coláiste na Tríonóide, Baile Átha Cliath
The University of Dublin

The Production and Characterization of Fluoroquinolone Amorphous Solid Dispersions

A dissertation submitted for the degree of
Doctor of Philosophy
at the School of Pharmacy & Pharmaceutical Sciences,
Trinity College Dublin,
the University of Dublin, Ireland

by Hanah N. Mesallati

Under the supervision of Dr. Lidia Tajber

June 2017

Declaration

I declare that this thesis has not been submitted as an exercise for a degree at this or any other university. A small proportion of the work described in this thesis was carried out by others, and this is duly acknowledged in the text wherever relevant. I declare that all other work is entirely my own.

I agree to deposit this thesis in the University's open access institutional repository or allow the Library to do so on my behalf, subject to Irish Copyright Legislation and Trinity College Library conditions of use and acknowledgement.

_____

Hanah Mesallati

Table of Contents

Summary ..... **i**

Acknowledgements ..... **iii**

Publications and Presentations ..... **iv**

List of Abbreviations and Symbols ..... **vi**

Chapter 1: General Introduction **1**

1.1 Bioavailability 2

1.1.1 Classification of Drugs 2

1.1.2. Solubility and Dissolution 3

1.1.3 Permeability 4

1.1.4 Methods of Improving Bioavailability 6

1.2 Amorphous Solids 9

1.2.1 Stability of Amorphous Solids 9

1.2.2 Amorphous Solid Dispersions 11

1.2.2.1 Stability of ASDs 11

1.2.2.1.1 Miscibility 12

1.2.2.2 Solubility and Dissolution of ASDs 15

1.2.3 Methods of Producing Amorphous Solids 17

1.2.3.1 Milling 18

1.2.3.2 Spray Drying 20

1.3 Ciprofloxacin 21

1.3.1 Ciprofloxacin Formulations 23

1.3.2 Enrofloxacin 25

1.4 Project Aims 26

Chapter 2: The Two Faces of Ciprofloxacin: Investigation of Proton Transfer in Solid State Transformations **29**

2.1 Introduction 30

2.2 Experimental Section 32

2.2.1 Materials 32

2.2.2 Methods 33

2.2.2.1 Production of Amorphous Ciprofloxacin 33

2.2.2.1.1 Ball Milling 33
2.2.2.1.2 Cryomilling 33
2.2.2.1.3 Spray Drying 33
2.2.2.2 Solid-State Characterization 33
2.2.2.2.1 Powder X-ray Diffraction (PXRD) 33
2.2.2.2.2 Differential Scanning Calorimetry (DSC) 34
2.2.2.2.3 High-Speed DSC (HSDSC) 34
2.2.2.2.4 Temperature-Modulated Differential Scanning Calorimetry (StepScan) 34
2.2.2.2.5 Thermogravimetric Analysis (TGA) 34
2.2.2.2.6 Solid-State Fourier Transform Infrared Spectroscopy (FTIR) 35
2.2.2.3 Thermal Degradation Study 35
2.2.2.4 High-Performance Liquid Chromatography (HPLC) 35
2.2.2.5 Dynamic Vapor Sorption (DVS) 36
2.2.2.6 Crystallographic Analysis 36
2.2.2.7 Computational Methods 36
2.2.2.8 Statistical Analysis 37
2.3 Results and Discussion 37
2.3.1 Crystal Forms of Ciprofloxacin 37
2.3.2 Production of Amorphous Ciprofloxacin 40
2.3.2.1 Ball Milling at Room Temperature 41
2.3.2.2 Cryomilling 42
2.3.2.3 Spray Drying 43
2.3.3 Quench Cooling - Thermal Degradation Studies 44
2.3.4 Solid-State Fourier Transform Infrared Spectroscopy 45
2.3.5 Conventional Thermal Analysis 48
2.3.6 Investigation of Proton Transfer in CIP 52
2.3.7 Physical Stability in Humid Conditions 56
2.4 Conclusions 58
Chapter 3: Amorphous Polymeric Drug Salts as Ionic Solid Dispersion Forms of Ciprofloxacin 59
3.1 Introduction 60
3.2 Experimental Section 61
3.2.1 Materials 61

3.2.2 Methods 63
3.2.2.1 Ball Milling 63
3.2.2.2 Solid-State Characterization 63
3.2.2.2.1 Powder X-ray Diffraction 63
3.2.2.2.2 Solid-State Fourier Transform Infrared Spectroscopy 64
3.2.2.2.3 Differential Scanning Calorimetry 64
3.2.2.2.4 Temperature-Modulated Differential Scanning Calorimetry (StepScan) 64
3.2.2.2.5 Calculation of Theoretical Glass Transition Values with Gordon-Taylor Equation 64
3.2.2.2.6 Thermogravimetric Analysis 65
3.2.2.3 Dynamic Vapor Sorption 65
3.2.2.4 Accelerated Stability Study 65
3.2.2.5 Dynamic Solubility Studies 65
3.2.2.6 Dissolution Study 65
3.2.2.7 UV Spectrophotometry 66
3.2.2.8 Parallel Artificial Membrane Permeability Assay (PAMPA) 66
3.2.2.9 High-Performance Liquid Chromatography 67
3.2.2.10 Bacterial Studies 67
3.2.2.11 Statistical Analysis 68
3.3 Results and Discussion 68
3.3.1 Production of Amorphous Solid Dispersions 68
3.3.2 Solid-State Characterization of Amorphous Solid Dispersions 72
3.3.2.1 Solid-State Fourier Transform Infrared Spectroscopy 72
3.3.2.2 Thermal Analysis 75
3.3.3 Stability Studies 77
3.3.4 Dynamic Solubility Studies 82
3.3.5 Dissolution Study 88
3.3.6 PAMPA Permeability Study 89
3.3.7 Bacterial Studies 92
3.4 Conclusions 94
Chapter 4: Polymer/Amorphous Salt Solid Dispersions of Ciprofloxacin 96
4.1 Introduction 97
4.2 Experimental Section 98
4.2.1 Materials 98

4.2.2 Methods 98
4.2.2.1 Sample Preparation 98
4.2.2.1.1 Ball Milling 98
4.2.2.1.2 Spray Drying 98
4.2.2.2 Solid-State Characterization 99
4.2.2.2.1 Powder X-ray Diffraction 99
4.2.2.2.2 Solid-State Fourier Transform Infrared Spectroscopy 99
4.2.2.2.3 Differential Scanning Calorimetry 99
4.2.2.2.4 Thermogravimetric Analysis 99
4.2.2.3 Determination of Solubility Parameters Using Inverse Gas Chromatography (IGC) 99
4.2.2.4 Dynamic Vapor Sorption 100
4.2.2.5 Long-term Stability Study 101
4.2.2.6 Dynamic Solubility Studies 101
4.2.2.7 UV Spectrophotometry 101
4.2.2.8 Parallel Artificial Membrane Permeability Assay 101
4.2.2.9 High-Performance Liquid Chromatography 101
4.2.2.10 Statistical Analysis 101
4.3 Results and Discussion 101
4.3.1 Production of Polymer/Amorphous Salt Solid Dispersions 101
4.3.2 Solid-State Characterization of Polymer/Amorphous Salt Solid Dispersions 103
4.3.2.1 Solid-State Fourier Transform Infrared Spectroscopy 103
4.3.2.2 Thermal Analysis and Estimation of Component Miscibility 106
4.3.3 Stability Studies 111
4.3.4 Dynamic Solubility Studies 117
4.3.5 PAMPA Permeability Study 121
4.4 Conclusions 122
Chapter 5: Preparation and Characterization of Amorphous Ciprofloxacin-Amino Acid Salts 123
5.1 Introduction 124
5.2 Experimental Section 126
5.2.1 Materials 126
5.2.2 Methods 127
5.2.2.1 Sample Preparation 127

5.2.2.2 Solid-State Characterization 127
5.2.2.2.1 Powder X-ray Diffraction 127
5.2.2.2.2 Solid-State Fourier Transform Infrared Spectroscopy 127
5.2.2.2.3 Solid-State Nuclear Magnetic Resonance (SSNMR) 127
5.2.2.2.4 Differential Scanning Calorimetry 128
5.2.2.2.5 High-Speed Differential Scanning Calorimetry 128
5.2.2.2.6 Thermogravimetric Analysis 128
5.2.2.3 Ciprofloxacin Aspartate and Glutamate Crystallization 128
5.2.2.4 Dynamic Vapor Sorption 128
5.2.2.5 Long-term Stability Study 129
5.2.2.6 Dynamic Solubility Studies 129
5.2.2.7 Parallel Artificial Membrane Permeability Assay 129
5.2.2.8 High-Performance Liquid Chromatography 129
5.2.2.9 Statistical Analysis 129
5.3 Results and Discussion 129
5.3.1 Sample Preparation 129
5.3.1.1 Ball Milling of Pure Amino Acids 129
5.3.1.2 Production of Ciprofloxacin/Amino Acid Solid Dispersions 130
5.3.2 Analysis of Drug-Amino Acid Interactions 133
5.3.2.1 Solid-State Fourier Transform Infrared Spectroscopy 133
5.3.2.2 Solid-State Nuclear Magnetic Resonance 136
5.3.3 Thermal Analysis 141
5.3.3.1 Glass Transition 142
5.3.3.2 Crystallization 143
5.3.3.3 Melting 148
5.3.4 Stability Studies 150
5.3.5 Dynamic Solubility Studies 156
5.3.6 PAMPA Permeability Study 161
5.4 Conclusions 162
Chapter 6: Production of Enrofloxacin Amorphous Solid Dispersions – A Comparison with Ciprofloxacin 164
6.1 Introduction 165
6.2 Experimental Section 167
6.2.1 Materials 167

6.2.2 Methods 167
6.2.2.1 Sample Preparation 167
6.2.2.2 Solid-State Characterization 167
6.2.2.2.1 Powder X-ray Diffraction 167
6.2.2.2.2 Solid-State Fourier Transform Infrared Spectroscopy 168
6.2.2.2.3 Differential Scanning Calorimetry 168
6.2.2.2.4 Modulated Temperature Differential Scanning Calorimetry (MTDSC) 168
6.2.2.2.5 Calculation of Theoretical Glass Transition Values with Gordon-Taylor Equation 168
6.2.2.2.6 High-Speed Differential Scanning Calorimetry 169
6.2.2.2.7 Thermogravimetric Analysis 169
6.2.2.3 Dynamic Vapor Sorption 169
6.2.2.4 Mathematical Modelling Using Young-Nelson Equations 169
6.2.2.5 FaSSIF Dynamic Solubility Study 170
6.2.2.6 Dissolution Study 170
6.2.2.7 UV Spectrophotometry 171
6.2.2.8 Bacterial Studies 171
6.3 Results and Discussion 171
6.3.1 Production of ENRO Amorphous Solid Dispersions 171
6.3.2 Solid-State Fourier Transform Infrared Spectroscopy 174
6.3.3 Thermal Analysis 179
6.3.4 Water Sorption Studies 183
6.3.5 Solubility and Dissolution Studies 189
6.3.6 Bacterial Studies 193
6.4 Conclusions 195
Chapter 7: General Discussion and Conclusions 196
7.1 General Discussion and Conclusions 197
7.2 Main Findings 205
7.3 Future Work 207
References 210
Appendices 236
Appendix 1 237
Appendix 2 242

Appendix 3 246
Appendix 4 251
Appendix 5 259

Summary

This thesis focuses on the poorly soluble fluoroquinolone antibiotic ciprofloxacin (CIP). Anhydrous CIP has the distinctive feature of being able to exist in either the zwitterionic or unionized form, however previous studies have generally only focused on one form of the drug. The ability of CIP to transform from one form to the other in the solid state was therefore investigated. The zwitterion was found to convert to the unionized form upon heating to its melting point, whereas the opposite transformation occurred when unionized CIP was exposed to water vapor.

Among the different formulation options available to improve the solubility of a drug, amorphization provides a number of advantages. However, very few examples of amorphous CIP formulations are mentioned in the literature. For the first time, the production of pure amorphous CIP is discussed in this thesis. This proved to be a challenging task due to the poor solubility, thermal degradation and strong crystal lattice of CIP. A fully X-ray amorphous sample was only obtained by spray drying a solution of the drug in pure water.

Due to the propensity of amorphous solids to crystallize, it is desirable to formulate them as amorphous solid dispersions (ASDs) using appropriate stabilizers. A number of polymers and small molecules were screened with CIP for their suitability in this regard. Ball milling was found to be a suitable production method for these ASDs. It was discovered that fully X-ray amorphous solid dispersions were only produced when CIP was milled with acidic polymers such as Eudragit L100, Eudragit L100-55, Carbopol and HPMCAS. Fourier transform infrared spectroscopy (FTIR) confirmed the presence of an ionic interaction between the piperazine amino group of CIP and carboxylate of the polymer in each ASD. The strength of these drug-polymer interactions contributed to the higher than expected glass transition temperatures (T_g's) of the samples, and rendered them resistant to crystallization during thermal and water sorption studies.

Although CIP remained partially crystalline when milled with neutral polymers such as PVP and Soluplus, it was possible to form a ternary ASD by dispersing amorphous CIP/succinic acid salts in these polymers. The addition of polymer increased the T_g's and crystallization temperatures of the salts, and they were also more stable during long-term stability studies.

However, all of the ASDs crystallized following exposure to high humidity. Similar results were obtained with ASDs containing CIP and various amino acids. Evidence of salt formation between the protonated secondary amine of the drug and α-carboxylate group of aspartic acid, glutamic acid, cysteine and arginine was found via FTIR and solid-state nuclear magnetic resonance analysis. In contrast, CIP was unable to interact fully with serine, alanine and glycine, resulting in semi-crystalline solid dispersions.

All of the ASDs produced in this project were more soluble than crystalline CIP in water and biorelevant media. A much greater increase in solubility was obtained with the ASDs containing more acidic counterions, such as succinic acid, glutamic acid and aspartic acid. However, the permeability of these samples was found to be lower than that of CIP in parallel artificial membrane permeability assays. In contrast, the ASDs containing cysteine, arginine and HPMCAS demonstrated higher effective permeability than the pure drug, while no decrease was seen with the other binary polymeric ASDs, giving them a more favorable solubility-permeability balance.

For comparison, a close analogue of CIP called enrofloxacin (ENRO), which bears an ethyl substituent on its piperazine ring, was subjected to a number of the same investigations as CIP. ENRO showed the same affinity as CIP for polymers, and only became fully X-ray amorphous when milled with those containing carboxylic acids. Like CIP, the tertiary amine of ENRO appears to be protonated in these ASDs, and forms an ionic bond with the carboxylate groups of the polymers. The stability of the ASDs was reflected in their elevated T_g's and lack of crystallization during water sorption studies. They also reached higher drug concentrations during solubility and dissolution studies than the pure drug. Like the corresponding polymeric CIP ASDs, no decrease in antibiotic efficacy was observed with the ENRO ASDs, while significant improvements were obtained with the ASDs containing HPMCAS. Therefore, ASDs may be a viable formulation option for improving the pharmaceutical properties of these fluoroquinolone drugs.

Acknowledgements

Firstly, I would like to express my sincere gratitude to my supervisor, Dr. Lidia Tajber, for all her support and guidance during my PhD studies. I was lucky to have a supervisor who was so understanding and easy to work with. I also wish to thank the past and current members of my lab, as well as the other researchers in the Panoz Institute, for all their help and friendship over the years, in particular Agnieszka, Naila, Svenja, Kate, Kieran, David, Peter, Zelalem and Emer. I am also thankful to the technical staff in the School of Pharmacy, Trevor, Brian and Ray, for their time and assistance.

I am grateful to Dr. Krzysztof Paluch, Dr. Anita Umerska and Dr. Sarah Hudson for conducting dynamic vapor sorption, bacterial and solid-state NMR studies, respectively, for my projects. I would also like to acknowledge the undergraduate students Eibhlin Fitzpatrick and Andrea Burke, and Masters student Daryl Conroy, who helped me with my laboratory work as part of their research projects.

This research project would not have been possible without the funding provided by the Science Foundation Ireland, under the Synthesis and Solid State Pharmaceutical Centre (SSPC). I also wish to acknowledge the other researchers in the SSPC, in particular those from Strand 3 P9, for listening to my presentations and participating in helpful discussions about my work.

Finally, I would like to thank my family for their constant moral support and encouragement, in particular my mum Jane. A special thank you to my husband Ivan for all of his motivation and problem solving help, and without whose support I would not have completed this PhD.

Publications and Presentations

Publications Associated with the Thesis:

- Mesallati, H.; Mugheirbi, N. A.; Tajber, L. Two Faces of Ciprofloxacin: Investigation of Proton Transfer in Solid State Transformations**.** *Crystal Growth & Design*. **2016**, 16, 6574–6585.
- Mesallati, H.; Umerska, A.; Paluch, K. J.; Tajber, L. Amorphous Polymeric Drug Salts as Ionic Solid Dispersion Forms of Ciprofloxacin. *Molecular Pharmaceutics*. **2017**, 14, 2209–2223.
- Mesallati, H.; Tajber, L. Polymer/Amorphous Salt Solid Dispersions of Ciprofloxacin. *Pharmaceutical Research.* **2017**. DOI: 10.1007/s11095-017-2250-z.
- Mesallati, H.; Conroy, D.; Hudson, S.; Tajber, L. Preparation and Characterization of Amorphous Ciprofloxacin-Amino Acid Salts. *European Journal of Pharmaceutics and Biopharmaceutics*. **2017.** DOI: 10.1016/j.ejpb.2017.09.009.
- Mesallati, H.; Umerska, A.; Tajber, L. Production of Enrofloxacin Amorphous Solid Dispersions – A Comparison with Ciprofloxacin. In preparation.

Other Publications:

- Knapik, J.; Wojnarowska, Z.; Grzybowska, K.; Tajber, L.; Mesallati, H.; Paluch, K. J.; Paluch, M. Molecular Dynamics and Physical Stability of Amorphous Nimesulide Drug and its Binary Drug–Polymer Systems. *Molecular Pharmaceutics*. **2016**, 13, 1937–1946.

Poster Presentations:

- Mesallati, H.; Conroy, D.; Tajber, L. Preparation of Amorphous Solid Dispersions of the Zwitterionic Drug Ciprofloxacin with Amino Acids. 51st AAPS Arden

Conference, Baltimore, MD, USA, **2016** Apr 18-20; T2006.

- Mesallati, H.; Tajber, L. Production of Amorphous Solid Dispersions to Improve the Solubility of Ciprofloxacin. 38th All Ireland Schools of Pharmacy Conference, RCSI, Dublin, Ireland. **2016** Mar 21-22.
- Mesallati, H.; Tajber, L. Production and Analysis of Amorphous Ciprofloxacin. SFI 2 year review of SSPC, University of Limerick, Ireland. **2015** Dec 10.
- Mesallati, H.; Tajber, L. Production of Binary Amorphous Salt Solid Dispersions of Ciprofloxacin. 2015 AAPS Annual Meeting and Exposition, Orlando, FL, USA, **2015** Oct 25-29; M1280.
- Mesallati, H.; Paluch, K. J.; Tajber, L. Production of Binary Amorphous Solid Dispersions of Ciprofloxacin. 37th All Ireland Schools of Pharmacy Conference, Queen's University Belfast, UK. **2015** Mar 30-31.

List of Abbreviations and Symbols

2θ	2 theta (diffraction angle)
δ_t	total solubility parameter
ΔE	energy band gap
η	absolute hardness
μ	chemical potential
χ	absolute electron negativity
ω	electrophilicity index
ALA	alanine
ANOVA	analysis of variance
API	active pharmaceutical ingredient
ARG	arginine
ASD	amorphous solid dispersion
ASP	aspartic acid
BCS	Biopharmaceutics Classification System
BHI	brain-heart infusion
BM	ball milled
CCDC	Cambridge Crystallographic Data Centre
CIP	ciprofloxacin
CIP HCl	ciprofloxacin hydrochloride
CP/MAS	cross polarization magic angle spinning
CS 1:1	ciprofloxacin hemisuccinate (CIP/succinic acid 1:1)
CS 2:1	ciprofloxacin succinate (CIP/succinic acid 2:1)
CSD	Cambridge Structural Database

CYS	cysteine
dm/dt	change in mass per unit time
DSC	differential scanning calorimetry
DVS	dynamic vapor sorption
ENRO	enrofloxacin
^exo	exothermic direction
FaSSGF	fasted state simulated gastric fluid
FaSSIF	fasted state simulated intestinal fluid
FTIR	Fourier transform infrared spectroscopy
GIT	gastrointestinal tract
GLU	glutamic acid
GLY	glycine
G-T	Gordon-Taylor
HOMO	highest occupied molecular orbital
HPLC	high-performance liquid chromatography
HPMCAS	hydroxypropyl methylcellulose acetate succinate
HSDSC	high-speed differential scanning calorimetry
^{1}H T_1	proton spin-lattice relaxation time
IGC	inverse gas chromatography
log P	n-octanol/water partition coefficient
LUMO	lowest unoccupied molecular orbital
MBC	minimum bactericidal concentration
MIC	minimum inhibitory concentration
MTDSC	modulated temperature differential scanning calorimetry

PAMPA	parallel artificial membrane permeability assay
P_e	effective permeability
pH_{max}	pH of maximum solubility
pK_a	negative base-10 logarithm of the acid dissociation constant
PM	physical mixture
PVA	poly(vinyl alcohol)
PVP	polyvinylpyrrolidone
PXRD	powder X-ray diffraction
r	correlation coefficient
R	gas constant
RH	relative humidity
rpm	revolutions per minute
RT	room temperature
S	global softness
SD	semi-crystalline solid dispersion
SDD	spray dried
SER	serine
SSNMR	solid-state nuclear magnetic resonance
T_g	glass transition temperature
TGA	thermogravimetric analysis

Chapter 1: General Introduction

1.1 Bioavailability

The bioavailability of a drug may be defined as the percentage of an administered dose that reaches the bloodstream. While an injected drug will theoretically have a bioavailability of 100%, this is not the case for oral dosage forms. Following oral administration, a formulation must disintegrate and dissolve in the gastrointestinal tract (GIT), before being absorbed through the intestinal wall into the circulatory system. The rate and extent to which this occurs will depend on an abundance of factors, in particular the physicochemical properties of the drug, the formulation used and the conditions in vivo. While the majority of these variables are outside the scope of this thesis, a number will be examined in relation to their effects on the fundamental properties of solubility, dissolution and permeability.

1.1.1 Classification of Drugs

The Biopharmaceutics Classification System (BCS) is used to classify drugs based on their aqueous solubility and gastrointestinal permeability.[1] The BCS was first proposed by Amidon et al in 1995, and is based on the fact that drug dissolution and gastrointestinal permeability are the major factors controlling the rate and extent of drug absorption. Accordingly, drugs can fall into one of the following four BCS groups: class 1: high solubility-high permeability drugs; class 2: low solubility-high permeability drugs; class 3: high solubility-low permeability drugs; and class 4: low solubility-low permeability drugs.[2] A modification of the BCS, called the developability classification system (DCS), further segregates class 2 drugs depending on whether their oral absorption is dissolution rate limited (class 2a) or solubility limited (class 2b).[3]

A drug may be described as highly soluble if the highest dose is soluble in less than 250 ml of aqueous media over the pH range 1–7.5, and a highly permeable drug should be more than 90% absorbed in humans. Regarding dissolution, a drug may be classified as rapidly dissolving if more than 85% of the dose dissolves in less than 900 ml of buffer within 30 minutes, using United States Pharmacopoeia apparatus I or II.[4]

1.1.2. Solubility and Dissolution

A major issue encountered during the development of many new active pharmaceutical ingredients (APIs) is poor aqueous solubility. It has been reported that almost 70% of new drug candidates have a solubility of less than 100 μg/ml in water, and therefore may be considered as practically insoluble.[5] In order to avoid problems with intestinal absorption, poorly soluble drugs may be developed as injectables. However, as oral formulations are the preferred drug delivery option due to patient acceptance and ease of administration, this route will be focused on here.

Solubility may be defined as the maximum amount of solute that can enter solution under certain conditions, such as temperature and pH. Dissolution on the other hand is the process of a solute disaggregating, dispersing and dissociating in a solvent to form a solution. Therefore, while solubility is a thermodynamic property of a solute, dissolution is a kinetic process, and is usually examined in terms of dissolution rate. As it is possible for an API to have a high dissolution rate but poor solubility, or vice versa, both of these processes are commonly examined during drug development.[6]

If a concentration in excess of the thermodynamic equilibrium solubility of a solute is achieved in solution, this is described as supersaturation.[7] Supersaturation may occur if the temperature or volume of a solution is rapidly decreased, or upon addition of a cosolvent in which the solute is less soluble. A supersaturated solution may also be generated in vivo when a weakly basic drug moves from the stomach into the higher pH of the small intestine. However, supersaturated systems are thermodynamically unstable, and thus the excess solute will eventually precipitate out of solution.[8]

The dissolution of a drug takes place in two stages. The first step involves the reaction of the solid (solute) and liquid (solvent), resulting in the release of solute molecules. This is followed by the transport of these solute molecules away from the solid/liquid interface into the bulk medium.[9] According to the Noyes-Whitney equation, the dissolution rate (DR) of a drug is related to the surface area available for dissolution (A), the diffusion coefficient of the drug (D), the volume of dissolution media (V), the thickness of the boundary layer

adjacent to the dissolving drug surface (h), the saturation solubility of the drug (C_s), and the amount of dissolved drug (X_d), as shown in the following equation:[10,11]

$$DR = \frac{A \times D}{V \times h} \times \left(C_s - \frac{X_d}{V}\right) \quad (1.1)$$

If the solvent volume is very large, or the drug is removed from the solvent faster than it dissolves, this is referred to as 'sink conditions'. This can occur in vivo when a drug is absorbed faster than it can go into solution.[9] If sink conditions are present, X_d will tend towards zero, and the second part of the Noyes-Whitney equation simplifies to C_s.

The diffusion of drug molecules from the particle surface into the bulk solution is often the rate limiting step of dissolution.[6] The diffusion coefficient may be increased by raising the temperature or decreasing the viscosity of the dissolution medium. While the temperature in vivo is very constant, the viscosity of the gastrointestinal fluids is influenced by the ingestion of food, and varies depending on the type and volume of food and fluids consumed.[11] The use of particle size reduction as a means of increasing drug solubility, via an increase in surface area, will be discussed in Section 1.1.4.

1.1.3 Permeability

In order for a drug to be absorbed into the systemic circulation it must have a certain permeability. Permeability may be defined as the ability of molecules to cross a cell, cell membrane, endothelium or epithelium. Permeability is usually described in terms of the rate at which this occurs, with units of 10^{-6} cm/s.[12] The movement of drug molecules across the intestinal epithelium can take place in a number of ways. Drugs may diffusive passively through the enterocytes (transcellular transport) or between the enterocytes (paracellular transport). Alternatively, carrier-mediated drug absorption may occur. This involves active transport, secondary active transport or facilitated (passive) diffusion of drug molecules across the cell membrane via a transmembrane protein. Receptor-mediated endocytosis may also be responsible for drug absorption.[13] Unlike passive absorption, carrier-mediated transport may be inhibited or become saturated.[14]

Most drugs are primarily absorbed by passive diffusion, which is driven by a concentration gradient across the cell membrane. However, a linear correlation between drug concentration

and membrane transport is generally only seen with uncharged molecules. During membrane partitioning, charged molecules can affect the surface potential of the lipid bilayer, resulting in a nonlinear concentration-permeation relationship.[14] The rate of passive transcellular transport of a drug is related to its lipophilicity, with more lipophilic drugs diffusing through cell membranes more quickly.[14] Drug absorption can also be reduced due to the presence of efflux transporters on the surface of enterocytes, such as P-glycoprotein, breast cancer resistance protein, multidrug resistance protein 2, organic anion transporter, and organic cation transporter.[13] In general, efflux transporters will only have a significant effect on drugs with low passive permeability.[14]

The intestinal cells lining the lumen of the GIT have a number of glycoproteins protruding from their apical surface, forming the glycocalyx. These cells are covered by a protective mucous layer produced by specialized epithelial cells called goblet cells. This layer differs in pH from that of the lumen contents, forming a "microclimate". The apical surface of the GIT also varies from pH 6.0–8.0 depending on location.[15] Before reaching the intestinal cell membranes, drugs must pass through a 30–100 μm thick aqueous boundary layer, which forms due to reduced agitation at the surface of the GIT. This is also known as the unstirred water layer. While diffusion through this layer may be the rate limiting step for lipophilic compounds, it does not significantly affect the absorption of poorly permeable drugs.[16]

There are a number of in vivo and in vitro models available for estimating the permeability of a drug, which differ in their complexity and speed. PAMPA, or the parallel artificial membrane permeability assay, was chosen for the projects described in the following chapters, as it is a relatively simple, non-cell based, high throughput technique, with good reproducibility.[17] More importantly, a number of studies have confirmed the suitability of PAMPA for predicting drug absorption in humans.[13,18] Briefly, PAMPA consists of two aqueous compartments separated by a phospholipid-coated filter, which forms an artificial cell membrane.[13] The proportion of drug that passes from the acceptor compartment to the donor compartment over a certain time frame is then measured. More details of this technique will be given in later chapters.

1.1.4 Methods of Improving Bioavailability

If a drug is poorly absorbed, a large dose must be administered in order to reach the necessary blood concentration range required to achieve the desired therapeutic effect. There are a number of drawbacks associated with the administration of large doses. For example, topical irritation and toxicity are more likely to occur in the GIT upon oral administration, which can reduce patient compliance. From a manufacturing point of view, the production of a drug product with a high drug load can be more problematic. This is often due to poor powder flowability and sticking during granulation and tableting. Another obvious disadvantage is the increase in manufacturing cost, as a larger amount of API will be consumed during development and manufacture of the drug product.[19]

Absorption can be increased by increasing the concentration of dissolved free drug at the site of absorption. A number of approaches may be taken to increase the solubility of an API. These include particle size reduction (micronization and nanoparticle formation), crystal modification (formation of metastable polymorphs, salts and cocrystals), cyclodextrin complexation, self-emulsification, pH modification and amorphization.[19] The suitability of these methods for a particular drug will depend on the chemical characteristics of the compound. For instance, ionizable APIs may be converted to different salt forms, whereas neutral drugs may be formulated as cocrystals.

Poorly soluble drugs may be divided into two categories depending on whether they suffer from solvation limited solubility or solid-state limited solubility. Drugs which are solvation limited are generally large and flexible, which increases their cavitation energy (the energy needed to disrupt the solvent and create a gap into which the solute molecule can fit). They are also lipophilic, which decreases their hydration due to reduced interaction with water molecules. The solubility of such compounds can be improved with excipients such as disintegrants, surfactants, cyclodextrins and lipids.[20] Drugs with solid-state limited solubility on the other hand are usually small, flat, rigid and inflexible molecules. The crystal lattices of such compounds are stabilized by intermolecular interactions, such as hydrogen bonding, Van der Waals and π–π interactions.[21] These structural features result in a high crystal packing energy (the energy required to disrupt the crystal lattice and release single molecules into solution), which is one of the main determinants of the solubility of a drug.[22] Due to the

strength of their intermolecular bonds, the dissociation of such drug molecules from the crystal lattice is hindered upon addition to water. In order to improve their solubility, the crystal lattice may be disrupted via salt formation, chemical modification or amorphization.[23]

As mentioned in Section 1.1.2, particle size reduction of a drug increases the surface area available for interaction with solvent, and thus the dissolution rate.[24] However, a number of potential problems may be encountered during the comminution process. Micronized particles may possess higher surface energy, which can result in agglomeration. This not only reduces the flowability of powders, but also decreases the surface area exposed to solvent during dissolution.[25] While particle size reduction can increase dissolution rate, this will not have a significant effect on the absorption of BCS class 2b (solubility limited) drugs.[3] The milling processes used to comminute particles also generate a large amount of heat and energy. This may bring about alterations in the physical state of the sample, for example partial conversion to the unstable amorphous form.[26] Although such a transformation is often undesirable, the amorphous state of a drug is in fact more soluble than its crystalline counterpart, and can offer more of a solubility improvement than other formulation options. The solubility difference between the amorphous and crystalline form of a drug can be several hundred fold, whereas polymorphs, for example, usually improve solubility by less than 10 times.[27] As the minimum particle size achievable by conventional milling is 2−3 μm, the solubility enhancement offered by comminution is also limited.[28] Therefore, a great deal of research has recently been carried out into the generation, characterization and stabilization of fully amorphous formulations. An overview of this area will be given in Section 1.2.

As the solubility and permeability of a drug are closely linked, these properties must be examined concurrently in order to enhance drug absorption. Permeability is directly proportional to the diffusion coefficient of the drug (the rate at which the drug crosses the cell membrane) and its membrane/aqueous partition coefficient (the ratio of the drug concentration within the phospholipid bilayer and the aqueous compartments), and therefore depends on the solubility of the drug in the GIT.[29] A number of studies have reported a trade-off in the solubility and permeability enhancement of many formulations.[29] Preparations such as surfactants, cyclodextrins and cosolvents increase the equilibrium solubility of drugs,

which leads to a decrease in the apparent cell membrane/intestinal lumen partition coefficient. This reduces the driving force for transport through the membrane.[30–32] When a drug is bound to cyclodextrins or incorporated into surfactant micelles, this also decreases the fraction of free drug in the GIT lumen, and thus the concentration gradient across the phospholipid barrier, which lowers the impetus for absorption.[29] Although a positive correlation between drug solubility and the concentration of cyclodextrin, surfactant or cosolvent has been found, this is associated with a corresponding decrease in passive permeability.[32]

As the passive permeation of a drug across a membrane is related to the concentration gradient,[14] the flux of drug molecules from the GIT lumen should be elevated by increasing the degree of supersaturation at the site of absorption. Supersaturation increases the kinetic or non-equilibrium solubility of a drug, and usually results in a greater concentration of free drug, without affecting its membrane/intestinal lumen partition coefficient.[31–33] A number of studies have demonstrated the benefit of amorphous formulations in this regard. Unlike other solubility-enhancing formulations, amorphous formulations do not appear to have the same negative effect on drug permeability. Combined with a significant solubility improvement, this results in a more favorable solubility-permeability balance, and higher transmembrane flux.[31,32] In addition, higher quantities of amorphous formulation were found to result in higher drug concentrations during solubility studies, while the permeability remained constant.[32]

As the degree of supersaturation is increased, the flux seen in permeability studies should also rise linearly.[32] However, this depends on the ability of an amorphous formulation to maintain supersaturation for a sufficient time, to allow for drug absorption to occur.[33] Higher levels of supersaturation are usually associated with greater or more rapid crystallization and precipitation of the solute. For this reason, a more moderate supersaturation level and release rate may be more effective at increasing the membrane flux of a drug.[8] This can be achieved in vivo if the drug steadily permeates through the wall of the GIT, as this will decrease the level of supersaturation in the lumen, and reduce the driving force for precipitation.[8] In addition, the inclusion of polymers in amorphous formulations may delay or prevent the

nucleation and crystallization of supersaturated drug solutions, as will be discussed in Section 1.2.2.2.

1.2 Amorphous Solids

Unlike crystalline materials, amorphous solids lack long range order. However, at the molecular level, the structure of amorphous solids is not always completely random, and they typically possess some short range order.[34] Due to their random orientation, each molecule in an amorphous system can undergo slightly different intra- and intermolecular interactions.[35] The non-uniform molecular arrangement of amorphous materials also results in a greater specific volume (volume per unit mass) and thus lower density than crystalline solids,[36] and higher free energy and entropy.[34] The amorphous form of a drug can therefore have very different physical properties to the corresponding crystalline state.[35]

The most pharmaceutically desirable trait of amorphous solids is their enhanced solubility relative to the crystalline state. The crystal packing energy, which is a significant barrier to dissolution, is reduced in amorphous materials due to their disrupted crystal lattice.[37] The high free energy of amorphous solids also increases their kinetic solubility, which enables the formation of supersaturated solutions.[38] Unfortunately, the amorphous state is metastable and prone to crystallization. This will be discussed in more detail in Section 1.2.1. Crystallization is particularly likely to occur in supersaturated solutions, which can negate the solubility advantage of an amorphous drug. In order to prevent or delay the crystallization of amorphous drugs, and to further enhance their solubility, composite amorphous formulations containing one or more stabilizers have been developed. These are known as amorphous solid dispersions (ASDs), and will be discussed in Section 1.2.2.

1.2.1 Stability of Amorphous Solids

The amorphous form of a substance is the most energetic solid state.[39] As a result of their excess free energy, amorphous solids are intrinsically unstable and prone to crystallization, leading to problems with manufacture and storage.[34] Amorphous solids undergo a glass to rubber (or supercooled liquid) transition at a characteristic temperature known as the glass

transition temperature or T_g. Great changes in viscosity and molecular mobility occur at this temperature.[40] Below the T_g the material is "kinetically frozen" in a thermodynamically unstable glassy state.[39] In the glassy state solids are usually hard and brittle, whereas in the rubbery state they become more soft and flexible, and the molecules have greater mobility.[41] Amorphous solids are therefore more prone to crystallization at temperatures above their T_g, as the increased molecular mobility facilitates nucleation and crystallization.[42] Some solids possess enough molecular mobility at temperatures below their T_g to crystallize over pharmaceutically relevant time frames.[43] However, at temperatures of 50 K below the T_g (known as the Kauzmann temperature, T_K) or more, molecular motions can be considered negligible.[44] A storage temperature of 50 ºC below the T_g has therefore been suggested as suitable for maintaining the stability of an amorphous medicinal product for the required shelf life.[39]

The process of crystallization begins with nucleation, which is believed to take place in two stages. According to this theory, nucleation commences with the formation of disordered clusters of drug molecules. When these clusters reach an adequate size, the molecules become organized into a crystal structure.[45] This is then followed by crystal growth. The rate of crystallization of an amorphous drug depends on a number of factors related to the molecule itself. Crystallization occurs more slowly for drugs with large molecular weights, as it takes longer for the drug molecules to diffuse to the growing crystal lattice, and requires more energy to reach the necessary conformation.[26] Molecules with a more complex structure and larger number of rotatable bonds will also take a longer time to crystallize, as they can exist in a number of different configurations. This increases the configurational entropy of the drug, and thus the time it takes for its molecules to reach a conformation matching that of the crystal lattice.[26,46]

The crystallization tendency of an amorphous solid is related to its T_g and melting point. The higher the T_g of a drug, the greater the kinetic barrier for molecular diffusion and thus crystallization, whereas the higher the melting point, the greater the thermodynamic driving force for crystallization. However, these factors may be altered by the presence of other components in composite formulations, as will be discussed in Section 1.2.2.1.

Amorphous drugs are more hygroscopic than their crystalline forms, as water can absorb into the internal structure of the material rather than just adsorb to the surface.[42,47] This is due to their larger free volume, as the irregularly arranged molecules in an amorphous solid are not as closely packed as those in a crystal.[39] It is therefore practically impossible to produce an amorphous formulation which does not contain any moisture.[48] Water absorption can negatively affect drug stability by increasing the rate and reducing the onset temperature of crystallization. This is due to plasticization of the sample by moisture, a lowering of the T_g and an increase in molecular mobility.[42,49]

1.2.2 Amorphous Solid Dispersions

As previously mentioned, a major drawback to amorphous drugs is their poor physical stability. This problem has been addressed by the development of amorphous solid dispersions, or ASDs. ASDs have been defined in a number of ways by different researchers. In this thesis the definition suggested by Crowley and Zografi will be used. According to these authors, an ASD may be defined as a miscible mixture of at least two chemical components that form a single amorphous phase.[40] An ASD may therefore contain one or more APIs, polymers, or low molecular weight compounds. A number of commercial polymeric ASDs have entered the market in recent years, proving that they can be a viable formulation option for poorly soluble drugs.[37] Some commercially available ASDs include: Cesamet® (nabilone/PVP), Kaletra® (lopinavir/ritonavir/copovidone), Prograf® (tacrolimus/HPMC) and Sporanox® (itraconazole/HPMC).[50] The mechanism by which such ASDs can improve the stability and solubility of amorphous drugs will be discussed in Section 1.2.2.1 and 1.2.2.2 respectively.

1.2.2.1 Stability of ASDs

ASDs are traditionally thought of as drug-polymer dispersions, and this is perhaps the most widely encountered amorphous formulation in the literature. Polymers have proven to be very efficient at stabilizing a wide range of poorly soluble drugs, and there are a number of possible mechanisms by which this can occur. Polymers can stabilize ASDs via antiplasticization, which is defined as a decrease in the plasticity of a substance, involving an increase in its T_g and a corresponding increase in the free energy required for

crystallization.[51] Polymers with long chains can also prevent crystallization by sterically hindering the diffusion of drug molecules, blocking sites of crystal growth, and increasing the viscosity of the formulation and the kinetic barrier to nucleation.[52,53] The free energy of an ASD may be decreased by the presence of polymers, as their high molecular weight and flexibility will increase the configurational entropy of the system.[51] The crystallization tendency of an ASD will also be decreased if there are interactions between the components, such as hydrogen bonding and acid-base interactions.[54] Intermolecular interactions reduce the molecular mobility of the drug and increase the energy required for crystallization.[52,55] However, polymers with high T_g's can increase the stability of ASDs in the absence of any drug-polymer interactions, as they will increase the overall T_g of the formulation relative to the pure amorphous drug.[56] Alternatively, if the T_g of a polymer is lower than that of the drug, an improvement in stability may still be obtained if there are strong interactions between the two components.[57]

As described in Section 1.2.1, amorphous solids are prone to water absorption, which decreases their T_g and reduces the barrier to crystallization. This property is more pronounced in ASDs, as hydrophilic polymers are often more hygroscopic than the amorphous form of a drug.[48] Water uptake can reduce the stability of an ASD due to plasticization, increased molecular mobility, and disruption of drug-polymer interactions.[37] However, despite their hygroscopic nature, polymers such as PVP can counteract these effects due to the stabilizing mechanisms described above. In addition, drugs that form stronger interactions with a polymer have been found to absorb less water during water uptake studies, as less hydrogen bonding sites will be available to water molecules.[40] Suitable packaging can also help to limit the absorption of water during storage.

1.2.2.1.1 Miscibility

ASDs will be more stable if their components are mixed on a molecular level, as this reduces their free energy, and thus the driving force for nucleation.[53] If an ASD is molecularly mixed it will consist of a single amorphous phase, with a single T_g. In contrast, if the constituents of an ASD are not homogeneously mixed, different regions of various compositions will exist, resulting in two or more amorphous phases, and a corresponding number of T_g's.[58] By examining the T_g of a binary ASD as a function of composition, one can estimate whether

the two constituents are miscible or compatible. If a drug and polymer are fully miscible, a single T_g should be obtained, in between the T_g of the pure drug and the polymer. If the constituents are fully immiscible on the other hand, two T_g's equal to those of the pure components will be seen at all possible compositions.[41] A simplified representation of this is shown in **Figure 1.1**.

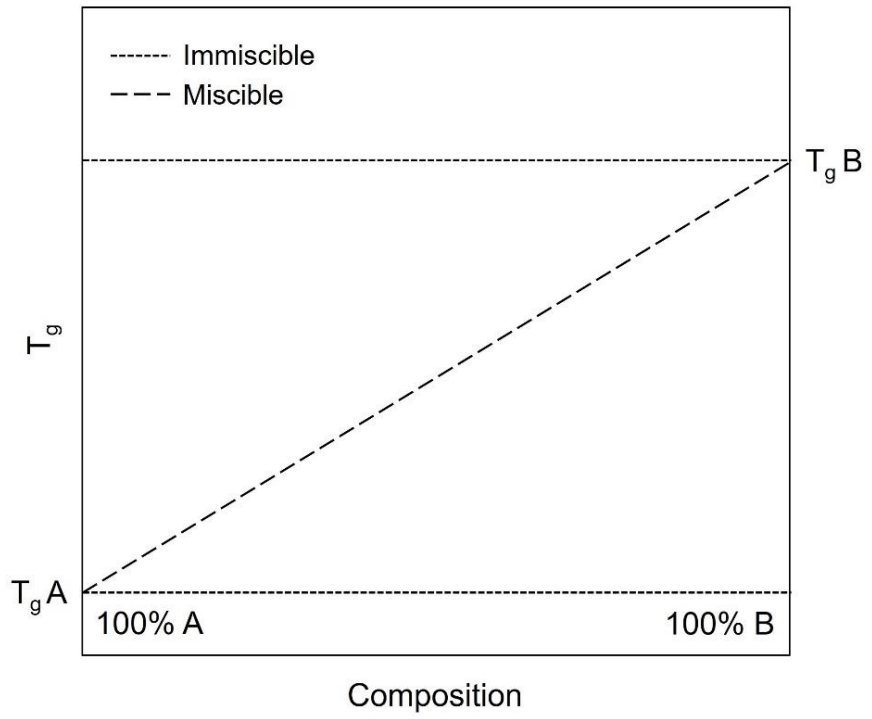

Figure 1.1. The effect of the ratio of components A and B on the overall T_g of a binary ASD. Adapted from Brostow et al.[41]

The miscibility of an ASD may also be estimated by comparing its experimental T_g to a theoretical value. Perhaps the most widely used equation for predicting the T_g of a mixture is the Gordon-Taylor equation, which takes into account the weight ratio, T_g and density of each component.[59] If the experimentally determined T_g of an ASD is very similar to that calculated by the Gordon-Taylor equation, it suggests that there is ideal mixing and a lack of specific interactions between the components.[60] If the experimental and calculated T_g of an ASD are not equal on the other hand, this indicates that the components are not completely miscible, and/or their volumes are not additive.[61] This can occur if there is a difference

between homo- and heteromolecular interactions in an ASD. For example, there may be ionic bonds between a drug and polymer, but weaker non-ionic interactions such as Van der Waals, polar or hydrogen bonds between relevant groups of the drug itself. Stronger drug-polymer intermolecular interactions will increase the density (and therefore decrease the volume) of an ASD, resulting in an increase in its T_g.[61] For this reason, higher than expected T_g's are commonly observed with amorphous salts.[62] Similarly, lower than predicted T_g values will be obtained if homomolecular drug-drug or polymer-polymer interactions are stronger than the heteromolecular interactions between a drug and polymer, as the free volume of the ASD will be higher than that of an ideal mixture.[63,64]

While the measurement of an ASD's T_g provides a rapid method of estimating the miscibility of its components, there are limits to the sensitivity of this technique. In particular, it is not possible to detect amorphous domains that are less than approximately 30 nm in size by DSC.[65] Similarly, if the T_g ranges of different amorphous areas overlap, DSC will be unable to separate them.[65] Therefore, additional techniques such as powder X-ray diffraction (PXRD), solid-state nuclear magnetic resonance (SSNMR) and Fourier transform infrared spectroscopy (FTIR) should be used to determine the phase composition of an ASD. These techniques can provide information on the kinetic miscibility of a mixture. For example, phase separation involving a domain size of 5–50 nm may be detected by SSNMR,[66] whereas such an ASD may be thermodynamically miscible and show a single T_g upon DSC analysis. Alternatively, if the components of an ASD are thermodynamically immiscible, they may still be kinetically miscible due to intimate mixing of the components during the production process, and this can also be determined by SSNMR analysis. Such a formulation would be expected to possess good physical stability,[67] highlighting the importance of using multiple techniques to examine the miscibility of an ASD.

The miscibility and compatibility of the components of an ASD may also be estimated by calculating their Hansen solubility parameters. The Hansen solubility parameter (δ_t) is a combination of partial solubility parameters, which represent the different kinds of interactions present in a molecule, i.e. dispersive forces (δ_d), dipole-dipole interactions between polar groups (δ_p) and hydrogen bonding (δ_h):[68,69]

$$\delta_t = \sqrt{\delta_d{}^2 + \delta_p{}^2 + \delta_h{}^2} \quad (1.2)$$

Two substances that have similar solubility parameters (differing by < 7 $MPa^{0.5}$) would be expected to have a high affinity for each other, and to form a miscible, single phase ASD.[69,70] On the other hand, if there is a difference of more than 10 $MPa^{0.5}$ in the solubility parameters of two components they are likely to be immiscible.[71] Hansen's solubility parameters can be found by group contribution calculations, inverse gas chromatography (IGC) or solubility studies.[38] In the former method, each functional group in a molecule is assigned a weighting related to its volume and potential for molecular interactions. The contributions from all of the functional groups are then combined to give the total solubility parameter of a substance.[72] While this is a relatively simple method due to the availability of functional group contribution values in the literature, there are a number of limitations to its application. For example, it will not give accurate results for salts, and in this case experimental approaches such as IGC must be used.[72]

1.2.2.2 Solubility and Dissolution of ASDs

The solubility and dissolution of amorphous drugs may be altered to different extents via ASD formation, depending on the stabilizers chosen. ASDs are generally quite porous. This allows water to penetrate the particles more easily, increasing the dissolution and drug release rates.[73] The formulation of a drug as an ASD containing a hydrophilic polymer can improve the solubility of a drug due to increased wetting and deagglomeration.[74] The inclusion of a polymer with self-emulsifying properties, or the addition of a surfactant, would also help in this regard.[75]

Polymers can improve the dissolution profile of drugs formulated as ASDs by enabling and prolonging supersaturation. This process has been analogized by Guzmán et al as a "spring" and "parachute".[76] The amorphous nature of an ASD enables rapid dissolution of a drug, which therefore acts as a "spring" for the formation of a supersaturated solution. Unfortunately, amorphous drugs tend to quickly convert from this high energy state to a more stable and less soluble crystal form, leading to precipitation and reduced absorption of the API. However, the polymers present in an ASD can inhibit the nucleation and crystallization

of the drug. In this way they act as "parachutes", helping to maintain supersaturation, and thus increase the extent of drug absorption.[76]

Polymers can prevent the nucleation and crystal growth of a drug in solution by interacting with the drug particles, thereby acting as a physical barrier and preventing the formation of drug-drug interactions.[45] In order for this to occur, a polymer must interact sufficiently with the solute, which requires a balance of hydrophobic and hydrophilic character. If a polymer is too hydrophilic or hydrophobic in comparison to a drug, it is more likely to interact with water or other polymer molecules, respectively. In order to maximize the degree of nonspecific interactions between a drug and polymer, the two components should have a similar hydrophobicity.[45] Polymers are more likely to prevent the crystallization of supersaturated solutions if they form stronger interactions with the drug, such as hydrogen or ionic bonds.[77] Therefore, for ionizable drugs, polymers containing oppositely charged functional groups are more likely to be effective crystallization inhibitors.[78] However, the efficacy of such a polymer will also depend on its pK_a and the pH of the surrounding medium, as this will determine whether it is ionized, and to what extent.[79] When a polymer is ionized, like charges will self-repulse, reducing the likelihood of polymer-polymer interactions, and increasing those between the drug and polymer.[45] In contrast, when such a polymer is unionized, it may adopt a more compact conformation in solution, leaving a smaller surface area available to block the crystal growth sites of the drug.[80] In addition to its chemical structure, the shape of a polymer may also affect its ability to prevent the crystal packing of a drug. For example, those with rigid, bulky side groups are more likely to sterically prevent drug molecules from coming into contact with one another.[45] Similarly, using a higher proportion of polymer, or a polymer with a higher molecular weight, will provide steric hindrance to drug diffusion and precipitation.[45,81] Such polymers may also form a viscous gel-like structure in solution. Although this can reduce the rate of drug dissolution, it can also prevent the organisation of drug aggregates into crystal nuclei, allowing them to redissolve.[82]

ASDs may dissolve rapidly or gradually, depending on their composition. In the former case, drug release may be described as dissolution-controlled.[83] This is commonly encountered when an ASD contains medium-soluble polymers. Upon addition to the dissolution medium,

the polymer dissolves rapidly. This is accompanied by the release of the amorphous drug. A high degree of supersaturation is thus rapidly produced, followed by nucleation and crystallization. Although this can be delayed to some extent by suitable polymers, they will be less effective in highly supersaturated solutions due to the increased rate of crystallization. Therefore, the drug concentration tends to spike and then fall rapidly with such formulations. With ASDs containing medium-insoluble polymers on the other hand, drug release is diffusion-controlled. The slower dissolution of the polymer and drug leads to a gradual increase in supersaturation and reduces the rate of nucleation and crystallization.[83] Although this also decreases the maximum achievable drug concentration, it can still enable significantly improved drug concentrations to be reached and, importantly, sustained for biologically relevant timeframes.[84] Therefore, higher oral bioavailability may be achieved with ASDs that gradually release the drug rather than those containing fast-releasing, soluble polymers.[83]

While much of the discussion thus far has focused on polymeric ASDs, amorphous salts containing a poorly soluble drug and suitable counterion may also provide a large solubility enhancement. Such ASDs will have the combined benefit of their amorphous nature and pH effect. In aqueous solutions, salts dissociate, allowing their counterions to alter the pH of the local environment. For instance, an acidic counterion will lower the pH of the medium surrounding a basic drug, resulting in ionization of the API and thus an improvement in its solubility.[85] Although the absence of a polymer may limit the duration of supersaturation obtained with amorphous salts, the strength of their ionic intermolecular interactions can improve their stability in the solid state.[86] Amorphous polymeric salts, in which an ionic interaction exists between a drug and polymer, would also be expected to remain stable during long-term storage.[61,87] These ASDs should have a greater ability to inhibit crystallization in solution than traditional amorphous salts, however their effect on pH is likely to be minimal.

1.2.3 Methods of Producing Amorphous Solids

The techniques used to prepare amorphous samples can fall into one of two categories.[88] One group involves the conversion of a crystalline material into a thermodynamically stable, non-crystalline, intermediate liquid form. For instance, during spray drying an intermediate

solution is rapidly precipitated in order to form an amorphous solid,[89] while during quench cooling a molten sample is rapidly cooled, freezing its molecules in a disordered state and producing a glass.[90] Freeze drying and solvent evaporation are other processes that fit within this category, which can be considered as the thermodynamic route of amorphous solid generation.[90] Alternatively, mechanical activation, such as ball milling, can be used to directly convert a crystalline solid to its amorphous form over a period of time.[88] This method of production is also known as the kinetic route.[90]

The level of short range order present in an amorphous solid will depend on the method of preparation, as will a number of its physicochemical properties. For example, the dissolution, water uptake behaviour and stability of otherwise comparable ASDs have been shown to vary depending on the techniques used to produce them. This may be due to differences in particle size and shape, or the level of disorder and/or extent of drug-polymer interactions within a sample.[91,92]

For reasons that will be discussed in the following chapters, the main method used to generate the amorphous solids described in this thesis was milling, followed by spray drying. A brief description of these techniques is given in Sections 1.2.3.1 and 1.2.3.2, respectively.

1.2.3.1 Milling

The vast majority of the milling discussed in this thesis was carried out with a planetary ball mill. This equipment consists of one or two milling chambers that rotate in a planetary motion around the mill. In addition, the chambers rotate in the opposite direction of their supporting disc, resulting in substantial centrifugal forces. The milling chambers contain a number of balls that collide with the sample and chamber walls. Samples are therefore subjected to a combination of compression, shear/attrition, and collision (particle-particle and particle-chamber wall) impacts, resulting in their comminution and the introduction of crystal defects.[93]

Although milling is usually used to reduce the particle size of pharmaceutical materials, it can also be used to bring about changes in the solid state of a material, as well as reactions between components. This is known as mechanochemistry. For example, when multicomponent mixtures are subjected to mechanical energy, a new substance, such as a

salt or cocrystal, may be formed. During mixing the reactants come into close contact, enabling interactions such as hydrogen bonding and proton transfer to occur.[94] Importantly, milling can also result in the conversion of drugs to their amorphous form. It has been hypothesized that the heat generated during milling may result in the amorphization of solids due to the occurrence of localized melting and quenching. However, the fact that milling at low temperatures facilitates the generation of the amorphous state contradicts this theory.[26,95] The mechanism of amorphization is more likely to be related to the accumulation of crystal defects due to the grinding and shearing effects particles are exposed to.[95] The mechanical energy of a mill can disrupt a drug's crystal lattice, resulting in an increase in free energy and loss of long range order, and may eventually lead to the formation of the amorphous phase.[26,96]

The operating conditions under which milling is carried out can have a significant impact on the solid-state properties of the product. High intensity milling is required to induce the defects and disorder necessary to obtain the amorphous state,[95] while it is easier to amorphize a solid at lower temperatures.[97] Milling should at least be carried out below the T_g of a drug in order to convert it to the amorphous state.[98] If milling is conducted at a temperature above the T_g, this can result in the formation of metastable crystal polymorphs instead.[97] Cryomilling is often a more efficient method of producing amorphous drugs than milling at room temperature. This process involves the use of liquid nitrogen to keep the temperature of the mill below 0 ^oC, which helps to prevent the crystallization of any amorphous material.[99] Longer milling times are also associated with greater molecular disorder and a reduced crystallization tendency.[100]

It is reasonable to assume that ASDs prepared by ball milling will be less homogeneous than those produced by processes such as spray drying or melt methods.[92,101] With the latter techniques, the components are initially present in a liquid form, allowing them to mix at a molecular level. This increases the likelihood that a complete glass solution will be formed upon particle solidification. In contrast, during milling the crystal lattice of a drug must first be disrupted before it can mix intimately with any other ingredients, and there is no guarantee that a molecular mixture will be achieved.[102] Amorphous milled solids also tend to have a higher surface energy than those prepared by other methods. This may be due to an increased

surface-to-bulk ratio, changes in the conformation of molecules, and/or increased surface exposure of reactive and high energy functional groups upon milling.[103]

1.2.3.2 Spray Drying

The spray drying process begins with the atomization of a solution or suspension of the compound of interest, followed by mixing with a drying gas, evaporation of the solvent, and collection of the dried particles.[104] Spray drying can be used to produce pure amorphous drugs, as well as composite formulations, as long as the components are sufficiently soluble in a suitable solvent system. The solubility of the drug will determine whether spray drying is a practical method for producing the amorphous state, and whether a reasonable yield is possible.[104]

The physical properties of spray dried formulations will depend on a number of processing conditions, as shown in **Table 1.1**.[105] Spray dried formulations generally have a high porosity and free volume, which increases the extent and rate of dissolution that they can achieve. However, their low density can also make them less stable than amorphous samples produced by other methods. The presence of residual solvent in spray dried samples may also reduce their T_g and thus stability.[106]

Table 1.1. Effect of Spray Drying Conditions on Particle Properties[a]

Parameter	Particle size	Particle smoothness	Porosity	Residual moisture
Inlet temperature ↑	↑	↓	↓	↓
Drying flow rate ↑	↓	↑	↑	↓
Feed rate ↑	↓	↑	↓	↑
Solute concentration ↑	↑	↓	↓	↓
Solution viscosity ↑	↑	↓	↓	↑

[a]Adapted from Vasconcelos et al.[105] ↑/↓: Increase/decrease in parameter/characteristic.

1.3 Ciprofloxacin

Ciprofloxacin (CIP) is a second generation fluoroquinolone antibiotic with a wide spectrum of activity. It has a bacteriostatic effect on bacterial cells by reversibly blocking DNA replication and cell growth. This involves the formation of a complex between the drug, the enzymes DNA gyrase and topoisomerase IV, and bacterial DNA, which prevents the cleavage and re-ligation of DNA.[107] CIP also has concentration-dependent bactericidal activity, via the production and release of free DNA ends.[108]

CIP contains both an acidic and a basic group, and can therefore exist in a number of ionization states depending on the pH of its environment. The pK_a of the secondary amine and carboxylic acid of CIP have been reported as approximately 8.6 and 6.2, respectively.[109] Therefore, in neutral media the drug can exist in either the unionized or zwitterionic form (**Figure 1.2**), although the latter is far more prevalent.[110] CIP can also easily convert between these forms due to the small difference in the pK_a of the carboxylic acid and amino group of the molecule.[109] In the solid state the drug usually exists as the zwitterion, as its oppositely charged groups can participate in extensive intermolecular interactions. This enables dense packing of the molecules in the crystal, and increases its stability relative to the unionized form of the drug.[21] Further details of these intermolecular bonds will be provided in Chapter 2, along with a thorough description of the crystal structure of both forms of CIP, and their interconversion.

(a)

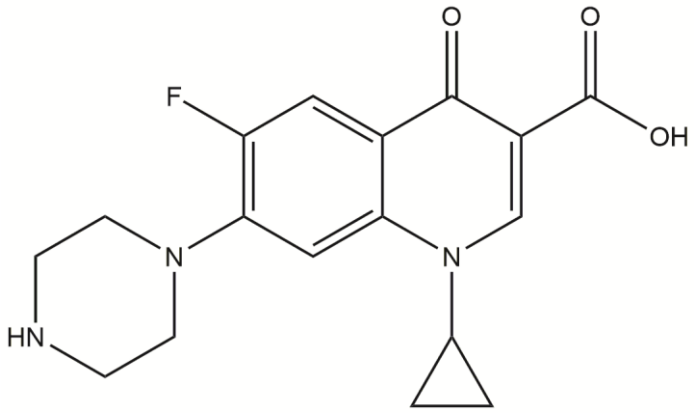

(b)

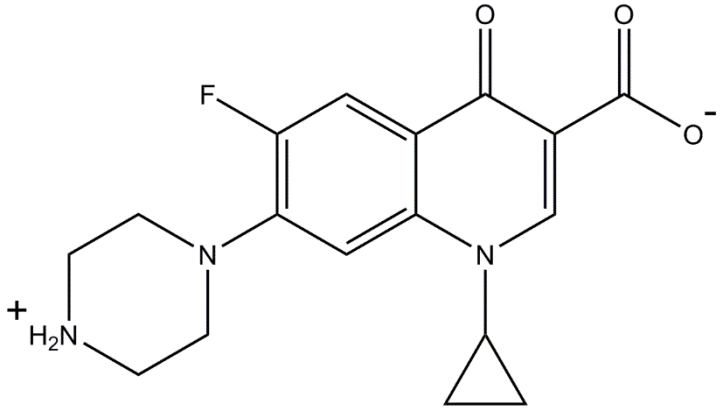

Figure 1.2. Chemical structure of (a) unionized and (b) zwitterionic ciprofloxacin.

The strength of a drug's crystal lattice may be represented by its melting point.[21] Given that zwitterionic CIP (the commercially available form of the drug) has a high melting point of around 270 ^{o}C, it is unsurprising that it is poorly water soluble. However, since it is an ionizable drug, its solubility will vary with pH, with a minimum around pH 7.5[110] (**Figure 1.3**). Therefore, CIP most likely dissolves in the acidic environment of the stomach, and is then absorbed upon entering the duodenum.[111]

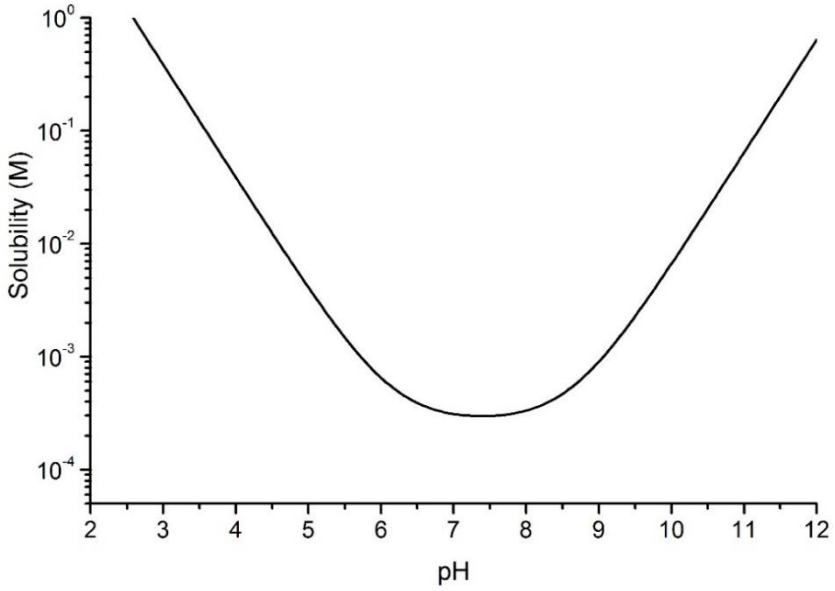

Figure 1.3. pH-solubility curve of ciprofloxacin.

In addition to its poor aqueous solubility, CIP has been classified as a poorly permeable drug.[112] Its log P has been reported as -0.8,[113] whereas a log P of at least 0.8 is recommended in order for a drug to be sufficiently permeable in vivo.[114] CIP therefore falls within the specifications of a BCS class 4 drug.[113] The low log P of CIP may be explained by the fact that only the unionized form of the drug will partition into an organic phase.[115] In aqueous solution, zwitterionic CIP molecules associate head-to-tail into "stacks", which are further stabilized by hydrogen bonding with water molecules. Although the formation of these stacks results in partial charge neutralization,[116] it is still unlikely that they will approach a lipid membrane.[117] However, the drug is also believed to be partly absorbed in the zwitterionic form in vivo via the paracellular route, as it can pass through the water-filled channels between intestinal epithelial cells.[118] Similarly, CIP may enter bacterial cells in the zwitterionic form by passing through water-filled porins, whereas only the unionized form can diffuse across the lipid bilayer.[119] Although the paracellular route is reportedly responsible for almost 20% of CIP's transport at pH 6.5,[118] the majority of CIP is believed to be absorbed via the transcellular pathway. While zwitterionic CIP is too hydrophilic to directly diffuse across the cell membrane, it is believed to undergo intramolecular proton transfer in the area adjacent to the phospholipid bilayer. The reduced dielectric constant and greater lipophilicity of this region facilitate the conversion of CIP to the more lipophilic unionized form,[15,109,120] which can cross the cell membrane with relative ease.[117]

1.3.1 Ciprofloxacin Formulations

Due to the poor solubility of CIP, no formulations containing the pure drug are available on the Irish market. Instead, the vast majority of products contain the hydrochloride salt, CIP HCl. This salt is available as 250, 500 and 750 mg tablets for oral administration, and in ear drops at a concentration of 3 mg/ml. The lactate salt of CIP is also available as a solution for infusion. CIP HCl is far more soluble than the pure drug in water, however their solubility is comparable in phosphate buffer. Although CIP HCl has been classified as a BCS class 4 drug,[121] the bioavailability of CIP following oral administration of this salt has been reported to be approximately 69%.[122]

Salt formation is clearly a suitable formulation option for CIP, and has been the focus of a number of research studies. Like the commercially available salts, these compounds all

contain acidic counterions, which interact with the protonated secondary amine of the drug. When the carboxylic acid of CIP is unionized, it forms an intramolecular hydrogen bond with the neighboring ketone group. For this reason, the pK_a of the carboxylic acid is unusually high,[109] and therefore this group is less likely to be involved in salt formation than the piperazine group of CIP.

The mesylate, gluconate and glycolate salts of CIP were recently shown to greatly improve the solubility of the drug, over and above that of CIP HCl, in water and simulated biological fluids.[123] CIP salts have also been produced using malonic, tartaric, oxalic, citric, succinic, maleic, fumaric and adipic acid. These formulations also improved the aqueous solubility of the drug and resulted in faster dissolution.[124–126] In addition to disrupting the crystal lattice and removing the dipole of CIP, such salts generate a low pH when they dissolve, which further increases the solubility of the drug.

Regarding amorphous formulations of CIP, there is little in the literature on this topic, while no mention of pure amorphous CIP could be found at all. Amorphous salts were produced by Paluch et al by spray drying and ball milling, respectively, a 1:1 and 2:1 mixture of CIP and succinic acid. Both salts significantly increased the solubility of the drug, however they were unstable in the presence of water, and crystallized during vapor sorption and solubility studies.[125] CIP nanoparticles prepared by Cheow et al were found to have a dissolution rate two times greater than the pure crystalline drug. These were prepared by mixing a solution of CIP in acetic acid with a solution of dextran sulphate and NaCl, and freeze drying the resulting suspension.[127] Although the authors claimed that these particles were amorphous, a slight peak is visible in their PXRD pattern, indicating the presence of residual crystallinity. In contrast, fully X-ray amorphous microparticles were successfully prepared by Osman et al by spray drying acidic solutions containing CIP and various concentrations of chitosan, dextran sulphate, or a combination of both polymers. The appearance of a new peak at 1716 cm^{-1} in the FTIR spectra of these ASDs suggested the formation of ionic interactions between the components. The authors also hypothesized that CIP may have formed salts with the acids present in the spray dried solutions. While the in vitro release of CIP was significantly improved by most of the spray dried ASDs, the release of the drug was hindered in some cases due to the formation of a thick polymer gel.[128]

1.3.2 Enrofloxacin

Enrofloxacin (ENRO) is a fluoroquinolone with a chemical structure very similar to that of CIP (**Figure 1.4**). Although the chemical formulae of the two drugs resemble each other closely, the additional ethyl substituent attached to the piperazine ring of ENRO results in distinct physical, chemical and biological properties. One of the most notable differences between anhydrous CIP and ENRO is that the former drug exists in the zwitterionic form in the solid state, whereas the latter is unionized.[129] It is therefore reasonable to assume that ENRO possesses a weaker crystal lattice than CIP, due to the absence of intermolecular ionic interactions. This may affect the solid state properties of ENRO, and make it easier to amorphize. This will be examined further in Chapter 6.

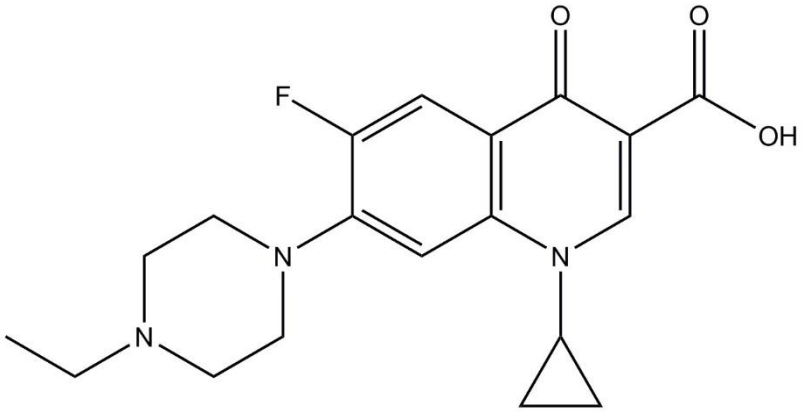

Figure 1.4. Chemical structure of enrofloxacin.

The pK_a of the carboxylic acid of ENRO is very similar to that of CIP, with a value of approximately 6.3.[130] As with the unionized form of CIP, this group participates in an intramolecular O−H•••O hydrogen bond with the neighboring ketone.[129] The presence of an ethyl substituent on the terminal amine of ENRO reduces the basicity of this group, giving it a pK_a of approximately 7.8. While the equivalent amino group of CIP participates in salt formation, the tertiary amine of ENRO may be less likely to interact with acidic counterions due to its lower basicity. However, a number of ENRO salts were successfully prepared by Karanam et al using highly ionizable acids, such as maleic, fumaric, succinic, oxalic and acetic acid.[129] The ability of ENRO to form ASD formulations by interacting with various polymers will also be investigated in Chapter 6.

Although ENRO is unionized in the solid state, in neutral solution it primarily exists as the zwitterion. Like CIP, it is practically insoluble in water, and is least soluble around pH 7.4.[131] The extra ethyl group of ENRO increases the lipophilicity of the drug, resulting in a log P of approximately 0.6.[132] However, ENRO was found to be more soluble than CIP at neutral pH,[132] perhaps due to its weaker crystal lattice. The higher permeability of ENRO compared to CIP has also been confirmed by rat in situ permeability studies.[130] Due to safety concerns, ENRO is only licensed as a veterinary medicine. Therefore, the extent to which the drug is absorbed in humans is unknown. Regarding other mammals, the bioavailability of ENRO varies widely depending on the species of animal treated. For example, while the drug is highly absorbed in pigs and dogs, a bioavailability of only approximately 34% was obtained in kittens. In general, ENRO has a higher oral bioavailability than CIP in small animals and horses. The drug is also primarily metabolized to CIP in vivo.[133]

1.4 Project Aims

Amorphization has proven to be a very effective means of improving the solubility of a variety of compounds.[27] To date, much of the research in this area has focused on a limited number of poorly soluble drugs with properties amenable to amorphization. Due to the scarcity of published research concerning CIP, the overall aim of this project was to produce a number of amorphous formulations of this API, in order to improve its pharmaceutical properties.

Before focusing on composite formulations, a greater understanding of the behavior of the CIP molecule in the solid state was required. For instance, while the crystal structure of the unionized and zwitterionic form of CIP have been described independently, a head-to-head comparison has not been carried out. The ability of CIP to transform from one form to the other in the solid state has also not been investigated. These topics are therefore examined in Chapter 2. In this chapter attempts to produce pure amorphous CIP are also described for the first time. The solid state properties of the amorphous form of the drug are then determined, in order to provide a reference point for subsequent studies of CIP ASDs.

It is well known that polymers can significantly improve the solubility and stability of amorphous drugs. Therefore, a major aim of this project was to prepare polymeric ASDs of CIP. A number of polymers were screened for their suitability in this regard, as described in Chapter 3. In order to determine the viability of the resulting ASDs, their physical stability, solubility, dissolution and permeability are also investigated. Finally, the minimum inhibitory concentration (MIC) and minimum bactericidal concentration (MBC) of the dispersions are compared to those of CIP to ensure that the pharmacology of the drug was not adversely affected by its formulation as an ASD.

Chapter 4 continues the work carried out by Paluch et al on CIP/succinic acid amorphous salts.[125] The authors found these salts to be significantly more soluble than crystalline CIP, however they were not particularly stable when exposed to water. The main goal of the work described in Chapter 4 was to improve the stability of these salts by combining them with a polymer. In addition to their stability, the solid state properties of these polymer/amorphous salt solid dispersions are also examined. Their solubility and permeability are then compared to those of the original salts to determine whether the addition of polymer had any effect on these properties.

A number of studies have recently demonstrated the suitability of amino acids as stabilizers for ASDs. In Chapter 5 the ability of a variety of amino acids to fulfill such a function for CIP is explored. Given that all amino acids contain a carboxylate and secondary amine functional group, as well as additional side chain groups, there are a number of possible means by which they could interact with CIP. Therefore, a major objective of Chapter 5 was to investigate the nature of the interactions present between the drug and amino acids in the ASDs. The behavior of the formulations when heated or exposed to water vapor is also examined, as well as their solubility and permeability.

Unlike the previous chapters, Chapter 6 focuses on another fluoroquinolone, ENRO, which is an analogue of CIP. The primary purpose of this work was to produce ASDs of ENRO, and in doing so to determine whether the ethyl substituent of the drug affects its ability to interact with polymers. The solid state properties of anhydrous ENRO and the successfully prepared ASDs are also analyzed, and their water uptake behavior is compared to crystalline

CIP and the equivalent CIP ASDs. The effect of ASD formation on the solubility, dissolution, MIC and MBC of the drug is then examined.

Finally, Chapter 7 contains a general discussion of the research conducted for this project, and the conclusions that may be drawn from it. This is followed by a synopsis of the main findings of the work, and an outline of possible future studies that may be initiated by it.

Chapter 2: The Two Faces of Ciprofloxacin: Investigation of Proton Transfer in Solid State Transformations

2.1 Introduction

Ciprofloxacin (CIP), or 1-cyclopropyl-6-fluoro-4-oxo-7-(piperazin-1-yl)-1,4-dihydroquinoline-3-carboxylic acid, is a second generation fluoroquinolone that was first marketed in 1986. It is a wide spectrum antibiotic, with high activity against Gram-negative species of bacteria and good-to-moderate activity against Gram-positive species.[134,135] It is also effective against atypical organisms such as Legionella pneumophila, Chlamydia trachomatis, Mycobacterium tuberculosis and Mycoplasma hominis.[136,137] Anhydrous CIP is an interesting molecule, as it can exist in two different forms: the unionized form (**Figure 2.1a**) and the zwitterion (**Figure 2.1b**). However, it is the zwitterion that is usually present in the solid state, and that is available commercially. The crystal structures of the unionized form of CIP and the zwitterion have been described by Mahapatra et al and Fabbiani et al, respectively.[138,139]

(a)

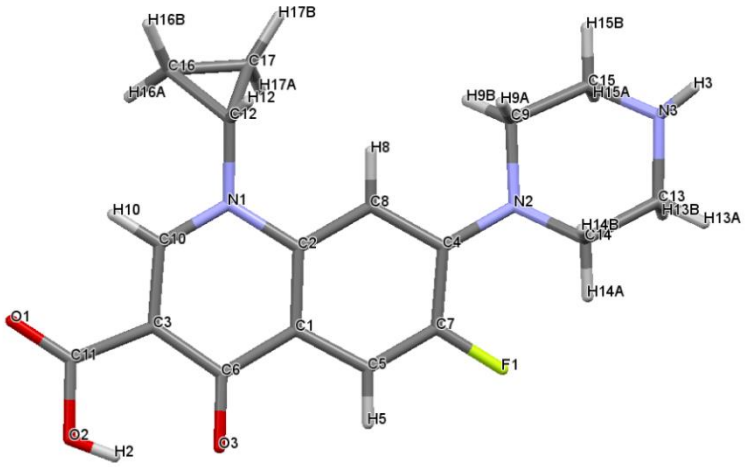

(b)

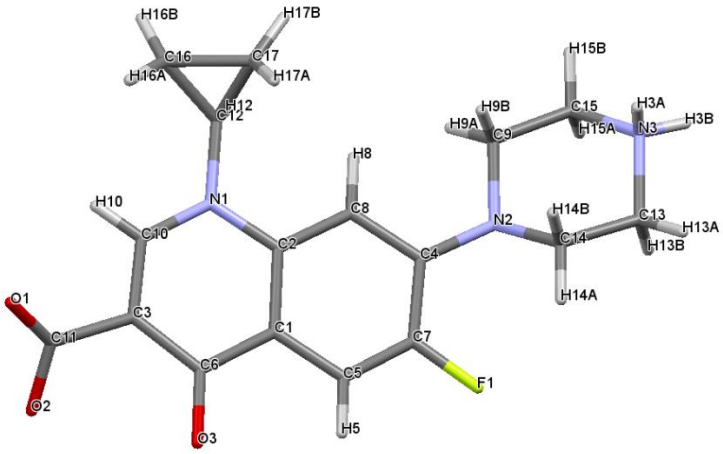

Figure 2.1. Chemical structures with atom labels of (a) unionized CIP and (b) zwitterionic CIP.

In solution, the carboxylic acid and secondary amine of CIP can ionize, depending on the pH of the surrounding media. In the neutral pH range CIP is predominantly zwitterionic and has an overall neutral charge, making it practically insoluble in aqueous media.[140] The solubility of CIP in water has been reported as 0.06 and 0.08 mg/ml at 25 ^{o}C and 37 ^{o}C, respectively.[125] CIP is also poorly soluble in other common solvents such as ethanol, methanol, propanol, dichloromethane, acetone and chloroform.[141,142,143]

The poor solubility of CIP may also be attributed to the strength of its crystal lattice, resulting in solid-state limited solubility. Intermolecular interactions, such as hydrogen bonding, Van der Waals and π−π interactions, inhibit the dissociation of drug molecules from the crystal lattice upon addition to water.[113] As described in Chapter 1, one method of improving the solubility of such drugs is amorphization. The amorphous form does not possess long range order, and is the most energetic solid state.[34,144] Amorphous drugs are therefore more soluble than their crystalline counterparts, as less energy is required for the molecules to enter solution.[145] However, unlike many other poorly soluble drugs, the preparation of pure amorphous CIP has not been described in the literature. In contrast, the production of other fluoroquinolones in the amorphous state has been more extensively reported. Norfloxacin, which possesses an ethyl group in the place of CIP's cyclopropyl group, has been produced

in the pure amorphous form via spray drying and quench cooling. This form of the drug was found to be in the unionized state, whereas anhydrous crystalline norfloxacin is zwitterionic.[146,147] Amorphous moxifloxacin HCl and levofloxacin HCl have also been prepared by spray drying and solvent evaporation, respectively,[148,149] whereas gemifloxacin has been synthesized in the amorphous form.[150]

Due to the absence of research in this area, the primary aim of this study was to prepare the pure amorphous form of CIP. Ball milling, cryomilling and spray drying were attempted for this purpose. Powder X-ray diffraction (PXRD), differential scanning calorimetry (DSC) and Fourier transform infrared spectroscopy (FTIR) were used to confirm the amorphous nature or otherwise of the resultant samples and their ionization state, and to find the T_g of CIP. CIP has been reported to undergo thermal decomposition following melting,[125] however this has never been fully investigated. In order to rule out the use of melting techniques, such as quench cooling, for the amorphization of CIP, its degradation upon heating to the onset and endset of melting was studied. The effect of such heating on its ionization state was also determined. In order to gain a better understanding of the unionized and zwitterionic forms of the drug, their crystal structures and chemical stability were examined via crystallographic and computational analysis. Finally, the effect of water uptake on the unionized form of CIP was explored using dynamic vapor sorption (DVS).

2.2 Experimental Section

2.2.1 Materials

Anhydrous ciprofloxacin was obtained from Carbosynth Limited, Berkshire, UK. Acetonitrile was obtained from Sigma-Aldrich Ireland Ltd., Arklow, Ireland. All other chemicals and solvents were of analytical grade.

2.2.2 Methods

2.2.2.1 Production of Amorphous Ciprofloxacin

2.2.2.1.1 Ball Milling

CIP was ball milled (BM) at room temperature (RT) using a Retsch planetary ball mill PM 100 (Haan, Germany). 2 g of powder was added to 50 ml stainless steel grinding bowls. Three stainless steel milling balls 20 mm in diameter and weighing 32 g each were used. The drug was milled for 6 hours in total, in intervals of 15 min with 10 min breaks in between. After 1, 2, 4 and 6 hours, small samples of powder were taken for analysis by PXRD.

2.2.2.1.2 Cryomilling

A Retsch CryoMill (Haan, Germany) was used to cryomill 0.5 g of CIP. The drug was sealed in a grinding jar and immersed in liquid nitrogen for a few minutes. CIP was then milled for 6 cycles, consisting of 3 min of grinding followed by a 2 min break.

2.2.2.1.3 Spray Drying

Spray drying was carried out by Dr. Lidia Tajber in Trinity College Dublin (TCD). A Büchi B-290 mini spray dryer (Flawil, Switzerland) with a 1.5 mm cap and 0.7 mm tip was used to spray dry CIP. The pump speed was set to 30% (9–10 ml/min), and the aspirator to 100%. A mixture of nitrogen (with a pressure of 6 bar) and air was used as the drying gas. Two different solvents were used to produce pure spray dried (SDD) CIP. In the first case, an excess of the drug was added to 1 L of a 9:1 mixture of ethanol and water, which was stirred overnight. The next day the solution was filtered to remove any undissolved drug, and then spray dried using an inlet temperature of 78 ^{o}C. This procedure was then repeated using pure water and an inlet temperature of 100 ^{o}C.

2.2.2.2 Solid-State Characterization

2.2.2.2.1 Powder X-ray Diffraction (PXRD)

PXRD was carried out at RT (22–25 ^{o}C) using a benchtop Rigaku MiniflexII X-ray diffractometer (Tokyo, Japan) and a Haskris cooler (Illinois, USA). The samples were scanned from 5 to 40 2θ degrees with a step width of 0.05, scan rate of 0.05^{o}/sec and signal

collection time per step of 1 sec. The tube (Cu, 1kW normal focus) output voltage and current were 30 kV and 15 mA, respectively.

2.2.2.2.2 Differential Scanning Calorimetry (DSC)

DSC was carried out using a Mettler Toledo DSC (Schwerzenbach, Switzerland) with a RP-100 LabPlant refrigerated cooling system (Filey, UK), which was calibrated using an indium standard. The purge gas used was nitrogen. Approximately 5–10 mg samples were analyzed in sealed 40 µl aluminum pans with pierced lids. All samples were heated from 25 to 300 ^{o}C at 10 ^{o}C/min. Mettler Toledo STARe software (version 6.10) was used to analyze the thermograms.

2.2.2.2.3 High-Speed DSC (HSDSC)

HSDSC was performed by Dr. Lidia Tajber in TCD using a PerkinElmer Diamond DSC (Waltham, MA, USA) and ULSP B.V. 130 cooling system (Ede, Netherlands). The instrument was calibrated using an indium standard. Approximately 3–5 mg samples were analyzed in 40 µl aluminum pans with sealed aluminum lids. A helium gas flow of 60 ml/min was controlled with a PerkinElmer Thermal Analysis Gas Station. Crystalline and cryomilled CIP were heated from 25 to 300 ^{o}C at 50–500 ^{o}C/min. To allow for water evaporation, cryomilled CIP was first heated from 25 to 70 ^{o}C, allowed to cool to 25 ^{o}C, and then reheated to 300 ^{o}C.

2.2.2.2.4 Temperature-Modulated Differential Scanning Calorimetry (StepScan)

A PerkinElmer Diamond DSC, as described above, was used to detect the T_g of amorphous CIP by Dr. Lidia Tajber in TCD. Nitrogen was used as the purge gas at a flow rate of 40 ml/min. Samples were prepared as described for HSDSC, and were heated at 5 ^{o}C/min in steps of 2 ^{o}C. Between each step the temperature was held constant for 1 min. The specific heat of the glass transition was calculated from the enthalpy flow using the area algorithm.

2.2.2.2.5 Thermogravimetric Analysis (TGA)

TGA was carried out on crystalline and cryomilled CIP using a Mettler TG50 measuring module coupled to a Mettler Toledo MT5 balance (Schwerzenbach, Switzerland). Approximately 8–10 mg samples were analyzed in open aluminum pans, using nitrogen as

the purge gas. Samples were heated from 25 to 300 ^{o}C at a rate of 10 ^{o}C/min. Mettler Toledo STARe software (version 6.10) was used to analyze the thermograms.

2.2.2.2.6 Solid-State Fourier Transform Infrared Spectroscopy (FTIR)

FTIR was performed using a Spectrum One FT-IR spectrometer (PerkinElmer, Connecticut, USA) equipped with Spectrum Software version 6.1. A spectral range of 450–4000 cm^{-1}, resolution of 4 cm^{-1}, scan number of 10 and scan speed of 0.2 cm/sec were used. KBr disks were produced by direct compression, using a pressure of approximately 10 bar for 1 min. A sample loading of 1% was used. Deconvolution of the carbonyl region of the spectra (1770–1550 cm^{-1}) was conducted in order to separate overlapping bands. Following subtraction of the baseline, Gaussian peak fitting was carried out on the spectra using OriginPro 7.5 software. In each case four to five overlapping peaks were detected in this region. Their combined area and shape were close to those of the original bands.

2.2.2.3 Thermal Degradation Study

Crystalline CIP was heated to the onset (~ 265 ^{o}C) and endset (~ 276 ^{o}C) of melting at 10 ^{o}C/min using a Mettler Toledo DSC. Cryomilled CIP was also heated to the melting endset (~ 284 ^{o}C). Crystalline CIP was then heated by HSDSC to 300 ^{o}C at 500 ^{o}C/min using a PerkinElmer Diamond DSC. The samples were diluted with mobile phase and analyzed by HPLC. The entire study was carried out at least in triplicate for each sample.

2.2.2.4 High-Performance Liquid Chromatography (HPLC)

The content of CIP was measured with a Shimadzu 10Avp HPLC system (Kyoto, Japan). A Luna 5u C8 column was used, with a length of 250 mm, internal diameter of 4.6 mm and 5 µm particle size. The mobile phase consisted of 13 volumes of acetonitrile and 87 volumes of a 2.45 g/L solution of phosphoric acid, previously adjusted to pH 3.0 with triethylamine. An injection volume of 10 µl and flow rate of 1.5 ml/min for 17 min was used. A Shimadzu SPD-10Avp UV-vis detector at 278 nm was used to detect the drug. A standard curve was prepared in order to find the concentration of CIP.

2.2.2.5 Dynamic Vapor Sorption (DVS)

DVS analysis was carried out on partially amorphous CIP that had been spray dried in ethanol/water, using an Advantage-1 automated gravimetric vapor sorption analyzer (Surface Measurement Systems Ltd., London, UK). The temperature was maintained at 25.0 ± 0.1 °C. Approximately 10 mg of powder was added to the sample basket and placed in the instrument. This was equilibrated at 0% relative humidity (RH) until a constant mass was obtained ($dm/dt \leq 0.002$ mg/min). The reference mass was recorded and sorption-desorption analysis was then carried out between 0 and 90% RH, in steps of 10% RH. At each stage, the sample mass was equilibrated ($dm/dt \leq 0.002$ mg/min for at least 10 min) before the RH was changed. An isotherm was calculated from the complete sorption and desorption profile. The sample was analyzed by PXRD when it reached 80% RH (during the sorption stage) and also when it returned to 0% RH at the end of the study.

2.2.2.6 Crystallographic Analysis

The crystallographic data was analyzed by Dr. Lidia Tajber and Naila Mugheirbi in TCD using PLATON (version 150216),[151] CrystalExplorer (version 3.1)[152] and Mercury (version 3.5.1)[153] using the 2015 version of the Cambridge Structural Database (CSD) software.

2.2.2.7 Computational Methods

Gaussian03 software[154] was used by Dr. Lidia Tajber in TCD to optimize the structures of unionized CIP (gas phase) and zwitterionic CIP (water). Due to the instability of zwitterionic CIP in the gas phase, solvation effects during minimization of this structure were achieved implicitly through application of the integral equation formalism polarizable continuum model (IEFPCM). The B3LYP/6-311++G(d,p) level of density functional theory was applied in all cases. No constrains on the geometry of molecules was imposed. Initial geometries were minimized using the 6-31++G(d,p) basis set and re-optimized. The GaussView03 package was then applied to visualize the frontier molecular orbitals and Mulliken charges.

The following global electronic descriptors were calculated according to Koopmans' theorem,[155] assuming that electron affinity (A) can be expressed in terms of HOMO (highest occupied molecular orbital) orbital energy (E_{HOMO}), while ionization energy (I) can be expressed as LUMO (lowest unoccupied molecular orbital) orbital energy (E_{LUMO}).

Therefore, global reactivity descriptors, including energy band gap (ΔE), absolute electron negativity (χ), chemical potential (μ), absolute hardness (η), global softness (S) and electrophilicity index (ω) can be determined using equations 2.1−2.6:[156,157]

$$\Delta E = (I - A) \tag{2.1}$$

$$\chi = \frac{I+A}{2} \tag{2.2}$$

$$\mu = -\chi \tag{2.3}$$

$$\eta = \frac{I-A}{2} \tag{2.4}$$

$$S = \frac{1}{\eta} \tag{2.5}$$

$$\omega = \frac{\mu^2}{2\eta} \tag{2.6}$$

2.2.2.8 Statistical Analysis

Statistical analysis was carried out using Minitab 16 software. Data was analyzed using one- and two-sample Student *t* tests, or one-way analysis of variance (ANOVA) with Tukey's multiple comparison test (Tukey's honestly significant difference, or HSD). A *p*-value of ≤ 0.05 was considered significant.

2.3 Results and Discussion

2.3.1 Crystal Forms of Ciprofloxacin

As previously mentioned, anhydrous CIP is known to exist in two crystalline forms. It may be unionized (CCDC number 757817, CSD refcode UHITOV01)[138] or zwitterionic (CCDC number 714344, CSD refcode UHITOV).[139] Detailed crystallographic information on these structures may be found in the publications of Mahapatra et al[138] and Fabbiani et al,[139] respectively. The structure overlay of unionized and zwitterionic CIP, produced using the

crystal structures from the CCDC (no. 757817 and no. 714344, respectively), is shown in **Figure 2.2**.

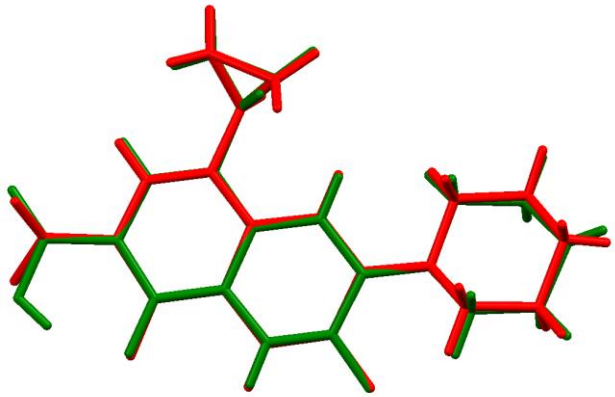

Figure 2.2. Structure overlay of unionized (green) and zwitterionic (red) CIP.

The root mean square deviation (RMSD) is defined as the square root of the mean squared error, and provides a measure of the difference between two sets of values. In Mercury the RMSD is used to measure the geometric difference between packing features or packing patterns in crystal structures. Three pairs of atoms, F1, C1 and C7, were used to compare the structures of unionized and zwitterionic CIP, resulting in a RMSD of 0.0264. The distances between the equivalent atoms were 0.023 Å for F1, 0.027 Å for C1 and 0.029 Å for C7, indicating that there is no significant conformational change between the two forms of CIP molecule.

Unionized CIP belongs to the triclinic crystal system and P-1 space group.[138] An O-H•••O intramolecular hydrogen bond is formed between the hydrogen of the carboxylic acid and the neighboring ketone oxygen (**Figure 2.3a**). This interaction is also found in CIP salts, where it stabilizes the protonated carboxylic acid and reduces the acidity of this group.[110] The unionized drug also contains an intermolecular N-H•••N hydrogen bond between the secondary amine groups of neighboring molecules. Therefore, each molecule is part of a dimer. In addition, intermolecular interactions between the carbonyl oxygen of the carboxylic acid and various C-H groups are present.[138] It is important to note that, according to Mahapatra et al, the crystal of unionized CIP that was used to obtain the structure shown in **Figure 2.3a** was not of the best quality.[138] Therefore, the hydrogen atom of the secondary

amine of CIP (H3 according to the numbering system shown in **Figure 2.1a)** is most likely either misplaced or disordered in the structure reported by the authors.

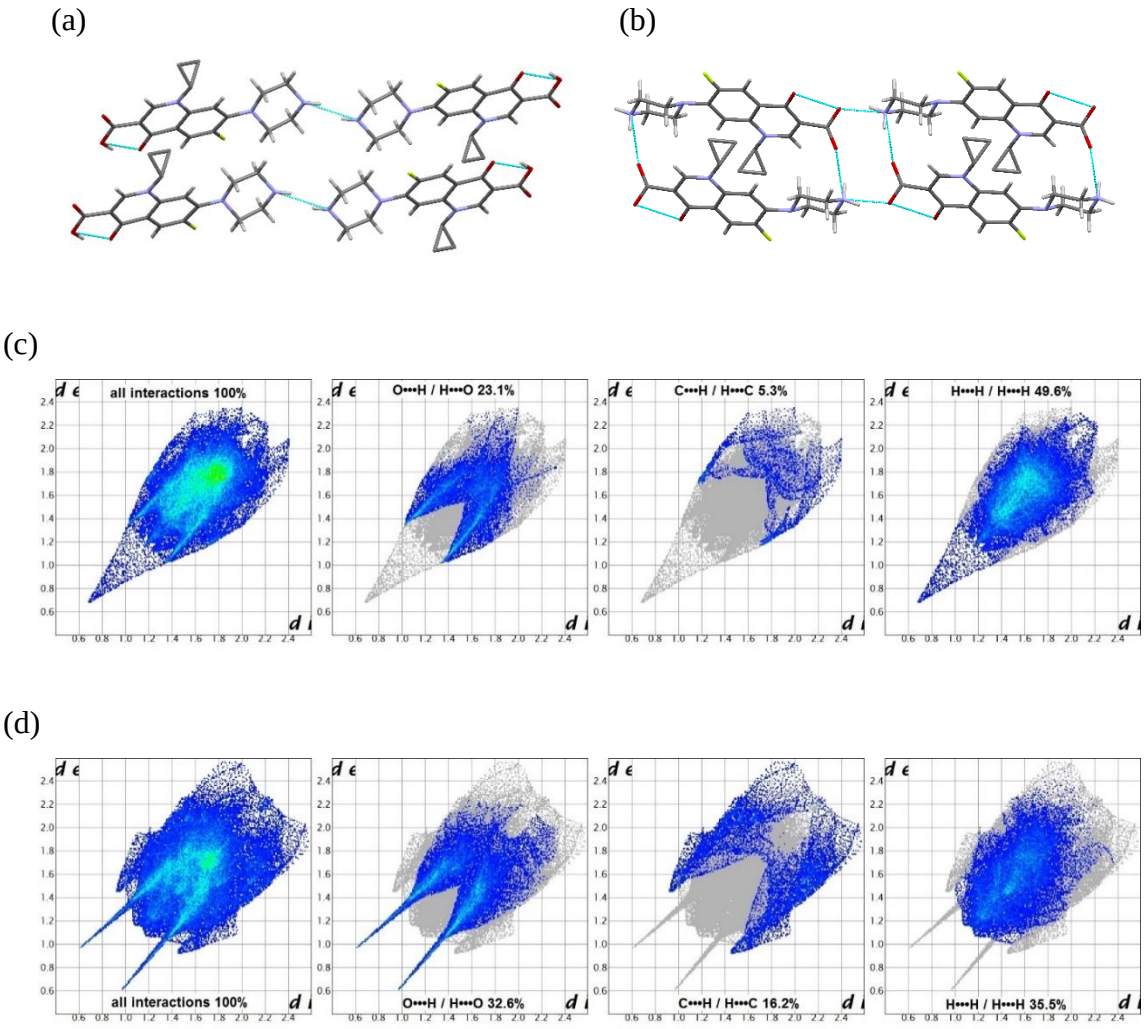

Figure 2.3. Principal hydrogen bond network in (a) unionized CIP and (b) zwitterionic CIP. Hirshfeld analysis as fingerprint plots with percent contribution of reciprocal interactions for (c) unionized CIP and (d) zwitterionic CIP.

In zwitterionic CIP, intermolecular ionic bonds are formed between the positively charged piperazine amino group and negatively charged carboxylate group of two neighboring molecules. This head-to-tail interaction results in the formation of a chain of molecules parallel to the a-axis of the unit cell (**Figure 2.3b**). In addition, adjacent chains are connected by strong intermolecular NH^{+}•••O^{-} hydrogen bonds, forming two-dimensional layers which

extend along the (-1 0 1) planes of the drug and are not interlinked.[139,158] Each CIP molecule is therefore linked to both neighboring and adjacent molecules, resulting in a tetramer-like structure. Intermolecular C-H π−π interactions between the aromatic rings and between the aromatic ring and cyclopropyl group are also present.[158] Such intermolecular bonding enables dense packing of the molecules in the crystal and the formation of a strong crystal lattice.[21] A weak halogen C-H•••F bond is also present in the crystal structures of unionized and zwitterionic CIP. A detailed analysis of the H-bonds present in both forms of CIP can be found in **Table A.1.1.**

Hirshfeld analysis of the crystal packing of unionized and zwitterionic CIP, using the fingerprint plot feature, reveals that their crystal structures are stabilized by 23.1% and 32.6% of reciprocal O•••H interactions, respectively. The contribution of other principal interactions (reciprocal C•••H/H•••C and H•••H) is presented in **Figure 2.3c** and **2.3d**. As mentioned above, the crystal structure of unionized CIP that was used for Hirshfeld analysis was likely not completely accurate in terms of the position of the H3 atom. Therefore, the extremely short H...H contact calculated for the unionized form is unrealistic and likely incorrect. The greater contribution of the O•••H interactions in zwitterionic CIP confers enhanced stability to the crystal lattice of this form of the drug in comparison to that of unionized CIP.[159] These combined O•••H and H•••O interactions are visible as "wings" in the fingerprint plot in **Figure 2.3d**. The UNI force-field calculations showed that the total packing energy of the crystal structures of unionized and zwitterionic CIP was -129.8 and -169.4 kJ/mol, respectively (**Appendix 1)**. Therefore, it can be concluded that the zwitterionic form of CIP is more stable. This explains the higher theoretical density of 1.50 g/cm^3 for the zwitterion, compared to 1.45 g/cm^3 for unionized CIP, as calculated using PLATON software.

2.3.2 Production of Amorphous Ciprofloxacin

The production of pure amorphous CIP has not been described in the literature to date. This is most likely due to the fact that it is not suitable for processing by the most common methods of amorphous solid generation. For example, CIP has been reported to decompose

after melting,[125] which would rule out the use of melting techniques. In addition, due to its very low solubility in common solvents, solvent evaporation, spray drying and freeze drying are also quite unattractive options. Nevertheless, a number of processing techniques were evaluated in terms of their suitability to amorphize CIP.

2.3.2.1 Ball Milling at Room Temperature

While milling is often used to micronize drugs, high energy milling can be used to bring about changes in the solid state of a drug, such as conversion from the crystalline to the amorphous form.[54] As can be seen from **Figure 2.4**, ball milling at RT for 4 hours did not produce the fully amorphous form of CIP; however, it did reduce the intensity of the peaks seen in PXRD over time. Like the starting material, the peaks of ball milled CIP match those of the anhydrous zwitterion. Increasing the duration of milling to 6 hours did not decrease the intensity of the peaks further (data not shown). Upon milling, the color of CIP also changed from off-white to pale yellow, which can be considered as mechanochromism.[160]

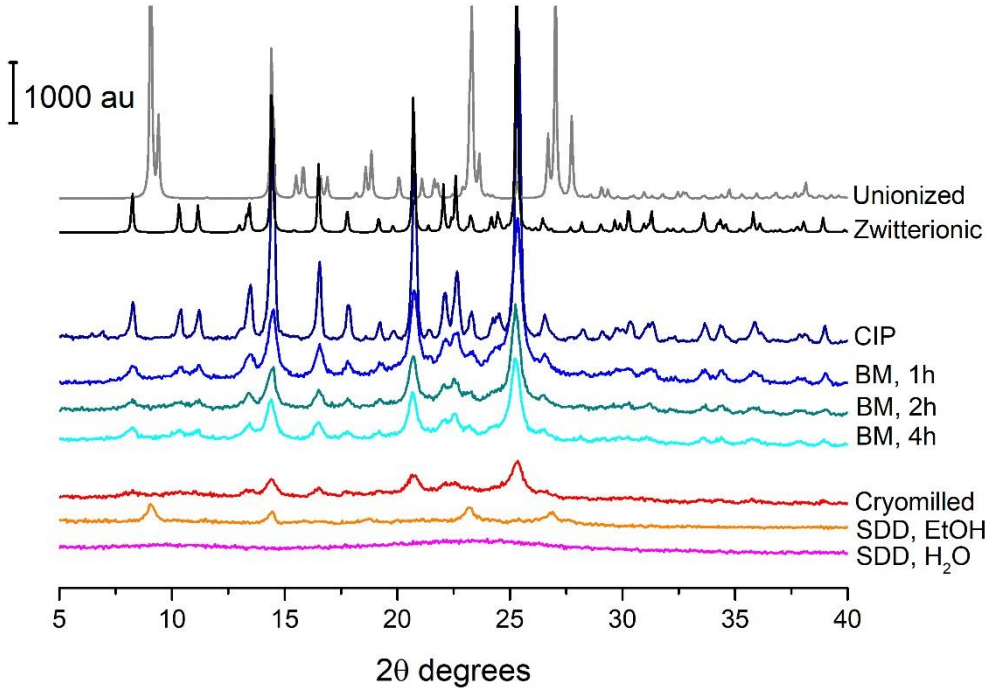

Figure 2.4. PXRD analysis of (from top to bottom) Unionized: powder pattern of unionized CIP calculated from CCDC number 757817; Zwitterionic: powder pattern of zwitterionic CIP calculated from CCDC number 714344; CIP: CIP powder starting material; BM,1h, 2h

and 4h: CIP powder starting material ball milled for 1, 2 and 4 hours; Cryomilled: CIP powder starting material cryomilled; SDD, EtOH: CIP spray dried from water/ethanol mixture; and SDD, H_2O: CIP spray dried from an aqueous solution.

The most intense peak in the PXRD pattern of CIP is located at 25.3 2θ degrees. This peak corresponds to the (1 2 -1) crystal face, and appears in the diffractogram of all of the samples that were produced by milling. The peaks at 14.4 (1 0 -1), 20.7 (1 0 -2) and 16.5 (1 1 1) 2θ degrees are the next most intense peaks, and also appear in the PXRD patterns of the milled drug. During mechanical stress, such as milling, crystals will fracture along specific crystallographic slip planes. This occurs in two possible manners, depending on the shape of the crystal. It will either break along its shortest dimension or along a cleavage plane with a low attachment energy.[161,162] Thus, the fracture of a crystal will occur where the interactions between adjacent planes are weakest. Slip planes are also likely to correspond to rigid crystallographic planes with a high molecular density and large d-spacing (distance between adjacent planes).[163] (1 2 -1) seems to be the most likely cleavage plane of the zwitterion, and therefore it appears as the most intense peak in the X-ray diffractogram of milled CIP. This plane is illustrated in **Figure 2.5**.

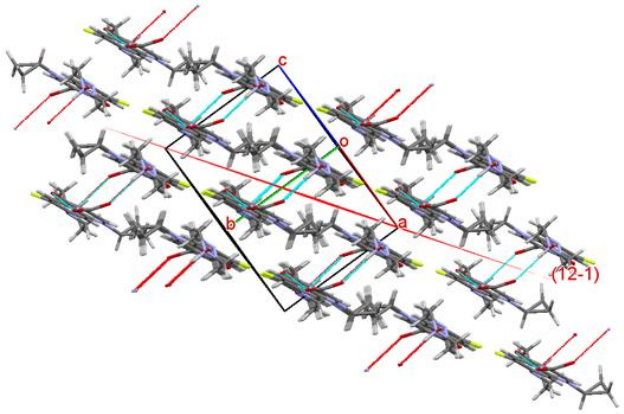

Figure 2.5. Cleavage plane (1 2 -1) of zwitterionic CIP.

2.3.2.2 Cryomilling

The inability to generate amorphous CIP by ball milling at RT may be due to the relatively high temperature at which the process was carried out. The lower the temperature used for milling, the easier it is to amorphize a drug.[97] It is also well known that in order to obtain an

amorphous product, milling should be performed below the T_g of the drug.[98] Therefore, cryomilling should be a more efficient method of producing amorphous CIP than milling at RT. Cryomilling holds the sample at a temperature below 0 ^oC, which helps to prevent its crystallization during milling.[99] However, as shown in **Figure 2.4**, following cryomilling CIP still had some residual crystallinity. The four most prominent peaks of the zwitterion are still present in the diffractogram of the cryomilled sample; however, they are less intense than those obtained with the drug milled at RT.

2.3.2.3 Spray Drying

Spray drying was the final technique attempted in order to produce amorphous CIP. Although CIP is described as practically insoluble in water and very slightly soluble in ethanol by the British Pharmacopoeia,[143] theoretically CIP can be spray dried in these solvents. However, a very large volume of dilute solution will be required. The sample of pure CIP produced by spray drying in ethanol/water 9:1 (v/v) possessed a small degree of residual crystallinity (**Figure 2.4**). However, in contrast to the partially amorphous CIP obtained with the other methods, this form of CIP displayed different PXRD peaks. These correspond to the simulated single crystal diffraction pattern of unionized CIP reported by Mahapatra et al.[138] Since the starting material was zwitterionic, it was the non-aqueous nature of the solvent used for spray drying that dictated the CIP form that crystallized from, presumably, a fully amorphous intermediate. The most prominent peaks in the PXRD pattern of unionized CIP are located at 9 (0 0 1), 14.4 (0 1 1), 23.3 (2 -1 0) and 27 (0 1 -3) 2θ degrees. These four peaks also appear in the diffractogram of CIP spray dried in ethanol/water, at a low intensity.

Spray drying in pure water on the other hand successfully yielded CIP that was fully X-ray amorphous (**Figure 2.4**). An earlier attempt to spray dry CIP in water resulted in a partially amorphous form of the drug. As with the milled products, the PXRD peaks of this sample corresponded to those of zwitterionic CIP (data not shown). Although this method was successful at producing fully amorphous CIP, a significant disadvantage of this spray drying procedure is that 1 L of solution is required in order to produce just a few milligrams of sample. This is therefore a very inefficient method of generating amorphous CIP.

2.3.3 Quench Cooling - Thermal Degradation Studies

It was noted that CIP changes color upon heating. DSC experiments showed that at the onset of melting (~ 265 ^{o}C) it is pale yellow/beige in color, whereas at the endset (~ 276 ^{o}C) it is dark brown. The proportion of drug that degraded in each sample under certain heating conditions is listed in **Table 2.1**. The content of CIP in the sample heated to ~265 ^{o}C (prior to melting) decreased slightly by 5.7 ± 2.5%, however a one-sample *t* test showed that this is not statistically significantly different from the starting material ($p = 0.19$). In contrast, for the CIP sample heated to ~276 ^{o}C (up to the endset of melting) it was found that 26.8 ± 8.1% of the drug had degraded. This confirms that quench cooling is not a suitable method for the production of amorphous CIP, as melting induces an unacceptable level of chemical degradation.

The use of higher heating rates should reduce degradation, as the sample will have less time to undergo structural changes.[164] Indeed, when a heating rate of 500 ^{o}C/min was used, a lower degree of degradation of 19.4% occurred. However, this was not statistically significantly different from the sample heated at 10 ^{o}C/min, according to a two-sample *t* test ($p = 0.29$). A lower proportion of degradation, of 12.7 ± 6.3%, was obtained with cryomilled CIP, as this sample was only heated to the endset of the first melting peak (~273 ^{o}C), prior to full degradation. ANOVA with Tukey's multiple comparison test showed that the level of thermal decomposition in this sample was statistically significantly different from that of crystalline CIP heated to ~276 ^{o}C (post-melt) at 10 ^{o}C/min ($p = 0.04$).

Table 2.1. Proportion of CIP that Degraded on Thermal Treatment

Sample	% Degraded
Crystalline CIP (heated up to ~265 ^{o}C at 10 ^{o}C/min)	5.7 ± 2.5
Crystalline CIP (heated up to ~276 ^{o}C at 10 ^{o}C/min)	26.8 ± 8.1
Cryomilled CIP (heated up to ~273 ^{o}C at 10 ^{o}C/min)	12.7 ± 6.3
Crystalline CIP Post HSDSC (heated up to ~276 ^{o}C at 500 ^{o}C/min)	19.4 ± 4.4

The TGA plots of crystalline and cryomilled CIP are shown in **Figure 2.6**. The mass of crystalline CIP decreased gradually up to a temperature of approximately 250 ^{o}C. Above this temperature a steep loss in mass occurred due to thermal degradation, resulting in a total mass loss of 12.8%. With the cryomilled sample on the other hand, an initial mass loss of 6.4% occurred between 25 and 65 ^{o}C due to water loss. The mass of this sample also decreased steeply above 250 ^{o}C due to degradation, leading to a total loss in mass of 17.3%.

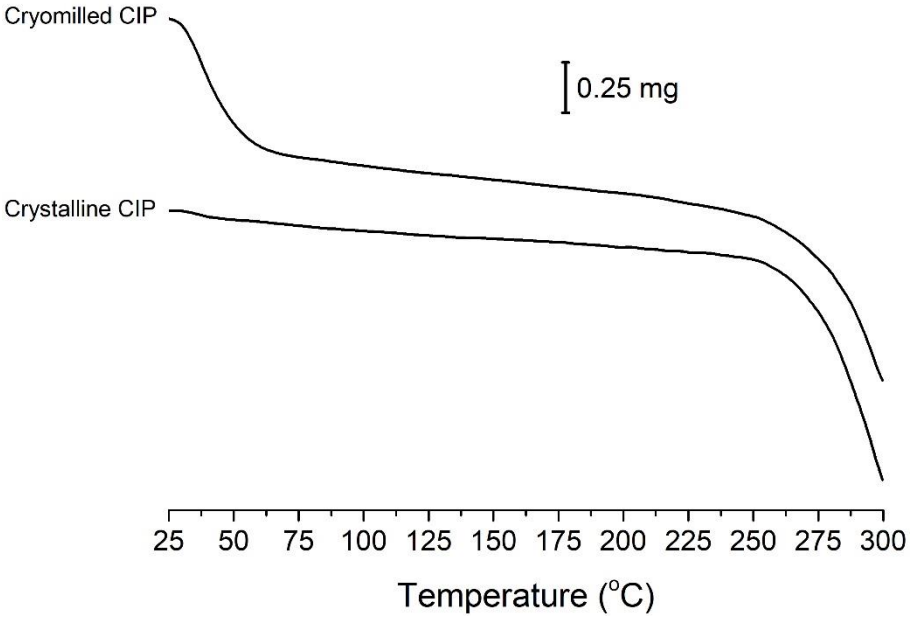

Figure 2.6. TGA analysis of crystalline and cryomilled CIP.

2.3.4 Solid-State Fourier Transform Infrared Spectroscopy

The FTIR spectra of the CIP starting material, amorphous and partially amorphous CIP samples are shown in **Figure 2.7a**. The spectrum of raw CIP contains a peak at 1590 and 1375 cm^{-1}, corresponding to the asymmetric and symmetric vibrations, respectively, of the carboxylate ion.[165] The spectrum of CIP that was spray dried in ethanol/water, on the other hand, has a clear peak at 1722 cm^{-1}, due to the presence of the COOH group. There may be some residual zwitterionic CIP present in this sample however, as small peaks matching those of the carboxylate ion of CIP may also be seen at 1590 and 1375 cm^{-1}. The spectra of the rest of the amorphous and partially amorphous CIP samples are missing a strong peak

above 1700 cm^{-1}, due to deprotonation of the carboxylic acid.[166] The asymmetric and symmetric vibrations of the COO^- group are far weaker than in the crystalline drug; however, amorphous solids are known to exhibit broader bands of lower intensity than their crystalline counterparts.[167] These samples also contain a minor amount of unionized CIP, as a small peak can be seen in their spectra at around 1720 cm^{-1}. The peak at approximately 1618 cm^{-1} in the spectrum of CIP can be assigned to the C=O stretch of the ketone carbonyl,[165] and this peak appears in the spectra of all of the partially amorphous samples.

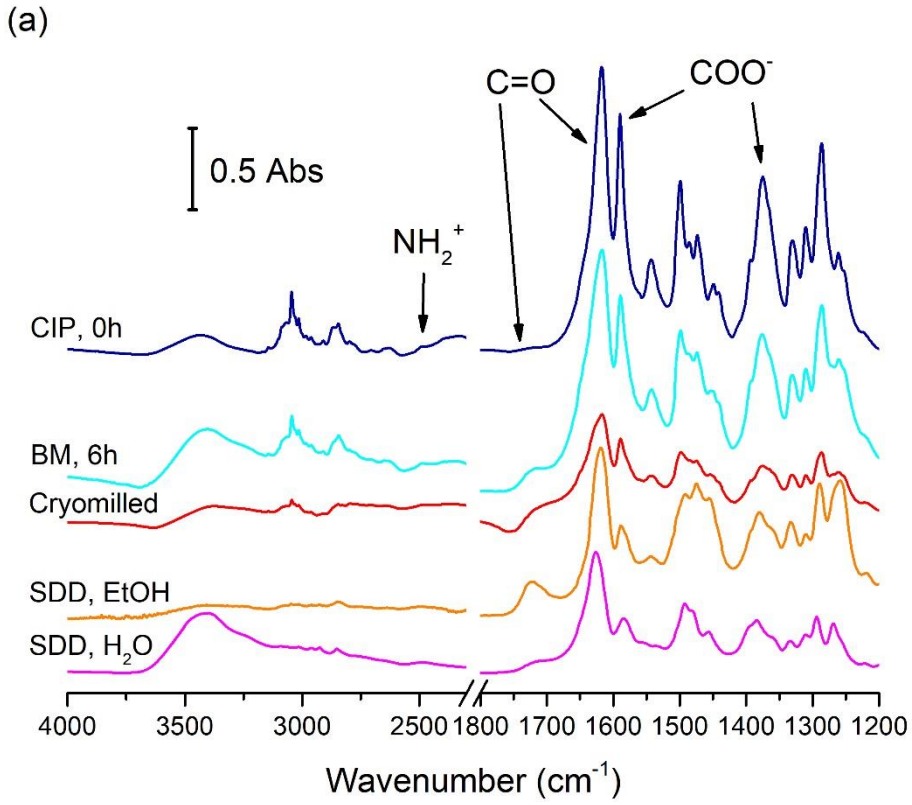

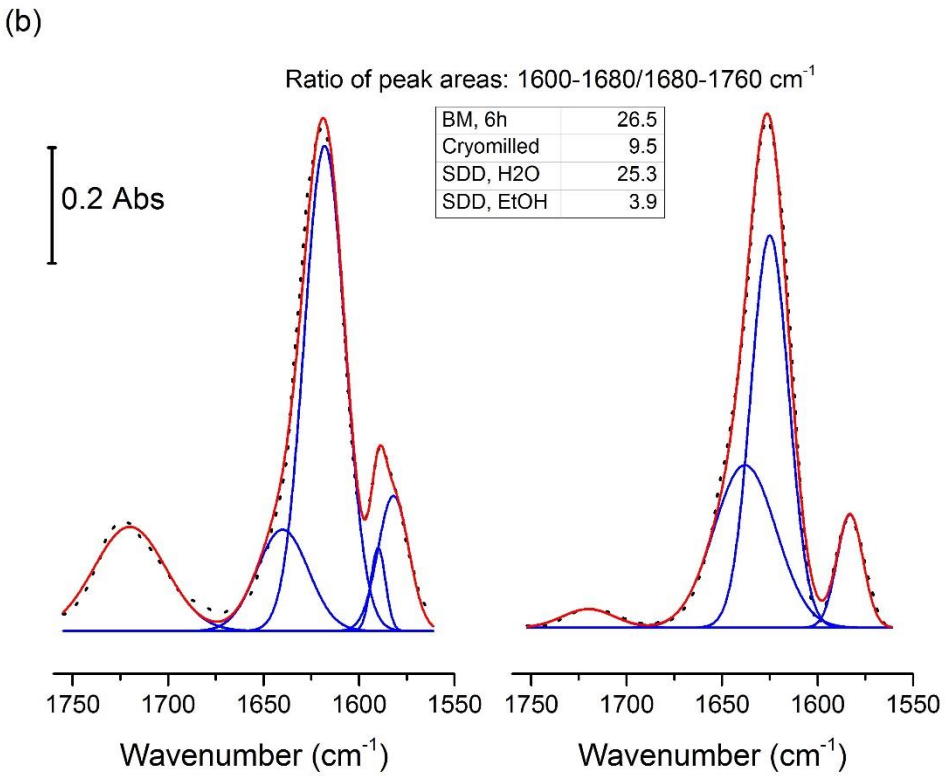

Figure 2.7. (a) FTIR spectra of (from top to bottom) unmilled CIP, CIP ball milled for 6 hours, cryomilled CIP, CIP spray dried from water/ethanol mixture and CIP spray dried from water. (b) Examples of peak deconvolution. CIP spray dried from ethanol/water mixture (left) and CIP spray dried from water (right). Dotted black line: recorded spectrum; solid blue lines: deconvoluted individual Gauss peaks; and solid red line: sum of the component peaks.

The peaks in the carbonyl region of the spectra, from 1770–1550 cm^{-1}, are quite broad, leading to overlap. In order to enhance their resolution, the spectra were deconvoluted, with Gaussian peak fitting. An example of the deconvoluted FTIR spectra obtained with spray dried CIP is shown in **Figure 2.7b**. In each case 4–5 peaks were found in the region examined, due to different vibrations of the carbonyl groups. For all four of the disordered samples, a peak of low area is present between 1680 and 1760 cm^{-1}, which corresponds to the unionized COOH group. This confirms the presence of a small amount of unionized CIP in all of these samples. The ratio of the area of the peak appearing at 1600–1680 cm^{-1} to that featuring between 1680 and 1760 cm^{-1} can be used to compare the proportion of unionized

carboxylic acid present in the four samples. As suggested by the FTIR spectra shown above, the lowest ratio was obtained with CIP that was spray dried in ethanol/water, which was equal to 3.9. This was followed by cryomilled CIP, at 9.5. A much lower proportion of unionized CIP was present in the samples prepared by ball milling at RT and spray drying in pure water, which had a ratio of 26.5 and 25.3, respectively. As previously mentioned, the peak at approximately 1590 cm^{-1} corresponds to the asymmetric vibration of the carboxylate ion.[165] This peak is present at 1583–1590 cm^{-1} in all of the spectra, confirming the presence of the zwitterion. Two peaks were found in this area for CIP that was ball milled at RT and that which was spray dried in ethanol/water. This may be due to the participation of this group in hydrogen bonding.

NH_2^+ stretching vibrations are present as weak bands at 2400–2600 cm^{-1} in the spectra shown in **Figure 2.7a**. Similar bands can be found in the FTIR spectra of CIP salts, in which the piperazine secondary amine is also ionized.[125,168] This peak appears to be absent from the sample spray dried in ethanol/water. These spectra therefore confirm the results of the PXRD analysis above, that is, that the CIP raw material, as well as the samples obtained by ball milling, cryomilling and spray drying in pure water, are zwitterionic. The CIP which was spray dried in ethanol/water, on the other hand, is largely unionized.

2.3.5 Conventional Thermal Analysis

DSC thermograms (using a heating rate of 10 ^oC/min) of amorphous and partially amorphous CIP, produced by the different methods described above, are shown in **Figure 2.8**. The CIP starting material displayed a sharp melting endotherm at 271.9 ^oC. In contrast, the drug that was ball milled at RT had a broad melting peak, at a lower temperature of 263.4 ^oC, as it is more disordered than the fully crystalline starting material. There appears to be a slight exothermic event in the thermogram of this sample at about 104 ^oC, due to crystallization of the amorphous material present.

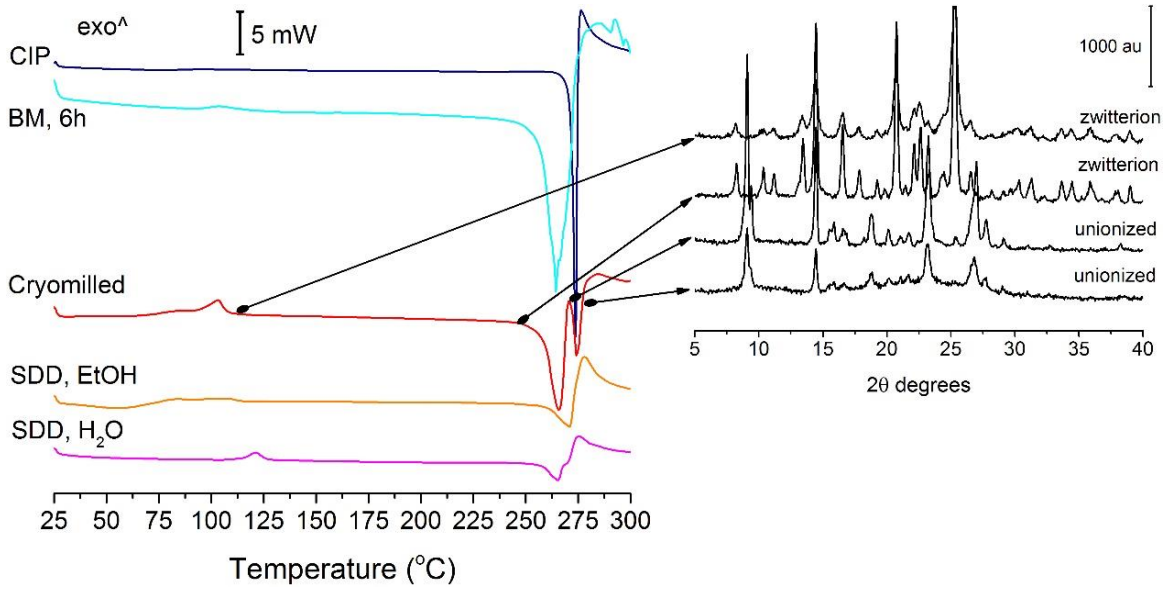

Figure 2.8. Conventional DSC thermograms of (from top) unmilled CIP, CIP ball milled for 6 hours, cryomilled CIP, CIP spray dried from water/ethanol mixture and CIP spray dried from water (left). The panel on the right shows the PXRD diffractograms of cryomilled CIP heated to various temperatures.

The DSC thermogram of cryomilled CIP shows a larger crystallization peak, at 103 °C. Interestingly, two endothermic peaks, at 266 °C and 278 °C, are also present. This sample was further investigated by heating it to various temperatures in the DSC instrument, and then immediately analyzing the sample by PXRD (**Figure 2.8**). As described above, the PXRD diffractogram of cryomilled CIP displayed small peaks corresponding to the zwitterion. At the endset of crystallization (110 °C) and prior to the onset of the first melting peak (251 °C), the drug was found to be in the same ionized state, with an increase in crystallinity occurring as the temperature increased. However, following both the first (270 °C) and second (276 °C) endothermic peaks, the drug was in the unionized state. FTIR analysis (data not shown) confirmed the ionization state of CIP, with the unionized carboxylic acid group producing a peak at 1726 cm^{-1}. Therefore, heating this form of CIP to a temperature near its melting point enables intramolecular proton transfer from the protonated piperazine amino group to the carboxylate anion.

These results are similar to those obtained by others with the crystalline zwitterionic form of CIP. Turel et al found that, when heated to 270 °C (before the drug melts or begins to

decompose), the carboxylate absorbance bands in the FTIR spectrum of the drug disappear and are replaced by the characteristic peak of a carboxylic acid carbonyl.[169] This is due to the conversion of the zwitterion to the unionized form, although this was not explicitly stated by the authors. This transformation was also found to occur with CIP hexahydrate upon heating to 280 ^{o}C.[166] Similarly, Mahapatra et al claimed that heating CIP to 250 ^{o}C resulted in the reversible formation of unionized CIP, as shown by PXRD.[138] However, in this case the changes in the PXRD pattern were incorrectly attributed to dehydration and hydration of the drug, rather than intramolecular proton transfer. In order to replicate Mahapatra et al's results, CIP was heated to 250, 260, 265 and 270 ^{o}C by DSC, then immediately analyzed by PXRD. However, at each stage the drug was found to still be in the ionized state. In contrast, when CIP was heated to the endset of melting (approximately 285 ^{o}C) and allowed to cool it was found to be X-ray amorphous (**Figure 2.9a**). When this sample was analyzed by DSC a T_g could be seen at 94.5 ^{o}C (**Figure 2.9b**). Its FTIR spectra also contained a peak at 1724 cm^{-1}, which corresponds to the unionized COOH group of CIP (**Figure 2.9c**). This confirms that CIP converted to the unionized form.

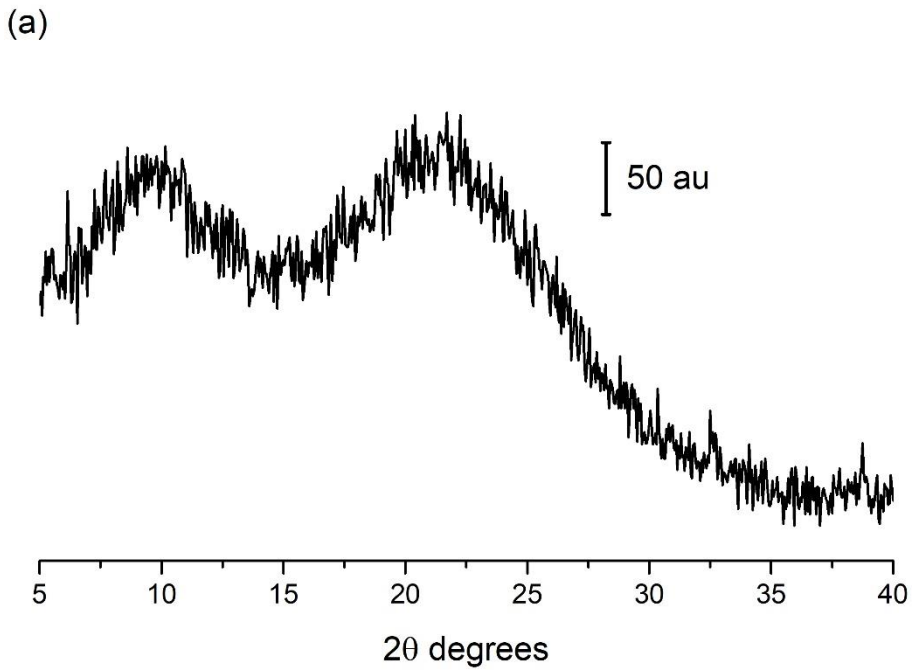

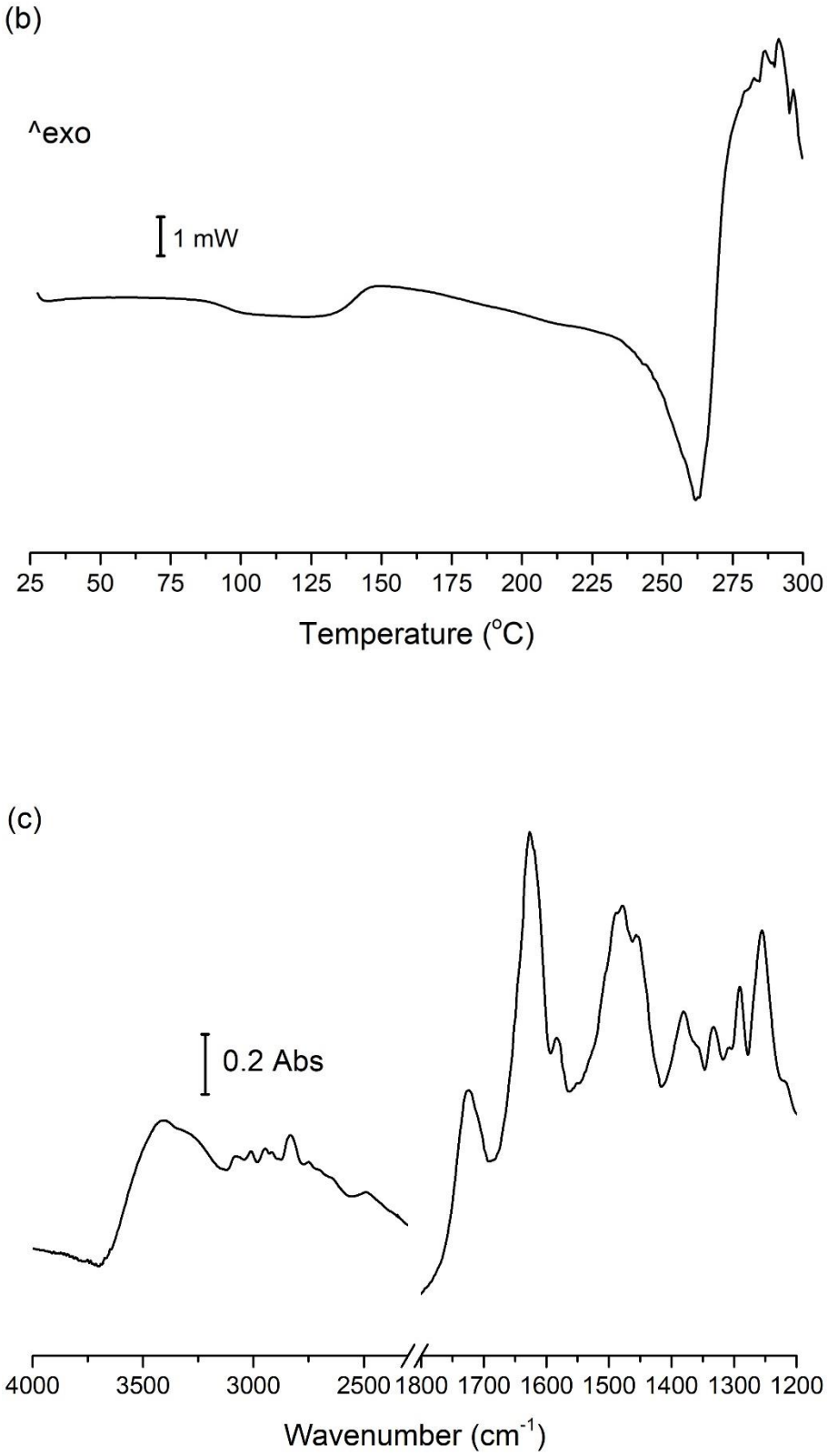

Figure 2.9. (a) PXRD (b) DSC and (c) FTIR analysis of quench cooled CIP.

The samples of CIP that were spray dried in ethanol/water and pure water also had broader and lower melting peaks than the crystalline drug, at 270.6 and 266.2 °C, respectively (**Figure 2.8**). Although the T_g's of these samples are difficult to distinguish, they appear to be located between 80 and 100 °C. Crystallization occurs soon after the glass transition, suggesting that the samples are thermally unstable. Temperature-modulated DSC (StepScan) was used to find the T_g of the fully amorphous CIP that was spray dried in pure water. This technique is more sensitive to changes in specific heat capacity, such as glass transition events, than standard DSC. It can therefore be used to accurately detect weak, broad or irregularly shaped glass transitions.[170] This allowed the detection of the T_g of CIP at 86.7 °C.

2.3.6 Investigation of Proton Transfer in CIP

HSDSC was used to analyze the partially amorphous cryomilled CIP. The use of a higher heating rate increases the sensitivity of the instrument, and produces a larger step change in the thermogram during the glass transition. Despite this, the T_g could not be seen clearly with a heating rate of 50–200 °C/min. However, when this was increased to 300 °C/min a glass transition was visible at 88.0 °C (**Figure 2.10a**). This was soon followed by crystallization, which shows that the sample has poor thermal stability. Increasing the heating rate did not have a significant effect on the crystallization temperature of the sample, with the onset remaining between 97.5 and 99.7 °C for all runs. This is unusual, as crystallization is generally a function of temperature and time. Therefore, the peak observed in the thermogram would be expected to shift to higher temperatures if the heating rate is increased.[171] The crystallization temperature may have remained constant due to the sample having a low energy barrier for crystallization. Regardless of the heating rate used, cryomilled CIP also displayed two endothermal peaks.

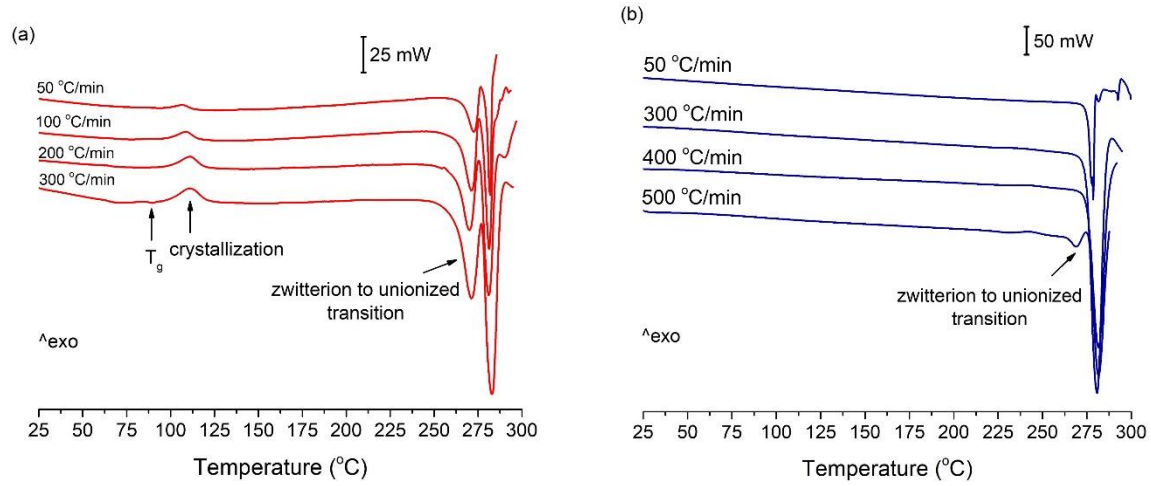

Figure 2.10. HSDSC of (a) cryomilled CIP and (b) crystalline CIP (as received).

Crystalline CIP was then analyzed by HSDSC, with heating rates of 50–500 °C/min. In DSC the change in heat flow signal seen during a transition is proportional to the heating rate. Therefore, high heating rates can be used to detect low energy transitions. At heating rates of up to 400 °C/min, a single melting peak was obtained (**Figure 2.10b**). However, heating at 500 °C/min enabled the elucidation of two endothermic peaks, with onsets at 269.3 and 275.6 °C. These can be attributed to the transition of the zwitterion to the unionized form, followed by its melting. A similar endothermic peak was seen in the DSC thermogram of crystalline norfloxacin immediately prior to melting, due to a solid-solid phase transition.[146] In contrast to conventional DSC, following HSDSC at 500 °C/min, CIP was still crystalline; however, its PXRD pattern matched that of unionized CIP.

The conversion of zwitterionic CIP to the unionized form is clearly a function of physical disorder in the sample. While both samples showed this transition, a much higher heating rate was required to visualize this event with crystalline CIP. Computational analysis was therefore performed to investigate the relative chemical stability of unionized and zwitterionic CIP. HOMO and LUMO are key parameters related to the reactivity and chemical stability of molecules. The energy gap between HOMO and LUMO helps to describe the chemical behavior and electrical properties of molecules, with lower energies indicating higher reactivity and lower stability.[156] Electron density on the HOMO/LUMO frontier orbitals of unionized CIP is distributed through various parts of the molecule. The

HOMO resides on the piperazine residue and in part on the quinoline ring, while the LUMO sits mainly on the quinoline system, stretching as far as the carboxylic acid group (**Figure 2.11**). In zwitterionic CIP on the other hand, the HOMO/LUMO are arranged only around the quinoline ring (**Figure 2.11**). The HOMO/LUMO energy gap for unionized and zwitterionic CIP, based on the computed structures, is 2.939 and 3.020 eV, respectively (**Table 2.2**). The zwitterion is therefore slightly more stable, although the difference in reactivity between the two forms of the drug is small. The greater stability of zwitterionic CIP is also reflected in the fact that its HOMO/LUMO is centered around the quinoline ring and not on the groups with the highest electron donor/acceptor capacity, in contrast to unionized CIP.

Global reactivity parameters, such as absolute electron negativity (χ), chemical potential (μ), absolute hardness (η), global softness (S) and electrophilicity index (ω), listed in **Table 2.2**, also indicate the greater stability of zwitterionic CIP. Hardness is a measure of resistance to change in the electron distribution in a molecule.[172] Therefore, higher values of hardness (and lower values of softness) suggest that a system is more stable. The chemical potential and electrophilicity index parameters provide an estimate of the propensity of an electrophile or nucleophile to give or accept an electron. Lower values of μ and ω are typical of a nucleophile (in this case zwitterionic CIP), while unionized CIP will exhibit electrophilic properties, confirming that proton transfer will occur from the (positively) charged piperazine nitrogen onto the carboxylate group. From the crystal lattice of zwitterionic CIP (**Figure 2.3**), it can be deduced that the intermolecular ionic interactions between the ionized molecules should facilitate such a transfer. As previously discussed, the crystal structures of unionized and zwitterionic CIP differ quite substantially. Unionized CIP consists of dimers connected by head-to-head N-H•••N hydrogen bonds, while the molecules in zwitterionic CIP form head-to-tail $N\text{-}H_2^+ \bullet\bullet\bullet {}^-OOC$ hydrogen bonds with both neighboring and adjacent molecules. Therefore, transformation between the two forms of the drug will involve reorientation of the molecules as well as proton transfer.

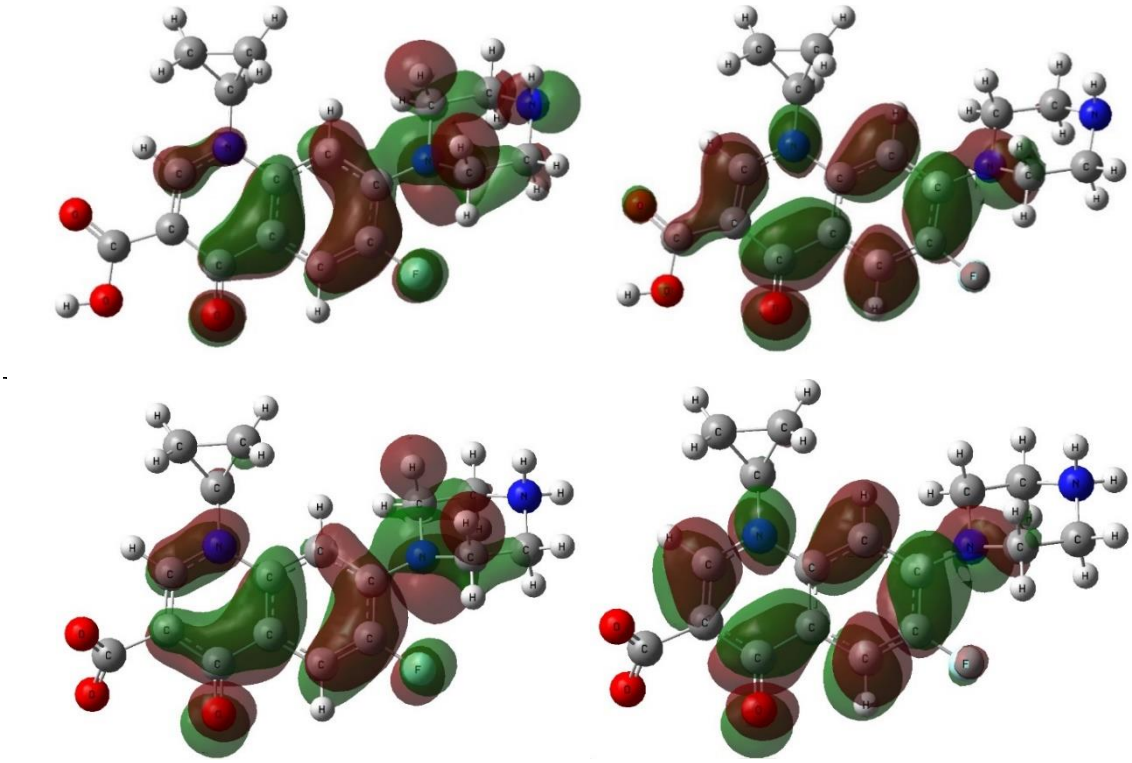

Figure 2.11. HOMO (left) AND LUMO (right) of unionized CIP (top) and zwitterionic CIP (bottom).

Table 2.2 Global Reactivity Parameters of Unionized and Zwitterionic CIP

	E_{HOMO} (eV)	E_{LUMO} (eV)	ΔE^a (eV)	χ^b	μ^c	η^d	S^e	ω^f
Unionized CIP	-8.762	-5.823	2.939	7.293	-7.293	1.469	0.340	18.097
Zwitterionic CIP	-8.871	-5.850	3.020	7.361	-7.361	1.510	0.331	17.938

[a]ΔE: energy band gap; [b]χ: absolute electron negativity; [c]μ: chemical potential; [d]η: absolute hardness; [e]S: global softness; and [f]ω: electrophilicity index of unionized and zwitterionic CIP.

Color change has been noted to occur when proton transfer is induced by external stimuli.[160] This may explain why CIP changes color upon milling and when heated close to its melting

point. Piroxicam is another zwitterionic drug that can undergo proton transfer upon processing. In contrast to CIP, crystalline piroxicam is unionized. It converts to the amorphous zwitterion upon cryomilling, leading to a significant change in the conformation of the piroxicam molecule.[160] The unionized form of piroxicam is colorless, while the zwitterion and melt are yellow.[173] The conversion of piroxicam between the unionized and zwitterionic form has been described as tautomeric polymorphism.[173] The zwitterionic and unionized form of CIP may therefore be considered as tautomers, which undergo thermal and mechanically induced tautomerism. The ΔE values for both forms of CIP are close to 3 eV (**Table 2.2**). This corresponds to the absorption of 410–430 nm light, rendering the substance yellow in color, consistent with our visual observations.

2.3.7 Physical Stability in Humid Conditions

The partially amorphous unionized CIP, produced by spray drying in ethanol/water, was analyzed by dynamic vapor sorption (DVS) in order to investigate the effect of water absorption on the crystal structure of the drug. As can be seen from the sorption-desorption isotherm (**Figure 2.12**), partially amorphous CIP was very hygroscopic, absorbing almost 16% of its mass in water at 90% RH.

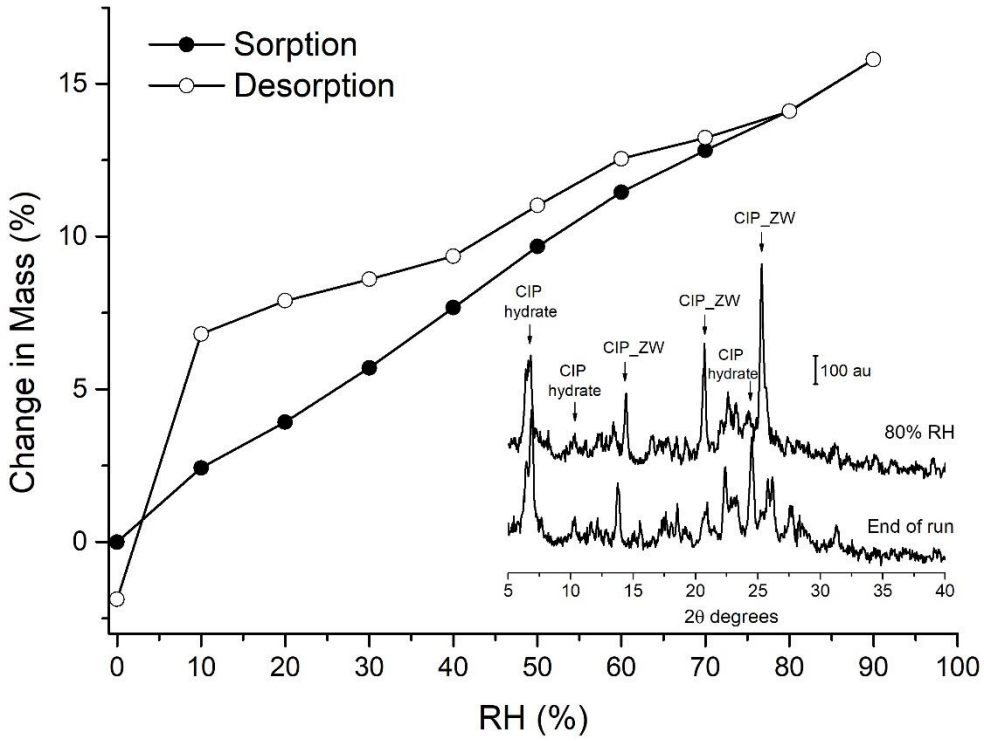

Figure 2.12. DVS analysis of partially amorphous CIP spray dried in ethanol/water 9:1. Inset: PXRD of the sample following DVS analysis, at 80% RH (on sorption, red line) and following the full sorption/desorption cycle (at 0% RH, black line). CIP_ZW: peaks corresponding to zwitterionic CIP.

The drug partially crystallized during the DVS study. This was confirmed by PXRD, which was carried out at 80% RH and at the end of the run (**Figure 2.12**, inset). At 80% RH, the diffractogram has four main peaks. The peak at 6–7 2θ degrees corresponds to that of the CIP hydrate which contains 3.7 water molecules for every molecule of CIP.[158] The peaks at 14.4, 20.7 and 25.3 2θ degrees on the other hand match the most prominent peaks of zwitterionic CIP. At the end of the analysis, at 0% RH, the PXRD pattern of the drug also contained the pronounced peak of the 3.7 hydrate at 6–7 2θ degrees. Peaks at 13.8 and 24.5 2θ degrees also belong to the hydrate, and those at 20.8 and 22.4 2θ to the zwitterion. Hydrates often crystallize more readily than the anhydrous form of a drug, as the molecules can pack together more easily. This may be due to their symmetry, changes in conformation, and the formation of hydrogen bonds between the drug and water molecules.[174] When hydrated, CIP also exists in the zwitterionic form.[166] Therefore, while anhydrous CIP can

exist in the unionized form, when exposed to water it reverts to the zwitterion. Similar results were obtained with norfloxacin, with the unionized drug converting to the zwitterion when exposed to high humidity.[175] Incorporation of water molecules has been found to lower the energy barrier for proton transfer, which enables this conversion to occur upon hydration.[176]

2.4 Conclusions

The production of pure amorphous CIP is very challenging due to its poor solubility, strong crystal lattice and thermal degradation. Despite these barriers, amorphous CIP was successfully prepared for the first time by spray drying in water, while partially amorphous products were obtained by ball milling, cryomilling and spray drying in an ethanol/water mixture. The unionized form of the drug was obtained using the latter method, whereas all others resulted in the zwitterion. Proton transfer, resulting in transformation to the unionized drug, was visualized using HSDSC. This was shown to occur upon heating the zwitterion to its melting point, and took place more readily in disordered systems. The reverse transformation occurred when unionized CIP was exposed to high humidity. Although the calculated differences between unionized and zwitterionic CIP, such as molecular conformation, packing energy and the HOMO/LUMO energy gap, were found to be small, the higher degree of hydrogen bonding in the crystal lattice of the charged drug results in greater stability and lower reactivity. Thus the zwitterion is the preferred form of CIP in the crystalline state.

Chapter 3: Amorphous Polymeric Drug Salts as Ionic Solid Dispersion Forms of Ciprofloxacin

3.1 Introduction

As previously discussed, CIP is both poorly soluble and poorly permeable, making it a class 4 BCS drug.[112] Upon addition to water, the dissociation of CIP's crystal lattice is hindered by the strength of its intermolecular interactions. The solubility of the drug can therefore be improved by disrupting its crystal lattice via salt formation or amorphization.[23] Salt formation is the most frequently used process for improving the solubility of acidic and basic drugs, and is also claimed to be the most effective.[28] For this reason, it has been the main focus of research aimed at improving the solubility of CIP. The commercially available hydrochloride salt of CIP has been reported to have a solubility of approximately 42 mg/ml in water.[168] However, due to the common ion effect, the solubility of HCl salts is decreased in the stomach.[177] The lactate salt of CIP is available commercially as a solution for infusion, and has an aqueous solubility of just over 100 mg/ml.[178] As an alternative to small molecules, polymers may be used as counterions in pharmaceutical salts. Although no such studies have been carried out on CIP, Willis et al found that the extent and rate of methapyrilene release in simulated gastric and intestinal fluid was improved by the formation of drug-polymer salts, in which the amino group of the drug and carboxyl groups of the polymer interacted.[179]

Another method of improving the aqueous solubility of drugs with solid-state limited solubility is amorphization. However, as discussed in Chapter 1, a major disadvantage of amorphous formulations is that they are intrinsically unstable and prone to crystallization.[34] The most common approach taken to overcome the poor stability of amorphous drugs is to formulate them as amorphous solid dispersions (ASDs). ASDs consist of an amorphous molecular dispersion of a drug in a solid carrier, which may be a small molecule or polymer.[180] The carrier used to form an ASD must be chosen carefully in order to maximize the stability and solubility of the product. The physical stability of an ASD is improved if there are interactions between the components, e.g. hydrogen bonding and acid-base interactions. This reduces the molecular mobility of the drug and increases the energy required for crystallization.[55] ASDs also enable faster drug dissolution, often resulting in supersaturation. The polymers present in an ASD help to prevent crystallization and precipitation of the drug in solution, and thus prolong this supersaturated state.[76]

Despite the benefits of amorphous formulations in terms of solubility, there is very little information in the literature regarding the formation of CIP ASDs. This study therefore focuses on the preparation of a number of solid dispersions of CIP by ball milling. The solid state properties of the successful ASDs were first investigated, in particular the nature of their drug-polymer interactions and thermal stability. As previously mentioned, a major issue associated with amorphous formulations is their poor physical stability, however this can be counteracted to some degree by the use of polymers with high T_g's that interact specifically with the drug. The stability of the ASDs during dynamic vapor sorption (DVS) analysis and under accelerated conditions was therefore examined in order to determine their resistance to crystallization.

Another major goal of this study was to determine the effect of ASD formation on the biopharmaceutical properties of CIP, specifically its solubility, permeability and antimicrobial activity, and how these characteristics are connected. ASDs have been found to increase the solubility of drugs via supersaturation, while maintaining a constant permeability. In contrast, the solubility advantage obtained with formulations containing cyclodextrins, surfactants and cosolvents is negatively correlated with permeability.[32] The solubility of crystalline CIP and the ASDs was therefore investigated in water and biorelevant media, and their permeability was compared using parallel artificial membrane permeability assay (PAMPA), to discover whether a similar relationship exists between the solubility and permeability of these preparations. Finally, it was of interest to determine whether the formulation of CIP as an ASD affected its antimicrobial activity, which should also be related to permeability. Therefore, the minimum inhibitory concentration (MIC) and minimum bactericidal concentration (MBC) of CIP and the ASDs were measured in a number of bacterial species.

3.2 Experimental Section

3.2.1 Materials

Ciprofloxacin hydrochloride (CIP HCl) salt was kindly donated by Hemofarm, Serbia. The following polymers were used to form solid dispersions with CIP: Polyvinylpyrrolidone K17

(PVP, Plasdone C-15, ISP Technologies, New Jersey, USA); poly(vinyl alcohol) (PVA, 98% hydrolyzed, M_r 13000–23000, Sigma-Aldrich, St. Louis, Missouri); polyvinyl caprolactam-polyvinyl acetate-polyethylene glycol graft copolymer (Soluplus, BASF SE, Ludwigshafen, Germany); polyethylene glycol 4000 (PEG 4000, BDH Ltd, Poole, England); methacrylic acid methyl methacrylate copolymer (Eudragit L100, Evonik Röhm GmbH, Darmstadt, Germany); methacrylic acid ethyl acrylate copolymer (Eudragit L100-55, Evonik Röhm GmbH, Darmstadt, Germany); poly(acrylic acid) (Carbopol 981, BF Goodrich, Ohio, USA); and hydroxypropyl methylcellulose acetate succinate grades LG and MG (HPMCAS-LG and HPMCAS-MG, Shin-Etsu Chemical Co., Ltd, Tokyo, Japan). The chemical structures of the latter five polymers are shown in **Figure 3.1**.

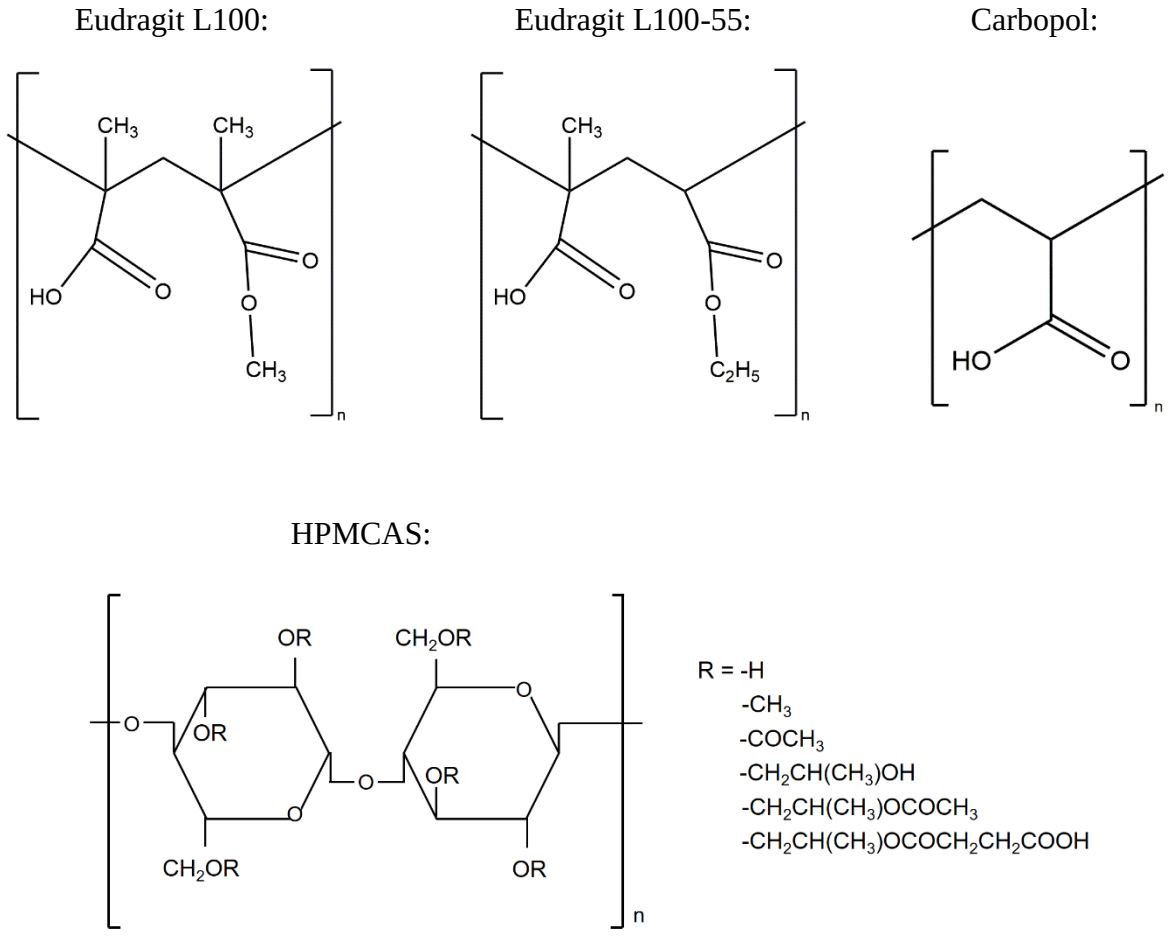

Figure 3.1. Chemical structures of polymers used in this study. The different grades of HPMCAS differ in their substituent content.

Fasted state simulated gastric fluid (FaSSGF) was produced by adding 60 mg SIF® Powder Original (biorelevant.com, Surrey, UK) to one liter of FaSSGF HCl solution, consisting of 34 mM NaCl adjusted to pH 1.6 with HCl. Fasted state simulated intestinal fluid (FaSSIF) was produced by adding 2.24 g SIF® Powder Original to one liter of FaSSIF phosphate buffer, consisting of 19.5 mM NaOH, 25 mM $NaH_2PO_4 \cdot H_2O$ and 106 mM NaCl, adjusted to pH 6.5 with NaOH. NaOH pellets were obtained from Riedel-de Haën, Seelze, Germany, $NaH_2PO_4 \cdot H_2O$ from Merck, Darmstadt, Germany and NaCl from Sigma-Aldrich Ireland Ltd., Arklow, Ireland. Dodecane, triethylamine, lecithin (L-α-phosphatidylcholine, Type XVI-E) and phosphate buffered saline (PBS) tablets were obtained from Sigma-Aldrich Ireland Ltd., Arklow, Ireland. Brain-heart infusion (BHI) broth was purchased from bioMérieux (Marcy l'Étoile, France). Plates with Columbia agar supplemented with sheep blood were obtained from Oxoïd (Dardilly, France). All other chemicals and solvents were of analytical grade.

3.2.2 Methods

3.2.2.1 Ball Milling

CIP was first milled with PVP at a concentration of 10–95% (w/w). Solid dispersions of CIP with Eudragit L100, Eudragit L100-55, Carbopol 981, HPMCAS-LG, HPMCAS-MG, PVA, Soluplus and PEG 4000 were also formed using 20–60% (w/w) polymer. Milling was conducted using the same apparatus and procedure described in Chapter 2. For each sample, milling was performed at RT, except for CIP/HPMCAS-LG and CIP/HPMCAS-MG ASDs, which were also milled at 2–5 ºC. The powder mixtures were each milled for 4–6 hours in total.

3.2.2.2 Solid-State Characterization

3.2.2.2.1 Powder X-ray Diffraction

PXRD was performed as described in Chapter 2.

3.2.2.2.2 Solid-State Fourier Transform Infrared Spectroscopy

FTIR was performed as described in Chapter 2. Physical mixtures (PMs) were also analyzed for comparison. These were prepared by blending together the drug and polymer starting materials in the same ratio as in the ASDs with a mortar and pestle.

3.2.2.2.3 Differential Scanning Calorimetry

DSC was carried out using the same apparatus described in Chapter 2. The ASDs were first heated from 25 to 70–100 ºC to remove any water present in the powder. When cool, the samples were reheated from 25 to 300 ºC at a rate of 10 ºC/min.

3.2.2.2.4 Temperature-Modulated Differential Scanning Calorimetry (StepScan)

StepScan DSC was performed by Dr. Lidia Tajber in TCD as described in Chapter 2.

3.2.2.2.5 Calculation of Theoretical Glass Transition Values with Gordon-Taylor Equation

The theoretical T_g's of the ASDs were calculated using the Gordon-Taylor equation:[59,64]

$$T_g = \frac{w_1 T_{g1} + K w_2 T_{g2}}{w_1 + K w_2} \quad (3.1)$$

where K is approximately equal to

$$K \approx \frac{T_{g1}\rho_1}{T_{g2}\rho_2} \quad (3.2)$$

w_1 and w_2 are the weight fractions, T_{g1} and T_{g2} are the glass transition temperatures, and ρ_1 and ρ_2 are the densities of the two components. As described in Chapter 2, the T_g of pure amorphous CIP has been determined as 86.7 ºC, while its density is 1.5 g/cm^3. The T_g's of the polymers were obtained from literature: Eudragit L100, 130 ºC;[181] Eudragit L100-55, 96 ºC;[182] HPMCAS-LG, 119 ºC;[183] and HPMCAS-MG, 120 ºC.[183] The average density values for the various components were also obtained from literature: Eudragit L100, 0.84 g/cm^3;[184] Eudragit L100-55, 0.83 g/cm^3;[185] and HPMCAS-LG and HPMCAS-MG, 1.29 g/cm^3.[186] The T_g's predicted by the Gordon-Taylor equation were then compared to the experimental values measured by DSC.

3.2.2.2.6 Thermogravimetric Analysis

TGA was performed as described in Chapter 2.

3.2.2.3 Dynamic Vapor Sorption

DVS studies were carried out by Dr. Krzysztof Paluch in Bradford University using the same apparatus and procedure described in Chapter 2. Following DVS analysis the samples were analyzed by PXRD in order to detect any crystallization.

3.2.2.4 Accelerated Stability Study

A stability study of the ASDs was conducted under accelerated storage conditions of 40 ^{o}C and 75% RH. Samples of each powder were taken every 2–3 days for a period of 2 weeks. PXRD was used to determine whether crystallization had occurred in any of the samples.

3.2.2.5 Dynamic Solubility Studies

10–20 ml of water, FaSSIF or FaSSGF was added to 40 ml glass vials. These were placed into jacketed beakers connected to a Lauda M12 water bath (Lauda-Königshofen, Germany) and allowed to equilibrate to 37 ^{o}C. A quantity of pure drug or ASD, in excess of the expected saturated solubility, was added to the stirred vials. Samples were drawn from the vials at specific time points over a 2 hour period. These aliquots were filtered with 0.45 μm PTFE membrane filters (VWR, USA). The filtered solutions were then diluted with a 2.45 g/L solution of phosphoric acid, previously adjusted to pH 3.0 with triethylamine. The concentration of CIP in each of the diluted samples was determined by UV spectrophotometry. The solubility studies were repeated at least in triplicate with each medium. The pH of the solutions was measured before the addition of the samples and at the end of the 2 hour study using a Thermo Orion 420A+ pH meter (Thermo Scientific, Hampshire, UK). The solid material left in the vials at the end of the studies was filtered and analyzed by PXRD.

3.2.2.6 Dissolution Study

Dissolution studies were carried out at 37 ^{o}C, using a paddle apparatus (Apparatus II) with a continuous rotation of 100 rpm. A quantity of sample corresponding to approximately 10%

of the final CIP concentration obtained in the solubility studies was added to 300 ml of FaSSIF. 1 ml aliquots were taken at specific time points over the 2 hour period of the study, and replaced with 1 ml of FaSSIF. Each sample was filtered with a 0.45 μm PTFE membrane filter and diluted with a 2.45 g/L solution of phosphoric acid, previously adjusted to pH 3.0 with triethylamine. The concentration of CIP in each of the diluted samples was then measured by UV spectrophotometry. The cumulative quantity of dissolved drug at each time point was calculated by taking account of the 1 ml aliquots taken for analysis. Each study was carried out at least in triplicate.

3.2.2.7 UV Spectrophotometry

UV analysis was carried out using a Shimadzu UV-1700 PharmaSpec UV-vis spectrophotometer (Shimadzu Corp., Kyoto, Japan). Quartz cells with a 1 cm optical path length were used for all measurements. UV absorbance was measured at 278 nm. The instrument was first blanked using a 2.45 g/L solution of phosphoric acid, previously adjusted to pH 3.0 with triethylamine. This buffer was also used to produce a range of concentrations of pure CIP, in order to construct a calibration curve.

3.2.2.8 Parallel Artificial Membrane Permeability Assay (PAMPA)

Permeability studies were carried out using the lipid-PAMPA method described by Merck Millipore.[187] A 96-well MultiScreen Filter Plate, with underdrain removed, and a 96-well MultiScreen Transport Receiver Plate (Millipore Corporation, Billerica, MA, USA) were used as the donor and acceptor plates, respectively. Solutions of CIP, CIP hydrochloride salt (CIP HCl), or ASD in PBS pH 7.4 and 6.4, at concentrations of 50–125 μg/ml, were prepared. 300 μl of PBS pH 7.4 was added to each well of the acceptor plate. 5 μl of a 1% (w/v) solution of lecithin in dodecane was added to the filter within each donor well to form an artificial membrane. 150 μl of the drug solutions were immediately added to each well of the donor plate in triplicate. The donor plate was then placed into the acceptor plate and incubated at RT for 16 hours. Following incubation, the contents of each well in the acceptor plate was diluted 1:4 with HPLC mobile phase and filtered with 0.45 μm PTFE membrane filters. The concentration of CIP in each sample was then measured using HPLC.

The effective permeability (P_e) of the samples was calculated using the following equation:[188]

$$P_e = -\ln(1 - r)\left(\frac{V_D V_A}{(V_D + V_A)At}\right) \quad (3.3)$$

where $r = \frac{[Drug]_{Acceptor}}{[Drug]_{Equilibrium}}$

V_D and V_A are the volumes of the donor and acceptor compartment, respectively, in cm^3, t is the incubation time in seconds, and A is the active surface area of the membrane (equal to the membrane area multiplied by the porosity ratio. For Millipore MultiScreen Permeability Filter Plate membranes this is equal to 0.24 cm^2 x 100%, or 0.24 cm^2).[187] $[Drug]_{Acceptor}$ is the concentration of the drug in the acceptor compartment at the end of the assay. $[Drug]_{Equilibrium}$ is determined by measuring the concentration of a reference solution, containing the drug at the equilibrium concentration (the overall concentration of the donor and acceptor solutions combined).[17] Given that the acceptor and donor compartments used in this study had a volume of 300 µl and 150 µl respectively, the equilibrium concentration of the drug should theoretically be one-third of that of the original solution added to the donor well.

3.2.2.9 High-Performance Liquid Chromatography

HPLC was carried out using the same apparatus and procedure described in Chapter 2, with a 15 min run time.

3.2.2.10 Bacterial Studies

Bacterial studies were carried out by Dr. Anita Umerska in Université Angers on the following bacterial strains: (1) *Staphylococcus aureus* ATCC 25923, (2) *Escherichia coli* ATCC 25922, (3) *Pseudomonas aeruginosa* ATCC 27853 and (4) *Klebsiella pneumoniae* DSM 16609. The bacteria were cultured on Columbia agar supplemented with sheep blood. The inoculum was prepared as described previously.[189] The density of the microorganism suspension was adjusted to equal that of the 1.1 McFarland standard for *S. aureus*, and the 0.5 McFarland standard for *P. aeruginosa, E. coli* and *K. pneumoniae*. The former suspension was further diluted 100-fold with BHI medium, while the latter were diluted 10-fold.

The minimum inhibitory concentrations (MICs) of CIP and the ASDs were determined using the broth microdilution method described by Umerska et al.[189] Several two-fold dilutions of the samples in BHI medium were prepared in order to obtain the desired concentration range. 50 µl of the bacterial suspension in BHI broth was then added to a well containing 50 µl of test sample or a control. The samples were incubated for 24 hours at 37 °C. All MIC assays were performed in triplicate on separate days. The MIC was taken to be the lowest concentration that completely inhibited the growth of bacteria, as detected by the unaided eye. The minimum bactericidal concentrations (MBCs) were determined by withdrawing 10 µl from each well, transferring it onto a plate containing Mueller Hinton agar, and incubating overnight at 37 °C. MIC and/or MBC values were considered as different if they varied by more than one dilution.[189]

3.2.2.11 Statistical Analysis

Statistical analysis was carried out as described in Chapter 2.

3.3 Results and Discussion

3.3.1 Production of Amorphous Solid Dispersions

A number of binary solid dispersions of CIP with different polymers, in various concentrations, were produced by ball milling. Ball milling was previously found to be a suitable method for forming the amorphous CIP/succinic acid 2:1 salt, as it did not result in any degradation of the drug.[125] The first polymer to be used was PVP, in a concentration range of 10–95% (w/w). PVP was chosen as it is a neutral, amorphous polymer, which is commonly used to produce ASDs of poorly soluble drugs.[180] Interestingly, CIP did not become amorphous when milled with any concentration of PVP tested. As the ratio of polymer to drug increased, the intensity of the peaks seen in the PXRD diffractograms decreased (**Figure A.2.1**). However, this was most likely due to a dilution effect. Although CIP may theoretically interact with PVP via hydrogen bonds, these interactions were evidently too weak to yield a fully amorphous solid dispersion. Similarly, when CIP was

milled with 40% (w/w) Soluplus or PEG 4000, both neutral polymers, a crystalline product was obtained (**Figure 3.2a**).

The next polymer chosen for milling with CIP was poly(vinyl alcohol) (PVA), whose hydroxyl group can act as both a hydrogen bond acceptor and donor. Following 4 hours of milling at RT with 40% (w/w) PVA, small peaks were still seen by PXRD (**Figure 3.2a**). Milling at RT can result in increased temperatures and a subsequent increase in molecular mobility.[97] This can induce nucleation and crystallization of amorphous material. The use of too low a concentration of polymer can also result in an unstable product.[54] Therefore, a higher concentration of 60% (w/w) PVA, 6 hour milling time and milling temperature of 2–5 ºC were implemented. This resulted in a product that was almost fully amorphous, however very small peaks could still be detected at approximately 20 and 25 2θ degrees due to the presence of residual crystalline CIP.

As polymers with neutral functional groups were ineffective at amorphizing CIP, it was hypothesized that perhaps a polymer with ionizable moieties is necessary for this. As previously discussed, many salts of CIP have been produced using acidic counterions, such as succinic acid. The secondary amine of CIP's piperazine ring is ionized in these salts, and forms hydrogen bonds with the negatively charged carboxylate groups of the acid.[125] Therefore, the processing of CIP with acidic polymers may be a suitable means of producing a stable amorphous formulation. Eudragit L100, Eudragit L100-55 and Carbopol 981 all contain carboxylic acid groups and were the first acidic polymers to be used. As can be seen from **Figure 3.2b**, each of these polymers resulted in the formation of an X-ray amorphous solid dispersion when milled with CIP for 4 hours at RT, at a concentration of 40% (w/w). While higher ratios of polymer were also successful, the use of lower quantities of the Eudragit polymers resulted in a partially crystalline product. Carbopol on the other hand still produced an ASD when used at a concentration of 20% (w/w). Each of these ASDs were dark yellow/orange in color, whereas the starting materials, as well as the semi-crystalline solid dispersions obtained with the neutral polymers, were off-white powders.

HPMCAS also contains acidic groups. The LG grade contains 5–9% acetyl and 14–18% succinoyl groups, and the MG grade 7–11% and 10–14% of each group, respectively.[183]

However, when these were milled with CIP using the same conditions as for the other acidic polymers, the product was only partially amorphous (**Figure 3.2a**). Higher concentrations of polymer and longer milling times still resulted in partially crystalline systems, as evidenced by PXRD peaks, although polymer concentration appears to have a greater effect on the crystallinity of these samples than milling time (**Figure A.2.2**). Milling was next conducted at 2–5 ºC, with a 60 % (w/w) concentration of HPMCAS, for 6 hours. These conditions resulted in the formation of X-ray amorphous solid dispersions (**Figure 3.2b**), which were dark yellow in color.

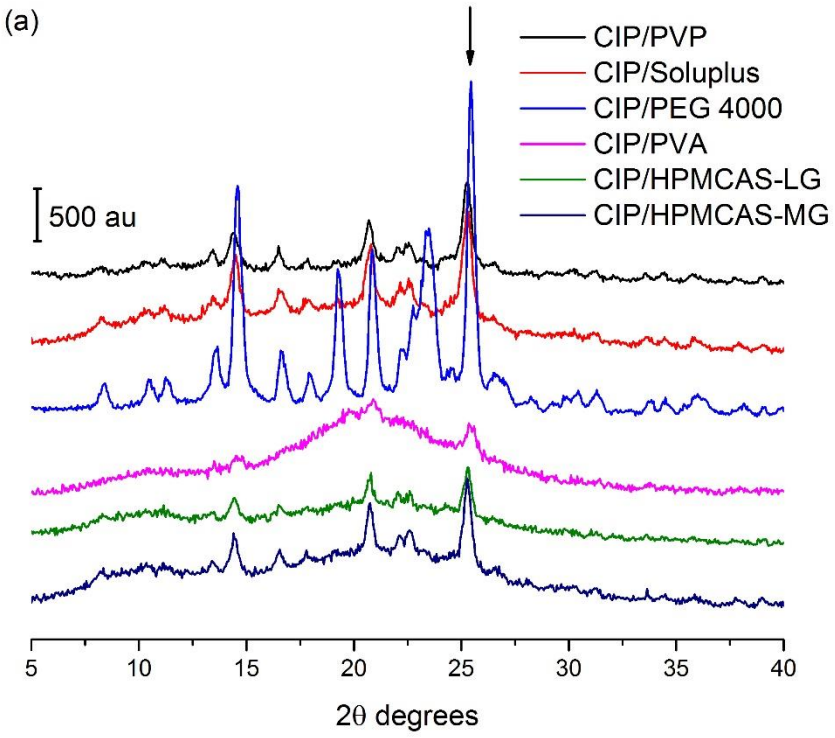

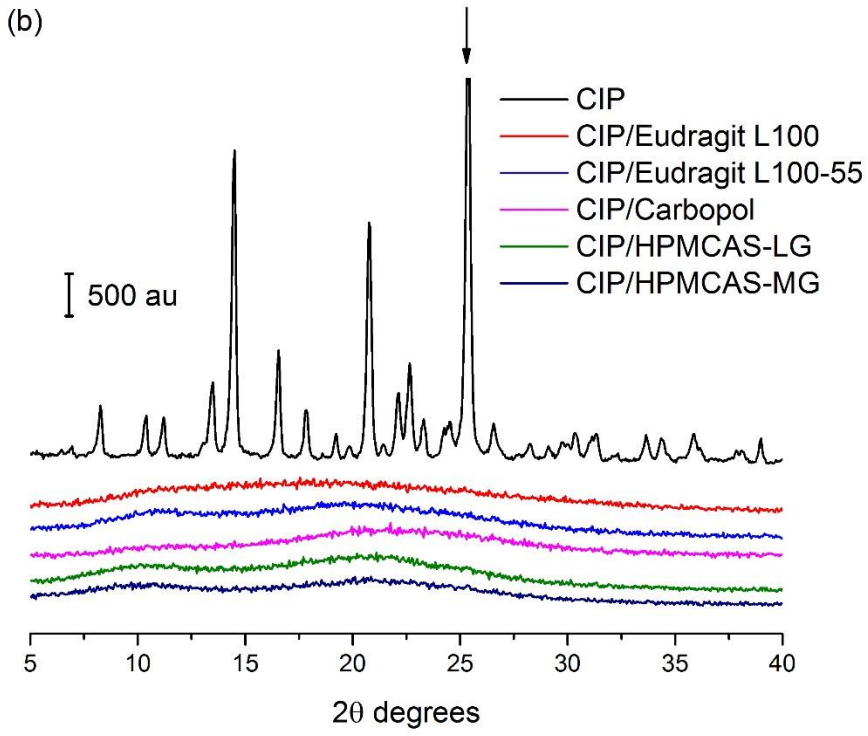

Figure 3.2. (a) PXRD analysis following milling of CIP with various polymers at a 40% (w/w) concentration, for 4 hours at RT and (b) PXRD analysis of CIP and CIP ASDs. The peak at 25.3 2θ degrees corresponds to the major slip plane in the crystal lattice of CIP, and therefore it is the most likely peak to be present following mechanical stress of the drug.

ASDs formed from the five acidic polymers discussed above (i.e. Eudragit L100, Eudragit L100-55, Carbopol 981, HPMCAS-LG and HPMCAS-MG) were chosen for further examination. While a higher proportion of polymer should increase the physical stability of an ASD,[52] it also necessitates the use of a larger preparation in order to deliver the required dose as an oral solid dosage form. This could result in problems with patient acceptability and compliance. Therefore, a polymer concentration of 40% (w/w) was chosen for the ASDs containing Eudragit L100, Eudragit L100-55 and Carbopol, and 60% (w/w) for those containing HPMCAS.

3.3.2 Solid-State Characterization of Amorphous Solid Dispersions

3.3.2.1 Solid-State Fourier Transform Infrared Spectroscopy

The FTIR spectra of the ASDs, polymers and crystalline CIP are shown in **Figure 3.3**. The spectra of the physical mixtures (PMs) are also shown for comparison. In the spectra of each of the polymers, a peak can be seen between 1709 and 1744 cm^{-1} due to the C=O stretch of their carboxylic acid groups. A matching peak is present in the spectra of the PMs. As discussed in Chapter 2, the spectrum of crystalline CIP contains a peak at 1590 and 1375 cm^{-1}, corresponding to the asymmetric and symmetric vibrations of the carboxylate ion, respectively.[165] The peak at 1590 cm^{-1} is absent from the spectra of the ASDs containing Eudragit and Carbopol, while those containing HPMCAS display a small peak, due to the presence of a residual amount of zwitterionic CIP. Interestingly, with all of the ASDs a strong peak is seen between 1723 and 1734 cm^{-1}, due to the C=O stretch of COOH. In each case, this peak is far more intense than the corresponding peak in the spectra of the PMs. Therefore, these peaks can be assigned to the carboxylic acid of CIP, and it can be concluded that this group is uncharged in the ASDs. This is in contrast to the semi-crystalline solid dispersions containing PVP and Soluplus, which also show the characteristic peaks of the ionized carboxylate group of CIP. These peaks are weaker and broader in the more disordered CIP/PVA solid dispersion, as the proportion of crystalline CIP is greatly reduced. In addition, like the ASDs, this sample has a peak at approximately 1720 cm^{-1}, which confirms the presence of the protonated carboxylic acid group of CIP (**Figure A.2.3**).

The strongest peak in the spectrum of crystalline CIP, at approximately 1618 cm^{-1}, can be assigned to the C=O stretch of the ketone carbonyl.[165] This peak is shifted to 1628 cm^{-1} in the spectra of the ASDs, which may be due to changes in the hydrogen bonding of this group. This peak was also found to shift to 1627–1629 cm^{-1} when zwitterionic CIP was heated to its melting point, which results in the formation of the unionized form of the drug (**Figure 2.9c**). When the carboxylic acid of CIP is unionized, an intramolecular hydrogen bond is formed between this ketone and the neighboring carboxylic acid. This hydrogen bond is also found in CIP salts, in which the carboxylic acid of CIP is also protonated.[125] In contrast, no such shift in the ketone carbonyl peak is seen in the spectra of the semi-crystalline solid dispersions, as they contain zwitterionic CIP.

In each of the ASD spectra a broad peak at 2400–2600 cm^{-1} can be assigned to the NH_2^+ stretching vibrations of CIP.[125] Therefore, the drug is in a similar ionization state in these ASDs as it is in crystalline salts formed using various acids, i.e. with a neutral carboxylic acid and positively charged secondary amine. The latter group most likely interacts with negatively charged carboxylate groups in the polymers, as was seen with CIP succinate salts.[125] As previously stated, the pK_a of the carboxylic acid of CIP has been reported as 6.16, while that of the piperazine amine is 8.62.[109] Given that the pK_a values of the polymers vary from 5 to 6.0,[181–183,190] the pK_a difference between the secondary amine of the drug and carboxylic acid of the polymers falls within the limits of salt formation of ≥ 2–3 in each case.[191] Therefore, these formulations could be considered as amorphous polymeric drug salts. Amorphous drug-polymer salts have also been produced by Weuts et al,[61] Song et al[87] and Maniruzzaman et al.[192] In each case an ionic interaction between the carboxylate groups of the polymers and amino groups of the drugs was detected.

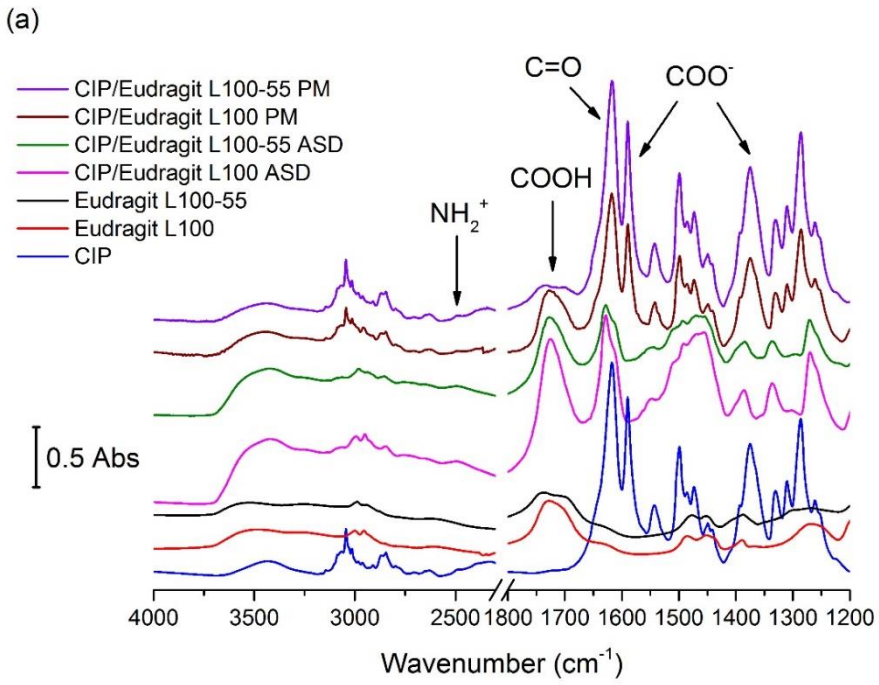

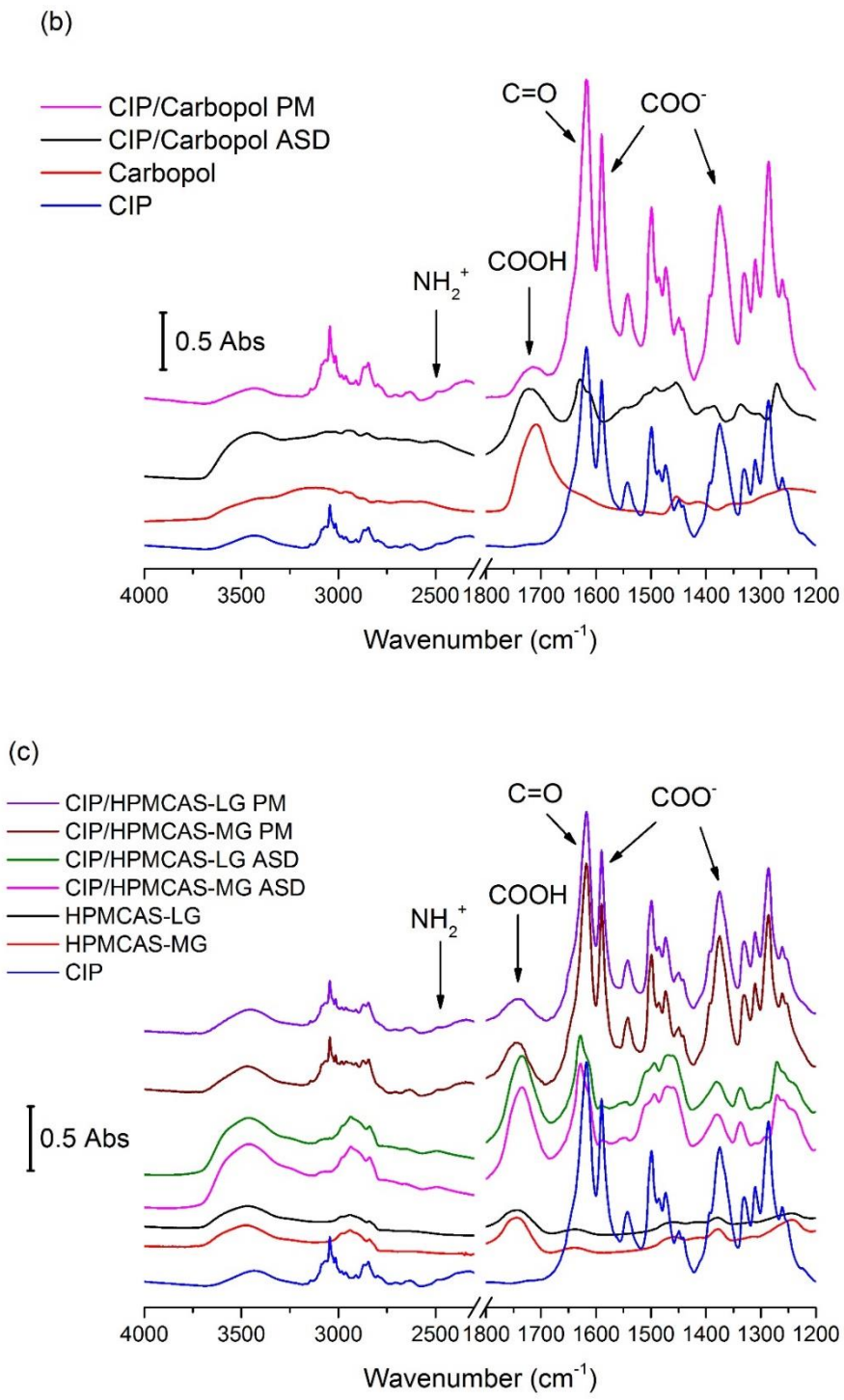

Figure 3.3. FTIR spectra of ASDs and PMs containing (a) Eudragit L100 and Eudragit L100-55 40% (w/w) (b) Carbopol 40% (w/w) and (c) HPMCAS-LG and HPMCAS-MG 60% (w/w).

3.3.2.2 Thermal Analysis

Conventional DSC, using a heating rate of 10 ºC/min, resulted in DSC thermograms that proved difficult to interpret for the ASDs (**Figure 3.4**). In each case it was impossible to pinpoint a definite T_g. Due to their high water content, the samples were first heated from 25–100 ºC to allow for evaporation of sorbed water.

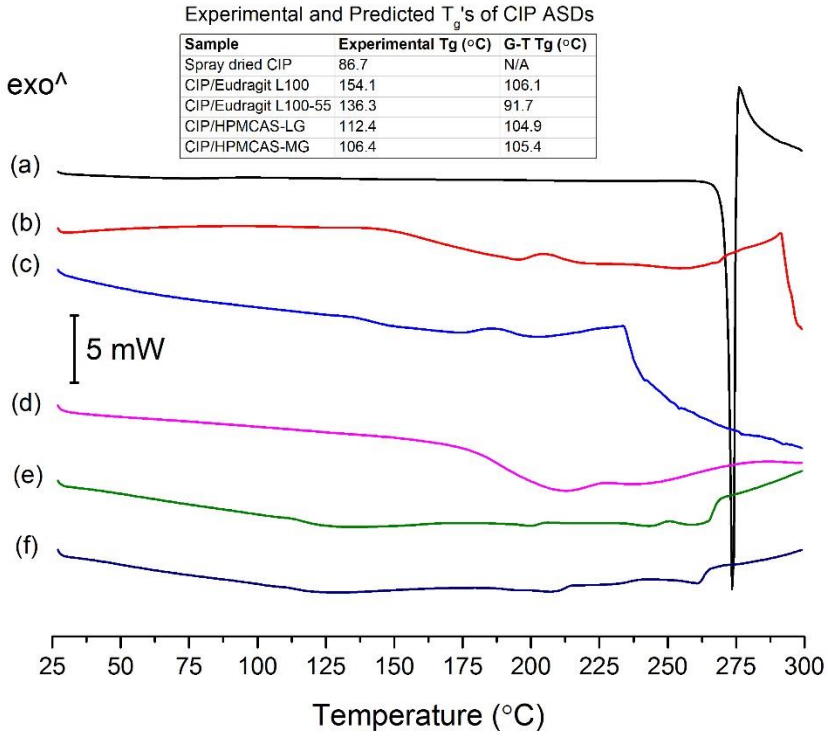

Figure 3.4. DSC thermograms of (a) crystalline CIP, and ASDs containing (b) Eudragit L100 40% (w/w) (c) Eudragit L100-55 40% (w/w) (d) Carbopol 40% (w/w) (e) HPMCAS-LG 60% (w/w) and (f) HPMCAS-MG 60% (w/w). The thermograms of the ASDs are those obtained from the second heating cycle, following initial heating to 100 ºC to allow for water evaporation. The T_g's obtained from temperature modulated DSC (StepScan) and calculated using the Gordon-Taylor (G-T) equation are also listed.

Crystalline CIP has a melting point of approximately 272 ºC, which is accompanied by degradation. The ASDs did not display a clear melting endotherm, which can be taken as confirmation of their amorphous nature.[193] Like the pure drug, the ASDs undergo thermal degradation, as shown by TGA (**Figure 3.5**). All of the ASDs initially undergo water

evaporation, followed by substantial degradation above ~ 230 ºC, leading to a total mass loss of 14–19%.

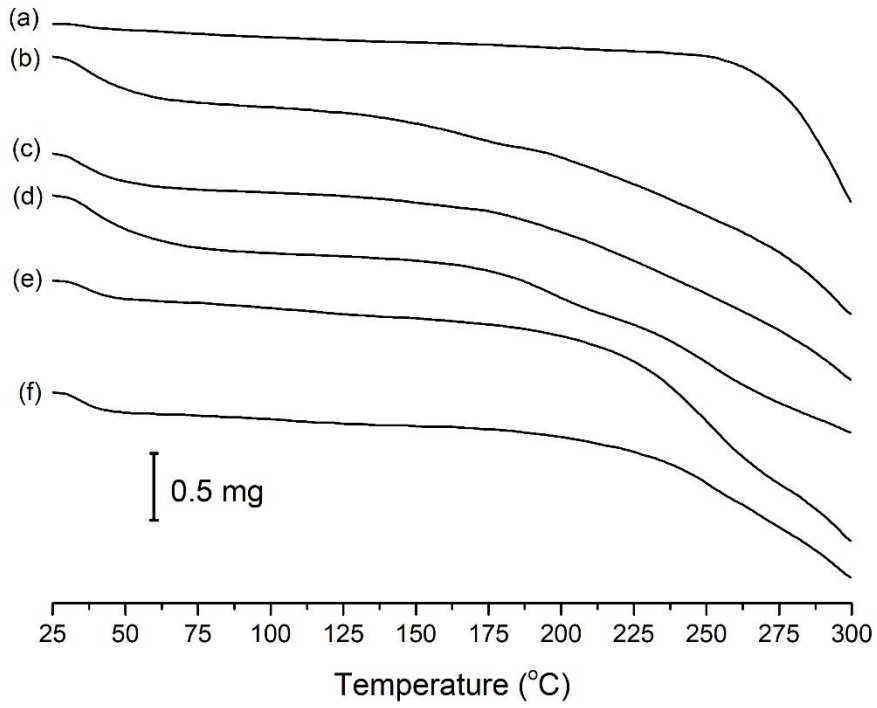

Figure 3.5. TGA analysis of (a) crystalline CIP, and ASDs containing (b) Eudragit L100 40% (w/w) (c) Eudragit L100-55 40% (w/w) (d) Carbopol 40% (w/w) (e) HPMCAS-LG 60% (w/w) and (f) HPMCAS-MG 60% (w/w).

Temperature-modulated DSC (StepScan) was used to locate the T_g's of the ASDs, and these are listed in **Figure 3.4**. A single T_g was seen in the thermograms of all of the ASDs. This suggests that CIP is miscible with each of these polymers[41] and that phase separation does not occur in the ASDs.[145] Unfortunately, despite the use of the StepScan method, the T_g of the CIP/Carbopol ASD could not be detected. The T_g's that were calculated using the Gordon-Taylor (G-T) equation are also shown in **Figure 3.4**. The G-T equation is based on the assumption that the components form an ideal mixture, with additive free volumes, but without any strong interactions between the constituents.[59,64] With all of the ASDs, the T_g values obtained experimentally were higher than those predicted theoretically. This was also found to be the case for the amorphous polymeric salts produced by Weuts et al and Song et al.[61,87] Particularly large positive deviations of approximately 48 and 45 ºC were obtained

for the ASDs containing Eudragit L100 and Eudragit L100-55, respectively. The G-T equation is known to underestimate the T_g of salts due to their ionic bonds, and larger deviations are obtained with counterions that form stronger electrostatic interactions with the drug.[62,194] Therefore, the FTIR spectra and higher than predicted T_g's of these ASDs suggest that ionic interactions exist between CIP and the polymers.

In contrast to the Eudragit-containing ASDs, the experimental and calculated T_g's of the CIP/HPMCAS-MG ASD were very similar, differing by only 1 ºC. This suggests that the drug and polymer are fully miscible and do not interact specifically with one another.[60] Alternatively, the strength of the interactions formed between the drug and polymer may be equal in strength to the homomolecular interactions in the pure components.[53] This formulation would therefore be expected to be less stable than the ASDs containing Eudragit L100 or L100-55. A larger deviation of 7.5 ºC was seen with CIP/HPMCAS-LG, suggesting that the drug interacts more substantially with this grade of HPMCAS, but less so than with the Eudragit polymers, possibly due to a larger content of succinoyl groups in this grade of HPMCAS. Similarly, stronger drug-polymer interactions may exist in the Eudragit-containing ASDs due to the higher proportion of carboxylic acid groups present in these polymers in comparison to HPMCAS (see polymer structures in **Figure 3.1**). This may explain why it was more difficult to amorphize the CIP/HPMCAS mixtures, with larger polymer concentrations, longer milling times and lower temperatures being required compared to the other ASDs.

3.3.3 Stability Studies

DVS analysis showed that all of the ASDs are capable of sorbing a large amount of water. At 90% RH, a change in mass of between 16% and 20% was seen for all of the samples. CIP/Eudragit L100 sorbed the greatest amount of water, and CIP/HPMCAS-MG the least. The sorption-desorption isotherms obtained with all of the samples had a similar sigmoidal shape and hysteresis (**Figure 3.6**). These results are to be expected, as amorphous drugs are more hygroscopic than their crystalline forms. The presence of hygroscopic polymers would also have contributed to the water uptake of the ASDs.

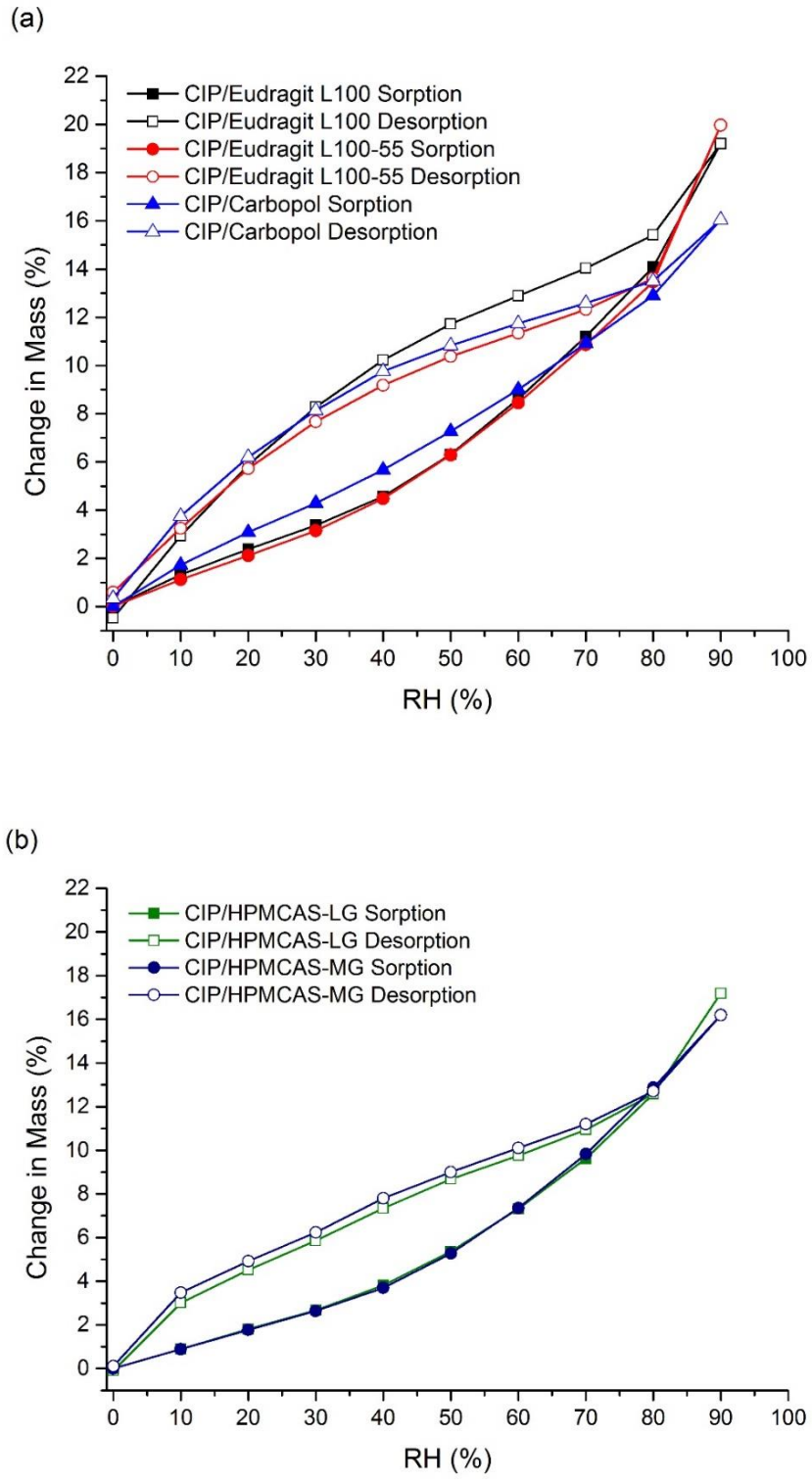

Figure 3.6. DVS analysis of CIP ASDs containing (a) Eudragit L100, Eudragit L100-55 and Carbopol 40% (w/w) and (b) HPMCAS-LG and HPMCAS-MG 60% (w/w).

As discussed in Chapter 1, water sorption can negatively affect drug stability by increasing the rate of crystallization.[42] However, all of the ASDs studied here remained X-ray amorphous following DVS analysis, as shown by PXRD **(Figure 3.7)**. Electrostatic forces between the amino group of CIP and carboxylates of the polymers most likely stabilized the ASDs and prevented their crystallization during the study. Similar interactions were responsible for the improved stability of loperamide-polyacrylic acid and lapatinib-hydroxypropylmethylcellulose phthalate ASDs during stability studies.[61,87] In addition, the long chains of polymers can delay crystallization by sterically hindering the diffusion of drug molecules, blocking sites of crystal growth, and increasing the kinetic barrier to nucleation.[52,53]

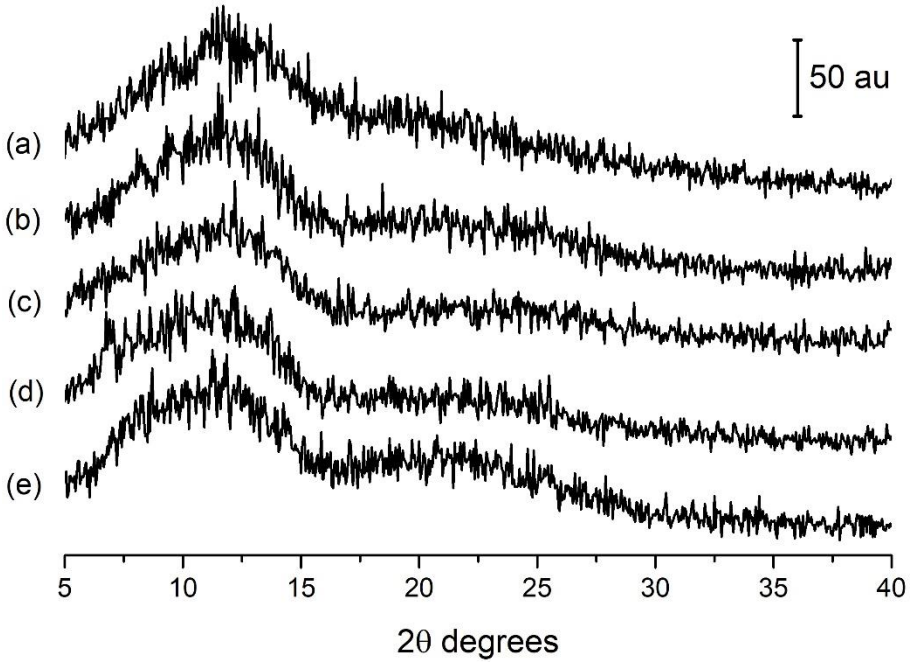

Figure 3.7. PXRD following DVS analysis of CIP ASDs containing (a) Eudragit L100 40% (w/w) (b) Eudragit L100-55 40% (w/w) (c) Carbopol 40% (w/w) (d) HPMCAS-LG 60% (w/w) and (e) HPMCAS-MG 60% (w/w).

All of the ASDs, except for CIP/Eudragit L100, began to crystallize after 24 hours in accelerated storage conditions of 40 ^{o}C/75% RH. However, by day 3 of the study this sample also began to show small crystallization peaks (**Figure 3.8a**). There was only a slight increase

in the intensity of the bands seen in the PXRD of the HPMCAS samples between day 1 and 14, and no noticeable change in the Carbopol sample during the same timeframe (**Figure 3.8**). As CIP/Eudragit L100 did not show prominent peaks until day 3 of the study, it is therefore slightly more resistant to crystallization than the other ASDs. After 14 days, all of the samples were partially crystalline by PXRD, displaying a number of low intensity peaks. Therefore, although the ASDs were physically stable under the high humidity conditions of DVS, when this was combined with high temperature, a small degree of crystallization occurred.

All of the ASDs, except for CIP/Carbopol, showed PXRD peaks corresponding to that of hydrated CIP, in particular the most characteristic peak of the 3.7 hydrate at approximately 6.5 2θ degrees.[158] Peaks corresponding to the 3.1 hydrate (see next section) were also identified. In contrast to the other ASDs, the peaks of hydrated CIP were absent from the diffractograms of the CIP/Carbopol ASD, which instead showed broad peaks corresponding to anhydrous zwitterionic CIP.

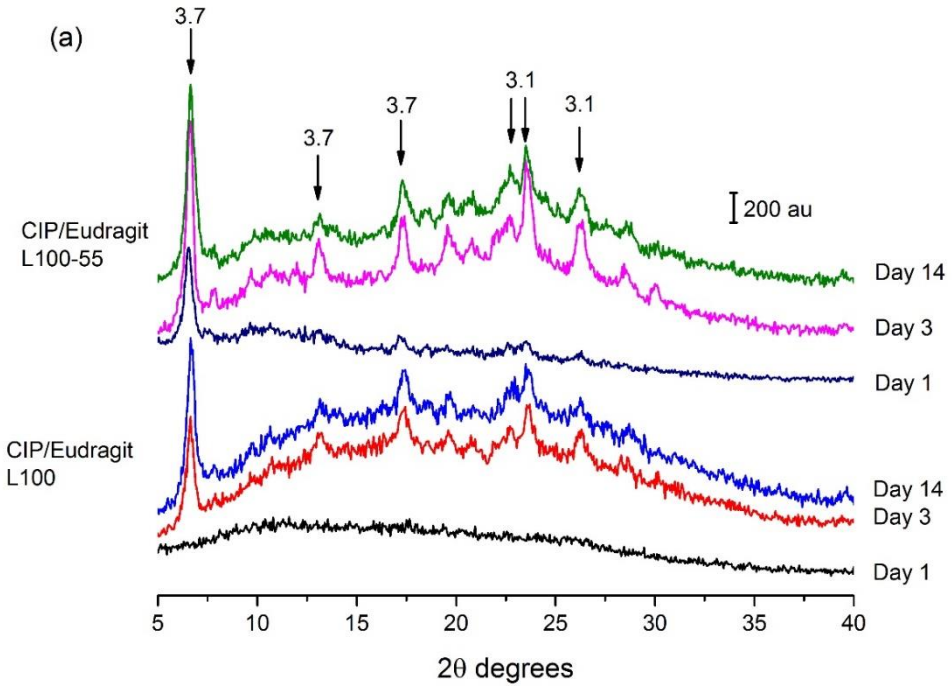

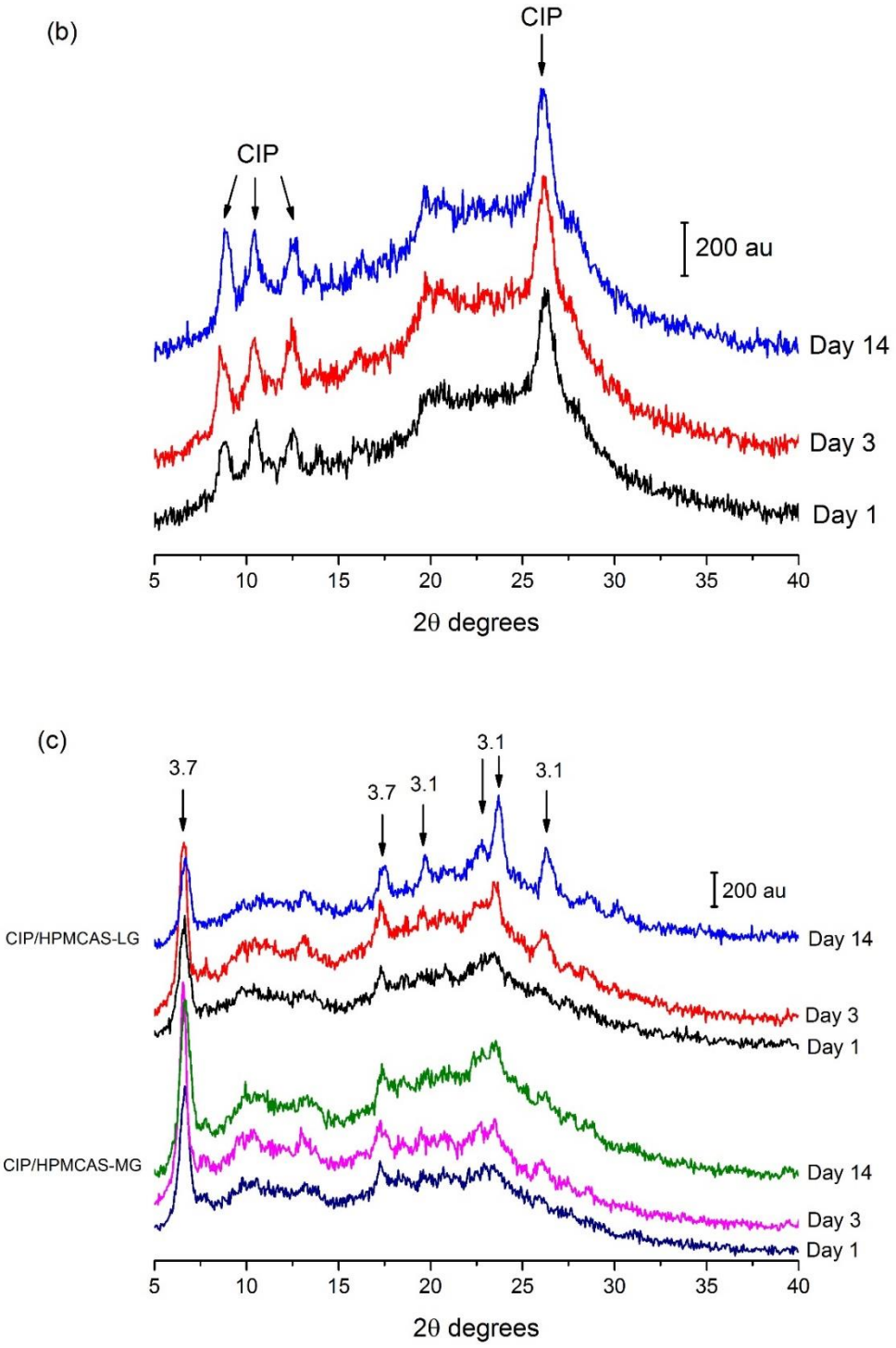

Figure 3.8. PXRD analysis of ASDs stored at 40 ºC/75% RH for 1, 3 and 14 days: (a) CIP/Eudragit L100 and CIP/Eudragit L100-55 (b) CIP/Carbopol and (c) CIP/HPMCAS-LG and CIP/HPMCAS-MG. The arrows identify the most prominent peaks, corresponding to CIP, CIP 3.7 hydrate (3.7) and CIP 3.1 hydrate (3.1).

3.3.4 Dynamic Solubility Studies

As previously mentioned, CIP is a zwitterionic compound, with a basic and an acidic group that can ionize depending on the pH of the solvent. Therefore, it is important to study the solubility of this drug in different media in order to estimate how it will behave in various sections of the gastrointestinal tract.[195] Solubility studies were carried out in water, FaSSIF (fasted state simulated intestinal fluid, pH 6.5) and FaSSGF (fasted state simulated gastric fluid, pH 1.6). Due to excessive clumping and the viscous nature of the solutions formed when the CIP/Eudragit L100-55 and Carbopol samples were added to the media, it was not possible to accurately carry out solubility tests on these ASDs.

CIP has low aqueous solubility, achieving a concentration of only 0.09 mg/ml in water after 2 hours. The Eudragit and HPMCAS ASDs showed superior solubility, obtaining concentrations approximately 7 and 19 times that of the pure drug, respectively, in the same time frame. After a steep initial increase in concentration within the first 10 min or so, these levels were then sustained for the duration of the experiment (**Figure 3.9a**). All three of these polymers are practically insoluble in water,[183,184] which may have limited their ability to improve the aqueous solubility of CIP. Although the LG grade of HPMCAS resulted in slightly higher drug concentrations in the initial portion of the study, after 2 hours no statistically significant difference was seen when compared to the MG grade ($p = 0.27$).

The solubility profiles of the ASDs are similar to the "spring" and "parachute" model described in Chapter 1. The disordered structure of the ASDs enables the rapid dissolution of CIP, while the polymers help to prevent its nucleation and crystallization.[76] PXRD analysis of the excess solid recovered at the end of the studies confirmed that a low proportion of CIP crystallized from the ASDs in solution overall (**Figure A.2.4**). CIP/Eudragit L100 was quite resistant to crystallization in water, with just one small peak appearing in the PXRD of the excess solid recovered at the end of the study, at 6.5 2θ degrees. The HPMCAS ASDs showed a greater number of peaks, of higher intensity, but still remained somewhat disordered. As demonstrated in the stability study, these ASDs have a greater propensity to crystallize when exposed to water than those containing Eudragit L100. The excess solids recovered at the end of the solubility studies in FaSSIF were also partially crystalline. A more crystalline product was obtained with CIP/HPMCAS-LG, indicating that

this ASD is less resistant to crystallization at basic pH. Unlike the ASDs, pure CIP formed a fully crystalline hydrate in all media; however, the PXRD pattern of the residue from solubility studies in water differed from those conducted in FaSSIF and FaSSGF (**Figure A.2.4d**). In the latter two cases, the CIP 3.7 hydrate was indentified,[158] while TGA of the former hydrate found it to contain 14.3% water. This corresponds to approximately 3.1 moles of water per mole of CIP. While the HPMCAS-LG ASD also formed the 3.7 hydrate in water, all the other ASD/media combinations resulted in the CIP 3.1 hydrate.

In FaSSIF crystalline CIP reached a peak concentration of 0.9 mg/ml after 1 min. This quickly fell over the first 10 min, and then remained fairly constant at approximately 0.15 mg/ml for the remainder of the study. The sodium taurocholate and lecithin present in FaSSIF mimic bile salts and phospholipids, respectively, in intestinal fluid.[196] The increased solubility of the pure drug in this medium compared to water may be due to the presence of these surfactants. The Eudragit L100 and HPMCAS ASDs behaved differently over the course of the study. The solubility of the former increased gradually over 2 hours, giving the plot in **Figure 3.9b** a convex shape. In contrast, the HPMCAS-LG and HPMCAS-MG ASDs reached a peak in CIP concentration after 5–10 min, and then slowly fell over the remainder of the study. The LG grade of HPMCAS reached a top concentration of 1.9 mg/ml, whereas the MG grade obtained a maximum of 1.5 mg/ml. Solid dispersions containing different grades of HPMCAS would be expected to show discrepancies in solubility at various pH values, due to differences in their succinoyl and acetyl content.[197] However, although the former sample remained at a higher concentration for the majority of the study, after 2 hours an equal concentration of 1.3 mg/ml was obtained with both HPMCAS ASDs. The decrease in the solubility of CIP/HPMCAS-LG over time may be due to the conversion of the drug to its hydrate, as detected by PXRD, as the aqueous solubility and dissolution rate of CIP hydrate is significantly lower than that of the anhydrous drug.[198] Although HPMCAS-LG and HPMCAS-MG are soluble at a pH above 5.5 and 6.0 respectively,[183] this did not result in a substantial increase in the solubility of these ASDs in FaSSIF.

In FaSSGF the Eudragit L100 and HPMCAS-LG ASDs showed very similar behavior to each other, achieving maximum CIP concentrations of 3.2 mg/ml after 2 hours. The HPMCAS-MG formulation was somewhat more soluble at low pH, reaching 4.1 mg/ml

(**Figure 3.9c**). The solubility of the pure drug however was approximately 3–4 times higher than that of the ASDs. This may be due to the fact that the polymers are insoluble in aqueous acidic solutions.[197] CIP on the other hand has high solubility at pH < 5, as it has a net positive charge. In contrast, it has minimal solubility at neutral pH, where it bears no overall charge.[112] Similar results were seen in solubility studies of malonic, tartaric and oxalic acid salts of CIP, which were also found to be less soluble than the pure drug in acidic media.[124] An amorphous solid was recovered at the end of this study for all of the ASDs, indicating that they are resistant to crystallization at low pH.

The pH of the solutions at the end of the studies was measured and is listed in **Figure 3.9**. Very small changes in pH, of ± 0.2 on average, occurred over the course of the study, with the exception of pure CIP in FaSSGF. In this case the high quantity of weakly basic drug in solution increased the pH to 4.7. Therefore, the differences in solubility described above cannot be attributed to changes in pH, but rather to the physical form of the drug and the presence of polymers.

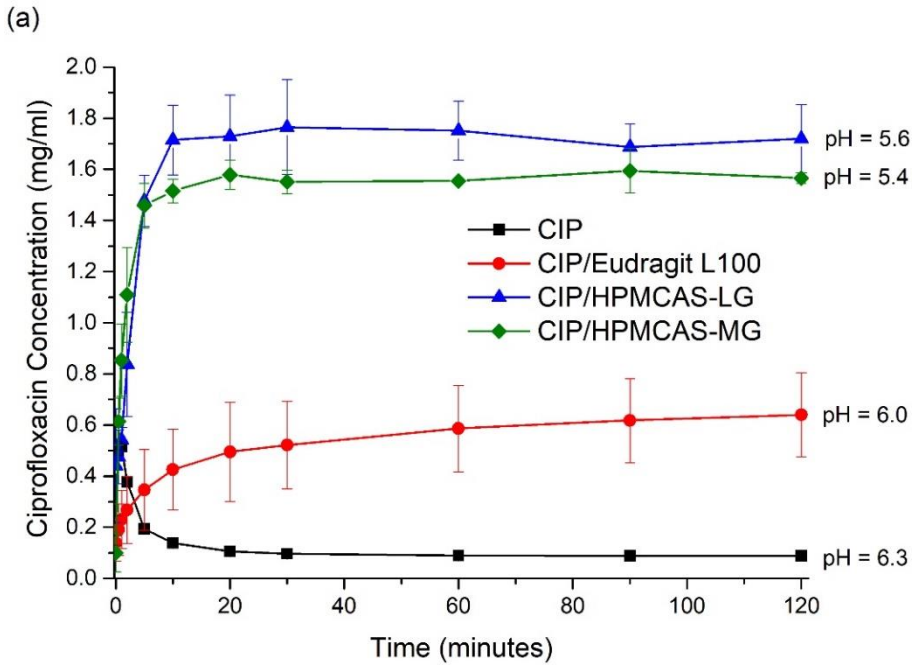

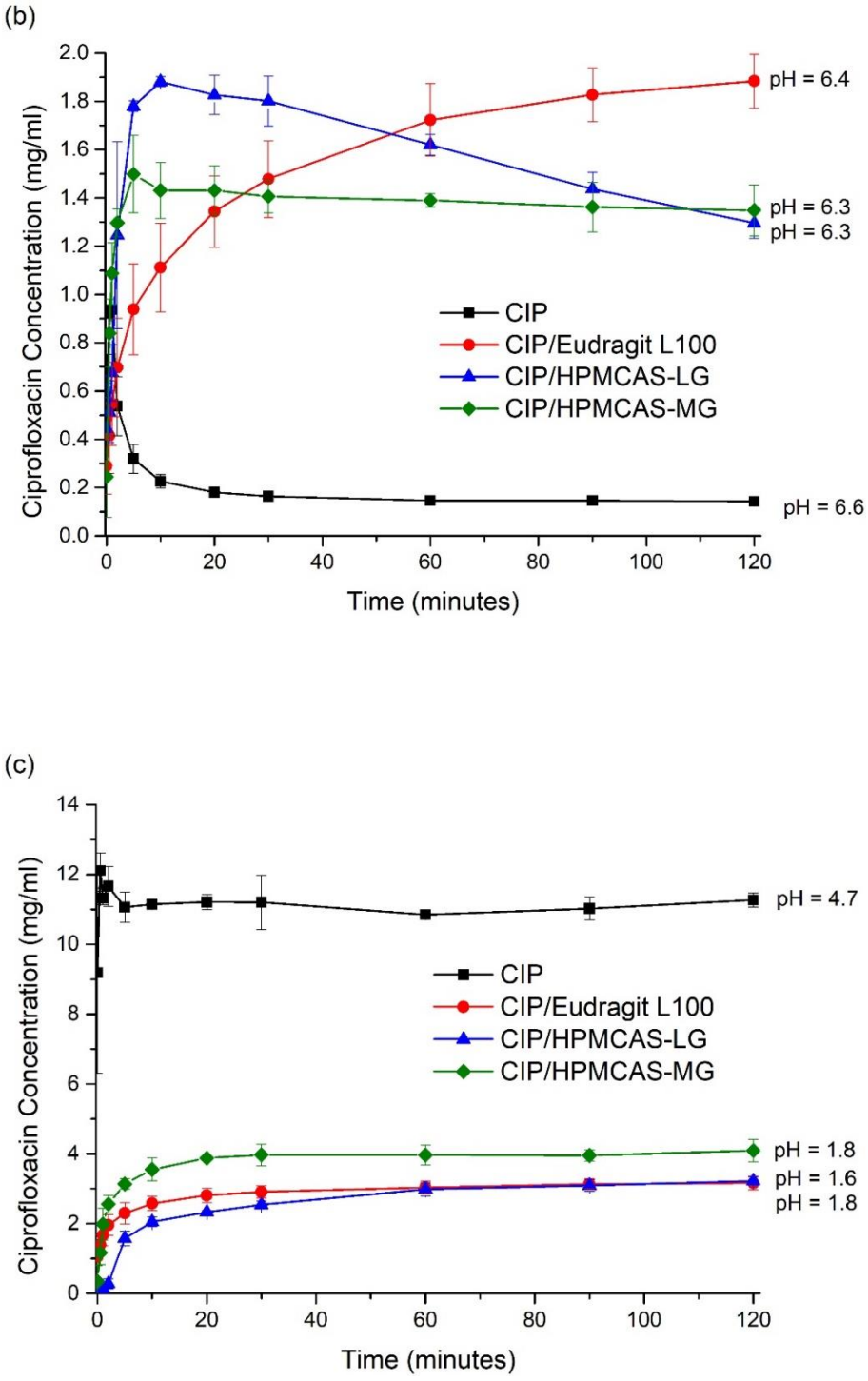

Figure 3.9. Solubility studies in (a) water (b) FaSSIF and (c) FaSSGF at 37 ºC. The average of at least 3 experiments is plotted, ± the standard deviation. The average pH of the solutions at the end of the study is also shown.

A modification of the Henderson-Hasselbalch equation was used to construct the theoretical pH-solubility profile of pure CIP and the commercial hydrochloride salt, CIP HCl:

$$S_T = [B]\,(1 + 10^{pKa1-pH} + 10^{pH-pKa2}) \quad (3.4)$$

S_T is the total solubility of the drug in moles/L and [B] is the concentration of the free base (approximately 0.000266 M for CIP and 0.0008 M for CIP HCl). As previously mentioned, the pK_a of the carboxylic acid of CIP (pK_{a1}) at 37 ^oC has been reported as 6.16, and that of the piperazine amine (pK_{a2}) as 8.62.[109] The CIP ASDs may be considered as basic salts, as they consist of an interaction between the positively charged amino group of the drug and negatively charged carboxylate groups of the polymers. According to Kramer and Flynn, the pH-solubility profile of a basic salt can be represented by two independent solubility profiles, one of which describes when the free base is the saturation species, and the other when the salt is the saturation species.[199] The point at which the two curves intersect is referred to as the pH_{max}, the pH of maximum solubility. In a saturated solution above pH_{max}, the dissolved solute is in equilibrium with the free base, and at a pH below pH_{max}, it is in equilibrium with the salt.[28] The following equation was used to predict the pH-solubility profile of the ASDs:

$$S_T\,(pH<pH_{max}) = [BH^+]_s\,(1 + 10^{pH\,-\,pKa}) \quad (3.5)$$

$[BH^+]_s$ is the concentration of the protonated amorphous salt. The subscript s highlights the fact that the salt is the saturation species at a pH below pH_{max}.[28]

As can be seen from **Figure 3.10**, the experimental data does not fit the theoretical pH-solubility curve of CIP exactly. The solubility of the drug from the ASDs in water and FaSSIF is higher than that predicted for CIP. These experimental data points align more closely with the profile of CIP HCl. Therefore, a more accurate pH_{max} for these amorphous polymeric salts may be the intersection of the curve for CIP HCl and the CIP ASDs, which occurs at a pH of 5.1. The three main outliers in **Figure 3.10** correspond to the particularly high solubility of the ASDs in FaSSIF. As previously mentioned, FaSSIF contains surfactants, which may enhance the solubility of these solids compared to water. This lack of fit also suggests that the solubility enhancement of these formulations is not due to their effect on pH. Instead, this may be attributed to their amorphous nature and polymer content.

The solubility of the pure drug in FaSSGF is also higher than that predicted, and aligns more closely with the CIP HCl curve. Due to the presence of HCl in FaSSGF, the drug is likely to be in a similar environment in this medium as CIP HCl in water. At a pH below pH_{max}, i.e. in FaSSGF, the ASDs no longer follow the solubility curve of CIP, as the equilibrium species is now the salt. At acidic pH they may be more accurately described by equation 3.5 above.

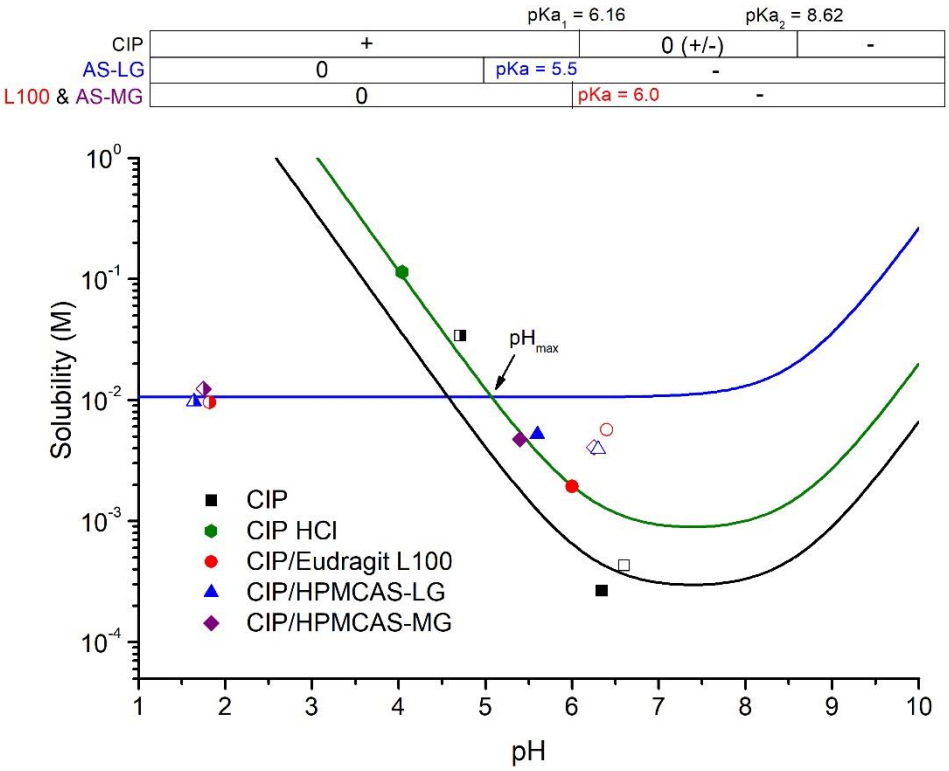

Figure 3.10. Theoretical pH-solubility profiles of CIP (black), CIP HCl (green), and CIP ASDs (blue). The symbols represent the average concentrations obtained from solubility studies after two hours in water (filled symbols), FaSSIF (empty symbols) and FaSSGF (half-filled symbols). The bars above the plot show the ionization state of the drug and the polymers in each pH range.

3.3.5 Dissolution Study

The dissolution profile of crystalline CIP began to plateau after 10 min, with an average concentration of 0.017 mg/ml being achieved at the end of the study (**Figure 3.11**). CIP/Eudragit L100 had a more gradual drug release pattern, without a clear plateau, resulting in a final concentration of 0.10 mg/ml. A similar convex profile was obtained with this formulation in solubility studies (**Figure 3.9**). A greater variance was also obtained with this ASD, as the powder clumped or dispersed to varying degrees upon addition to the vessel, leading to differences in the surface area exposed to the dissolution medium. This behavior may also be responsible for delaying and limiting the dissolution and diffusion of CIP from the formulation. In addition, the interactions between the drug and polymer may have been sufficiently strong as to hinder the dissociation of CIP and thus delay its dissolution.[200] The presence of stronger interactions between the drug and polymer in this ASD may also explain its higher T_g and lower degree of crystallization in solubility studies than the HPMCAS-containing formulations. Similar to CIP, the dissolution profiles of the HPMCAS-LG and HPMCAS-MG ASDs also began to plateau after about 10 min, reaching a CIP concentration of 0.12 mg/ml and 0.15 mg/ml respectively over the course of the study. Like the pure drug, these powders dispersed rapidly when added to the dissolution medium, resulting in a greater rate and extent of dissolution compared to the Eudragit L100 ASD.

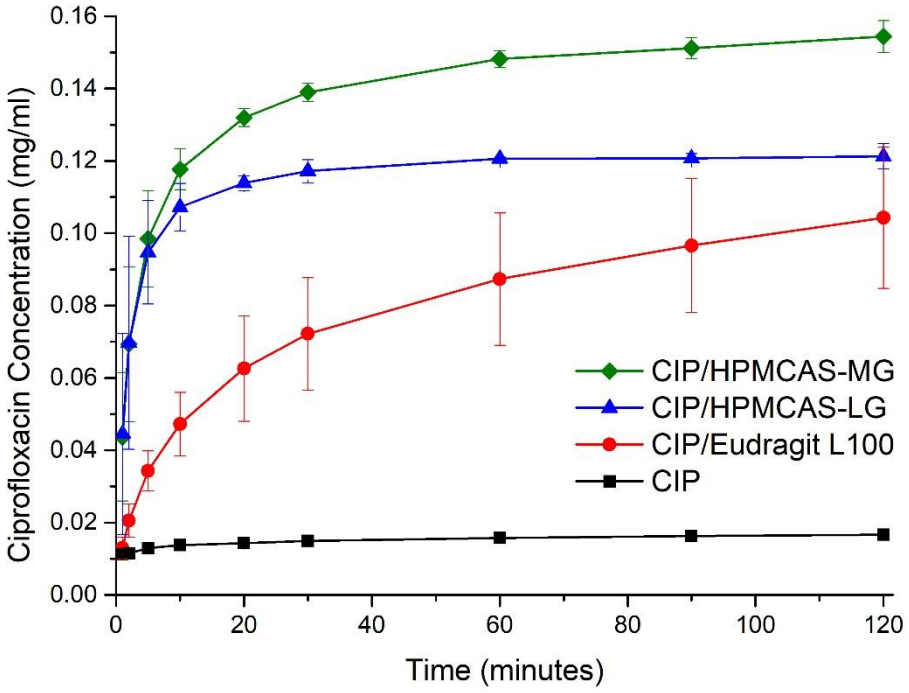

Figure 3.11. Dissolution studies in FaSSIF at 37 ºC. The average of at least 3 experiments is plotted, ± the standard deviation.

3.3.6 PAMPA Permeability Study

The results of the PAMPA study, under iso-pH and pH gradient conditions, are shown in **Table 3.1**. The commercially available hydrochloride salt, CIP HCl, was included in the study for comparison. PAMPA is usually carried out using donor and acceptor solutions of the same pH (iso-pH conditions), however this does not accurately mimic what occurs in vivo. Fortuna et al obtained the best correlation between apparent permeability from PAMPA studies and human intestinal absorption for a range of drugs, including the fluoroquinolone norfloxacin, with a pH of 6.5 and 7.4 in the donor and acceptor compartments, respectively.[201] The pH of the blood and the cytosol of intestinal cells lining the duodenum is about 7.4, therefore this is a suitable pH to use for the acceptor compartment.[15] CIP is believed to be absorbed from the upper section of the duodenum, which has a pH of 6.4.[202,203] A donor/acceptor pH of 6.4/7.4 was therefore chosen for this study in order to more closely represent the pH gradient present in vivo at the site of CIP absorption.[15] In addition, as the permeability of ionizable drugs, such as CIP, depends on pH, it is useful to carry out PAMPA

at two different pH values for such compounds, to prevent under- or overestimation of permeability.

Table 3.1. PAMPA Permeability Values of CIP

	Iso-pH P_e^a x 10^6 (cm/s)	**pH gradient P_e^a x 10^6 (cm/s)**	***p*-value[b]**
Crystalline CIP	0.56 ± 0.06	0.62 ± 0.08	0.42
CIP HCl	0.32 ± 0.00	0.32 ± 0.01	0.22
CIP/Eudragit L100	0.52 ± 0.00	0.50 ± 0.06	0.50
CIP/HPMCAS-LG	0.75 ± 0.06	0.64 ± 0.10	0.20
CIP/HPMCAS-MG	0.64 ± 0.03	0.67 ± 0.03	0.34

[a]P_e: effective permeability. The average of three measurements is shown, ± the standard deviation. [b]*p*-value from *t* test comparing P_e from regular and pH-gradient PAMPA.

According to Sugano, a permeability of less than 1×10^{-6} cm/s can be considered as low permeability.[204] As can be seen from **Table 3.1**, all of the samples may therefore be described as poorly permeable. A similarly low P_e of 0.19 x 10^{-6} cm/s was obtained for CIP by Tehler et al in Caco-2 studies.[113] Two-sample *t* tests were used to compare the results of the individual samples under both pH conditions, and in each case no statistically significant difference was found (see *p*-values in **Table 3.1**). The pI of CIP is around 7.4–7.5.[110] The passive absorption of this drug would therefore be expected to be highest at this pH. As the pH is decreased below the pI, the carboxylate group of CIP will become protonated, and the proportion of drug bearing an overall positive charge will increase. This should reduce its passive transport through a lipid membrane. However, at neutral pH the drug exists primarily as the zwitterion, with only about 2% expected to be present in the unionized form at the pI.[110] While the membrane penetration and diffusion of unionized CIP is energetically favorable, the transmembrane translocation of zwitterionic CIP is unlikely to occur.[117] Evidently, dropping from pH 7.4 to 6.4 does not have a large effect on the proportion of unionized CIP present, and thus no significant difference in P_e was seen when the donor solution pH was changed in the above study.

ANOVA and Tukey's multiple comparison test were carried out to compare the P_e of the different samples. CIP from ASDs containing HPMCAS-LG and HPMCAS-MG possessed the highest permeability, with a P_e of 0.75×10^{-6} and 0.64×10^{-6} cm/s respectively under iso-pH conditions, and 0.64×10^{-6} and 0.67×10^{-6} cm/s respectively with a pH-gradient; however, these samples were not statistically significantly different from each other under either pH condition. In addition, the CIP/HPMCAS-MG system did not differ significantly from the pure drug in either study, while CIP from the HPMCAS-LG sample was only significantly more permeable than CIP under iso-pH conditions. CIP as the HCl salt had a significantly lower permeability than the other samples, with a P_e of 0.32×10^{-6} cm/s under both pH conditions. The drug from the ASD containing Eudragit L100 had a slightly lower average P_e than the pure crystalline drug in both PAMPA experiments; however, this difference was not statistically significant. The lower P_e obtained with the CIP/Eudragit L100 ASD compared to those containing HPMCAS may be due to the formation of drug/polymer complexes in solution. As shown previously by Friesen et al, upon addition to aqueous solutions, ASDs may rapidly disperse to form a number of species.[205] These can potentially include large drug/polymer aggregates, which may form a slowly dissolving amorphous precipitate, and thus reduce the concentration of free drug in solution.[205] This would be more likely to occur with CIP/Eudragit L100 due to the stronger drug-polymer interactions present in this ASD, as suggested by its particularly high T_g.

A number of studies have found that other solubility enhancing formulations such as cyclodextrins, surfactants and cosolvents decrease the permeability of drugs in both PAMPA and intestinal perfusion assays, leading to a trade-off between solubility and permeability.[31,32] According to Miller et al, preparations such as these increase the equilibrium solubility of drugs, which results in a decrease in their apparent cell membrane/intestinal lumen partition coefficient. As the permeability of a drug is directly related to this coefficient, the solubility advantage provided by these formulations is accompanied by a decrease in permeability.[31] In contrast, ASDs increase the solubility of drugs via supersaturation, which does not affect the apparent membrane/lumen partition coefficient. Amorphous formulations can therefore significantly increase the concentration of drug in solution, while also maintaining a constant effective permeability, giving them a superior solubility-permeability balance.[31,32] The results of this study are therefore in line

with those of other researchers, with all of the CIP ASDs enhancing the solubility of the drug in water and FaSSIF, without a subsequent decrease in permeability. The crystalline CIP HCl salt on the other hand significantly reduced the permeability of the drug, most likely due to greater ionization of CIP. Although the P_e of a drug is not affected by its concentration (as long as the drug is free to pass through the membrane), the increased solubility afforded by ASDs should increase the transmembrane flux of a drug, and thus may also improve its in vivo absorption.[31]

According to Tam et al, 18% of CIP is absorbed via the paracellular route at pH 6.5.[118] As the PAMPA model does not take account of paracellular transport, it is possible that the results above underestimate the in vivo absorption of CIP. PAMPA is also unable to predict active transport, and will therefore underestimate the permeability of compounds that are absorbed via drug transporters.[206] This could explain why the effective permeability of CIP reported here is lower than that obtained by others in rat in situ and Caco-2 cell studies.[118,207] While CIP is mainly absorbed by passive transport, it is also a substrate for active transporters in the intestine, such as organic anion transporting polypeptide 1A2 (OATP1A2).[208] In addition, it is a substrate for the efflux protein breast cancer resistance protein (BCRP), which reduces the bioavailability of the drug.[209] Despite this, Bermejo et al showed that for fluoroquinolones such as CIP, there was a good correlation between the results of PAMPA and that of Caco-2 and in vivo rat in situ permeability studies.[109] As the main aim of the permeability assay performed in this study was to determine whether ASD formation affects the permeability of CIP, PAMPA was suitable for this comparative analysis. However, in order to obtain a more accurate quantitative estimate of the permeability of the drug and ASDs, more representative permeability studies would be required, such as rat in situ perfusion assays, which more closely mimic the environment in vivo.

3.3.7 Bacterial Studies

The minimum inhibitory concentration (MIC) and minimum bactericidal concentration (MBC) of CIP and the ASDs in a number of bacterial species are shown in **Table 3.2**. The values that differ significantly from those of pure crystalline CIP are shown in bold. The

MBC is expected to be larger than the MIC, as a larger quantity of API is required to kill bacteria rather than just inhibit their growth. MICs ≤ 1.0 μg/ml indicate that the microorganism is susceptible to CIP, whereas MICs ≥ 2.0 μg/ml indicate resistance to this antibiotic.[210] All of the organisms used in this study can therefore be considered as sensitive to CIP, with MICs ≤ 1 μg/ml. The MIC and MBC values obtained with CIP are close to those obtained by other researchers in these species.[211–213] *E. coli* was found to be the most susceptible strain to CIP, with a MIC of 0.008–0.032 μg/ml. This was followed by *K. pneumoniae* (MIC 0.032–0.125 μg/ml), *P. aeruginosa* (MIC 0.125–1.0 μg/ml) and *S. aureus* (MIC 0.25–1.0 μg/ml). The MBCs also followed the same order of susceptibility. A drug is generally considered bactericidal if it has a MBC to MIC ratio of ≤ 4.[214] Therefore, all of the samples in this study were bactericidal, with ratios of 1–2.

The formulation of CIP as an ASD did not result in a decrease in antibacterial activity in any case. In fact, CIP/HPMCAS-MG had a significantly lower MIC and MBC in all bacterial species studied compared to the pure drug. The MIC of CIP/HPMCAS-LG was also significantly improved in *E. coli*, while its MBC decreased in both *E. coli* and *S. aureus*. As described above, these ASDs had the highest P_e in PAMPA permeability studies, whereas CIP/Eudragit L100 did not differ significantly from the pure drug. Therefore, the improved permeability of these samples may have aided the penetration of CIP into the bacterial cells, most likely via the passive diffusion route through the cell membranes.

Table 3.2. Minimum Inhibitory Concentration and Minimum Bactericidal Concentration of Ciprofloxacin and ASDs in Various Bacteria[a]

Sample	***S. aureus***	***E. coli***	***P. aeruginosa***	***K. pneumoniae***
Minimum Inhibitory Concentration (μg/ml)				
Crystalline CIP	1	0.032	0.5	0.125
CIP/Eudragit L100	1	0.032	0.5–1	0.125
CIP/HPMCAS-LG	0.5	**0.008–0.016**	0.25–0.5	0.063–0.125
CIP/HPMCAS-MG	**0.25–0.5**	**0.008–0.016**	**0.125–0.25**	**0.032–0.063**
Minimum Bactericidal Concentration (μg/ml)				
CIP	1.0–2.0	0.032–0.064	1.0	0.25
CIP/Eudragit L100	1	0.032	1.0	0.25
CIP/HPMCAS-LG	**0.5**	**0.016**	1.0	0.125
CIP/HPMCAS-MG	**0.5**	**0.016**	**0.25–0.5**	**0.063–0.125**

[a]The values shown in bold differ significantly from those of pure crystalline CIP.

3.4 Conclusions

Amorphous solid dispersions are one formulation option for poorly soluble drugs, however the polymers used in these preparations must be carefully chosen. This work has shown that an acidic polymer is necessary to produce CIP ASDs by ball milling, as it enables the formation of stabilizing ionic interactions between the two components. These bonds resulted in high T_g values, above those predicted by the Gordon-Taylor equation. While the CIP ASDs crystallized quickly under accelerated stability conditions of 40 ºC/75% RH, they remained amorphous following exposure to humidity levels of up to 90% at 25 ºC during DVS analysis. Therefore, although the stabilizing effects of the polymers were not sufficient to prevent crystallization of CIP when exposed to a combination of high heat and humidity, these ASDs may remain stable if stored at ambient temperatures.

The ASDs chosen for further examination showed superior solubility in water and FaSSIF compared to the pure drug, which can be attributed to their amorphous nature, rather than

any effect on pH. The polymer content of the ASDs also enabled the maintenance of supersaturation for at least two hours in most cases. In addition, no decrease in the passive permeability of CIP occurred with any of these ASDs, while a modest increase in effective permeability was seen with the ASD containing HPMCAS-LG. In contrast, the crystalline CIP HCl salt significantly decreased the permeability of the drug, highlighting the benefit of amorphous polymeric formulations in this regard. In line with the results of the permeability assay, the formulation of CIP as an ASD did not reduce its antibacterial potency in the bacterial species studied, and a decrease in MIC and MBC was also obtained with the ASDs containing HPMCAS. This indicates that ASD formation with HPMCAS increases the proportion of CIP capable of diffusing through bacterial cell membranes. Therefore, ASDs may be a viable alternative for formulating CIP with improved solubility, bioavailability and antibacterial activity.

Chapter 4: Polymer/Amorphous Salt Solid Dispersions of Ciprofloxacin

4.1 Introduction

As discussed in Chapter 1, a number of crystalline CIP salts containing various acidic counterions have been produced, all of which significantly increased the solubility of the drug.[123,125,215] Removal of the dipole in zwitterions such as CIP via salt formation will often result in improved solubility, due to a decrease in crystal lattice energy.[216] Salts may also increase the solubility of drugs by altering the pH as they dissolve.[217] For the reasons discussed in the previous chapters, amorphous salts could be expected to be more soluble than their crystalline counterparts. However, there is also a risk that they will crystallize during storage or dissolution, and thus negate their solubility advantage. For instance, Paluch et al prepared amorphous CIP/succinic acid salts with a 1:1 (CS 1:1) and 2:1 (CS 2:1) molar ratio. Although these amorphous salts increased the solubility of CIP in water at 37 ^{o}C by over 300 times, both samples crystallized during DVS and solubility studies.[125] In contrast, the polymeric ASDs discussed in Chapter 3 either remained amorphous during the same analyses, or crystallized to a small degree.

Following the promising results obtained with the binary ASDs of Chapter 3 and the CS 1:1 and CS 2:1 salts, the main aim of this study was to determine whether a combination of these two approaches could improve the stability of these salts. Polymer/amorphous salt solid dispersions, consisting of the CS 1:1 or CS 2:1 salt dispersed in 20–60 % (w/w) PVP or Soluplus, were produced by spray drying and ball milling. The stability of these ASDs during DVS analysis and long-term storage at RT was then investigated. Patel et al used a similar approach to improve the physical properties of the amorphous tenoxicam/arginine 1:2 salt. The authors found that the formulation of spray dried ASDs with 10–50% (w/w) PVP resulted in much higher T_g's than the pure 1:2 amorphous salt, and also helped to maintain supersaturation during solubility studies.[218] Ternary ASDs consisting of an indomethacin-meglumine salt plus PVP have also been produced by Telang et al by solvent evaporation. Although these samples were found to have greater physical stability than a binary indomethacin/PVP ASD, no studies directly comparing the stability of the ternary ASD and the amorphous indomethacin-meglumine salt were carried out.

The miscibility and interactions between the CIP succinate salts and the polymers were also of interest in this study, as ASDs will have greater stability if their components interact specifically with one another and are mixed on a molecular level.[53] FTIR was used to investigate the intermolecular interactions present in the ternary ASDs, and their miscibility was examined by DSC and IGC. In addition, the solubility of the ASDs in water and simulated biological fluids was compared to that of the amorphous CS 1:1 and CS 2:1 salts, in order to determine whether the addition of polymer offered any advantages in this regard. Finally, the effect of salt formation on the permeability of CIP was determined using the PAMPA model.

4.2 Experimental Section

4.2.1 Materials

Succinic acid was obtained from Aldrich, Milwaukee, USA. The details of all other materials and solvents used in this study are listed in Chapter 3.

4.2.2 Methods

4.2.2.1 Sample Preparation

4.2.2.1.1 Ball Milling

Ball milling was conducted using the same apparatus and procedure described in Chapter 2. Amorphous ciprofloxacin hemisuccinate (CS 1:1) and ciprofloxacin succinate (CS 2:1) salts were produced by milling CIP and succinic acid in a 1:1 and 2:1 molar ratio, respectively, for a total of 6 hours at RT. Polymer/salt ASDs were produced by adding 40% (w/w) PVP or Soluplus to either of these salts, and milling for a further 60 min in total.

4.2.2.1.2 Spray Drying

Ternary ASDs were produced using the same apparatus and procedure described in Chapter 2. 2% (w/v) solutions of a 1:1 molar ratio of CIP and succinic acid, plus 20–60% (w/w) PVP

were prepared in water. This was also repeated using 40% (w/w) Soluplus. The solutions were then spray dried with an inlet temperature of 150 ºC.

4.2.2.2 Solid-State Characterization

4.2.2.2.1 Powder X-ray Diffraction

PXRD was performed as described in Chapter 2.

4.2.2.2.2 Solid-State Fourier Transform Infrared Spectroscopy

FTIR was performed as described in Chapter 2.

4.2.2.2.3 Differential Scanning Calorimetry

DSC was performed as described in Chapter 3. All measurements were carried out in triplicate.

4.2.2.2.4 Thermogravimetric Analysis

TGA was performed as described in Chapter 2.

4.2.2.3 Determination of Solubility Parameters Using Inverse Gas Chromatography (IGC)

IGC was carried out on the CS 1:1 and CS 2:1 amorphous salts using a Surface Measurement Systems (SMS) iGC 2000 (London, UK) equipped with a flame ionization detector (FID). Samples were sieved through a 180 μm mesh and packed into a glass column. The carrier gas used was helium, with a flow rate of 5 ml/min. The column was held at a temperature of 30 ºC (303 K). Methane was used as a non-interacting internal standard for dead time correction. Nine different solvents were used in this study. These were classified according to the type of interactions they can form with the stationary phase. Nonane, octane and heptane (the n-alkanes) may form dispersion interactions; acetone, dichloromethane, chloroform and ethyl acetate form polar bonds; and ethanol and 2-propanol participate in hydrogen bonding. The retention time of each solvent was determined by measuring the peak maximum. The solubility parameters of the salts were calculated using the method described by Kitak et al:[72]

$$\chi_{1,2}^{\infty} = \ln\left(\frac{273.15R}{P_1^0 V_g M_{r,1}}\right) - \frac{P_1^0}{RT}(B_{11} - V_1) + \ln\left(\frac{\rho_1}{\rho_2}\right) - \left(1 - \frac{V_1}{V_2}\right) \quad (4.1)$$

$\chi_{1,2}^{\infty}$ is the interaction parameter, R is the gas constant, T is the temperature, P_1^0 is the saturated vapor pressure of the solvent, V_g is the specific retention volume, $M_{r,1}$ is the molecular mass of the solvent, B_{11} is the second virial coefficient, V_1 and V_2 are the molar volumes of the solvent and solute respectively, and ρ_1 and ρ_2 are their respective densities. The molar volumes of CS 1:1 and 2:1 were estimated by dividing their molecular weight by their density.

$\chi_{1,2}^{\infty}$ is linearly correlated to δ_{1i} as follows:[72]

$$\frac{\delta_{1i}^2}{RT} - \frac{\chi_{(1,2)i}^{\infty}}{V_1} = \frac{2\delta_2}{RT}\delta_{1i} - \left(\frac{\delta_2^2}{RT} + \frac{\chi_s^{\infty}}{V_1}\right) \quad (4.2)$$

δ_2 is the solubility parameter of the solute, which can be found from the intersection of the straight line with the y-axis (equal to the term in brackets in equation 4.2).

Partial solubility parameters may be calculated using the following equations:[72]

$$\delta_d = \frac{m_{alkanes} RT}{2} \quad (4.3)$$

$$\delta_p = \frac{(m_{polar} - m_{alkanes})RT}{2} \quad (4.4)$$

$$\delta_h = \frac{(m_{h-bond} - m_{alkanes})RT}{2} \quad (4.5)$$

$m_{alkanes}$, m_{polar}, and $m_{h\text{-}bond}$ are the slopes obtained from the group of alkane solvents, polar solvents, and the solvents that form hydrogen bonds, respectively. R is the gas constant, and T is temperature.

Following IGC analysis CS 1:1 and CS 2:1 were analyzed by PXRD.

4.2.2.4 Dynamic Vapor Sorption

DVS was carried out using the same apparatus and procedure described in Chapter 2. Following DVS analysis the samples were analyzed by PXRD.

4.2.2.5 Long-term Stability Study

The ASDs and amorphous CS 1:1 and 2:1 salts were stored at RT (22–25 ºC) under dry storage conditions in a desiccator (silica gel). Samples of each powder were taken at regular intervals for a period of 12 months. PXRD was used to determine whether crystallization had occurred in any of the samples.

4.2.2.6 Dynamic Solubility Studies

Solubility studies were performed as described in Chapter 3.

4.2.2.7 UV Spectrophotometry

UV analysis was carried out as described in Chapter 3.

4.2.2.8 Parallel Artificial Membrane Permeability Assay

PAMPA was carried out as described in Chapter 3. The samples were dissolved in PBS pH 7.4, at concentrations of 70–200 µg/ml.

4.2.2.9 High-Performance Liquid Chromatography

HPLC was carried out as described in Chapter 3.

4.2.2.10 Statistical Analysis

Statistical analysis was carried out as described in Chapter 2.

4.3 Results and Discussion

4.3.1 Production of Polymer/Amorphous Salt Solid Dispersions

Amorphous CS 1:1 and CS 2:1 were previously produced by Paluch et al via spray drying and ball milling respectively,[125] whereas in this study ball milling was used to prepare both amorphous salts. Six hours of high intensity milling (600 rpm) was required to obtain fully X-ray amorphous powders. Like the polymeric ASDs discussed in the previous chapter, both of these amorphous salts were yellow in color. PVP was chosen as the primary polymer to

include in the CIP/succinic acid ASDs as it is hydrophilic and amorphous, and is commonly used to produce ASDs of poorly soluble drugs.[51] However, when a 1:1 molar ratio of CIP and succinic acid, plus 20–60% (w/w) PVP, were ball milled (BM) together for 4 hours, a partially crystalline product was obtained, with PXRD peaks primarily matching those of CIP, along with one small peak of the CS 1:1 salt at approximately 5.5 2θ degrees (**Figure A.3.1**). The sample containing 20% (w/w) PVP possessed the lowest degree of crystallinity following milling, as detected by PXRD, whereas more crystalline products were obtained when the proportion of PVP was increased to 40 or 60% (w/w). The polymer therefore appears to have hindered the formation and amorphization of the salt, although the degree of crystallinity (by PXRD) of the components did decrease over time during milling. Similarly, as described in Chapter 3, binary ASDs of CIP could not be formed with neutral polymers such as PVP and Soluplus, as the interactions between the drug and excipient were too weak to yield a fully amorphous solid dispersion.

As initial milling of all three individual starting materials was unsuccessful, CIP and succinic acid were then pre-milled, in order to form the amorphous 1:1 or 2:1 salt. These salts were subsequently milled with 40% (w/w) PVP for a further 60 min (BM CS 1:1/40% PVP and BM CS 2:1/40% PVP). The CS 1:1 salt was also milled with Soluplus for one hour (BM CS 1:1/40% Soluplus). Like PVP, this polymer is amorphous, and has been used successfully to form ASDs of other poorly soluble drugs by ball milling [219]. As can be seen in **Figure 4.1**, the use of pre-milling resulted in an X-ray amorphous product for each of these systems.

Spray drying was also used to produce ASDs containing CS 1:1. The required amount of succinic acid was first dissolved in warm water, followed by CIP, and then various quantities of PVP. Due to the poor solubility of CIP, solutions of CS 2:1 could not be prepared, and thus milling was the only suitable method of production for this salt. CS 1:1 with 20–60% (w/w) PVP resulted in fully X-ray amorphous ASDs (labelled as SDD CS 1:1/20% PVP, 40% PVP and 60% PVP, **Figure 4.1**). However, when a solution of CS 1:1 with 40% (w/w) Soluplus was spray dried (SDD), a partially crystalline product was obtained, as shown by PXRD and DSC (**Figure A.3.2**). The PXRD diffractogram of this sample contained a number of peaks corresponding to the CS 1:1 salt, as well as the most intense peak of CIP and succinic

acid at approximately 25–26 2θ degrees. Therefore, the process used to form the ASDs, as well as the type and proportion of polymer, affects the solid state of the product.

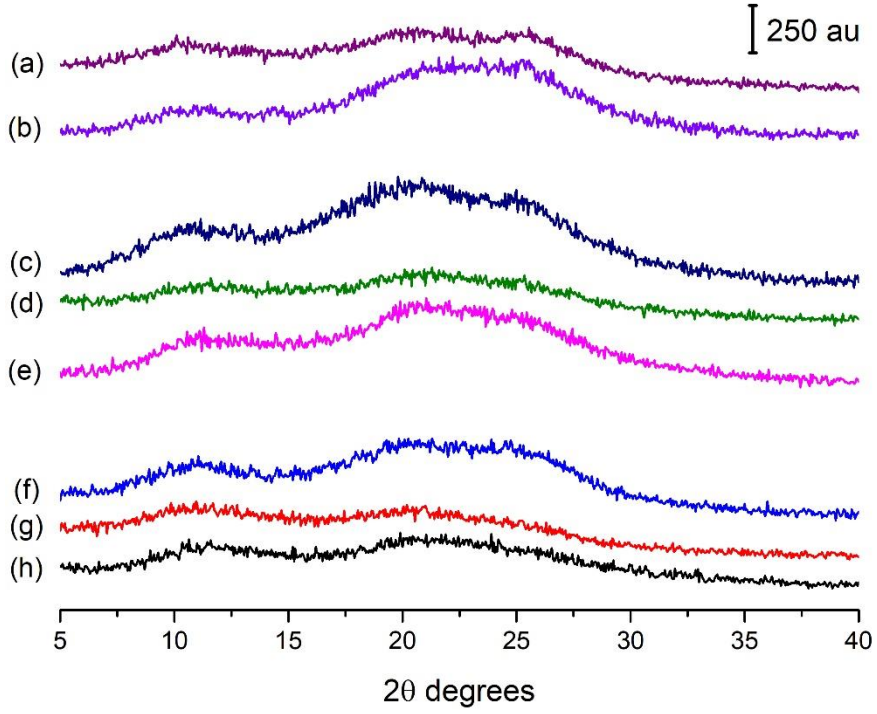

Figure 4.1. PXRD analysis of (a) CS 1:1 (b) CS 2:1 (c) BM CS 1:1/40% Soluplus (d) BM CS 2:1/40% PVP (e) BM CS 1:1/40% PVP (f) SDD CS 1:1/20% PVP (g) SDD CS 1:1/40% PVP and (h) SDD CS 1:1/60% PVP.

4.3.2 Solid-State Characterization of Polymer/Amorphous Salt Solid Dispersions

4.3.2.1 Solid-State Fourier Transform Infrared Spectroscopy

The FTIR spectra of the ASDs, CS 1:1, CS 2:1 and the starting materials are shown in **Figure 4.2**. As was the case with the binary ASDs of Chapter 3, the peaks corresponding to the asymmetric and symmetric vibrations of the carboxylate ion of CIP are absent from the spectra of these polymer/salt ASDs. Instead, a peak can be seen at 1721–1727 cm^{-1}. Therefore, the carboxylic acid of CIP is protonated in these ASDs, which was also found to be the case for the CS 1:1 and CS 2:1 salts.[125] The fact that the peak corresponding to the

C=O stretch of CIP's ketone group shifted from 1618 cm^{-1} to 1627–1629 cm^{-1} in the spectra of the ASDs provides further confirmation of the protonated state of the carboxylic acid of CIP, as previously discussed. Regarding the ionization state of the piperazine amino group of CIP, the spectra of the ASDs contain a broad peak at approximately 2490 cm^{-1}, which can be assigned to the NH_2^+ stretching vibrations of this group.[168] This positively charged group forms an ionic bond with the carboxylate groups of succinic acid within the salts.[125]

I.

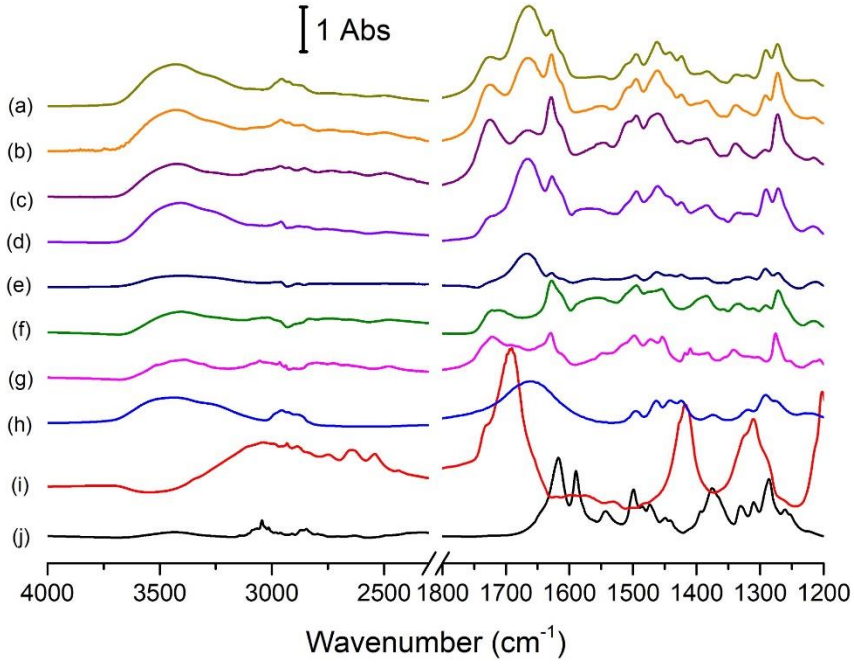

II.

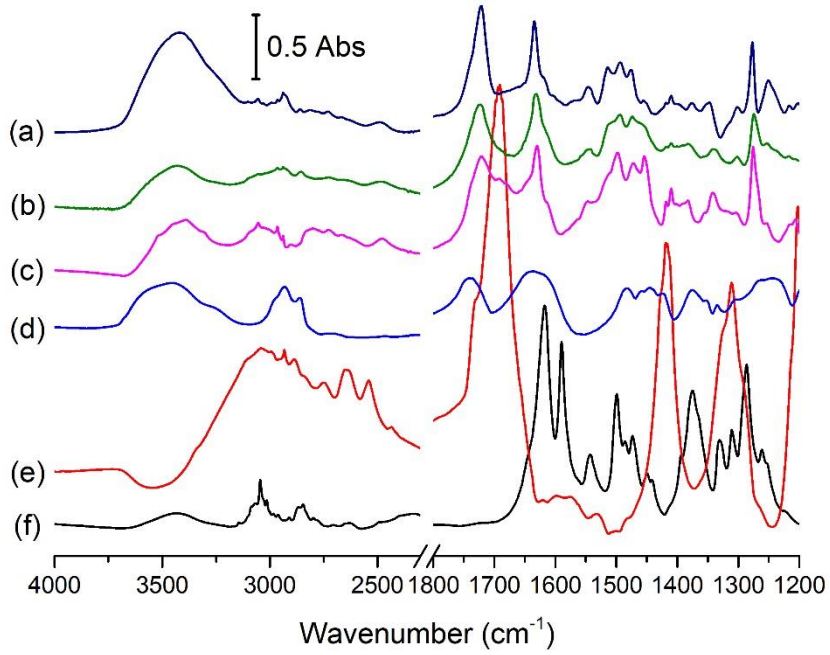

Figure 4.2. FTIR spectra of CIP ASDs. I. Containing PVP: (a) SDD CS 1:1/60% PVP (b) SDD CS 1:1/40% PVP (c) SDD CS 1:1/20% PVP (d) BM CS 2:1/40% PVP (e) BM CS 1:1/40% PVP (f) CS 2:1 (g) CS 1:1 (h) PVP (i) succinic acid and (j) CIP. II. Containing Soluplus: (a) BM CS 1:1/40% Soluplus (b) CS 1:1/40% Soluplus PM (c) CS 1:1 (d) Soluplus (e) succinic acid and (f) CIP.

The spectrum of PVP shows a broad peak from about 1600–1750 cm^{-1}, with a maximum at 1659 cm^{-1}, due to the C=O stretch of the pyrrolidone carbonyl group. This is the most likely functional group of PVP to participate in hydrogen bonding, and the formation of such interactions is usually associated with a shift in the corresponding peak to lower wavenumbers.[40] Chen et al observed a peak at 1657 cm^{-1} in the FTIR spectrum of PVP, even after it was dried under vacuum at 40 ºC for 24 hours, due to the participation of this group in hydrogen bonding with absorbed water. When the polymer was more thoroughly dried this peak shifted to 1667 cm^{-1}.[220] The carbonyl stretch of PVP also shifted to 1663–1667 cm^{-1} in the spectra of the ASDs (**Figure 4.2.I**), which may be due to a reduction in the hydrogen bonding of PVP's carbonyl group with water molecules in the ASDs. Similarly, the carbonyl peak of the polymer was found to shift to higher wavenumbers in nimesulide/PVP ASDs, as the more hydrophobic environment of the ASD resulted in a decrease in PVP-water hydrogen

bonds.[56] The fact that the carbonyl peak of PVP did not shift to lower wavenumbers in the spectra of the ASDs suggests that this polymer did not form hydrogen bonds with the CS 1:1 and 2:1 salts.

The peaks at 1637 cm^{-1} and 1741 cm^{-1} in the spectrum of Soluplus correspond to the C=O stretch of the caprolactam carbonyl and ester carbonyl, respectively. These bands are overlapped with those of the ketone and COOH carbonyl stretches of CIP in the spectrum of BM CS 1:1/40% Soluplus, with the combined peaks appearing at 1634 and 1721 cm^{-1}, respectively (**Figure 4.2.II**). This makes it difficult to say with any certainty whether the carbonyl peaks of Soluplus are shifted in this ASD. However, as the caprolactam peaks of the ASD and pure polymer differed by only 3 cm^{-1}, this shift may simply be due to experimental error. Regarding the peak at 1721 cm^{-1} in the spectrum of the ASD, a slight shoulder was visible at ~ 1738 cm^{-1}, which may be assigned to the ester carbonyl stretch of the polymer. Therefore, neither carbonyl peak of Soluplus underwent significant shifts upon ASD formation. In addition, upon comparison of the FTIR spectra of the ASD and a physical mixture, containing the CS 1:1 amorphous salt and Soluplus in the same ratio as in the ASD, no significant differences were seen. Therefore, like PVP, no evidence of hydrogen bonding between CS 1:1 and Soluplus could be detected in this ASD.

4.3.2.2 Thermal Analysis and Estimation of Component Miscibility

DSC thermograms of the ASDs are shown in **Figure 4.3**, and a summary of their thermal properties is given in **Table 4.1**. The T_g of CS 1:1 was detected at 86.7 ± 0.5 ^oC, which is identical to the T_g of pure amorphous CIP. The T_g of CS 2:1 on the other hand was only 69.3 ± 1.0 ^oC. The low T_g of the CS 1:1 and 2:1 salts may be partially attributed to the presence of succinic acid, whose T_g is believed to be less than 30 ^oC.[221]

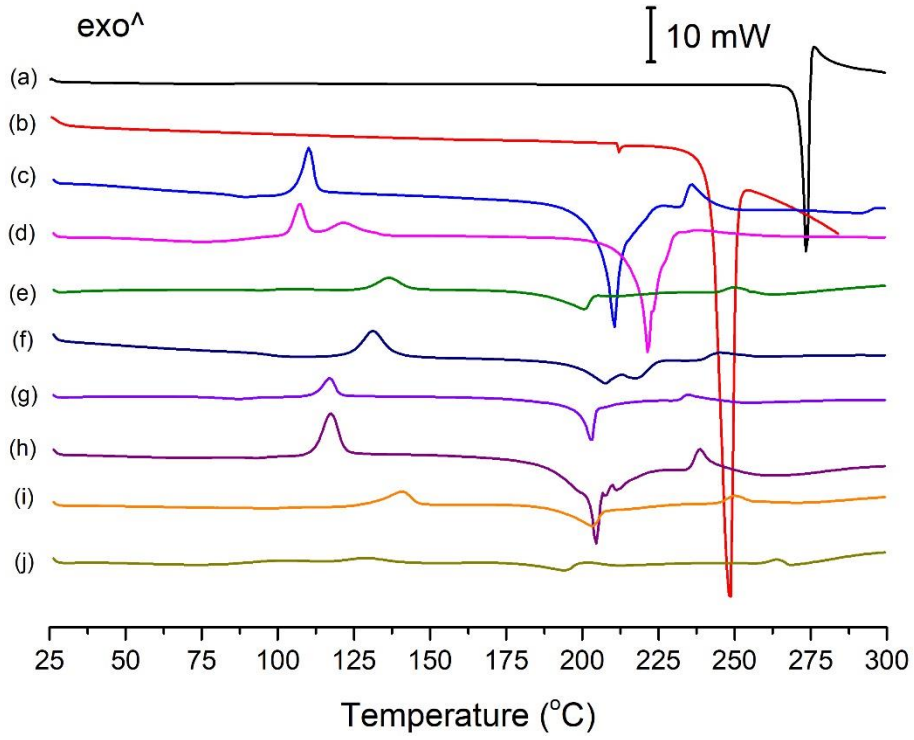

Figure 4.3. DSC thermograms of (a) CIP (b) succinic acid (c) CS 1:1 (d) CS 2:1 (e) BM CS 1:1/40% PVP (f) BM CS 2:1/40% PVP (g) BM CS 1:1/40% Soluplus (h) SDD CS 1:1/20% PVP (i) SDD CS 1:1/40% PVP and (j) SDD CS 1:1/60% PVP.

Table 4.1. Thermal Properties of CIP Amorphous Salts and ASDs

Sample	**T_g (°C)**	**Crystallization onset (°C)**	**Crystallization peak (°C)**
CS 1:1	86.7 ± 0.5	105.3 ± 1.2	110.3 ± 1.0
CS 2:1	69.3 ± 1.0	103.8 ± 0.5/ 115.3 ± 0.4	107.6 ± 0.2/ 121.8 ± 0.1
BM CS 1:1/40% PVP	91.2 ± 0.8	129.1 ± 0.2	136.9 ± 0.2
BM CS 2:1/40% PVP	98.4 ± 0.9	125.2 ± 0.8	132.3 ± 0.7
BM CS 1:1/40% Soluplus	81.7 ± 0.8	112.6 ± 0.4	117.5 ± 0.4
SDD CS 1:1/20% PVP	90.2 ± 0.1	111.3 ± 1.2	116.7 ± 1.4
SDD CS 1:1/40% PVP	93.0 ± 0.8	130.6 ± 0.0	140.8 ± 0.1
SDD CS 1:1/60% PVP	122.4 ± 1.6	145.0 ± 0.3	159.2 ± 1.0

DSC is commonly used to determine whether the components of an ASD are miscible or not. A single T_g was seen in the thermograms of all of the ASDs. This suggests that the amorphous salts are miscible with PVP and Soluplus, and that phase separation does not occur in the ASDs.[41] The T_g's of PVP K17 and Soluplus have been reported as 125.2 and 72 ºC, respectively.[219,222] If the two components of an ASD are miscible, its T_g should be located in between the T_g of the pure drug (or salt in this case) and the polymer,[41] and this was found to be the case for all of the ASDs. With the ASDs containing PVP this resulted in an increase in T_g relative to the relevant pure amorphous salt, whereas the T_g of BM CS 1:1/40% Soluplus was approximately 5 ºC lower than CS 1:1, due to the comparatively low T_g of the polymer. An additional indication of miscibility in the spray dried samples is that as the proportion of PVP increased, so did the T_g.

Another common approach for determining the miscibility of the components in an ASD is to calculate their solubility parameters. As mentioned in Chapter 1, the group contribution method may be used to find the solubility parameters of drugs and polymers, however it will not give accurate results for salts.[72] The total solubility parameters (δ_t) of the amorphous CS 1:1 and 2:1 salts were therefore determined by IGC, while those of the polymers were obtained from literature. The δ_t values were 19.9, 20.3, 22.7 and 19.4 $MPa^{0.5}$ for CS 1:1, CS 2:1, PVP[72] and Soluplus,[223] respectively. According to Greenhalgh et al, a difference of less than 7 $MPa^{0.5}$ between the solubility parameters of two components indicates that they are miscible, whereas if they differ by more than 10 $MPa^{0.5}$ they are expected to be immiscible.[71] These results therefore confirm the miscibility of the amorphous salts and the polymers, with a δ_t difference of $\leq$ 2.8 $MPa^{0.5}$ being obtained in each case.

The DSC thermograms of all of the ASDs contained exothermic peaks due to cold crystallization of their amorphous content. It is clear from **Figure 4.3** that the CS 2:1 amorphous salt differs from the other samples by the presence of two crystallization exotherms, peaking at 107.6 ºC and 121.8 ºC. PXRD analysis was carried out on the sample immediately following each crystallization event. Identical PXRD peaks were obtained in both cases, matching those of crystalline anhydrous CS 2:1;[125] however, they became more intense after the second crystallization event. Similar double exothermic peaks have been reported for a number of drugs following milling. Trasi et al attributed the first peak in the

thermogram of milled griseofulvin to the surface crystallization of particles that had nuclei on their surfaces, while the second peak was due to crystallization of the bulk of these particles, as well as particles that were not nucleated.[103] Therefore, the occurrence of two crystallization peaks in the thermogram of CS 2:1 indicates that the particles may have contained a number of surface crystal nuclei following milling, which were too small to be detected by PXRD.

All of the ASDs crystallized at higher temperatures than the corresponding salt, which can be attributed to the presence of polymer. The long chains of polymers can delay crystallization by sterically hindering the diffusion of drug molecules and formation of a crystal lattice, and the higher the proportion of polymer in an ASD, the more stable it should be to crystallization.[52] Indeed, as the ratio of PVP in the SDD dispersions increased, a linear increase in their crystallization temperature was observed. The high T_g of PVP should help to stabilize the ASDs, by reducing the molecular mobility and thus crystallization tendency of the salt.[56] The ASD containing Soluplus crystallized at a slightly lower temperature than those containing 40% (w/w) PVP; however, this is expected considering the significantly lower T_g of this polymer.

The method of production had a small but significant effect on the crystallization temperature of the ASDs containing CS 1:1 and 40% (w/w) PVP, with that of the SDD sample being almost 4 ºC higher than BM CS 1:1/40% PVP (*p*-value = 0.001). In contrast, no significant difference in the T_g values of BM CS 1:1/40% PVP and SDD CS 1:1/40% PVP was found (*p*-value for *t* test = 0.06). A reduction in crystallization temperature is expected for milled samples, as they contain a lot of exposed surfaces. Molecules located at the surface of particles possess more molecular mobility and are less confined than those in the bulk, which allows them to crystallize more easily.[103] Ball milled solids generally possess higher surface energy than ASDs produced by other methods, which reduces the activation energy for nucleation and crystal growth, resulting in a lower crystallization temperature.[103]

PMs consisting of the amorphous CS 1:1 and CS 2:1 salts and appropriate ratios of polymers were also analyzed by DSC, and their thermograms and thermal properties are shown in Figure **A.3.3** and **Table A.3.1**. Individual two-sample *t* tests were used to compare the results

obtained with the ASDs and corresponding PMs. In each case, the ASDs showed a statistically significantly higher T_g and lower melting endotherm than the corresponding PMs (p-value < 0.05). A statistically significantly higher crystallization temperature was also obtained for all the ASDs compared to the PMs, except for SDD CS 1:1/20% PVP, which was almost statistically significant (p = 0.07). Unlike the ASDs, the PMs did not offer an increase in T_g relative to the pure amorphous salts, and only the PM containing CS 2:1 and 40% (w/w) PVP demonstrated a statistically significant increase in crystallization temperature. These results indicate that simply mixing the amorphous salts with polymer offers negligible benefits in terms of thermal stability. Formulation as an ASD on the other hand significantly increases the T_g and crystallization temperature of CS 1:1 and CS 2:1, as it allows more intimate mixing of the components. The ASDs would therefore be expected to have higher physical stability during storage than the corresponding amorphous salts.

The water content and thermal degradation of the ASDs was investigated using TGA (**Figure 4.4**). Between 25 and 120 ºC, all of the samples underwent mass loss due to water evaporation. The greatest water loss was obtained with BM CS 2:1/40% PVP and BM CS 1:1/40% PVP, equal to 4.5 and 4.4%, respectively. As the proportion of PVP increased in the SDD samples, so did the degree of water loss, due to the high hygroscopicity of this polymer. A smaller mass loss of 2.1% occurred between 25–120 ºC with the ASD containing Soluplus, suggesting that this polymer is less hygroscopic than PVP. Although they did not contain any polymer, the amorphous CS 1:1 and CS 2:1 salts were found to have a water content of 4.25 and 4.1%, respectively. In addition to water loss, TGA analysis also showed that all of the samples undergo significant thermal degradation above ~200 ºC, as seen with the binary polymeric CIP ASDs discussed in Chapter 3. The thermograms of each of the amorphous samples contained broad endotherms above 180 ºC due to melting accompanied by decomposition (**Figure 4.3**).

TGA Mass Loss of Polymer/Salt ASDs

Sample	Total Mass Loss
CS 1:1	19.6%
CS 2:1	11.1%
BM 1:1/40% Soluplus	19%
BM 2:1/40% PVP	12.6%
BM 1:1/40% PVP	17.7%
SDD 1:1/20% PVP	15.3%
SDD 1:1/40% PVP	16%
SDD 1:1/60% PVP	15.1%

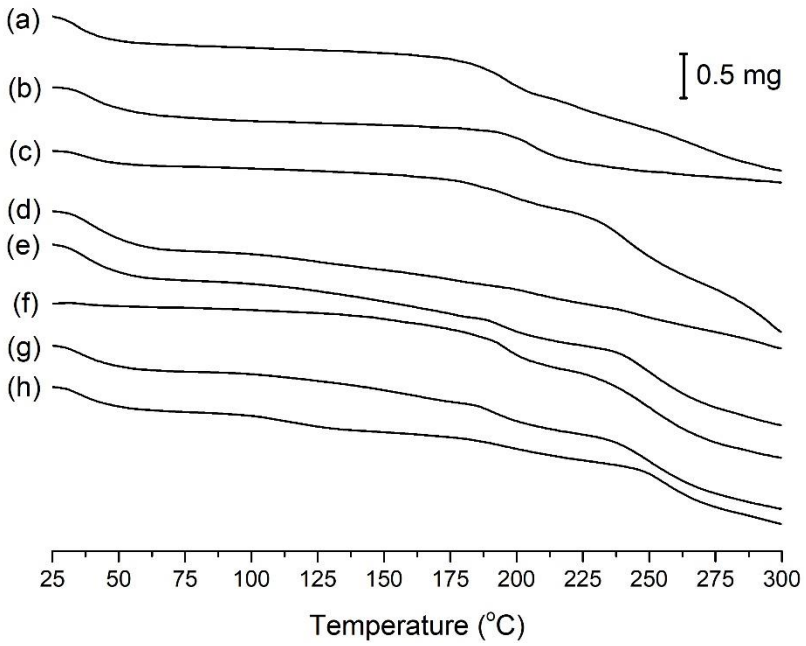

Figure 4.4. TGA analysis of (a) CS 1:1 (b) CS 2:1 (c) BM CS 1:1/40% Soluplus (d) BM CS 2:1/40% PVP (e) BM CS 1:1/40% PVP (f) SDD CS 1:1/20% PVP (g) SDD CS 1:1/40% PVP and (h) SDD CS 1:1/60% PVP. The total mass loss obtained at 300 ºC for each sample is also listed.

4.3.3 Stability Studies

The irregular arrangement of molecules in amorphous solids enables the absorption of large quantities of water, which was shown to be the case with all of the ASDs during DVS analysis (**Figure 4.5**). SDD CS 1:1/60% PVP absorbed the highest amount of water (37.8%), followed by BM CS 2:1/40% PVP (29.1%). The smallest change in mass was obtained with SDD 1:1/20% PVP (15.4%) and BM CS 1:1/40% Soluplus (15.9%). SDD and BM CS 1:1/40% PVP had similar mass changes of 28.0 % and 26.1% (w/w) respectively; therefore the method of production did not have a major effect on the water uptake behavior of these samples. In comparison to the ASDs, the mass of the amorphous CS 1:1 and CS 2:1 salts increased by approximately 10% during DVS analysis.[125] Therefore, the significantly larger water uptake of the ASDs can be attributed to the presence of hygroscopic polymer. A large degree of water absorption is expected in samples containing a molar excess of PVP monomer,[40] which was the case in all of the ASDs studied here.

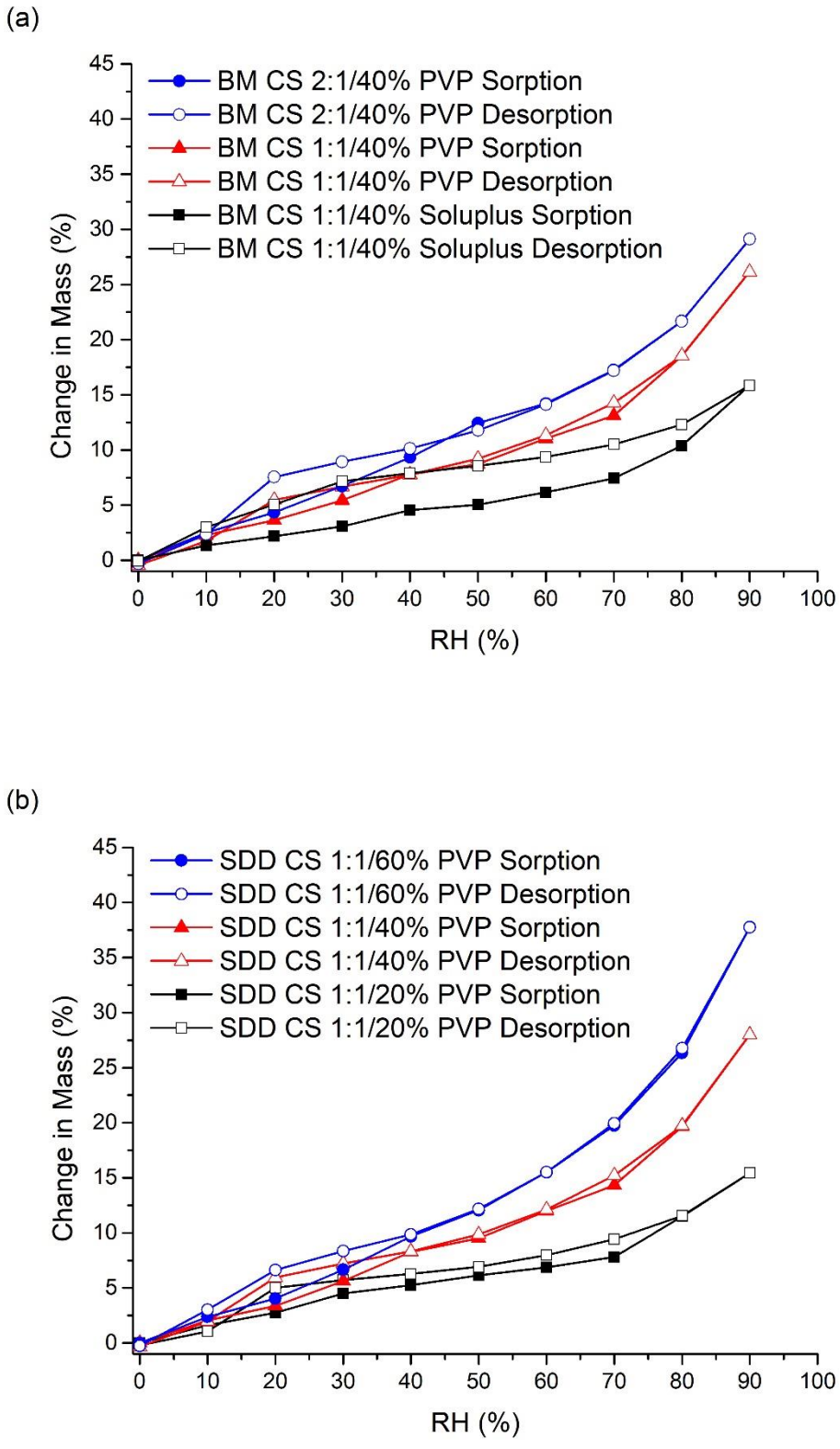

Figure 4.5. DVS analysis of polymer/salt ASDs produced by (a) ball milling and (b) spray drying.

The isotherm of BM CS 1:1/40% Soluplus shows a large degree of hysteresis. This indicates that water absorbs into the bulk of the particles, and that the diffusion of water from the surface to the interior is faster than diffusion in the opposite direction.[224] In contrast, only a small amount of hysteresis was seen with the PVP-containing ASDs, suggesting that water is mainly adsorbed to the surface of particles in these samples.

PXRD analysis of the samples following a full DVS cycle (at 0–90–0% RH) revealed that all the ASDs containing CIP and succinic acid in a 1:1 molar ratio crystallized as anhydrous CS 1:1, while BM 2:1/40% PVP formed anhydrous crystalline CS 2:1 (**Figure 4.6**). DVS analysis of the pure amorphous CS 1:1 and CS 2:1 salts resulted in the crystallization of CS 1:1 trihydrate and CS 2:1 tetrahydrate, respectively, at 40–50% RH. The latter salt then converted to the respective anhydrate during the dehydration cycle.[125] All of the ASDs studied here also appear to crystallize during the sorption stage at 40–50% RH. Therefore, it can be concluded that the presence of polymer did not improve the physical stability of the amorphous salts in high humidity conditions.

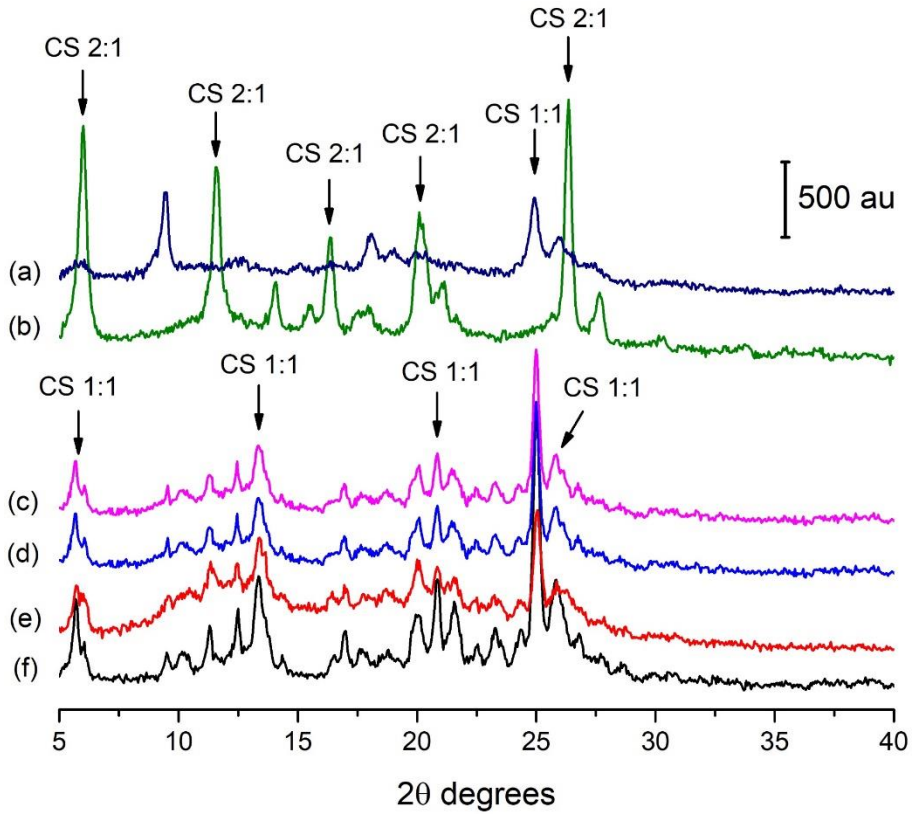

Figure 4.6. PXRD following DVS analysis of (a) BM CS 1:1/40% Soluplus (b) BM CS 2:1/40% PVP (c) BM CS 1:1/40% PVP (d) SDD CS 1:1/60% PVP (e) SDD CS 1:1/40% PVP and (f) SDD CS 1:1/20% PVP. The arrows point to the most prominent peaks of anhydrous CS 1:1 and CS 2:1.

Long-term stability studies were also carried out on the ASDs at RT (22–25 ^{o}C) under dry conditions. All of the ASDs containing PVP remained X-ray amorphous for at least 12 months, while a small peak appeared at 25.0 2θ degrees in the PXRD pattern of BM CS 1:1/40% Soluplus after 10 months, corresponding to the most prominent peak of crystalline anhydrous CS 1:1. This ASD therefore appears to be somewhat less stable than those containing PVP, which could be expected given its correspondingly lower T_g. In contrast, a small peak appeared in the PXRD pattern of CS 1:1 after only one month, and after two months both amorphous salts were partially crystalline, with peaks matching those of the corresponding anhydrous CIP succinate salts.[125] These peaks then grew in intensity over time due to increasing crystalline content (**Figure 4.7**).

(i)

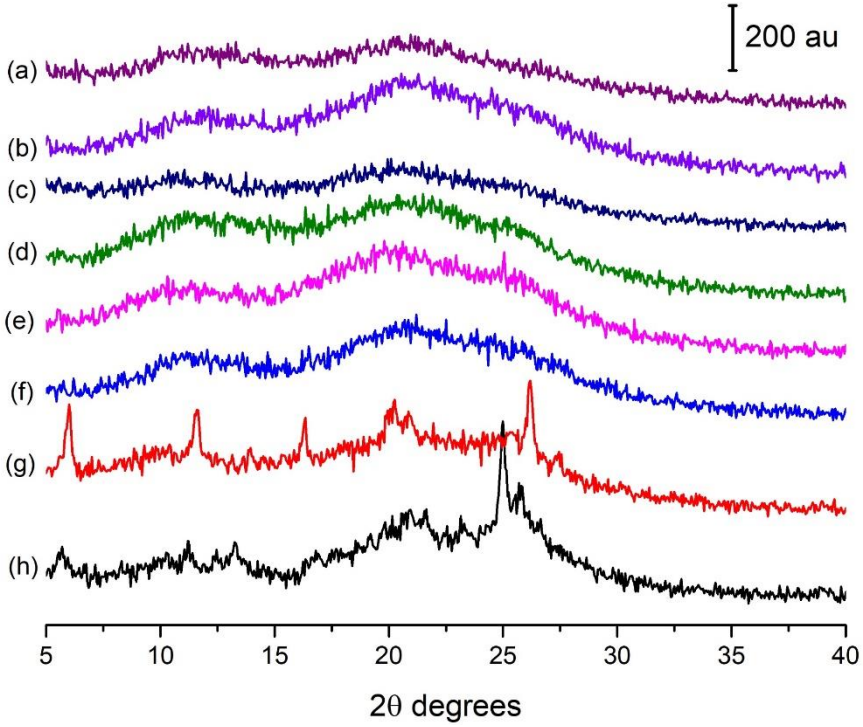
200 au
(a)
(b)
(c)
(d)
(e)
(f)
(g)
(h)
5
10
15
20
25
30
35
40
2θ degrees

(ii)

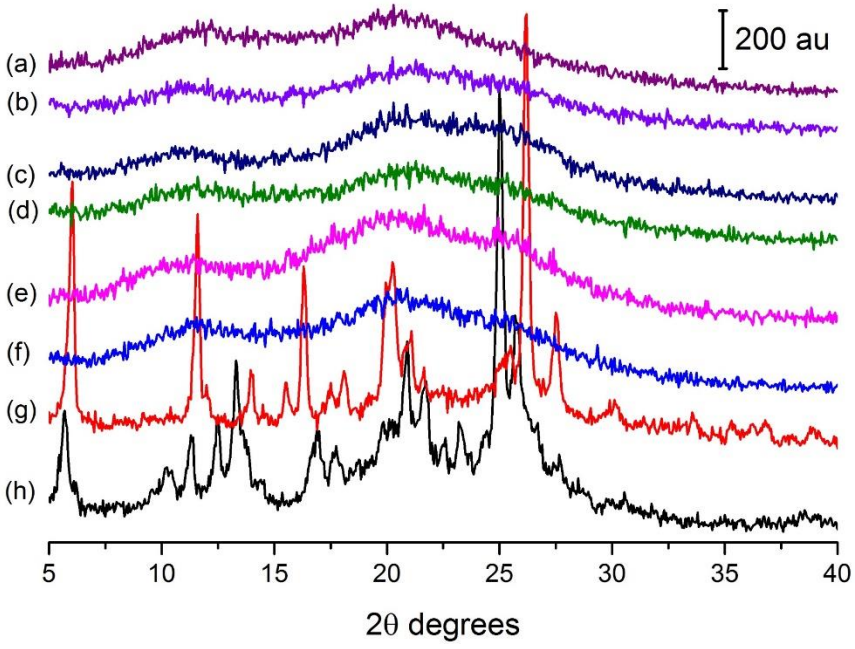
200 au
(a)
(b)
(c)
(d)
(e)
(f)
(g)
(h)
5
10
15
20
25
30
35
40
2θ degrees

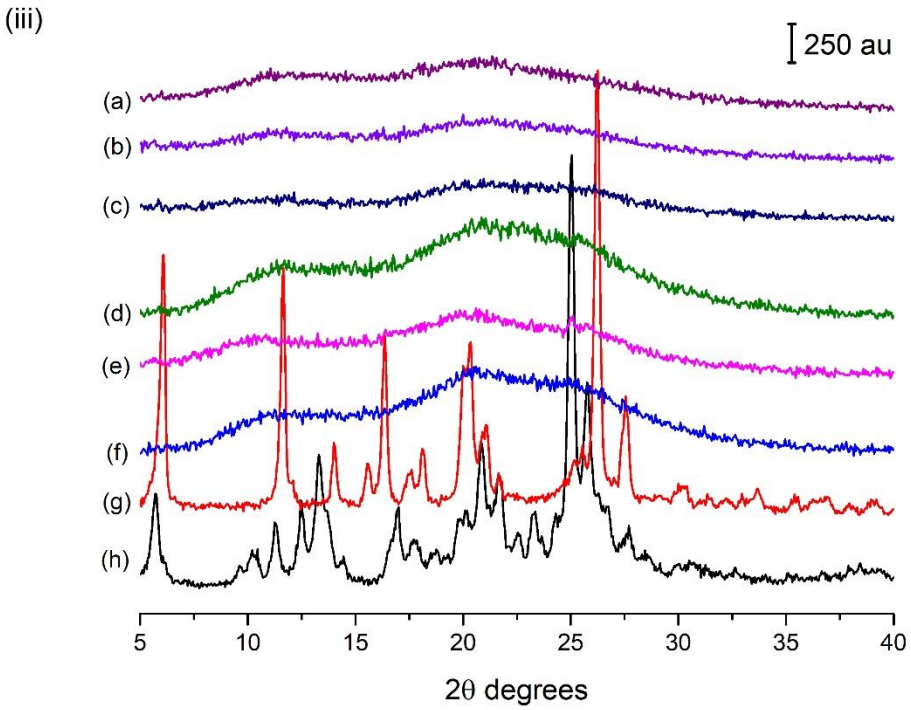

Figure 4.7. PXRD analysis of ASDs after storage at RT for (i) two months (ii) four months and (iii) twelve months: (a) SDD CS 1:1/60% PVP (b) SDD CS 1:1/40% PVP (c) SDD CS 1:1/20% PVP (d) BM CS 2:1/40% PVP (e) BM CS 1:1/40% Soluplus (f) BM CS 1:1/40% PVP (g) CS 2:1 and (h) CS 1:1.

The presence of PVP and Soluplus in the ASDs prevented the crystallization of CS 1:1 and CS 2:1 during long-term storage, allowing them to remain amorphous for an extended period of time. Similarly, as described in the previous section, the crystallization temperatures of all of the ASDs were significantly higher than the polymer-free salts in DSC studies. Polymers with high glass transition temperatures such as PVP are often used to stabilize ASDs, as they will help to reduce the molecular mobility and crystallization tendency of the drug.[56] However, as the T_g of Soluplus is relatively low, this is clearly not the only explanation for the improved stability of the ASD containing this polymer. The free energy of an amorphous formulation may be decreased by the presence of polymers, as their high molecular weight and flexibility will increase the configurational entropy of the system, and thus reduce the driving force for crystallization.[51] In addition, polymers can provide a physical barrier to crystallization by hindering the movement of drug molecules and blocking their access to crystal growth sites.[52] For instance, ASDs containing nimesulide and PVP were shown to

greatly increase the resistance of the drug to crystallization, despite having lower than predicted T_g's and lacking specific interactions between the components. The improved stability of the ASDs was attributed to the steric hindrance and antiplasticization effect of the polymer. This resulted in a reduction in the molecular mobility of the drug, as shown by broadband dielectric spectroscopy.[56] A combination of these factors most likely resulted in the improved stability of these ASDs.

4.3.4 Dynamic Solubility Studies

Due to the generation of a viscous gel when BM CS 1:1/40% Soluplus was added to the media, it was not possible to accurately carry out solubility tests on this sample. Similar issues have been encountered with this polymer by other researchers, and significant decreases in drug release from ASDs containing Soluplus have been reported due to hydrogel formation.[225] In contrast, the ASDs containing PVP demonstrated superior dispersion and wettability behavior, and full solubility tests were successfully carried out on all of these samples.

As can be seen in **Figure 4.8a**, a substantial improvement in the solubility of CIP was obtained with CS 1:1 and the ASDs containing this salt in water. An average maximum concentration of 30–34 mg/ml was achieved for all of these samples, however the differences between them were not statistically significant, as shown by ANOVA ($p = 0.27$). Similarly, Patel et al found that the solubility of tenoxicam doubled when formulated as an amorphous 1:2 salt with arginine, however the formation of an ASD with PVP did not provide any additional improvement.[218] With each of the ASDs, the concentration of CIP increased sharply within the first 60 sec of the study and did not fall substantially over the remainder of the experiment, although there was some fluctuation. CS 2:1 offered less of a solubility advantage in water than the 1:1 salt, with a maximum CIP concentration of 21.2 mg/ml. Therefore, a drug-acid ratio of 1:1 enables more of the drug to enter solution in water. This may be due to a greater reduction in the pH due to the higher proportion of succinic acid. In contrast to CS 1:1, the formulation of CS 2:1 as an ASD with PVP decreased its aqueous solubility significantly to 2.10 mg/ml, suggesting that the presence of polymer impeded the dissolution of the drug in this case. The aqueous solubility of CS 1:1, CS 2:1 and all of the

ASDs is significantly higher than that of the binary polymeric ASDs described in Chapter 3. This is most likely due to the presence of succinic acid in the former samples, which is more acidic and soluble than these polymers.

BM CS 2:1/40% PVP showed a similar profile to CIP in FaSSIF, reaching a peak concentration of 1.5 mg/ml after 30 sec, then quickly falling to approximately 0.5 mg/ml (**Figure 4.8b**). As in water, a significantly higher concentration was obtained with CS 1:1 and the other ASDs in FaSSIF. After 1 min, concentrations in excess of 39 mg/ml were obtained with all of these samples, which remained at this level for the remainder of the study. Again, the differences in the maximum concentration of these samples was not statistically significant, as shown by ANOVA ($p = 0.93$).

In contrast to water and FaSSIF, in FaSSGF BM CS 2:1/40% PVP had a comparable solubility to the other ASDs. Similarly, the CS 2:1 amorphous salt demonstrated superior solubility in this medium, achieving a concentration of 54.5 mg/ml at the end of the study. A maximum concentration of 38.9–43.9 mg/ml was obtained with all of the other ASDs in FaSSGF (**Figure 4.8c**). Again, the presence of polymer in BM CS 2:1/40% PVP reduced the solubility of the drug relative to the 2:1 salt, as it did in water and FaSSIF. ANOVA with Tukey's multiple comparison test revealed that the maximum solubility of SDD CS 1:1/60% PVP was significantly higher than that of BM CS 1:1/40% PVP in FaSSGF, however none of the other ASDs differed significantly. Therefore, it can be concluded that the processing method (dry ball milling vs. spray drying) did not affect the solubility of CS 1:1/40% PVP. Similarly, the proportion (w/w) of PVP in the ASDs prepared by spray drying did not have a significant effect on their solubility.

The pH of the solutions at the end of the solubility studies was measured and is listed in **Table A.3.2**. As expected, very similar values were obtained with CS 1:1 and the ASDs containing this salt. In water and FaSSIF the pH decreased to 4.6 ± 0.1 and 4.7 ± 0.1 respectively with these samples, and in FaSSGF it increased to 4.1 ± 0.1. CS 2:1 gave slightly higher values of 4.7–4.9 in the three media, while the pH was higher again with BM CS 2:1/40% PVP (final pH 5.4, 6.0 and 4.9 in water, FaSSIF and FaSSGF, respectively) due to the lower quantity of salt entering solution with these samples.

PXRD analysis of the excess powder left at the end of the experiments revealed that all of the amorphous solids crystallized (**Figure A.3.4**). The same crystal form was obtained for all of the samples containing CS 1:1 in the three different media, which was identified as CS 1:1 trihydrate.[125] In contrast, CS 2:1 and BM CS 2:1/40% PVP did not crystallize to the corresponding salt, but instead formed CIP hydrate. In FaSSIF the PXRD patterns of the precipitates matched that of the CIP 3.1 hydrate, while in water the CIP 3.7 hydrate[158] was obtained.. In FaSSGF, CS 2:1 crystallized to a mixture of the 3.1 and 3.7 hydrates. Unlike the other samples, the precipitate recovered from solubility studies with BM CS 2:1/40% PVP in this medium was only slightly crystalline, with low intensity peaks matching those of the CIP 3.7 hydrate. The significantly improved solubility observed for this sample in FaSSGF compared to the other media may therefore be partly due to a delay in crystallization. The crystallization behavior of the samples may also explain the superior solubility of those containing CS 1:1 compared to CS 2:1. Crystalline CS 1:1 has been shown to have a solubility of approximately 30 mg/ml in water,[125] and therefore its formation during solubility studies would still result in a large amount of CIP entering solution. CIP hydrate on the other hand is significantly less soluble than CS 1:1 trihydrate,[198] and its formation may have limited the solubility of CS 2:1 in water and FaSSIF.

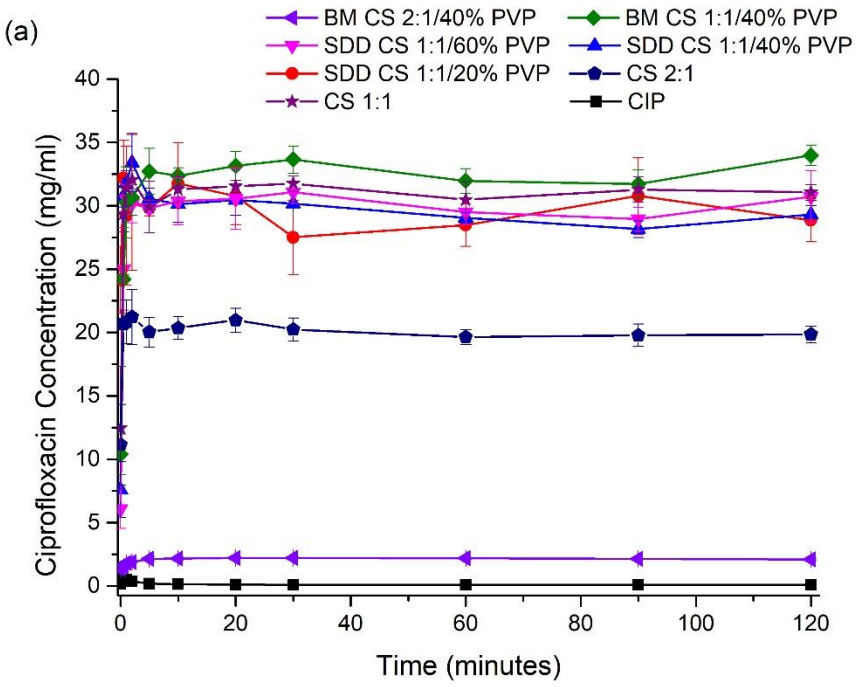

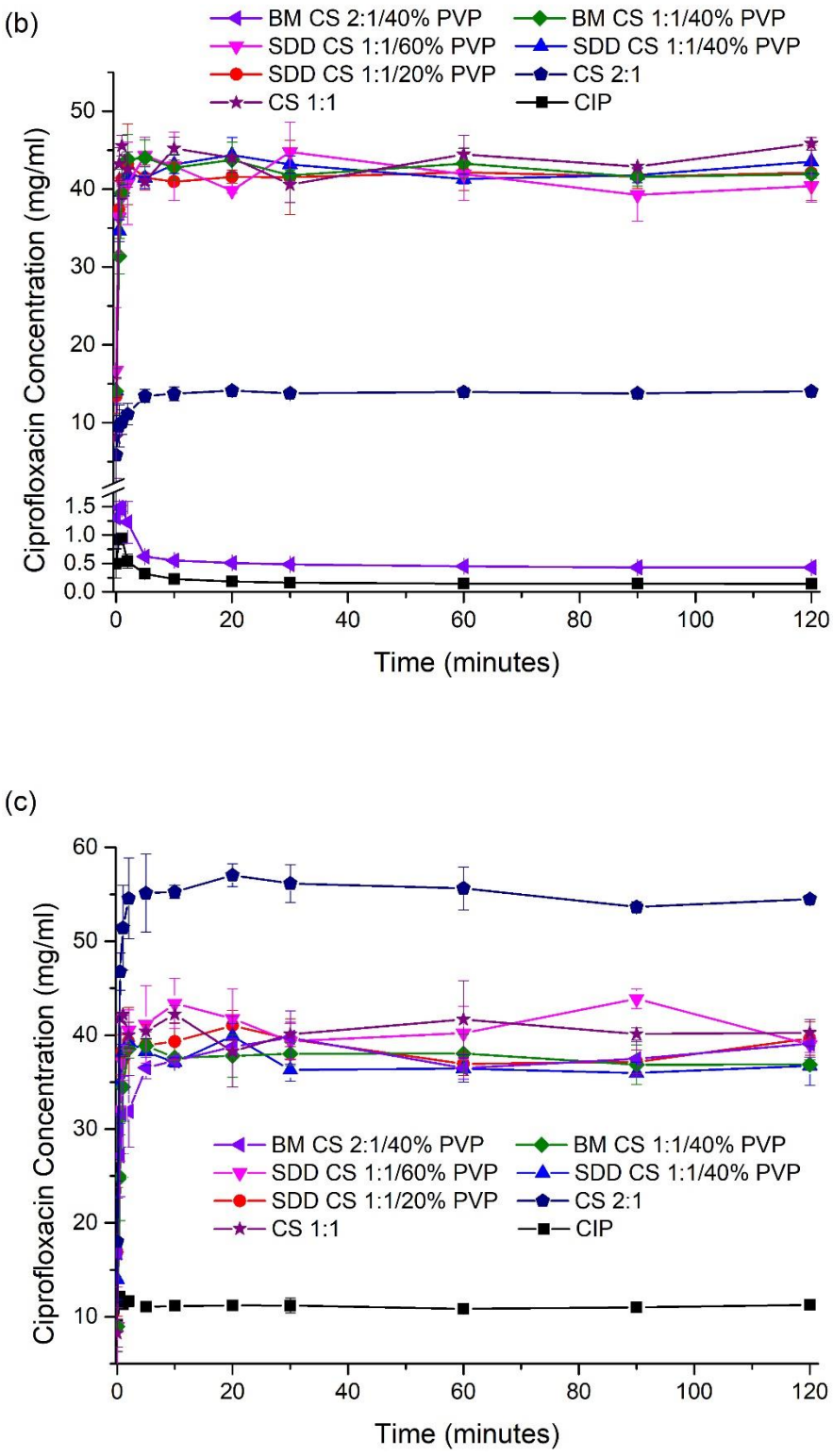

Figure 4.8. Solubility studies in (a) water (b) FaSSIF and (c) FaSSGF at 37 ºC. The average of at least 3 experiments is plotted, ± the standard deviation.

4.3.5 PAMPA Permeability Study

The results of the PAMPA study on CS 1:1, CS 2:1 and the ASDs containing PVP are shown in **Table 4.2**. As the effective permeability of CIP and the ASDs described in Chapter 3 did not differ significantly under iso-pH and pH gradient conditions, a pH of 7.4 was used in both the donor and acceptor compartments for this assay. All of the samples demonstrated low effective permeability (P_e) of less than 1×10^{-6} cm/s, and therefore would be expected to be poorly absorbed in vivo. Although the differences in P_e between the amorphous samples were not significant, they all had a significantly lower permeability than crystalline CIP, as shown by ANOVA and Tukey's multiple comparison test. Similarly, as described in the previous chapter, crystalline CIP HCl was also significantly less permeable than pure CIP. This may be due to the fact that the proportion of CIP bearing a net positive charge is increased by these salts, making it more hydrophilic, and less likely to diffuse across the lipid membrane. In contrast, no decrease in the permeability of the drug was seen with the ASDs containing Eudragit L100, HPMCAS-LG and HPMCAS-MG, as these excipients are unlikely to have a significant effect on the ionization state of the drug in solution.

Table 4.2. PAMPA Permeability Values of CIP

Sample	P_e x 10^6 (cm/s)
CIP	0.56 ± 0.06
CS 1:1	0.13 ± 0.02
CS 2:1	0.11 ± 0.01
BM CS 1:1/40% PVP	0.12 ± 0.01
BM CS 2:1/40% PVP	0.12 ± 0.02
SDD CS 1:1/20% PVP	0.12 ± 0.03
SDD CS 1:1/40% PVP	0.12 ± 0.02
SDD CS 1:1/60% PVP	0.12 ± 0.00

As discussed in Chapter 3, as PAMPA only provides an estimate of passive transcellular transport, it is possible that the in vivo absorption of these formulations was underestimated by this study. Although there is some evidence that CIP is a substrate for active transporters

and efflux proteins in the intestine,[208] it is believed to be largely absorbed passively, which includes the transmembrane and paracellular pathways.[207] As CIP can be transported via the paracellular route in the both the zwitterionic and cationic form,[118] at least a portion of the ionized drug should be absorbed by passing through the aqueous channels in between intestinal cells. Therefore, the in vivo permeability of CIP from these samples is likely to be higher than that obtained in this PAMPA study.

4.4 Conclusions

ASDs containing amorphous CS 1:1 and 2:1 salts dispersed in PVP or Soluplus were successfully produced via ball milling and spray drying. Although no clear evidence of specific interactions between the salts and polymers were found via FTIR analysis, DSC and IGC indicated that the salts and polymers form a miscible mixture in each case. All of the ASDs were superior to the corresponding salts in terms of thermal stability, with higher T_g's and crystallization temperatures, and these were positively correlated with the weight ratio of PVP. In addition, the ASDs remained fully X-ray amorphous for at least 10 months during long-term stability studies, whereas the amorphous salts began to crystallize after 1–2 months. However, all of the ASDs took up a large amount of water during DVS studies due to their polymer content, and crystallization occurred in each case at 40–50% RH. All of the ASDs containing CS 1:1 were over 300 times more soluble than pure CIP in water and FaSSIF, however no significant improvement was seen compared to the pure amorphous salt. CS 2:1 and the ASD containing this salt offered less of a solubility advantage, although they were still superior to crystalline CIP in all media. No decrease in the effective permeability of CIP was seen with the ASDs containing PVP compared to amorphous CS 1:1 and CS 2:1. However, all samples were significantly less permeable than pure crystalline CIP.

In conclusion, the formulation of CS 1:1 and CS 2:1 amorphous salts as ASDs with PVP or Soluplus improved their thermal and long-term stability, but did not significantly increase their stability in humid conditions, solubility or permeability. Although the amorphous salts and ASDs offered a significant advantage over pure crystalline CIP in terms of solubility, this was offset by a decrease in permeability.

Chapter 5: Preparation and Characterization of Amorphous Ciprofloxacin-Amino Acid Salts

5.1 Introduction

As demonstrated in Chapter 3 and 4, the solubility and stability of CIP may be increased by the production of ASDs containing suitable polymers and/or small molecules. A number of studies have recently focused on ASDs consisting of poorly soluble drugs and amino acids. Amino acids are attractive stabilizers for such formulations as they are inexpensive GRAS (generally recognized as safe) compounds,[226] that have been shown to improve the physical stability of many amorphous drugs.[62,86,227,228] The α-carboxylate, α-amino group or side chains of amino acids can all potentially form bonds with drugs, providing many possibilities in terms of intermolecular interactions. Amino acids may stabilize amorphous drugs via hydrogen bonding, hydrophobic and/or ionic interactions,[226] however amorphous formulations that lack specific drug-amino acid interactions have also been produced.[227] A number of amorphous salts have also been prepared with the basic amino acids, in particular arginine (ARG), via ball milling and spray drying.[86,218,229] In each of these salts an ionic interaction between the positively charged side chain guanidyl group of ARG and a carboxylate group of the drug was detected.[218,227,229]

From the results of the previous chapters, it could be predicted that successful amorphization of CIP would be most likely with the acidic amino acids, i.e. aspartic acid (ASP) and glutamic acid (GLU). A study by ElShaer et al supports this hypothesis. The authors found that CIP formed salts with ASP and GLU when freeze dried in a 1:1 molar ratio.[230] In both cases the positively charged piperazine amino group of CIP was found to form an ionic interaction with the carboxylate groups of ASP and GLU. In contrast, the authors were unable to form salts with the basic amino acids arginine, lysine and histidine.[230] Similarly, as described in Chapter 3, when CIP was milled with neutral polymers, such as PVP and Soluplus, a semi-crystalline product was obtained. However, since all amino acids contain an α-carboxyl group, they would be more likely to interact with the amino group of CIP, and potentially form an amorphous salt, than such polymers.

The major goal of this study was to explore the possibility of forming CIP ASDs with amino acids. Seven amino acids with differing side chain properties were chosen for analysis: glycine (GLY), alanine (ALA), serine (SER), arginine (ARG), cysteine (CYS), glutamic acid

(GLU) and aspartic acid (ASP). Their chemical structures are shown in **Figure 5.1**. Their side chains, or R groups, may be classified as nonpolar and aliphatic (GLY and ALA); polar and uncharged (SER and CYS); basic (ARG); and acidic (ASP and GLU). Solid dispersions were produced by ball milling CIP with the amino acids in a 1:1 molar ratio. PXRD, DSC, TGA, FTIR and solid-state nuclear magnetic resonance (SSNMR) were used to investigate the physical form and thermal behavior of the preparations, and the interactions between the components. The long-term stability of the successful CIP/amino acid ASDs, as well as the effect of water sorption on their physical state, was then examined. The solubility and dissolution rate of a range of poorly soluble drugs have been found to increase via the production of amino acid ASDs,[62,227,231] while the CIP aspartate and glutamate salts were significantly more soluble in water than crystalline CIP.[230] It was therefore of interest to determine whether this is also the case with the amorphous samples prepared in this study. Lastly, the passive permeability of the amino acid ASDs was compared to that of pure crystalline CIP using the PAMPA model.

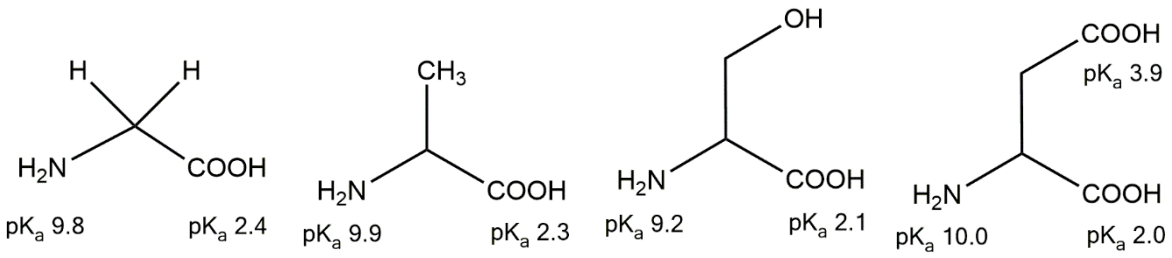

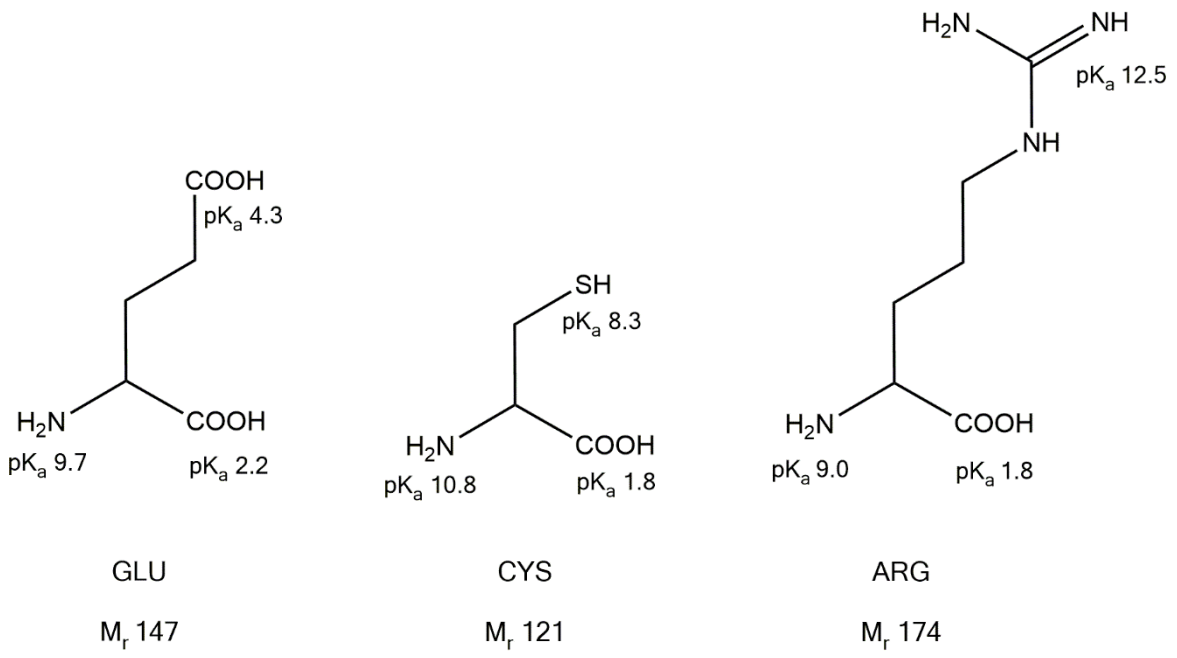

Figure 5.1. Chemical structures, pK_a values and molecular weights of the amino acids used in this study.

5.2 Experimental Section

5.2.1 Materials

The following amino acids were used to form solid dispersions with CIP: glycine (GLY: Sigma-Aldrich, St. Louis), L-alanine (ALA: Acros Organics, New Jersey), L-cysteine (CYS: SAFC, Sigma-Aldrich, St. Louis), L-serine (SER: Acros Organics, New Jersey), L-arginine (ARG: Sigma-Aldrich, St. Louis), L-glutamic acid (GLU: Acros Organics, New Jersey) and L-aspartic acid (ASP: Sigma-Aldrich, Dorset). The PXRD patterns of the starting materials are shown in **Figure A.4.1**. The details of all other materials and solvents used in this study are listed in Chapter 2 and 3.

5.2.2 Methods

5.2.2.1 Sample Preparation

Ball milling was carried out as described in Chapter 2. CIP was co-milled with the amino acids in a 1:1 molar ratio for 4–6 hours in total. PMs were prepared by mixing 1:1 molar quantities of CIP and the amino acid powders in a pestle and mortar for a few minutes. The amino acids were also milled individually for 4 hours by Ms. Daryl Conroy in TCD.

5.2.2.2 Solid-State Characterization

5.2.2.2.1 Powder X-ray Diffraction

PXRD was performed as described in Chapter 2.

5.2.2.2.2 Solid-State Fourier Transform Infrared Spectroscopy

FTIR was performed as described in Chapter 2.

5.2.2.2.3 Solid-State Nuclear Magnetic Resonance (SSNMR)

SSNMR analysis was carried out by Dr. Sarah Hudson in the University of Limerick. Carbon-13 NMR spectra were acquired on a Bruker Avance III HD NMR spectrometer operating at B_0 = 9.4 T, with corresponding ^{1}H and ^{13}C resonance frequencies of $\nu_0(^{1}H)$ = 400.1 MHz and $\nu_0(^{13}C)$ = 100.6 MHz. Samples were packed in 4 mm o.d. zirconia rotors with Kel-F caps under ambient atmosphere, and experimental ^{13}C NMR spectra were acquired at natural abundance using a 4 mm triple channel (H/X/Y) Bruker MAS probe operating in double resonance mode. The magic angle was optimized using a rotor packed with KBr and spun at 5 kHz. NMR spectra were referenced to TMS at δ_{iso} = 0 ppm by setting the high frequency ^{13}C resonance in adamantane to 38.48 ppm.[232] The ^{13}C CP/MAS NMR spectra were acquired in a single spectral window using the cross-polarization pulse sequence, with a magic angle spinning (MAS) rotor frequency of 10 kHz, a ^{1}H 90° pulse width of 2.5 μsec, and 50 kHz ^{1}H decoupling during acquisition. Proton decoupling was carried out with the SPINAL64[233] decoupling sequence at 100%. A contact time of 2.5 msec was optimized using a crystalline sample of CIP, and was used for the acquisition of all ^{13}C CP/MAS NMR spectra. Recycle delays were varied from 5 sec (more amorphous samples) to 20 sec (more crystalline samples), depending on the measured ^{1}H T_1 relaxation time for

each sample. For each sample, the ^{1}H T_1 relaxation time(s) were checked using the saturation recovery pulse sequence to ensure that the recycle delay allowed for adequate relaxation between the collection of subsequent transients. The NMR spectra varied from 128 to 4k transients, with more transients being collected for the amorphous samples to get a suitable signal to noise ratio. Samples were dried overnight in an oven at 50 °C prior to SSNMR analysis.

5.2.2.2.4 Differential Scanning Calorimetry

DSC was carried out as described in Chapter 3. All measurements were carried out in triplicate.

5.2.2.2.5 High-Speed Differential Scanning Calorimetry

HSDSC was carried out using the equipment and procedure described in Chapter 2. The samples were first heated from 25–80 °C and cooled to 5 °C to allow for water evaporation. They were then heated from 5–300 °C with a heating rate of 50–300 °C/min.

5.2.2.2.6 Thermogravimetric Analysis

TGA was performed as described in Chapter 2.

5.2.2.3 Ciprofloxacin Aspartate and Glutamate Crystallization

1:2 molar ratio solutions of CIP and ASP or GLU were prepared in a mixture of ethanol and water (approximately 3:1 volume ratio) at a concentration of 1% (w/v). These solutions were allowed to evaporate slowly at RT. When dry, the crystals were analyzed by PXRD. A portion of the ball milled CIP/ASP and CIP/GLU ASDs were also left exposed at RT (22–25 °C) for a number of months to encourage their crystallization. The samples were analyzed regularly by PXRD.

5.2.2.4 Dynamic Vapor Sorption

DVS studies were carried out using the same equipment and procedure described in Chapter 2. The samples were analyzed by PXRD following completion of the desorption cycle. DVS was repeated on fresh samples under the same conditions, however they were removed for PXRD analysis upon crystallization during the sorption cycle.

5.2.2.5 Long-term Stability Study

A long-term stability study was conducted on the CIP/amino acid ASDs as described in Chapter 4.

5.2.2.6 Dynamic Solubility Studies

Solubility studies were performed as described in Chapter 3.

5.2.2.7 Parallel Artificial Membrane Permeability Assay

PAMPA was carried out as described in Chapter 3. The samples were dissolved in PBS pH 7.4 at concentrations of 50–100 µg/ml.

5.2.2.8 High-Performance Liquid Chromatography

HPLC was carried out as described in Chapter 3.

5.2.2.9 Statistical Analysis

Statistical analysis was carried out as described in Chapter 2.

5.3 Results and Discussion

5.3.1 Sample Preparation

5.3.1.1 Ball Milling of Pure Amino Acids

Ball milling was first carried out on the amino acids themselves. This proved ineffective at amorphizing the amino acids, with only slight decreases in the intensity of their PXRD patterns noted after 4 hours of milling (**Figure 5.2**). Similarly, when CIP was ball milled on its own it became more disordered, but remained partially crystalline. Löbmann et al were also unable to produce amorphous amino acids via ball milling.[227] Like CIP, amino acids have a rigid structure and strong crystal lattice, making them difficult to amorphize on their own.[62] They are also relatively small and simple molecules, and can therefore recrystallize quickly.[26] In addition to ball milling, spray drying, vacuum drying and cryomilling have all proven unsuccessful at amorphizing amino acids, while quench cooling results in their

degradation.[86,227,228] Pure amorphous ARG has been generated via freeze drying, however this production method was unsuccessful for other amino acids.[86]

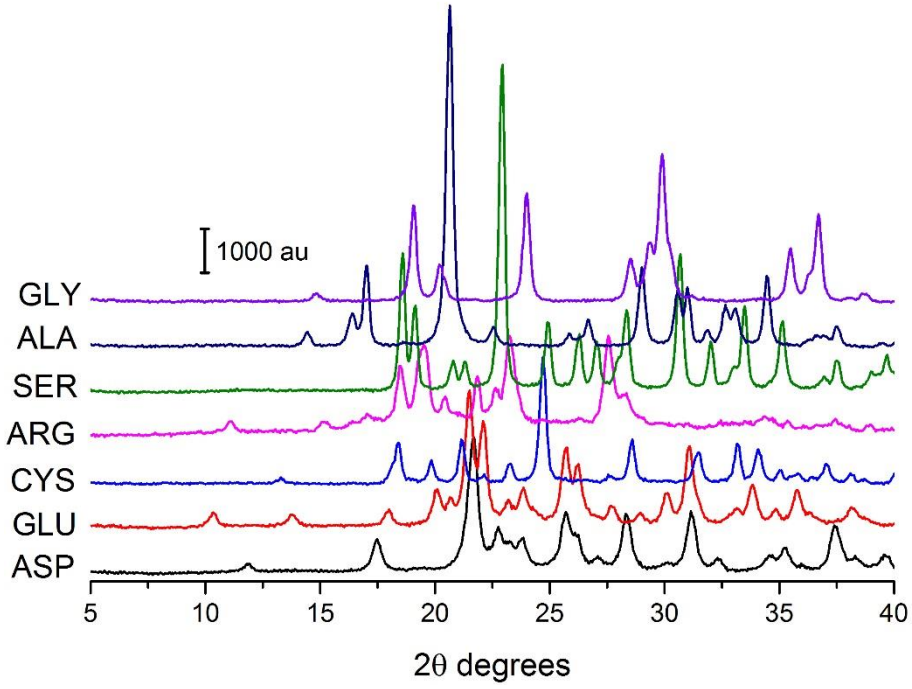

Figure 5.2. PXRD analysis of ball milled amino acids.

5.3.1.2 Production of Ciprofloxacin/Amino Acid Solid Dispersions

Similar to CIP, the α-carboxylate and amino groups, as well as the side chains of relevant amino acids, are involved in a number of intermolecular hydrogen bonds in the crystal lattice of these compounds. The formation of CIP/amino acid salts should therefore facilitate amorphization of both moieties, by disrupting this bonding network and preventing nucleation during processing.[234] This was attempted by ball milling CIP with the seven amino acids mentioned above in a 1:1 molar ratio. This ratio has been used for most amorphous drug-amino acid formulations described in the literature to date, and has been shown to result in the most stable ball milled preparations.[235]

Following the successful production of CIP aspartate and glutamate salts reported by ElShaer et al,[230] it was predicted that CIP would also form an ASD with these amino acids via ball milling. After four hours of milling, a few small peaks remained in the PXRD diffractograms of CIP/ASP and CIP/GLU. However, when milled for a further two hours they became fully

X-ray amorphous (**Figure 5.3**). Surprisingly, when CIP was milled with CYS and ARG, fully X-ray amorphous formulations were obtained after only four hours of milling. This was particularly unexpected for ARG, as ElShaer et al were unable to produce CIP salts with any of the basic amino acids.[230] Similarly, when the twenty essential amino acids were screened by Kasten et al for their suitability as amorphous co-formers for several drugs, it was discovered that ARG could only amorphize acidic compounds. In addition, the authors concluded that ASP and GLU were poor stabilizers for all drugs included in their study, while CYS was only successful for the acidic drug furosemide. The amino acids SER, ALA and GLY were also unsuccessful co-formers for all of the drugs included in Kasten et al's study.[236] Likewise, when CIP was milled with these amino acids for four hours, semi-crystalline solid dispersions (SDs) were obtained, with PXRD patterns matching the most intense peaks of the starting materials (**Figure 5.3**).

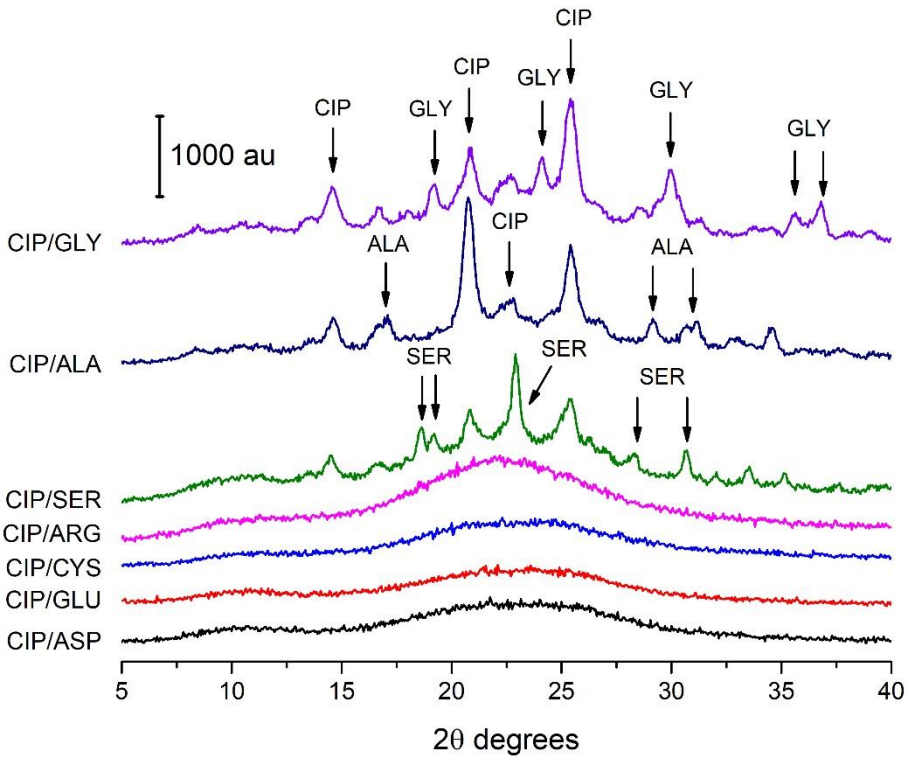

Figure 5.3. PXRD analysis of CIP/amino acid ASDs and SDs. The arrows identify the most prominent peaks of CIP, SER, ALA and GLY.

There are a number of possible explanations as to why some amino acids formed ASDs with CIP, while others did not. It is possible that the size of the amino acids had an influence on their ability to interact with CIP. It could be hypothesized that the smaller size of GLY, ALA and SER would facilitate their interaction with the drug. However, these simple amino acids all resulted in partially crystalline SDs when ball milled with CIP. On the other hand, the bulkier side chains and higher molecular weight of ASP, GLU, CYS and ARG may have increased the configurational entropy of the ASDs containing these amino acids, and thus hindered their crystallization.[26]

The reason why only some of the amino acids were successful co-formers for the amorphization of CIP may be due to pK_a differences. As previously mentioned, the pK_a values of CIP have been reported as 6.16 and 8.62 for the carboxylic acid and piperazine secondary amine, respectively.[109] The pK_a values of the α-carboxylic acid groups, α-amino groups and relevant side chains of the amino acids have been reported by Berg et al, and are shown in **Figure 5.1**.[237] All of the CIP ASDs discussed in the previous chapters have involved the interaction of the piperazine amino group of CIP with carboxylate groups of the excipients, and a similar interaction is believed to occur in the amino acid ASDs studied here (see Section 5.3.2). From **Figure 5.1** it can be seen that the amino acids with the lowest α-COOH pK_a values (thereby providing the greatest difference in pK_a from that of the piperazine amino group of CIP) are ARG and CYS. These amino acids formed ASDs most readily with the drug, requiring only four hours of milling. ASP and GLU have slightly higher pK_a values for their α-COOH groups, and required a further two hours of milling with CIP to become fully X-ray amorphous. Due to their higher pK_a values, the side chain carboxylic acid groups of ASP and GLU are less likely to form an ionic interaction with CIP than their α-carboxylate groups. Although the equivalent pK_a difference of SER is on par with than that of ASP and GLU, it was unable to form an ASD with CIP via ball milling. This suggests that a combination of factors influences the successful amorphization of CIP with an amino acid, such as the pK_a of the α-carboxylic acid group and its molecular weight.

5.3.2 Analysis of Drug-Amino Acid Interactions

5.3.2.1 Solid-State Fourier Transform Infrared Spectroscopy

The FTIR spectra of crystalline CIP, the amino acids, ASDs and PMs are shown in **Figure 5.4**. The characteristic peaks corresponding to the asymmetric and symmetric stretching vibrations of the carboxylate carbonyl of CIP, at 1590 cm^{-1} and 1375 cm^{-1} respectively,[165] are either absent from the spectra of the ASDs, or greatly decreased in intensity and shifted to lower wavenumbers. Therefore, like the ASDs of Chapter 3 and 4, the carboxylic acid of CIP appears to be protonated in these preparations. In contrast, this group is ionized in the SDs containing SER, ALA and GLY, as evidenced by the presence of peaks at 1590 cm^{-1} and 1375 cm^{-1}. NH_2^+ stretching vibrations are present as weak bands at 2400–2600 cm^{-1} in the FTIR spectrum of CIP,[125] and small bands may also be seen in this region in the spectra of all of the ASDs and semi-crystalline SDs. Therefore, it appears that CIP is in the same ionization state in these amorphous formulations as in CIP salts and CIP/polymer ASDs, i.e. with an unionized carboxylic acid group and a protonated secondary amine.

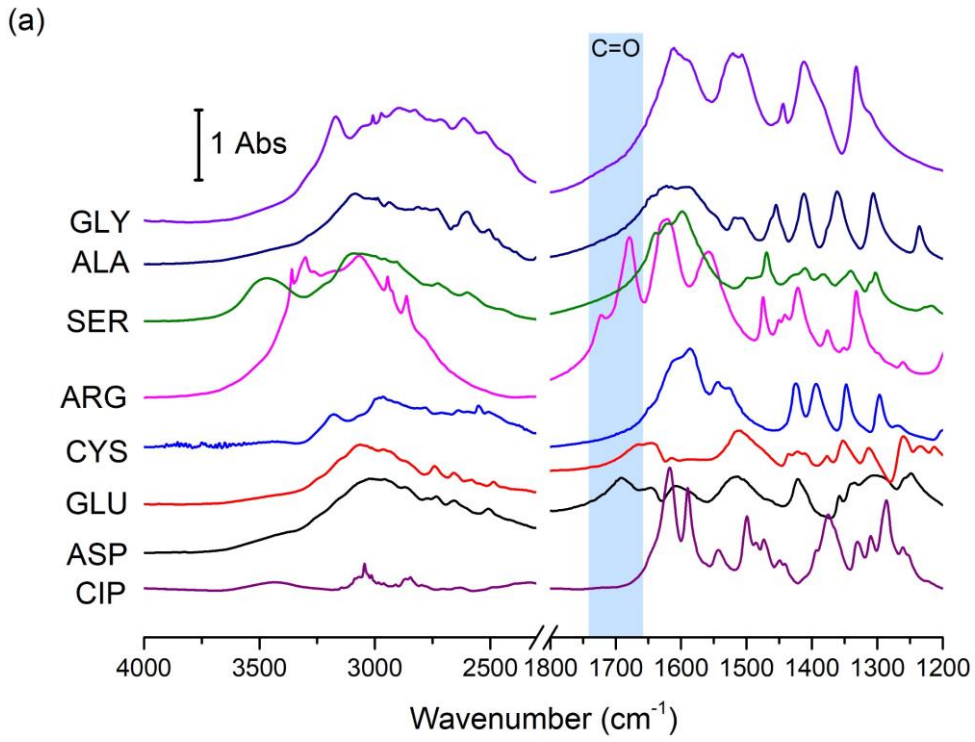

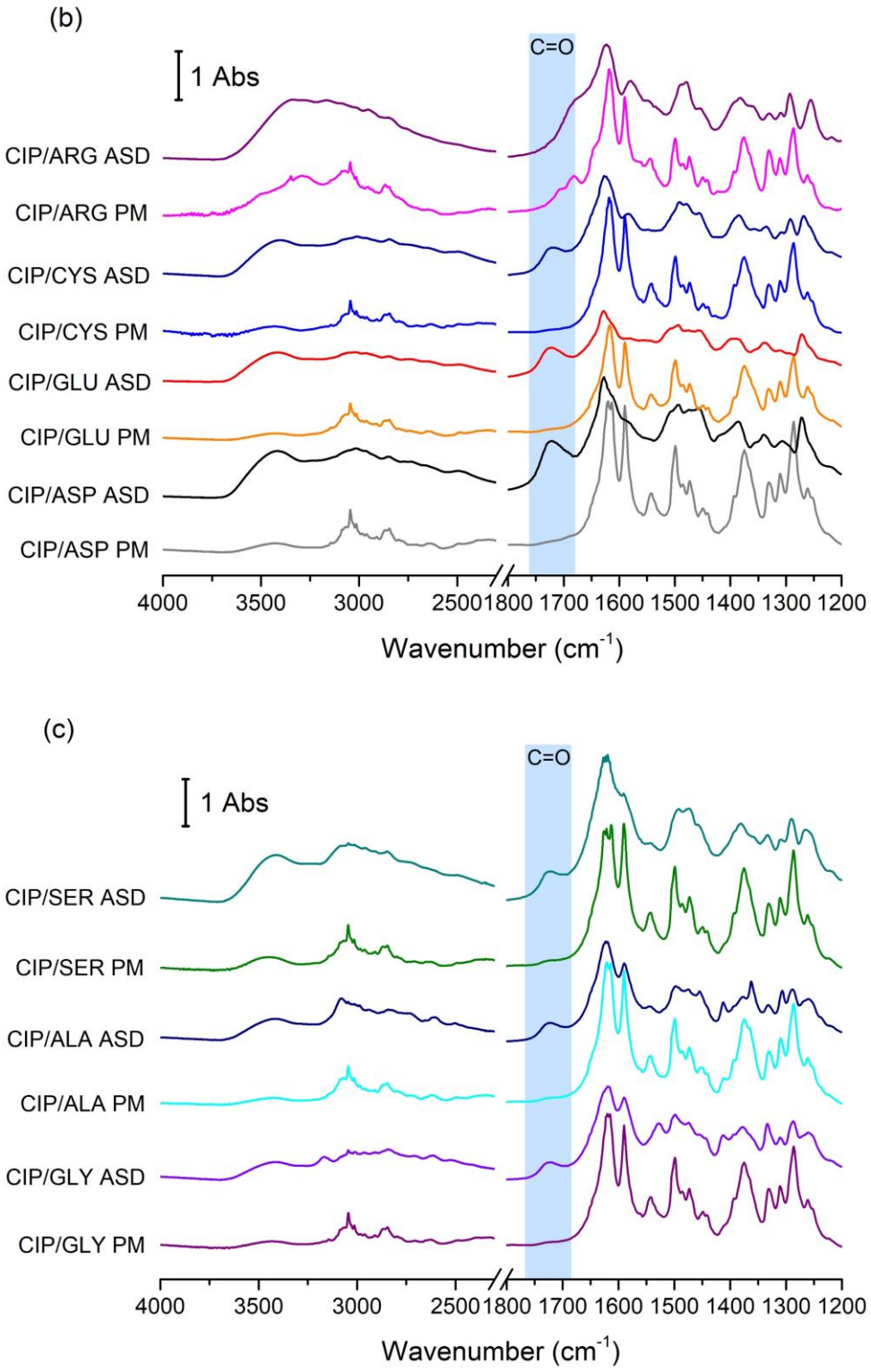

Figure 5.4. FTIR spectra of (a) starting materials (b) ASDs and corresponding PMs and (c) semi-crystalline SDs and corresponding PMs. Peaks corresponding to the C=O stretch of carboxylic acid groups are highlighted in blue.

Amino acids usually exist in the zwitterionic form at neutral pH and in the solid state,[238] and FTIR analysis of the starting materials was used to confirm their ionization state. The FTIR spectra of most of the amino acids are missing the characteristic peak of the unionized carboxylic acid C=O stretch above 1700 cm^{-1}, indicating that their α-carboxylic acid groups are ionized (**Figure 5.4a**). Peaks at 1600–1560 cm^{-1} and 1400–1422 cm^{-1} in each of the spectra may be assigned to the asymmetric and symmetric stretch of the α-carboxylate carbonyl, respectively. In contrast to the other amino acids, the spectra of ASP and GLU contain peaks around 1670–1730 cm^{-1} due to the C=O stretch of the protonated side chain carboxylic acid group.[238] The FTIR spectra of all of the amino acids, except ARG, contain a peak at 2120–2040 cm^{-1}, due to the symmetric stretch of the NH_3^+ group. They also contain a broad medium intensity band around 3200–3000 cm^{-1} due to the asymmetric stretch of this group,[239] while peaks at 1650–1610 cm^{-1} and 1530–1500 cm^{-1} can be assigned to the asymmetric and symmetric bending vibrations, respectively, of NH_3^+.[238] This indicates that the amino acid starting materials are in the zwitterionic form. These peaks are absent from the spectra of the ASDs. Instead, a medium intensity peak is present from 3415–3330 cm^{-1}, which can be assigned to the N-H stretch of the unionized primary amine group.[240] Therefore, the α-amino groups of the amino acids appear to be unionized in the ASDs.

Unlike the other amino acids used in this study, a small peak is present at 1721 cm^{-1} in the spectrum of crystalline ARG, suggesting the presence of the unionized form of this amino acid. The PXRD pattern of the ARG starting material (**Figure A.4.1**) matches that reported by Patel et al. The authors claimed that the crystalline ARG used in their study was a mixture of phases, consisting of the zwitterionic dihydrate plus unionized ARG.[218] Therefore, although the zwitterion has been shown to be the most stable form of ARG,[241] the raw material used in this study appears to be a mixture of the unionized and zwitterionic form. The FTIR spectrum of ARG is also somewhat more complicated than the other amino acids due to its larger and more complex side chain. The α-amino group of zwitterionic ARG is unionized, while the side chain guanidyl group is positively charged. The peaks at 1679 cm^{-1} and 1620 cm^{-1} in the spectrum of ARG may therefore be attributed to the asymmetric and symmetric stretch, respectively, of the guanidyl ($CN_3H_5^+$) group.[242] Like the other amino acids, the α-carboxylic acid of zwitterionic ARG is deprotonated. Although the asymmetric

stretch of the carboxylate C=O group could not be detected due to overlap with the guanidyl peaks, the symmetric stretch of this group is located at around 1421 cm^{-1}.[243]

As can be seen in **Figure 5.4b**, the spectra of all of the CIP/amino acid ASDs contain a peak at 1720–1725 cm^{-1}, although in the case of CIP/ARG this appears as a broad shoulder due to significant overlap with the neighboring guanidyl peak. A peak was also found in this region of the FTIR spectra of the polymeric ASDs discussed in the previous chapters. Therefore, CIP appears to be in the same ionization state in these amino acid ASDs, i.e. with an unionized carboxylic acid group and positively charged piperazine amino group. Similarly, ElShaer et al observed a peak at around 1720 cm^{-1} in the FTIR spectra of the CIP aspartate and glutamate salts. The authors concluded that an ionic interaction exists between the secondary amine of CIP's piperazine group and the carboxylate group of the amino acids in these salts.[230] CIP most likely interacts with the α-carboxylate groups of the amino acids used in this study in a similar manner, thereby forming amorphous salts. Interestingly, a small peak is also present at 1720–1725 cm^{-1} in the spectra of the three semi-crystalline SDs (**Figure 5.4c**). This suggests that a portion of CIP underwent proton transfer when milled with SER, ALA and GLY, however the drug-amino acid interactions were apparently not of sufficient strength to amorphize these samples completely.

The ketone carbonyl stretch of CIP appears at approximately 1618 cm^{-1} in the spectrum of the zwitterion,[165] but is shifted to 1627–1628 cm^{-1} in the spectra of the amino acid ASDs. As previously discussed, this shift also occurs with unionized CIP and CIP polymeric ASDs, and may be attributed to changes in the hydrogen bonding of the ketone upon protonation of the drug. The partial conversion of the carboxylate group of CIP to the protonated form in the CIP/SER and CIP/ALA SDs was verified by the location of the ketone carbonyl stretch at 1627 cm^{-1} and 1623 cm^{-1}, respectively. With CIP/GLY on the other hand, no such shift was detected.

5.3.2.2 Solid-State Nuclear Magnetic Resonance

The ^{13}C CP/MAS NMR spectra of crystalline CIP, the ball milled amino acids, and the ASDs and corresponding PMs are shown in **Figure 5.5**. As the side chains of the acidic amino acids differ by only one CH_2 group, SSNMR was not carried out on the samples containing ASP.

The ^{13}C spectrum of crystalline CIP matches that obtained by Mafra et al for the zwitterionic form of the drug.[158] Full peak assignment has been carried out by this group, and this was used to identify the peaks in the spectra of the CIP-amino acid ASDs. The ^{13}C spectra of the ball milled pure amino acids match those of crystalline GLU,[244] CYS[245] and ARG,[246] which have previously been described. The peaks present in these spectra are sharp in appearance, confirming that ball milling did not alter the crystallinity, ionization state or intermolecular interactions of the amino acids. Similarly, no significant differences were seen in their FTIR spectra following ball milling (data not shown). In contrast, the ^{13}C NMR spectra of the ASDs contain broad and overlapped peaks, which is typical of disordered solids and confirms their amorphous nature.[247] The spectra of the PMs consist of a direct combination of those of crystalline CIP and the ball milled amino acids, and no changes in peak chemical shift were detected.

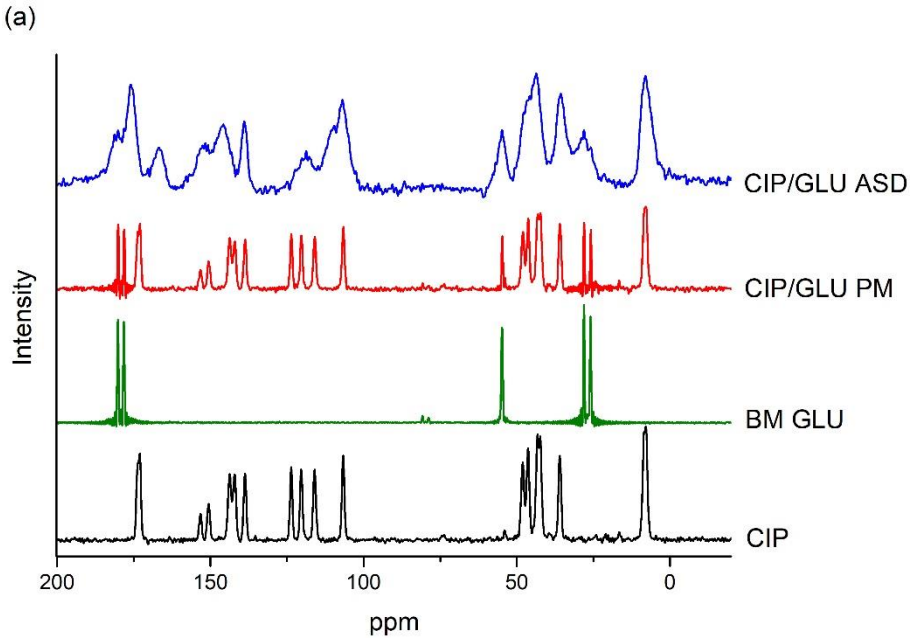

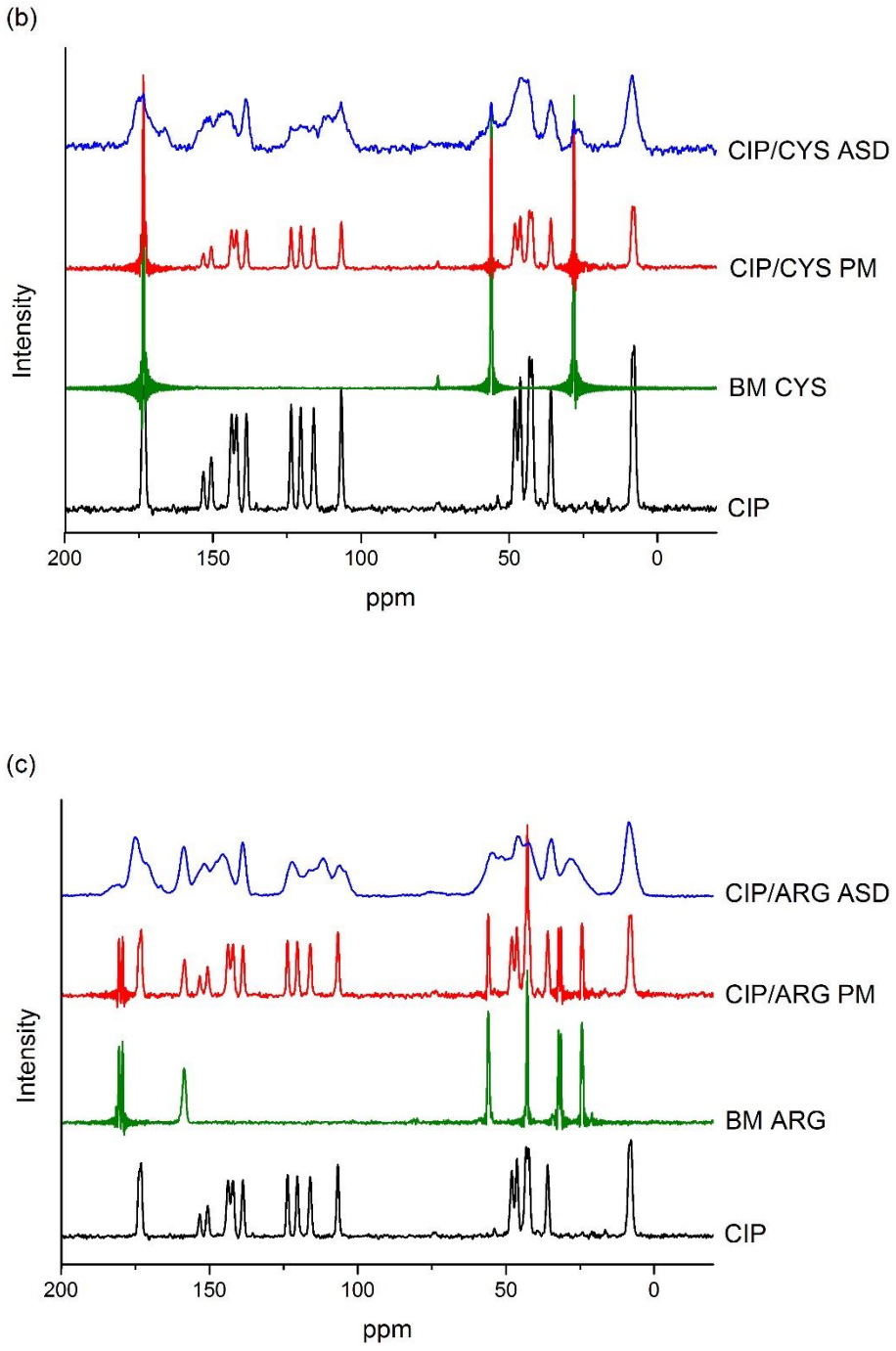

Figure 5.5. ^{13}C CP/MAS NMR spectra of samples containing (a) GLU (b) CYS and (c) ARG. BM: ball milled.

Of particular interest in this study was the location of the peaks corresponding to the carbonyl groups of CIP. If the hypothesis concerning the ionization state of CIP in the ASDs is correct, these peaks should undergo certain shifts due to protonation of the carboxylate group of the

drug. Therefore, the carbonyl region of the spectra (~160–190 ppm) will be focused on here. The relevant peak shifts for the samples are listed in **Table 5.1**.

Table 5.1. SSNMR ^{1}H T_1 Spin-Lattice Relaxation Times and Carbonyl Peak Assignment

Sample	^{1}H T_1 (s)	Chemical Shift (ppm)	Assignment
CIP	12	173.0	$C{=}OO^-$
		173.7	$C_{KET}{=}O$[a]
BM GLU	7.2	178.2	$C_{SC}{=}OOH$[b]
		180.2	$C_{\alpha}{=}OO^-$
BM CYS	3.3	173.5	$C_{\alpha}{=}OO^-$
BM ARG	13.5	179.4	$C_{\alpha}{=}OOH$
		180.6	$C_{\alpha}{=}OO^-$
CIP/GLU ASD	2.0	166.7	$C_{CIP}{=}OOH$[c]
		175.5	$C_{KET}{=}O$
		178.2	$C_{SC}{=}OOH$
		180.2 & 181.2	$C_{\alpha}{=}OO^-$
CIP/CYS ASD	1.9	166.2	$C_{CIP}{=}OOH$
		173.5	$C_{\alpha}{=}OO^-$
		175.4	$C_{KET}{=}O$
CIP/ARG ASD	1.2	166.4	$C_{CIP}{=}OOH$
		175.1	$C_{KET}{=}O$
		180.7	$C_{\alpha}{=}OO^-$

[a]$C_{KET}{=}O$: ketone carbonyl of CIP; [b]$C_{SC}{=}OOH$: side chain carboxylic acid carbonyl of GLU; [c]$C_{CIP}{=}OOH$: carboxylic acid carbonyl of CIP.

The peak corresponding to the carboxylate carbonyl carbon of zwitterionic CIP appears at 173.0 ppm.[158] In the spectra of the ASDs this peak is shifted to 166.2–166.7 ppm. In the zwitterion, this carbonyl is part of an electronegative carboxylate group, resulting in greater deshielding than in the unionized form of the drug, and thus a higher chemical shift. A similar shift was seen with the equivalent peak in the ^{13}C spectrum of sparfloxacin. The carboxylate carbonyl peak of zwitterionic sparfloxacin trihydrate appears at 169 ppm, whereas that of the

unionized form of the drug is located at 164.5 ppm.[248] The ^{13}C SSNMR spectrum of the CIP saccharinate salt, in which the carboxylic acid of CIP is unionized, was also found to contain a peak at 166.5 ppm, whereas this peak was absent from the spectra of the raw materials.[249]

In contrast to the carboxylic acid carbonyl of CIP, the ketone carbonyl, which appears at 173.7 ppm in the spectrum of the crystalline drug, is shifted slightly downfield in the ASDs, to 175.1–175.5 ppm (**Table 5.1**). Similarly, the equivalent carbonyl group demonstrated a higher chemical shift in the ^{13}C NMR spectrum of unionized sparfloxacin compared to the zwitterion.[248] As discussed in the previous section, the peak corresponding to the ketone carbonyl stretch also shifted to higher wavenumbers in the FTIR spectra of the ASDs. The participation of this group in intramolecular hydrogen bonding with the neighboring unionized carboxylic acid results in the formation of a constrained six-membered ring, which appears to have a deshielding effect on the ketone carbon. The results of the SSNMR studies therefore reinforce the hypothesis that the carboxylic acid of CIP is unionized in these ASDs, and it can be concluded that proton transfer to the carboxylate group of the drug occurred during the milling process. This is unlikely to be due to the conversion of zwitterionic CIP to the unionized form, as ball milling has been proven to be ineffective at bringing about this transformation, as described in Chapter 2. Therefore, the piperazine amino group of CIP is most likely ionized in the ASDs, as suggested by the results of FTIR analysis. The interaction of this positively charged group with the anionic α-carboxylate groups of the amino acids would result in proton transfer from the amino acid to the drug, and the formation of a salt. No significant changes in the chemical shifts of the carbonyl groups of the amino acids were seen in the ^{13}C NMR spectra of the ASDs compared to the pure ball milled amino acids, and therefore their α-carboxylate groups appear to remain ionized in the ASDs. As previously mentioned, CIP is more likely to form ionic bonds with the α-carboxylate groups of ASP and GLU rather than the side chain carboxylic acids due to their lower pK_a values.

Another indicator that proton transfer occurs from the amino acids to CIP upon milling is that the four ASDs were an intense yellow color, whereas the starting materials are white or off-white. A similar change in color was also observed with the polymeric CIP ASDs and amorphous CS 1:1 and 2:1 salts, as described in Chapter 3 and 4. This supports the assumption that CIP is forming a salt with the amino acids in these ASDs. In contrast, the

semi-crystalline SDs were pale yellow following milling, due to the smaller degree of proton transfer that occurred in these samples.

As previously discussed, the crystalline ARG raw material used in this study appears to be a mixture of the unionized and zwitterionic form of the amino acid. This would explain the presence of two peaks in the carbonyl region of ARG's ^{13}C SSNMR spectrum (**Figure 5.5c** and **Table 5.1**). The peak corresponding to the α-carboxylate carbonyl of ARG appears upfield when it is protonated, due to the increased shielding effect of the unionized carboxylic acid group.[218] Therefore, the peaks at 180.6 ppm and 179.4 ppm in the ^{13}C spectrum of ball milled ARG may be attributed to the zwitterionic and unionized form of the amino acid, respectively.

In addition to the determination of intermolecular interactions, SSNMR can also provide information on the mobility and miscibility of an ASD, via measurement of the spin-lattice relaxation time (^1H T_1). The ^1H T_1 of a solid decreases upon amorphization due to an increase in molecular mobility, which enables energy transfer.[247] The ^1H T_1 values of all of the ASDs were significantly lower than those of crystalline CIP and the amino acids, which confirms their amorphous nature (**Table 5.1**). If the two components of a mixture are molecularly mixed they will have a common T_1.[247] This was the case with the CIP/amino acid ASDs, which suggests that they consist of a single amorphous salt phase.

5.3.3 Thermal Analysis

The DSC thermograms of the amino acid ASDs and SDs obtained with a heating rate of 10 ^oC/min are shown in **Figure 5.6**, and a summary of their thermal properties is given in **Table 5.2**. DSC thermograms of the amino acid starting materials and CIP/amino acid PMs are shown in Figure **A.4.2**.

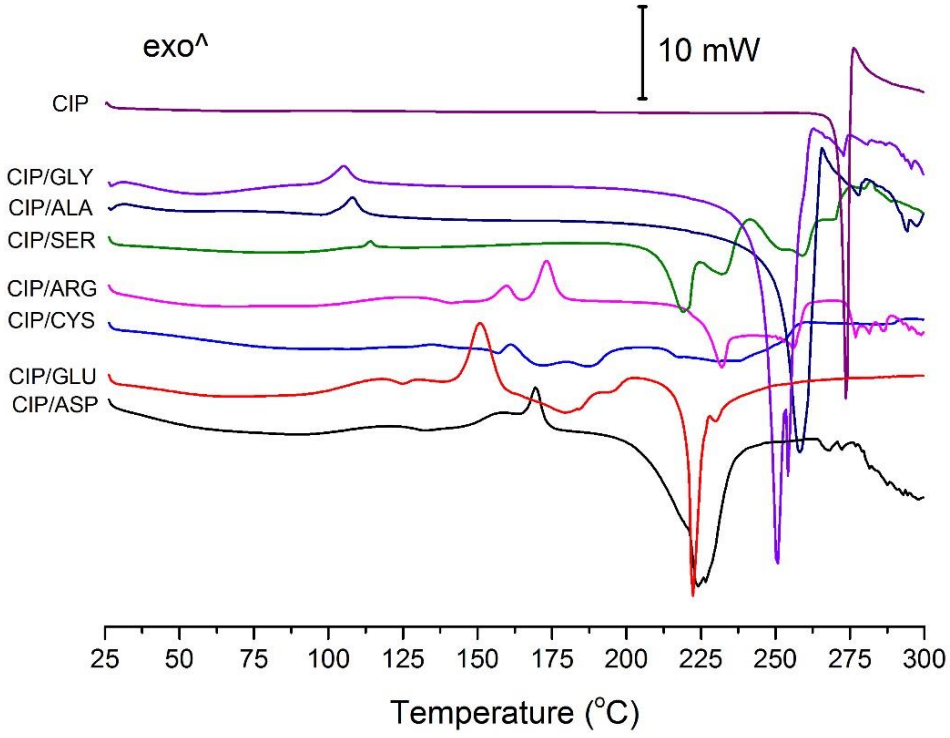

Figure 5.6. DSC thermograms of CIP/amino acid ASDs and SDs.

Table 5.2. Thermal Properties of CIP/Amino Acid ASDs and SDs Heated at 10 °C/min

Sample	T_g (°C)	Crystallization onset (°C)	Crystallization peak (°C)
CIP/ASP	135.8 ± 0.6	168.4 ± 0.5	171.3 ± 0.3
CIP/GLU	121.7 ± 0.9	149.2 ± 0.3	154.5 ± 0.1
CIP/CYS	104.0 ± 0.1	157.8 ± 0.0	161.1 ± 0.1
CIP/ARG	136.9 ± 0.5	153.7 ± 0.7/ 166.4 ± 1.7	158.8 ± 0.9/ 169.7 ± 0.2
CIP/SER	N.D.	111.3 ± 0.6	113.8 ± 0.5
CIP/ALA	N.D.	102.8 ± 0.2	108.1 ± 0.2
CIP/GLY	N.D.	98.2 ± 0.8	104.3 ± 0.8

5.3.3.1 Glass Transition

With each of the ASDs, a T_g was detected above that of pure amorphous CIP (86.7 °C). Due to the inherent difficulty in producing amorphous amino acids, there is little information in

the literature concerning the glass transition of pure amino acids. However, the T_g of freeze dried amorphous ARG has been independently reported as 55 ºC[250] and 18.4 ºC,[62] while the T_g's of freeze dried solutions containing 5% gelatin plus 10% ALA or SER in water were found to be -21.55 and -18.75 ºC, respectively.[251] The T_g's of GLY and GLU have also been reported as approximately 7 ºC[252] and -17 ºC,[253] respectively. Unfortunately, the T_g's of ASP and CYS could not be found in the literature. However, based on the published T_g values of other amino acids, it is reasonable to assume that they are significantly lower than those of the ASDs. Therefore, the measured T_g's of the CIP/amino acid ASDs are much higher than what would be expected if the two components were simply mixed intimately together. This provides further evidence of amorphous salt formation. The presence of a single T_g in the thermograms of each of the ASDs indicates that the components are mixed on a molecular level and form a single amorphous phase,[41] as suggested by the results of SSNMR analysis.

Due to their low amorphous content, a T_g could not be detected for the three semi-crystalline SDs. High-speed DSC (HSDSC) was therefore carried out on the samples. When a higher heating rate is used for DSC, the same heat flow will occur over a shorter length of time. This causes signals to become larger, enabling low-energy transitions to be detected and measured.[254] As the heating rate was increased, the glass transitions of the ASDs appeared as larger step changes in the thermograms (**Figure A.4.3**). However, despite the use of heating rates of up to 300 ºC/min, the T_g's of the SDs could not be detected.

5.3.3.2 Crystallization

All of the ASDs underwent cold crystallization during DSC analysis, with onset temperatures approximately 30 ºC above the T_g. Small crystallization peaks could also be seen in the thermograms of the semi-crystalline SDs, confirming that a small portion of material was transformed to the amorphous phase. The onset of crystallization occurred at much higher temperatures with the ASDs than the SDs, indicating that they possess superior physical stability.[228]

In order to determine the species that crystallized from the ASDs and SDs during DSC analysis, PXRD and FTIR were carried out on all of the samples following the endset of crystallization. In the case of the semi-crystalline SDs containing GLY, ALA and SER, the

PXRD patterns matched those obtained after ball milling, i.e. with low intensity peaks matching those of zwitterionic CIP and the amino acid starting materials (**Figure 5.7a**). The PXRD pattern of CIP/SER contained an additional peak at 9.2 2θ degrees, which corresponds to the unionized form of CIP. Despite the fact that CYS appears to form a salt with CIP following four hours of ball milling, the ASD containing this amino acid also crystallized to zwitterionic CIP during DSC analysis. This suggests that the interactions between the drug and CYS were not of a sufficient strength to maintain the salt structure upon heating.

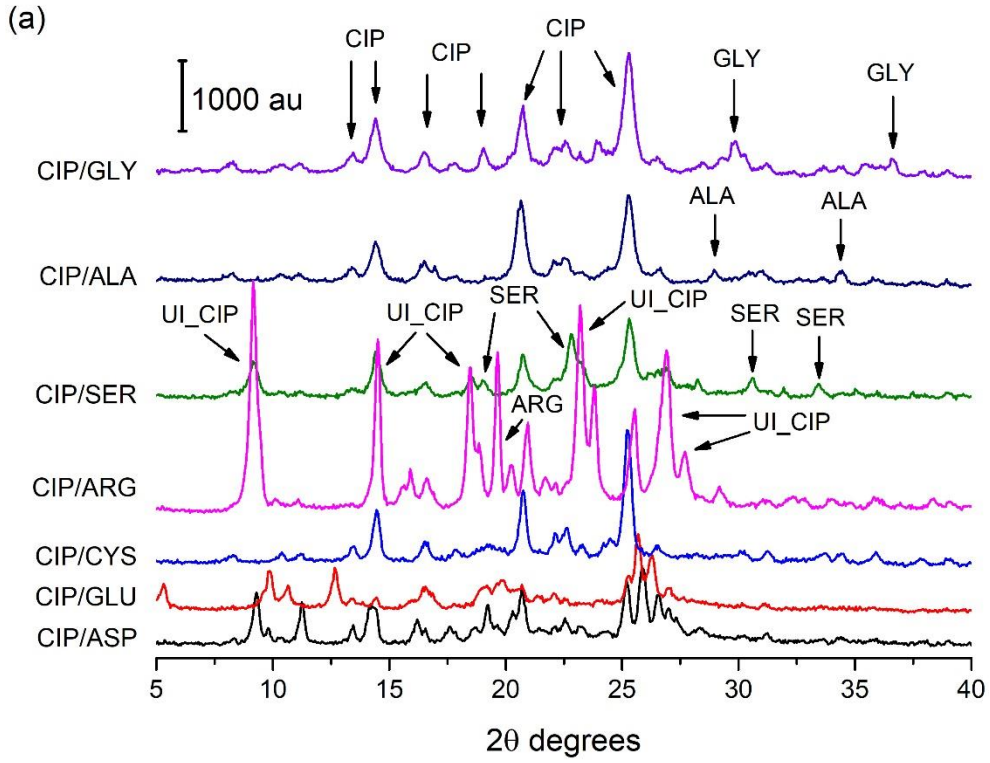

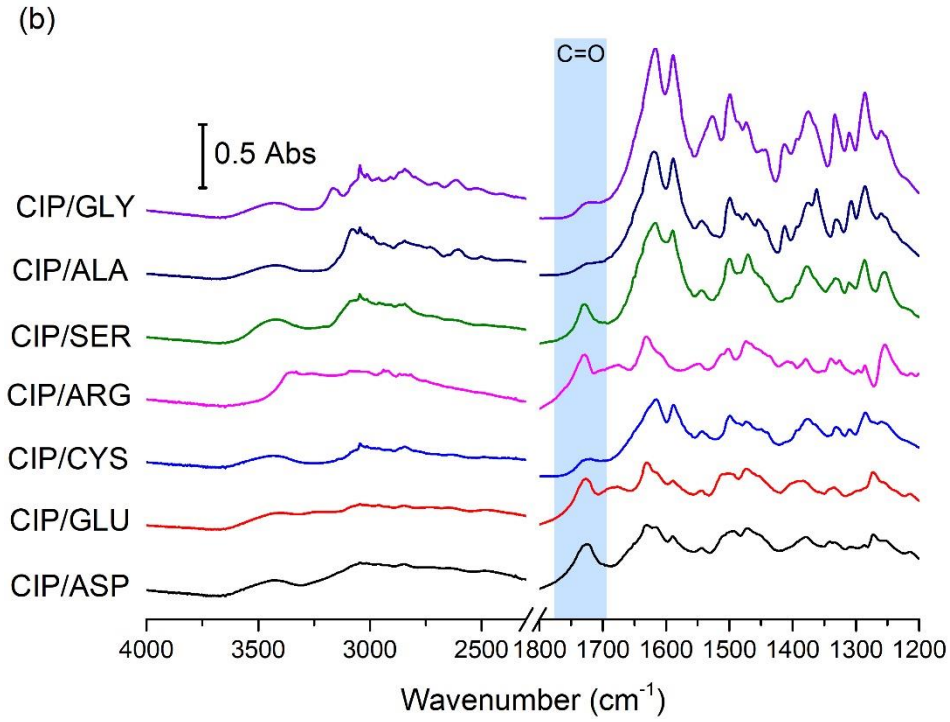

Figure 5.7. (a) PXRD analysis of ASDs and SDs following DSC crystallization. The arrows identify the principal peaks of the phases (see **Figure 5.8** for identification of phases with CIP/GLU and CIP/ASP). UI_CIP: unionized CIP. (b) FTIR analysis of ASDs and SDs following DSC crystallization. Peaks corresponding to the C=O stretch of carboxylic acid groups are highlighted in blue.

The DSC thermogram of the CIP/ARG ASD differs from the other samples by the presence of two exotherms. Double exothermic peaks are not unheard of for ball milled solids, as discussed in relation to the amorphous CIP/succinic acid 2:1 salt in Chapter 4. If crystal nuclei remain following ball milling, an initial exotherm will appear during DSC analysis due to surface crystallization, while a second peak will develop due to bulk crystallization.[103] In order to determine whether these peaks correspond to a two stage crystallization process, or to the formation of an intermediate phase, CIP/ARG was analyzed by PXRD immediately after both crystallization events. The diffraction patterns obtained in both instances were almost identical, but grew in intensity following the second crystallization exotherm. Therefore, it can be concluded that the formation of an intermediate phase did not occur.[103] Instead, the appearance of two exothermic peaks suggests that the CIP/ARG particles may have contained a number of surface crystal nuclei following milling, which were too small

to be detected by PXRD.[103] Increasing the heating rate during DSC analysis should reduce the rate of surface crystallization of an amorphous solid; however, a double exotherm was still observed when the CIP/ARG ASD was heated at 300 ^{o}C/min (**Figure A.4.3d**). This indicates that the surface of this sample crystallizes very quickly.[26] In contrast to the other samples, the major phase identified following the crystallization of CIP/ARG was that of the unionized form of CIP, while a peak of ARG was also present at approximately 19.6 2θ degrees (**Figure 5.7a**). The FTIR spectrum of this sample also matched that of the unionized form of CIP, with a peak at 1729 cm^{-1} due to the presence of the protonated carboxylic acid of the drug (**Figure 5.7b**). Therefore, like CIP/CYS, the arginine salt dissociated upon heating.

Unlike the other CIP/amino acid formulations, the PXRD patterns of the solids collected after crystallization of the CIP/ASP and CIP/GLU ASDs did not entirely match those of the starting materials. However, their FTIR spectra were very similar to those obtained with the freshly milled ASDs, although there were differences in peak intensity (**Figure 5.7b**). This indicates that CIP, ASP and GLU are in the same ionization state following crystallization, and that their ionic hetermolecular interactions remain intact. It was therefore hypothesized that the unidentified PXRD peaks belong to crystalline CIP aspartate and CIP glutamate salts. In order to verify this, attempts were made to produce these salts. However, this proved very difficult due to the poor solubility of CIP in water and other common solvents. In most cases pure CIP hydrate, aspartic acid or glutamic acid crystallized. Only slow crystallization of a 1:2 molar solution of CIP and amino acid in a water/ethanol mixture resulted in a solid with PXRD peaks resembling those obtained following DSC crystallization of these ASDs (**Figure 5.8**). Unfortunately, it was not possible to obtain pure crystals of a sufficient quality for single crystal X-ray analysis, and therefore the chemical composition of these samples could not be ascertained.

For comparison, a portion of the CIP/ASP and CIP/GLU ASDs were left exposed at RT to enable their slow crystallization. In the case of CIP/ASP, the crystals produced by slow solvent evaporation and RT crystallization of the ASD had very similar PXRD patterns (**Figure 5.8**). Additional peaks were present at 21.7, 22.9 and 23.8 2θ degrees in the diffractogram of the former sample due to contamination with residual crystalline ASP. The

peak at 5.1 2θ degrees in the diffractogram of this sample does not correlate with any of the raw materials, and may be due to the formation of a new phase, such as a hydrate of CIP aspartate. The PXRD diffractogram of the CIP/ASP ASD that crystallized during DSC analysis contained distinctive peaks at approximately 9.3, 9.9, 26.0 and 27.3 2θ degrees, and these were also present in the diffractograms of the other CIP/ASP crystals. Additional peaks in the diffractogram of the solid obtained following DSC crystallization match those of anhydrous zwitterionic CIP. Therefore, this sample crystallizes to a mixture of phases during DSC analysis.

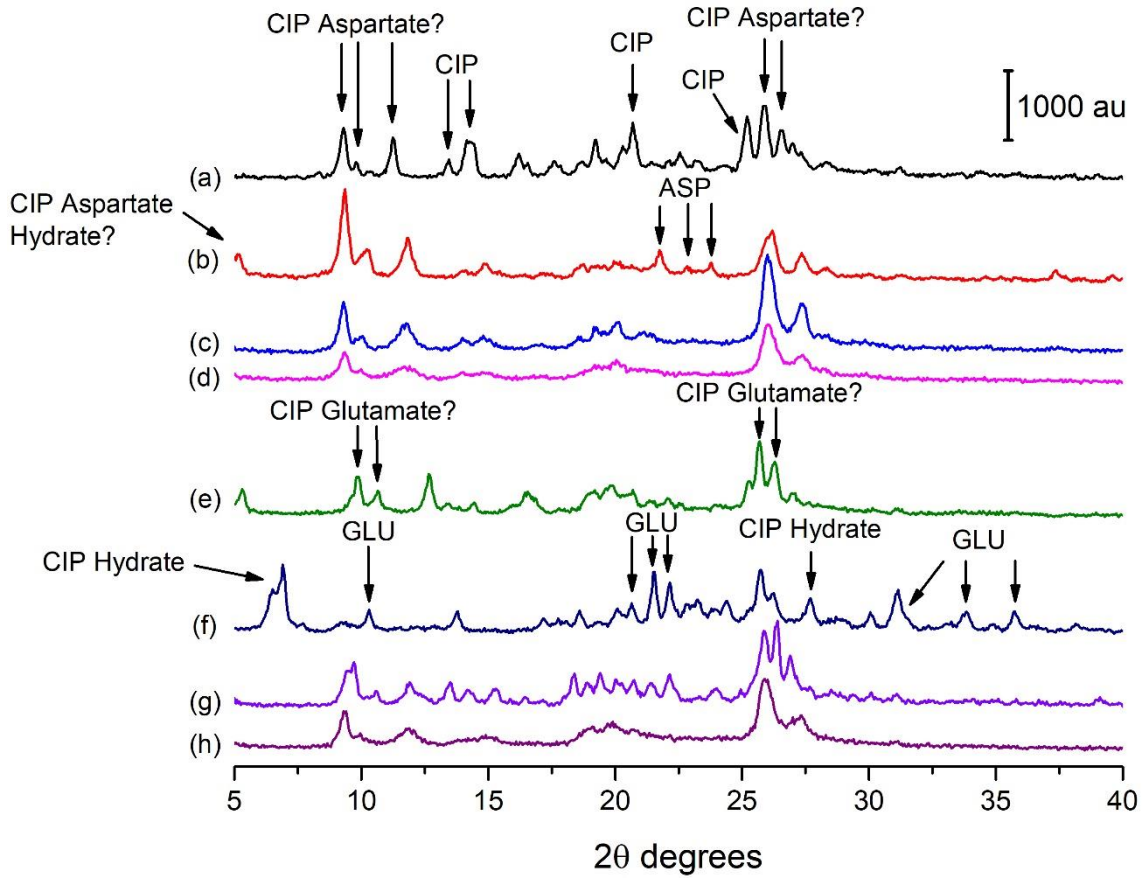

Figure 5.8. PXRD analysis of CIP/ASP and CIP/GLU crystals: (a) CIP/ASP ASD post DSC crystallization (b) CIP/ASP slow crystallization in ethanol/water (c) CIP/ASP ASD slow RT crystallization x 2.5 months (d) CIP/ASP ASD slow RT crystallization x 1 week (e) CIP/GLU ASD post DSC crystallization (f) CIP/GLU slow crystallization in ethanol/water (g) CIP/GLU ASD slow RT crystallization x 2.5 months (h) CIP/GLU ASD slow RT crystallization x 1 week. The arrows identify the principal peaks of the phases.

Solvent evaporation of a solution of CIP and GLU was unsuccessful at producing the CIP glutamate salt, and instead resulted in the crystallization of CIP 3.7 hydrate and GLU starting material. In contrast, when the CIP/GLU ASD was left exposed at RT for one week, its PXRD pattern did not correspond to any of the starting materials. However, it was almost identical to that of the CIP/ASP ASD that was crystallized in the same manner (**Figure 5.8**). If we are correct in our assumption that the CIP aspartate and glutamate salts are crystallizing from the corresponding ASDs, then the similarity of the PXRD patterns of these salts suggests that they are isostructural, i.e. they have a similar molecular packing but different chemical composition. Similarly, the PXRD patterns of a number of lamotrigine salts were found to closely resemble each other, and this was attributed to their isostructural nature. Although they were formed using different solvents and contained various dicarboxylic acids as counterions, the salts had the same packing arrangements and hydrogen bonding motifs.[255]

Following 2.5 months of exposure at RT, the peaks present in the diffractogram of the CIP/GLU ASD became more distinct, and a number of additional peaks appeared. Matching peaks were identified at approximately 9.8, 10.6, 21.4, 22.1, 25.8 and 26.3 2θ degrees in the diffractograms of the CIP/GLU ASDs crystallized at RT and during DSC analysis. The latter sample also contained a number of additional peaks, which did not correspond to any of the starting materials. Therefore, this ASD also seems to crystallize to a mixture of phases during DSC analysis, possibly consisting of the CIP glutamate salt, plus an unidentified phase or phases.

5.3.3.3 Melting

All of the ASDs and SDs undergo melting accompanied by decomposition at temperatures above 200 °C, which is not surprising given the high melting point of crystalline CIP and the amino acids (**Figure A.4.2a**). The crystalline drug and the amino acid starting materials also appear to undergo significant decomposition upon melting, resulting in broad melting peaks and complex thermograms. TGA was used to quantify this thermal degradation (**Figure 5.9**). An initial decrease in mass occurred from 25–100 °C with the four ASDs, due to the loss of sorbed water. This is expected for amorphous formulations due to their hygroscopic nature. A substantial total loss in mass of 20–34% was obtained with the ASDs, and they began to degrade at lower temperatures than the corresponding PMs. This may be due to the higher

molecular mobility of the amorphous samples, which can increase their reactivity and thus make them more prone to chemical degradation.[247]

(a)

TGA Mass Loss of CIP/Amino Acid ASDs

Sample	Mass Loss	Sample	Mass Loss
CIP/ASP	20.7%	CIP/GLU	17.9%
CIP/CYS	31.2%	CIP/ARG	34.2%

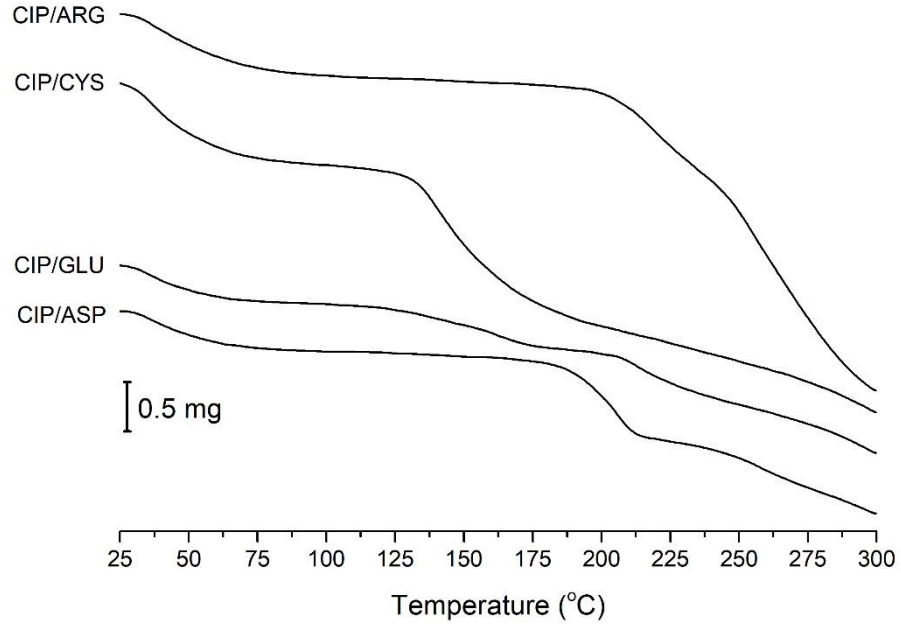

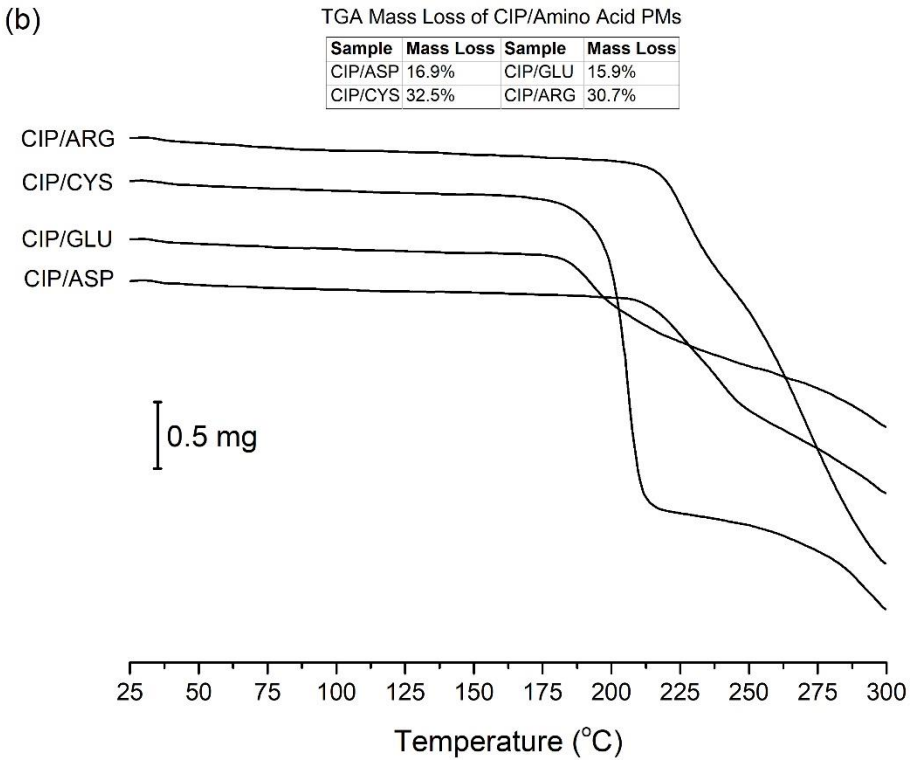

Figure 5.9. TGA analysis of (a) CIP/amino acid ASDs and (b) PMs.

The higher heating rates used in HSDSC should reduce the degree of degradation of a sample, as there will simply be less time for this to occur.[164] Although the thermograms of the ASDs and SDs were smoother when heated at 300 °C/min, substantial degradation still occurred with each sample upon melting, as can be seen from the complexity of the thermograms above 200–250 °C (**Figure A.4.3)**.

5.3.4 Stability Studies

The DVS isotherms of the CIP/amino acid ASDs are shown in **Figure 5.10**. Like the ASDs described in the previous chapters, these samples have a great propensity for water sorption. The greatest increase in mass during DVS analysis was obtained with CIP/ASP, reaching 31.0% at 90% RH, followed by CIP/ARG (23.9%), CIP/CYS (21.1%) and CIP/GLU (17.9%).

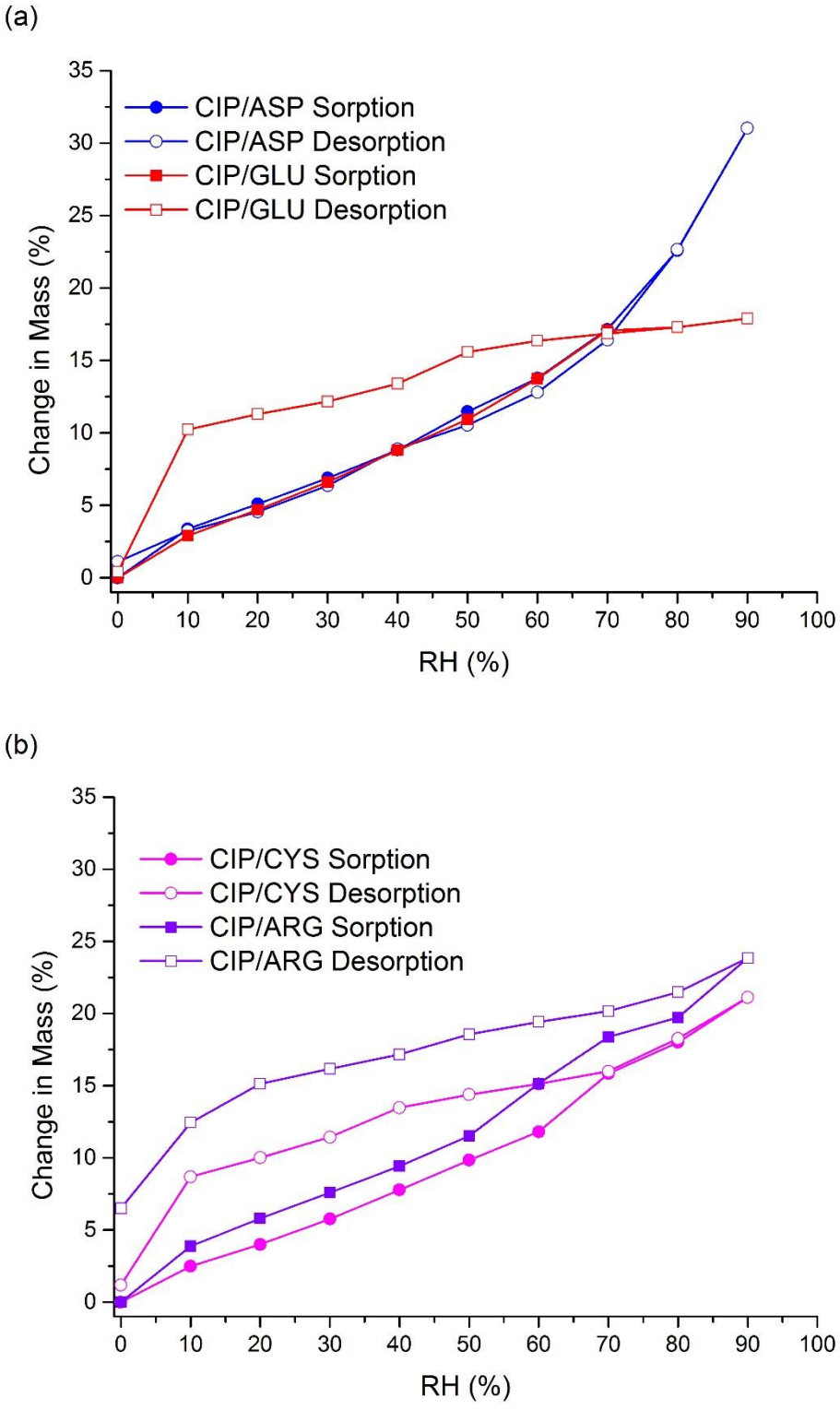

Figure 5.10. DVS analysis of CIP/amino acid ASDs: (a) CIP/ASP and CIP/GLU (b) CIP/CYS and CIP/ARG.

Unlike the other ASDs, the isotherm of CIP/ASP is convex in shape and shows minimal hysteresis. This suggests that water is mainly adsorbed to the surface of particles in this sample, and does not enter the interior significantly. In contrast, considerable hysteresis was observed with the other ASDs. Hysteresis is commonly encountered with amorphous solids due to water absorption into the bulk of the particles.[256] Therefore, the water uptake mechanism of the ASDs containing GLU, CYS and ARG differs from that of CIP/ASP, which may be due to differences in porosity.

Hysteresis was particularly evident in the isotherm of the CIP/ARG ASD, as the sample mass did not return to its original value at the end of the desorption cycle. Hysteresis may occur due to the failure of the sample to equilibrate fully during DVS analysis, i.e. if too short an equilibration time is used.[257] The full sorption-desorption cycle was therefore repeated on CIP/ARG using a maximum equilibration time of six hours, rather than the usual time of three hours. However, at the end of the study the mass of the sample was still significantly larger than its starting value (**Figure A.4.4**). The plot of change in mass vs. time for this sample also showed that it did not remain at any RH stage for longer than 180 min, meaning that it had sufficient time to equilibrate fully. Therefore, this hysteresis is not due to inadequate equilibration time. A possible alternative explanation may be that the diffusion of water from the interior of these particles to the surface is significantly slower than water uptake, and therefore a portion of absorbed water remained in the sample at the end of the study.[224]

PXRD analysis at the end of the desorption cycle showed that all of the ASDs crystallized during the DVS study (**Figure 5.11a**). As previously described, absorbed water can act as a plasticizer for amorphous materials, increasing their molecular mobility and decreasing their T_g, leading to crystallization.[42] The PXRD diffractograms obtained with the CIP/ARG, CIP/CYS and CIP/GLU ASDs matched those of the amino acid starting materials plus the CIP 3.7 hydrate. In contrast, the PXRD pattern obtained with CIP/ASP at the end of the DVS experiment resembled that obtained by slow solvent evaporation of an ethanolic solution of CIP and ASP (**Figure 5.8b**), with matching peaks at approximately 5.2, 26.1 and 27.3 2θ degrees. As discussed above, the product obtained from this slow crystallization process is believed to contain CIP aspartate, plus an unidentified phase, possibly a hydrate of this salt.

Additional unidentified peaks were present at approximately 10.3, 13.8 and 20.0 2θ degrees in the diffractogram of CIP/ASP following DVS, which possibly may also correspond to a hydrate of CIP aspartate.

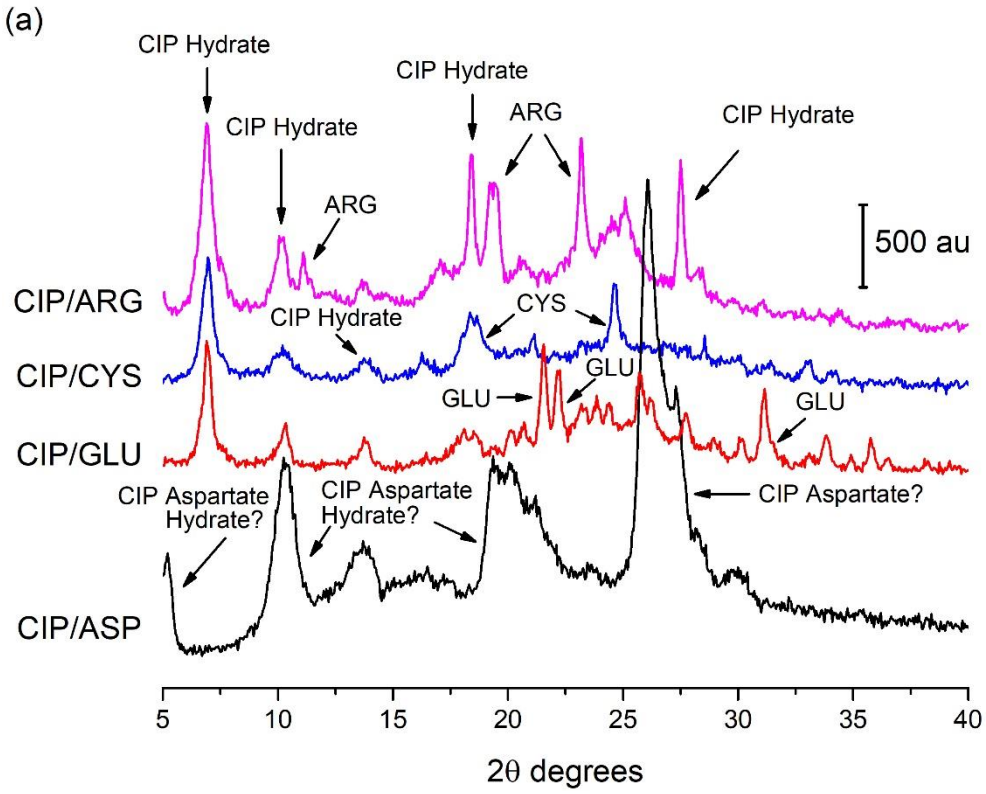

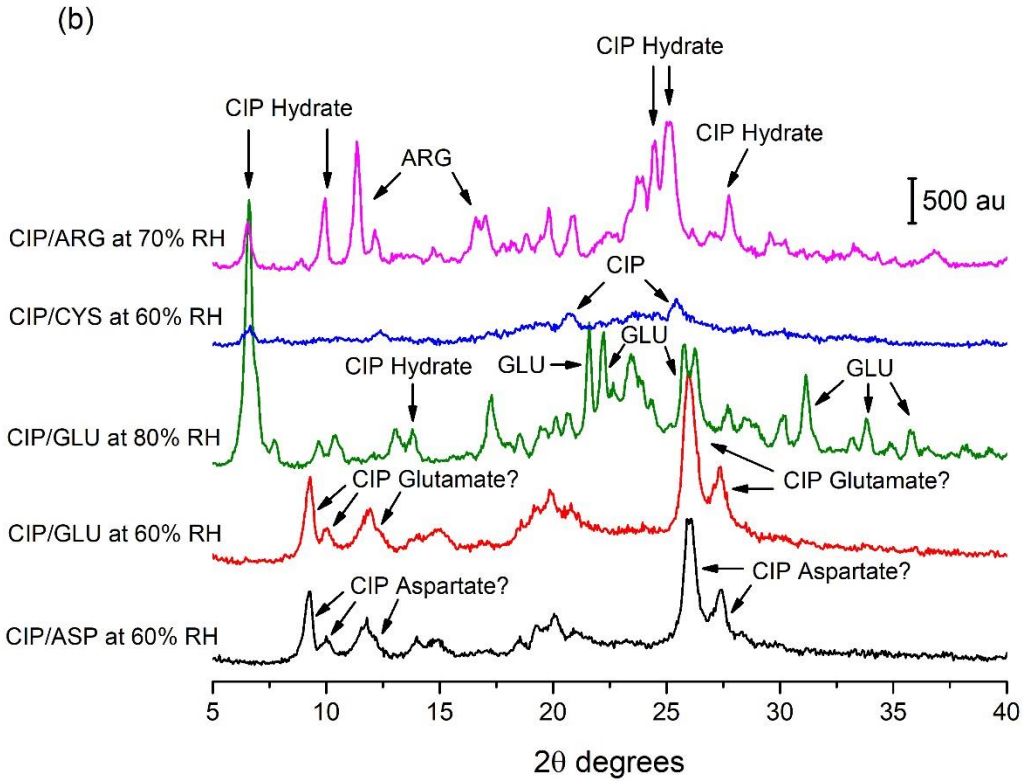

Figure 5.11. PXRD analysis of CIP/amino acid ASDs following DVS studies (a) at the end of desorption stage and (b) at various RH values during the sorption stage. The arrows identify the principal peaks of the phases.

Crystallization during water sorption can usually be identified by weight loss, as the crystalline solid cannot retain all of the water absorbed by the amorphous material.[91] From the change in mass vs. time plots of these samples, it could be seen that the ASD containing ARG crystallized at 70% RH during the sorption stage, whereas the other ASDs crystallized at 60% RH (data not shown). PXRD was also carried out on the samples following these crystallization events to determine whether the phase which initially crystallized differs from that obtained at the end of the study (**Figure 5.11b**). A similar PXRD pattern was obtained with the CIP/ARG ASD at both time points, although there were some differences in peak intensity. In the case of CIP/CYS, at 60% RH only small peaks corresponding to zwitterionic CIP and the CIP 3.7 hydrate could be identified. The drug therefore appears to crystallize at a lower RH level than the amino acid in these samples.

Although the PXRD patterns of CIP/ASP were quite similar at both time points, the sample which crystallized at 60% RH more closely matched that obtained when the ASD was allowed to crystallize slowly at RT via exposure to the air (**Figure 5.8c**). Two crystallization events were detected with the CIP/GLU ASD, at 60% and 80% RH. Following the second crystallization the PXRD pattern was very similar to that obtained at the end of the desorption stage, but the peaks were of a higher intensity. At 60% RH however, the PXRD pattern of the sample was almost identical to that of CIP/ASP at the same RH level. The same pattern was also obtained when both of these ASDs were left exposed at RT for one week, during which time they would have experienced a similar temperature to that used in DVS analysis. As discussed above, the fact that very similar X-ray diffractograms were obtained with CIP/ASP and CIP/GLU upon RT crystallization of the ASDs may be due to the formation of isostructural CIP aspartate and CIP glutamate salts. Therefore, these ASDs appear to initially crystallize to their corresponding salts during the water sorption stage of DVS analysis. The glutamate salt then dissociates to the raw materials at higher RH levels, whereas CIP aspartate forms an additional unidentified phase, perhaps due to hydration of the salt. A summary of the major phases identified following crystallization of the ASDs during DSC and DVS analysis is presented in **Figure A.4.5**.

As all of the ASDs crystallized when exposed to high humidity during DVS analysis, a long-term stability study was carried out under dry conditions at RT. All of the ASDs remained fully X-ray amorphous for 10 months under these storage conditions; however, at the 12 month time point a small peak was visible at 25.3 2θ degrees in the X-ray diffractogram of CIP/CYS, which corresponds to the most prominent PXRD peak of anhydrous zwitterionic CIP (**Figure A.4.6**). This ASD would be expected to have the lowest stability of these samples due to its lower T_g. In addition, the fact that CIP/CYS crystallized to zwitterionic CIP during DSC and DVS analysis, whereas CIP/ASP and CIP/GLU appear to have formed the corresponding crystalline salts, indicates that the interactions between the drug and amino acid are somewhat weaker in the former formulation. The higher T_g's obtained with the other ASDs suggests that CIP interacts more extensively with ASP, GLU and ARG. which would help to reduce the molecular mobility of the drug and increase the energy barrier to crystallization.[52,55]

5.3.5 Dynamic Solubility Studies

The concentration of CIP obtained during solubility studies in water, FaSSIF and FaSSGF is shown in **Figure 5.12**. Expanded sections of the plots are also shown for clarity. The samples behaved very similarly in water and FaSSIF. In each case the highest CIP concentration was obtained with the CIP/ASP ASD, which reached a maximum concentration of 49.6 ± 7.1 mg/ml and 44.5 ± 3.0 mg/ml in each medium, respectively. This was followed by the CIP/GLU ASD, which attained 36.6 ± 2.1 mg/ml and 31.3 ± 0.5 mg/ml, respectively, in these media. The concentration of CIP increased rapidly with both ASDs in the first few minutes, and then remained fairly constant for the duration of the study.

While the CIP/ASP and CIP/GLU PMs behaved similarly to the equivalent ASDs, a significantly higher concentration was obtained with the amorphous samples. This solubility advantage can be attributed to their solid state, i.e. formulation as an amorphous salt. However, high CIP concentrations of 20.3 ± 0.7 mg/ml and 16.9 ± 2.3 mg/ml were still obtained with the CIP/ASP and CIP/GLU PMs, respectively, in water. The ability of these PMs to increase the solubility of CIP may be explained by their effect on pH. The pH of 2% (w/v) solutions of the pure amino acids in water was therefore measured, which resulted in a pH of 2.9, 3.1, 4.7 and 11.6 with ASP, GLU, CYS and ARG, respectively. The solubility of CIP is greatly increased at low pH, as it bears a net positive charge. Therefore, a significant improvement in drug solubility would be expected for mixtures containing ASP and GLU. The pH of the solutions at the end of the solubility studies was also measured, and a comparison of these values is shown in **Figure A.4.7**. Like other pharmaceutical salts, the amino acids most likely dissociate rapidly upon addition to solvent, altering the pH of the dissolution layer around the drug and increasing its solubility and dissolution rate.[217] As expected, the lowest final pH was obtained with the samples containing the acidic amino acids. Both the PMs and ASDs containing ASP and GLU had a pH of 4.4–4.9 at the end of the study, no matter what the original pH of the medium.

The ASDs containing CYS and ARG offered less of a solubility advantage than the acidic amino acids. Crystalline CIP has a low aqueous solubility of 0.09 mg/ml. ANOVA and Tukey's multiple comparison test showed that statistically significantly higher concentrations of 1.3 ± 0.3 mg/ml and 1.1 ± 0.04 mg/ml were obtained with the CIP/CYS

and CIP/ARG ASDs in water, respectively. While the PM containing ARG was approximately 7 times more soluble than the pure drug in water, the CIP/CYS PM did not offer a significant advantage. The increased solubility of the former PM is most likely due to its effect on pH. At the end of the study the pH was found to be 9.6 with this PM, compared to 6.4 for CIP/CYS. This should result in a greater proportion of ionized CIP (in this case negatively charged), and thus higher drug solubility. In FaSSIF pure CIP reached a slightly higher concentration of approximately 0.14 mg/ml at the end of the study. As in water, a significantly higher concentration was obtained with the CIP/ARG and CIP/CYS ASDs, however they were substantially less soluble than the ASDs containing ASP and GLU, reaching only 0.5 ± 0.0 mg/ml and 0.3 ± 0.0 mg/ml, respectively. In contrast, the CIP/ARG PM did not differ significantly from the pure drug, and the CIP/CYS PM also had a low solubility of approximately 0.2 mg/ml. Therefore, the improved solubility of these ASDs compared to the PMs may be attributed to their amorphous nature.

A much higher concentration was obtained with all of the samples in FaSSGF compared to FaSSIF and water. As discussed in Chapter 3, CIP is positively charged at pH 1.6, and thus far more soluble, reaching a concentration of 11.3 ± 0.2 mg/ml at the end of the study. Each ASD was more soluble than the equivalent PM at this pH, confirming the solubility advantage of the amorphous formulations. Again, the samples containing the acidic amino acids had the highest solubility, with the CIP/ASP and CIP/GLU ASDs reaching concentrations of 240.1 ± 38.6 mg/ml and 120.4 ± 6.4 mg/ml, respectively. These samples are therefore significantly more soluble in FaSSGF than the polymer/CIP succinate salt ASDs described in Chapter 4, whereas a similar concentration was obtained with all of these ASDs in water and FaSSIF. The solubility of the CIP/ASP and CIP/GLU PMs was approximately 15 and 8 times greater than that of the crystalline drug, respectively. The CIP/CYS ASD and PM were also significantly more soluble in FaSSGF, reaching approximately 17.0 ± 0.4 mg/ml and 15.1 ± 1.6 mg/ml, respectively. In contrast, the solubility of the CIP/ARG ASD only increased modestly to 3.7 ± 0.2 mg/ml, while that of the CIP/ARG PM decreased compared to water to 0.18 ± 0.0 mg/ml. Again, this may be explained by pH effects. While the samples containing ARG produced a basic pH in water and FaSSIF, the lower starting pH of FaSSGF resulted in a more neutral overall pH upon dissolution of these samples, and thus lower CIP solubility.

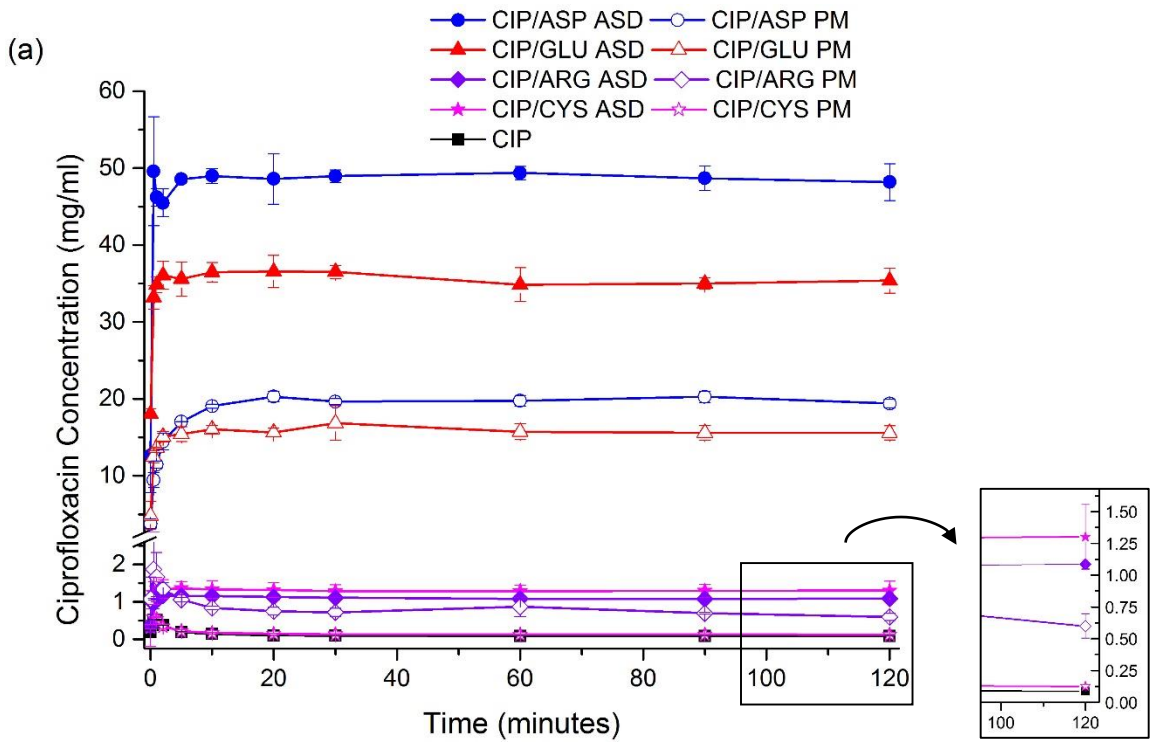
(a)
CIP/ASP ASD
CIP/ASP PM
CIP/GLU ASD
CIP/GLU PM
CIP/ARG ASD
CIP/ARG PM
CIP/CYS ASD
CIP/CYS PM
CIP
Ciprofloxacin Concentration (mg/ml)
Time (minutes)

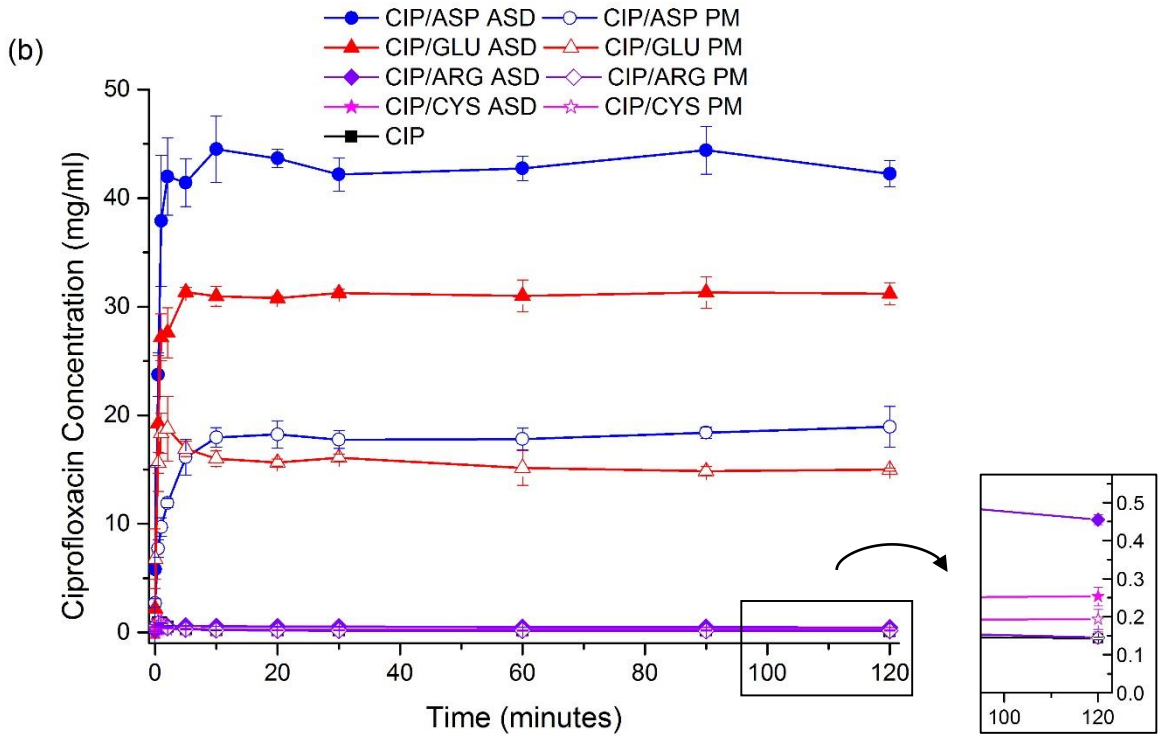
(b)
CIP/ASP ASD
CIP/ASP PM
CIP/GLU ASD
CIP/GLU PM
CIP/ARG ASD
CIP/ARG PM
CIP/CYS ASD
CIP/CYS PM
CIP
Ciprofloxacin Concentration (mg/ml)
Time (minutes)

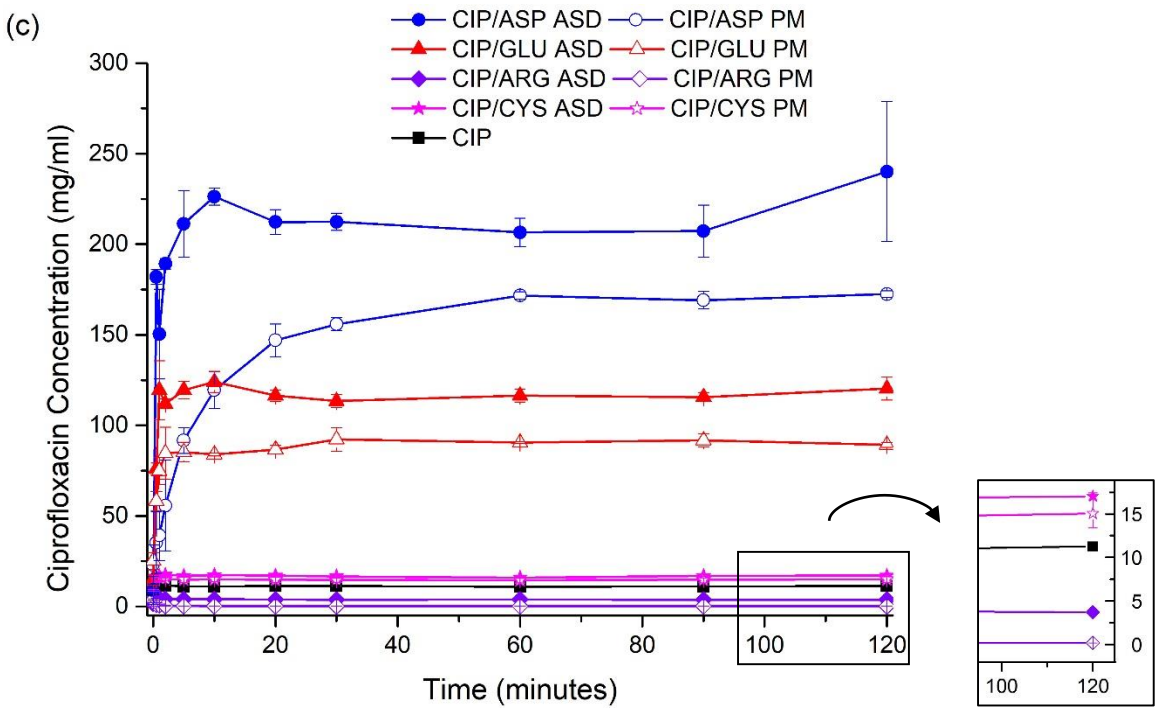

Figure 5.12. Solubility studies in (a) water (b) FaSSIF and (c) FaSSGF at 37 ºC. The average of at least 3 experiments is plotted, ± the standard deviation.

PXRD analysis of the solid residues left at the end of the solubility studies showed that all of the samples crystallized in each solvent (**Figure A.4.8**). In each case, less intense PXRD peaks were obtained with the ASDs than the PMs. The CIP 3.7 hydrate crystallized from all of the samples containing CYS and ARG, the CIP/GLU and CIP/ASP ASDs and CIP/GLU PM in FaSSIF, and the CIP/ASP ASD and PM in water. The PXRD patterns of the remaining ASP and GLU ASDs and PMs on the other hand matched that of the CIP 3.1 hydrate.

In order to confirm that the solubility advantage of the ASDs was not purely due to their effect on pH, a theoretical pH-solubility profile was constructed for CIP, as described in Chapter 3. CIP HCl was also included for comparison. As can be seen from **Figure 5.13**, the experimental solubility data did not fit the theoretical pH-solubility curve of CIP exactly. The experimental data points obtained in water with the ASDs and PMs containing ARG and CYS align quite well with the theoretical curve of CIP, whereas in FaSSIF they displayed slightly higher than predicted solubilities. This may be due to the presence of surfactants in this medium, which should improve the solubility of the drug via solubilization. Both of

these ASDs were more soluble than the equivalent PMs in all media. This suggests that the solid state changes introduced by ball milling contributed to their improved solubility. Like the pure drug, the solubility of these samples was increased in FaSSGF, so that the data points lay closer to the CIP HCl curve. The CIP/ASP and CIP/GLU PMs also behaved similarly to CIP HCl in water and FaSSIF. In FaSSGF the combination of an acidic counterion and low pH medium enabled an even larger amount of drug to enter solution from these samples. However, with the corresponding ASDs, a greater divergence from the theoretical pH-solubility plot was observed. Therefore, while pH certainly plays a part in the solubility enhancement of these samples, their disordered nature resulted in an additional increase in solubility in each case.

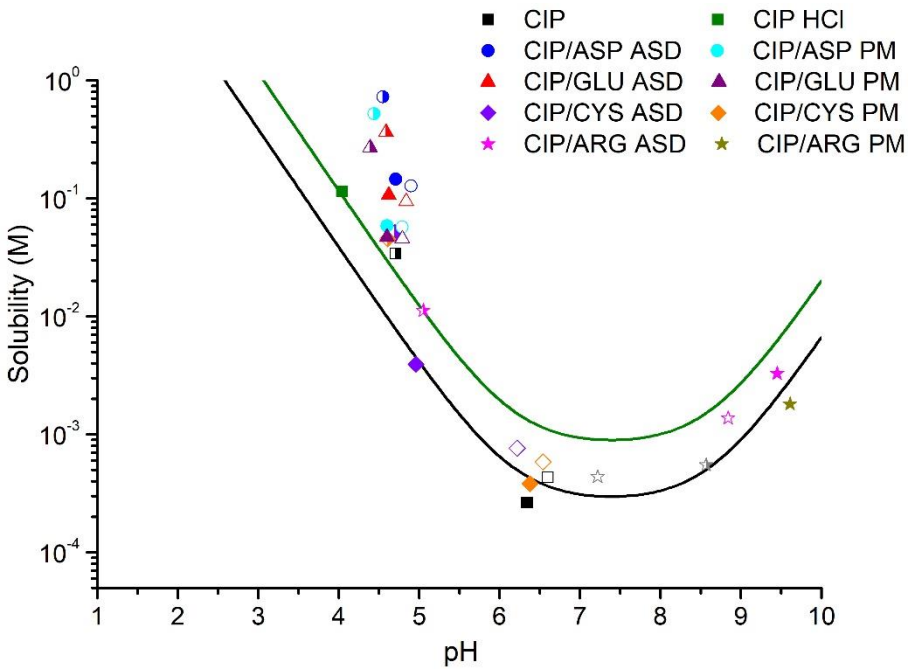

Figure 5.13. Theoretical pH-solubility profiles of CIP (black) and CIP HCl (green). The symbols represent the average concentrations obtained from solubility studies after two hours in water (filled symbols), FaSSIF (empty symbols) and FaSSGF (half-filled symbols).

5.3.6 PAMPA Permeability Study

The results of the PAMPA study on the CIP/amino acid ASDs are shown in **Table 5.3**. The values calculated for CIP and CIP HCl are listed again for comparison. Again, a pH of 7.4 was used in both the donor and acceptor compartments for these samples. As shown in **Table 5.3**, all of the samples had a P_e value less than 1 x 10^{-6} cm/s, and can therefore be described as poorly permeable.[204] CIP HCl, CIP/GLU and CIP/ASP had the lowest permeability, however they were not statistically significantly different from each other, as shown by Tukey's multiple comparison test. CIP/CYS had the highest permeability, followed by CIP/ARG, and then CIP. While the P_e of CIP was significantly lower than that of CIP/CYS, CIP/ARG did not differ significantly from either sample. The lower permeability of CIP HCl, CIP/ASP and CIP/GLU may be attributed to their acidic counterions. The presence of these acidic compounds in solution will increase the proportion of positively charged CIP, making the drug more soluble, but decreasing its lipophilicity. Similarly, the amorphous CIP succinate salts described in Chapter 4 were also found to be less permeable than the pure drug. Such a trade-off between increased solubility and decreased permeability is a common issue with solubility-enhancing formulations.[31] In contrast, CYS and ARG, like the polymers studied in Chapter 3, do not appear to significantly increase the proportion of ionized CIP in solution, and therefore the formulation of CIP as an ASD with these amino acids did not decrease its permeability.

Table 5.3. PAMPA Permeability Values of CIP

Sample	P_e x 10^6 (cm/s)
CIP	0.56 ± 0.06
CIP HCl	0.32 ± 0.00
CIP/ASP	0.38 ± 0.05
CIP/GLU	0.31 ± 0.01
CIP/CYS	0.87 ± 0.15
CIP/ARG	0.73 ± 0.04

As previously discussed, due to its simplicity, the PAMPA model only estimates passive transcellular drug absorption. As the tight junctions in between epithelial cells are believed to be selective for positively charged molecules,[258] the cationic form of CIP should be able to cross the intestinal barrier relatively easily via the paracellular route. Therefore, the total in vivo absorption of these samples, in particular the ASDs containing ASP and GLU, is likely to be somewhat higher than that estimated here. However, PAMPA is a convenient method for quickly comparing the permeability of the ASDs to that of the pure drug, which is why it was carried out in this study.

5.4 Conclusions

Amino acids have recently emerged as efficient ASD stabilizers for a number of drugs, and in this study the ability of a variety of amino acids to fulfill such a function for CIP was investigated. While semi-crystalline SDs were obtained with SER, ALA and GLY, dry milling with ASP, GLU, CYS and ARG resulted in fully X-ray amorphous solid dispersions. In each case, FTIR and SSNMR confirmed the formation of an amorphous salt, with an ionic interaction between the positively charged piperazine amino group of CIP and the negatively charged α-carboxylate groups of the amino acids. The T_g's of the ASDs were significantly higher than those of the starting materials, which is also indicative of salt formation.

The ASDs remained fully X-ray amorphous for at least 10 months when stored under dry conditions, however after 12 months CIP/CYS showed some evidence of crystallization. This indicates that CIP does not interact as strongly with CYS as it does with the other amino acids. All of the ASDs also began to crystallize at 60–70% RH during vapor sorption studies. Significant improvements in the solubility of CIP were seen with all of the ASDs, in particular with those containing ASP and GLU. This can be attributed to the pH-lowering effect of the acidic amino acids. In each case, the ASDs were significantly more soluble than the corresponding PMs, confirming that their amorphous state offers an additional boost in solubility. However, a trade-off between the solubility and permeability of the samples was observed. Like the commercial CIP HCl salt, the ASDs containing ASP and GLU were significantly less permeable than pure crystalline CIP, as the acidic counterions induce

protonation of the drug. In contrast, CIP/CYS showed a small but significant improvement in permeability compared to CIP, while CIP/ARG did not differ significantly. However, further studies with more representative permeability models would be necessary to determine whether any of these samples provide a true benefit in terms of in vivo absorption.

Chapter 6: Production of Enrofloxacin Amorphous Solid Dispersions – A Comparison with Ciprofloxacin

6.1 Introduction

Enrofloxacin (ENRO), or 1-cyclopropyl-7-(4-ethylpiperazin-1-yl)-6-fluoro-4-oxo-1,4-dihydroquinoline-3-carboxylic acid, is a fluoroquinolone antibiotic which is licensed solely for veterinary use. ENRO differs from the more widely known fluoroquinolone CIP by the presence of an ethyl substituent in the N3 position (**Figure 6.1**). Unlike CIP, ENRO is unionized in the solid state, and its crystal lattice is stabilized by a number of weak C–H•••O and C–H•••N hydrogen bonds,[129] in contrast to the extensive intermolecular interactions of CIP described in Chapter 2.

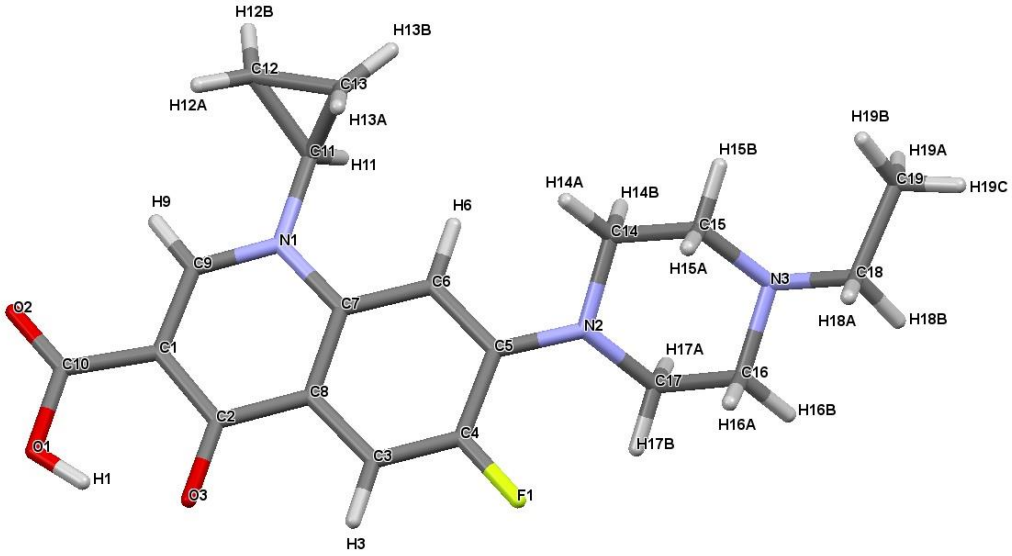

Figure 6.1. Chemical structure of enrofloxacin with atom labels.

Like CIP, ENRO is a poorly water soluble drug, with an intrinsic solubility of approximately 0.4 mg/ml,[130] and minimal solubility around pH 7.4.[131] Despite the theoretically higher hydrophilicity of CIP due to the absence of an aliphatic group in the N3 position, the strong crystal lattice of this drug reduces its aqueous solubility below that of ENRO. The greater lipophilicity of ENRO has been demonstrated in octanol/phosphate buffer pH 7.4 distribution experiments,[132] and it was also found to be more permeable than CIP in rat in situ permeability studies.[130] However, the permeability of ENRO still falls within the limits of poorly permeable,[132] and therefore it may be classified as a class 4 BCS drug.

In a recent study conducted by Karanam et al, a number of novel crystalline ENRO salts were found to be significantly more water soluble than the pure drug.[129] Single-crystal X-ray diffraction showed that the piperazine N3 nitrogen of ENRO is positively charged in the salts containing acidic counterions, such as succinic acid, fumaric acid and maleic acid, and forms an ionic bond with the carboxylate groups of the acids. The carboxylic acid of the drug remains unionized in these salts. In the ammonium salt on the other hand, ENRO was found to be in the anionic state, with a negatively charged carboxylate group and unionized piperazine group.[129] The solubility of ENRO was also increased significantly via formulation as the saccharinate salt by Romañuk et al. Like the equivalent CIP saccharinate salt, an ionic interaction between the positively charged N3 amino group of ENRO and negatively charged saccharin molecule was detected in this compound.[249]

As discussed in previous chapters, the solubility of a drug may be increased by converting it to the amorphous form, however suitable excipients are required to prevent its crystallization. This stabilization is usually brought about via interactions between the components, such as hydrogen or ionic bonds, and/or through steric hindrance, e.g. by polymers with long chains.[52] Unlike many other poorly soluble drugs, there is very little in the literature regarding amorphous solid dispersions of ENRO, and no mention of the pure amorphous form of the drug. However, one study by Chun and Choi describes the preparation of an enrofloxacin-Carbopol "complex" by mixing a solution of ENRO in 1% acetic acid with that of Carbopol in water, filtering and washing the precipitate, and then drying and milling the resultant powder.[259] The product was found to be X-ray amorphous, but lacked a clear T_g. The authors hypothesized that the positively charged tertiary amine of the drug formed an ionic bond with the carboxylate anions of Carbopol. Consequently, when the dissolution rate of the complex was found to be lower than that of the pure drug, this was attributed to the strength of the drug-polymer interactions.

Due to the absence of research in this area, the main aim of this study was to prepare ASDs of ENRO, and to examine their solid-state and pharmaceutical properties. As previously mentioned, the chemical structure of ENRO differs from that of CIP by the presence of an ethyl group on its N3 piperazine amino group. It was therefore of interest to determine whether this has an impact on the ability of the drug to interact with various polymers. The

water uptake behavior of the ENRO ASDs was also examined and compared to those of the equivalent CIP ASDs described in Chapter 3. In addition, the effect of ASD formation on the biopharmaceutical properties of ENRO was investigated via solubility, dissolution and bacterial studies.

6.2 Experimental Section

6.2.1 Materials

Enrofloxacin (ENRO) was obtained from Glentham Life Sciences (Wiltshire, UK). The details of all other materials and solvents used in this study are listed in Chapter 3.

6.2.2 Methods

6.2.2.1 Sample Preparation

Solid dispersions were produced by ball milling ENRO at RT with various polymers at a concentration of 40–60% (w/w), using the equipment described in Chapter 2. Each mixture was milled for 4–6 hours in total, in intervals of 15 min with 10 min breaks in between. Amorphous succinate salts were produced by ball milling ENRO and succinic acid in a 1:1 and 2:1 molar ratio for one hour. Crystalline ENRO was also milled alone for a total of 4 hours. ENRO was quench cooled by heating the crystalline drug to the endset of melting (~235 ºC) at 10 ºC/min in a DSC machine, and then immediately removing the sample to allow it to cool quickly at RT. Physical mixtures (PMs) were prepared by mixing relevant concentrations of ENRO and the polymers in a pestle and mortar for a few minutes.

6.2.2.2 Solid-State Characterization

6.2.2.2.1 Powder X-ray Diffraction

PXRD was performed as described in Chapter 2.

6.2.2.2.2 Solid-State Fourier Transform Infrared Spectroscopy

FTIR was performed as described in Chapter 2. Deconvolution of the FTIR spectra was conducted to facilitate their comparison. OriginPro 7.5 software was used to subtract the baseline and carry out Gaussian peak fitting on the spectra from ~1650–1400 cm^{-1}. In each case seven overlapping peaks were detected in this region, whose combined area and shape were similar to those of the original bands.

6.2.2.2.3 Differential Scanning Calorimetry

DSC was carried out using the same apparatus described in Chapter 2. To allow for water evaporation, the ASDs were first heated from 25 to 65 ^{o}C. When cool, the samples were reheated from 25 to 250 ^{o}C at a rate of 10 ^{o}C/min.

6.2.2.2.4 Modulated Temperature Differential Scanning Calorimetry (MTDSC)

MTDSC was carried out using a Q200 DSC instrument and TA Instruments DSC refrigerated cooling system (TA Instruments, New Castle, Delaware). Samples of 3–4 mg were heated in aluminum pans with sealed aluminum lids. Nitrogen was used as the purge gas at a flow rate of 20 ml/min. Samples were heated from 0 °C to 110–185 °C at 2 °C/min, with an amplitude of ± 0.318 °C and a modulation period of 60 sec. Results were analyzed with the Universal Analysis 2000 software (TA Instruments). The midpoint of the transition was taken as the T_g. Sapphire was used to calibrate the heat capacity, while indium was used for the calibration of enthalpy and temperature. All measurements were carried out in triplicate.

6.2.2.2.5 Calculation of Theoretical Glass Transition Values with Gordon-Taylor Equation

The theoretical T_g's of the ASDs were calculated using the Gordon-Taylor equation, as described in Chapter 3. Like the other polymers, the T_g (105 ^{o}C)[50] and average density (1.4 g/cm^3)[260] of Carbopol were obtained from literature, as was the average density value for ENRO (1.385 g/cm^3).[261]

6.2.2.2.6 High-Speed Differential Scanning Calorimetry

HSDSC was carried out using the equipment described in Chapter 2. Samples were heated from 25 to 300 ^{o}C at a rate of 300–500 ^{o}C/min.

6.2.2.2.7 Thermogravimetric Analysis

TGA was performed as described in Chapter 2.

6.2.2.3 Dynamic Vapor Sorption

DVS studies were carried out as described in Chapter 2.

6.2.2.4 Mathematical Modelling Using Young-Nelson Equations

In order to determine how water uptake occurs in the ASDs, the experimental sorption and desorption data was fitted to equations using the Young-Nelson model, as described previously:[262,263]

$$M_s = A(\beta + \theta) + B(\theta)RH \quad (6.1)$$

$$M_d = A(\beta + \theta) + B(\theta)RH_{max} \quad (6.2)$$

M_s and M_d are the amount of water sorbed and desorbed, respectively, at each RH value. This is expressed as a fraction of the dry mass of the sample. A and B are constants that can be defined as follows:

$$A = \frac{\rho_w Vol_M}{W_m} \quad (6.3)$$

$$B = \frac{\rho_w Vol_A}{W_m} \quad (6.4)$$

ρ_w is the density of water, W_m is the weight of the dry sample, and Vol_M and Vol_A are the volume of adsorbed and absorbed water, respectively. In equation 6.1 and 6.2, θ represents the fraction of sample surface that is covered by at least one layer of water molecules, and β is the mass of absorbed water at 100% RH. B(θ)RH is therefore the mass of absorbed water at a particular fraction of monolayer coverage, θ, and level of RH. A(β + θ) is equal to the total amount of adsorbed water, while Aθ is the mass of water in an entire adsorbed

monolayer, as a fraction of dry mass of the material. Aβ is the mass of water adsorbed in a multilayer. θ and β may be further defined as follows:[263]

$$\theta = \frac{RH}{RH + E(1 - RH)} \tag{6.5}$$

$$\beta = -\frac{ERH}{E-(E-1)RH} + \frac{E^2}{(E-1)} \ln\left[\frac{E-(E-1)RH}{E}\right] - (E+1)\ln(1-RH) \tag{6.6}$$

E is an equilibrium constant between water in the monolayer and condensed water adsorbed externally to the monolayer:

$$E = e^{-\left[\frac{q_1 - q_L}{k_B T}\right]} \tag{6.7}$$

q_1 is the heat of adsorption of water on the solid, and q_L is the heat of condensation of water, both in Joules/mole, T is the temperature in Kelvin, and k_B is Boltzmann's constant (1.38 x 10^{-23} J/K).

The experimental data obtained from DVS analysis of the ENRO ASDs, as well as the equivalent CIP ASDs described in Chapter 3, were fitted to equations 6.1 and 6.2 by iterative multiple linear regression. The sum of the squares of the residuals between the experimental and calculated values was used as fitting criteria. The multiple correlation coefficient (r) was calculated using Microsoft Excel 2007. Using the calculated values of A, B, θ and β, the profiles of water adsorbed in monolayer (Aθ) and multilayer (Aβ), and of absorbed water (Bθ), were determined.[263]

6.2.2.5 FaSSIF Dynamic Solubility Study

Solubility studies were carried out in FaSSIF as described in Chapter 3. The filtered aliquots were diluted with a 2.9 g/L solution of phosphoric acid, previously adjusted to pH 2.3 with triethylamine. The concentration of ENRO in each of the diluted samples was determined by UV spectrophotometry.

6.2.2.6 Dissolution Study

Dissolution studies were carried out as described in Chapter 3. Samples were diluted with a 2.9 g/L solution of phosphoric acid, previously adjusted to pH 2.3 with triethylamine. The

concentration of ENRO in each of the diluted samples was measured by UV spectrophotometry.

6.2.2.7 UV Spectrophotometry

UV analysis was carried out using the same equipment described in Chapter 3. The instrument was first blanked using a 2.9 g/L solution of phosphoric acid, previously adjusted to pH 2.3 with triethylamine. This buffer was also used to produce a range of concentrations of pure ENRO, in order to construct a calibration curve. The λ_{max} of these solutions was found to be 277 nm, therefore UV absorbance was measured at this wavelength.

6.2.2.8 Bacterial Studies

Bacterial studies were carried out by Dr. Anita Umerska in Université Angers as described in Chapter 3.

6.3 Results and Discussion

6.3.1 Production of ENRO Amorphous Solid Dispersions

Ball milling was first carried out on pure crystalline ENRO to determine whether it is possible to amorphize the drug in this manner. However, like CIP, following four hours of milling at RT, a disordered, semi-crystalline solid was obtained (**Figure 6.2a**). The most intense peaks in the X-ray diffractogram of ENRO may be seen at 7.4, 9.8, 14.9 and 25.8 2θ degrees. These peaks are also present in the diffractogram of ball milled ENRO, however their intensity is reduced. With quench cooled ENRO on the other hand, only one very small peak was visible at approximately 38.5 2θ degrees (**Figure 6.2a**).

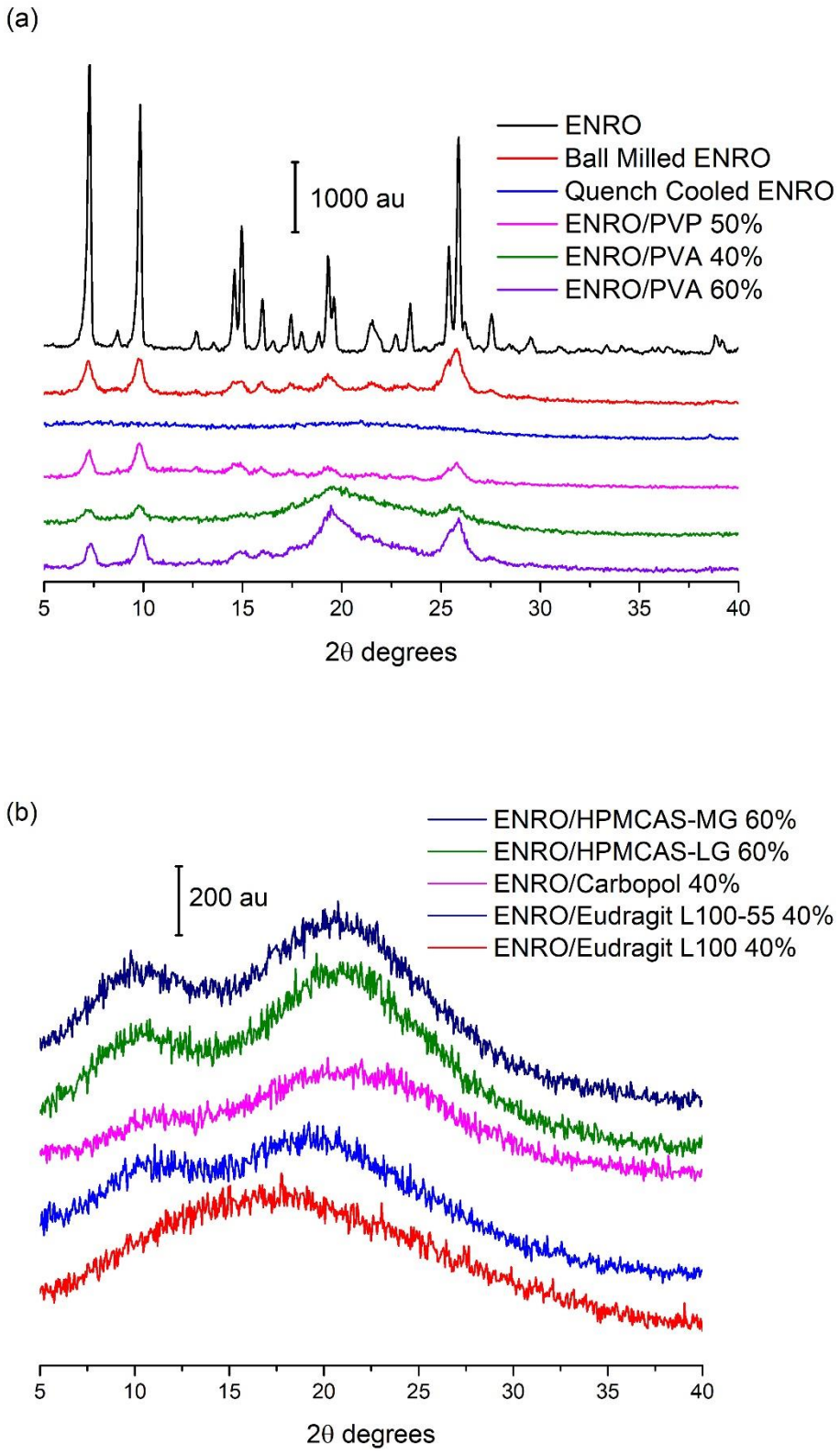

Figure 6.2. PXRD analysis of (a) ENRO and semi-crystalline solid dispersions and (b) ENRO ASDs.

As described in Chapter 3, fully X-ray amorphous solid dispersions were obtained when CIP was ball milled with Eudragit L100, Eudragit L100-55, Carbopol, HPMCAS-LG and HPMCAS-MG, and these acidic polymers also proved to be suitable co-formers for ENRO, with each resulting in a fully X-ray amorphous formulation (**Figure 6.2b**). In common with CIP, an obvious color change was observed following the milling of ENRO with each of these polymers, from off-white to various shades of orange and peach. Like CIP, a polymer concentration of 60% (w/w) was required to fully amorphize mixtures of CIP and HPMCAS, whereas 40% (w/w) was adequate for Eudragit L100, Eudragit L100-55 and Carbopol. Although the product obtained with 40% (w/w) HPMCAS-LG was almost X-ray amorphous following 4 hours of milling, very small peaks could still be detected by PXRD at 9.8 and 25.8 2θ degrees, corresponding to the most prominent peaks of anhydrous ENRO (**Figure A.5.1**). A slightly more crystalline product was obtained with HPMCAS-MG under the same conditions, which decreased in intensity following a further 2 hours of milling, but did not disappear entirely. In contrast to CIP, which required a total of 6 hours of milling and a reduced temperature of 2–5 ºC to form ASDs with 60% (w/w) HPMCAS, 4 hours of milling at room temperature was adequate for the corresponding ENRO ASDs (**Figure A.5.1**). This may be due to the weaker crystal lattice of ENRO, which would facilitate its amorphization. These results show that the presence of an extra ethyl group in the structure of ENRO does not appear to negatively affect its ability to interact with these acidic polymers. To enable closer comparison with the equivalent CIP ASDs, the ENRO/HPMCAS ASDs containing 60% (w/w) polymer that were milled for 6 hours were used for further studies.

Succinic acid has been used to produce crystalline salts of both ENRO and CIP,[125,129] and, as described in Chapter 4, amorphous salts were also prepared by ball milling CIP with this acid in a 1:1 and 2:1 molar ratio. Ball milling was also used successfully in this study to produce the equivalent amorphous ENRO salts. However, while six hours of milling was necessary to obtain fully X-ray amorphous formulations with CIP, only one hour was required for ENRO.

In contrast to the acidic excipients, when CIP was milled with neutral polymers such as PVP and PVA at a concentration of 40–60% (w/w), a semi-crystalline product was obtained. This was also the case with ENRO (**Figure 6.2a**). The fact that fully X-ray amorphous solid

dispersions were only formed when ENRO was milled with acidic polymers containing carboxylic acid groups suggests that the drug is interacting with these substances via ionic bonds, as was the case with CIP. Likewise, in all of the ENRO salts produced by Karanam et al containing an acidic counterion, proton transfer from the acid to the piperazine tertiary amine (N3) of the drug occurred, resulting in an ionic interaction between the two moieties.[129] A similar reaction may take place between the N3 of ENRO and the polymers in these ASDs.

6.3.2 Solid-State Fourier Transform Infrared Spectroscopy

The results of FTIR analysis of the ASDs, PMs and starting materials are shown in **Figure 6.3**. A sharp peak is located at 1737 cm^{-1} in the spectrum of crystalline ENRO due to the carbonyl stretch of its unionized carboxylic acid group. While the process of ball milling introduced some disorder to the crystal lattice of ENRO, the FTIR spectrum of the ball milled drug was almost identical to the crystalline ENRO starting material. The greater molecular disorder of quench cooled ENRO on the other hand is evident in the broader and less intense peaks of its spectrum (**Figure 6.3d**). Slight peak shifts were also seen with this sample, in particular the carboxylic acid C=O stretch, which shifted to 1728 cm^{-1}. This can be attributed to changes in the drug's intermolecular interactions upon amorphization, such as hydrogen bonding.[264] Interestingly, the COOH carbonyl stretch of the drug also shifted to lower wavenumbers in the spectrum of the crystalline ENRO saccharinate salt, in which the piperazine N3 amino group of the drug is positively charged.[249] This carbonyl peak also underwent a similar shift with all of the ASDs. Therefore, while the carboxylic acid of ENRO remains unionized in the ASDs, changes in the hydrogen bonding of this group clearly occur upon amorphization. This shift may also be related to changes in the ionization state of the drug.

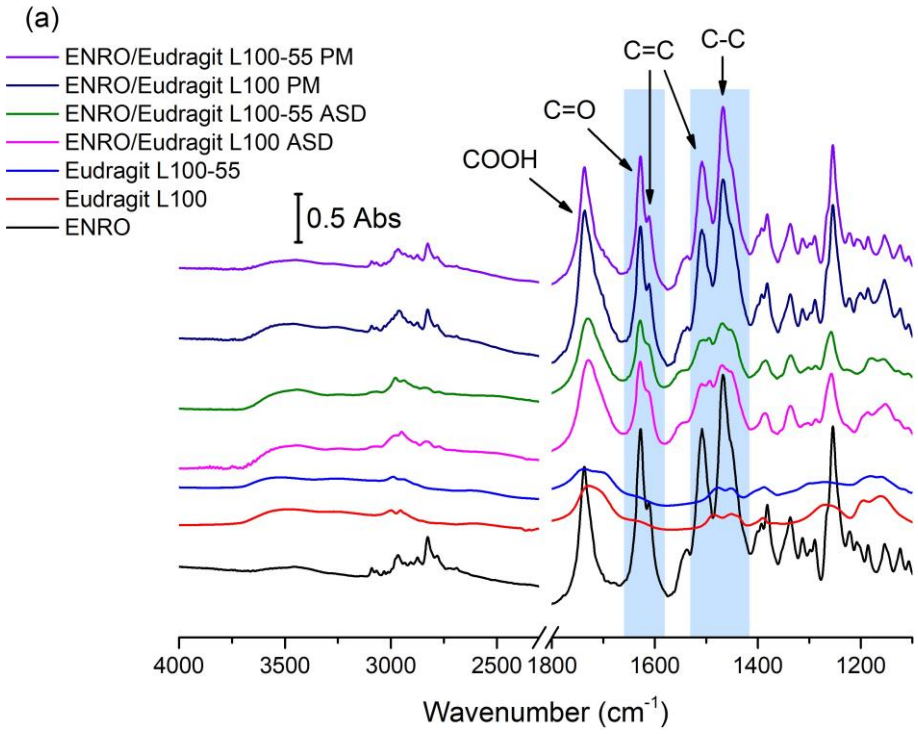
(a)
ENRO/Eudragit L100-55 PM
ENRO/Eudragit L100 PM
ENRO/Eudragit L100-55 ASD
ENRO/Eudragit L100 ASD
Eudragit L100-55
Eudragit L100
ENRO
0.5 Abs
COOH
C=O
C=C
C-C
4000
3500
3000
2500
1800
1600
1400
1200
Wavenumber (cm-1)

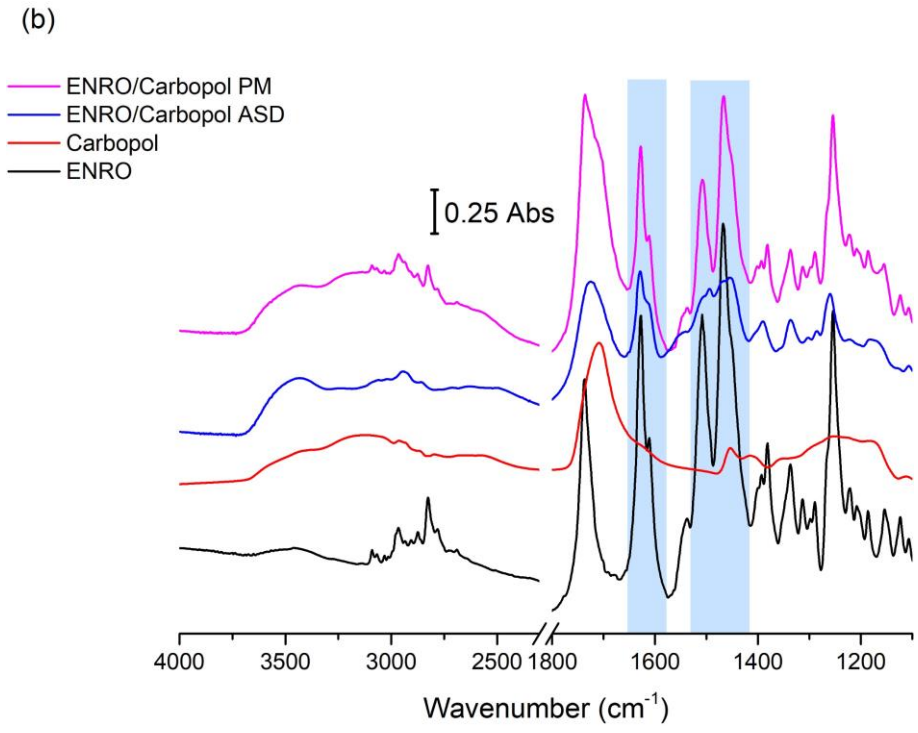
(b)
ENRO/Carbopol PM
ENRO/Carbopol ASD
Carbopol
ENRO
0.25 Abs
4000
3500
3000
2500
1800
1600
1400
1200
Wavenumber (cm-1)

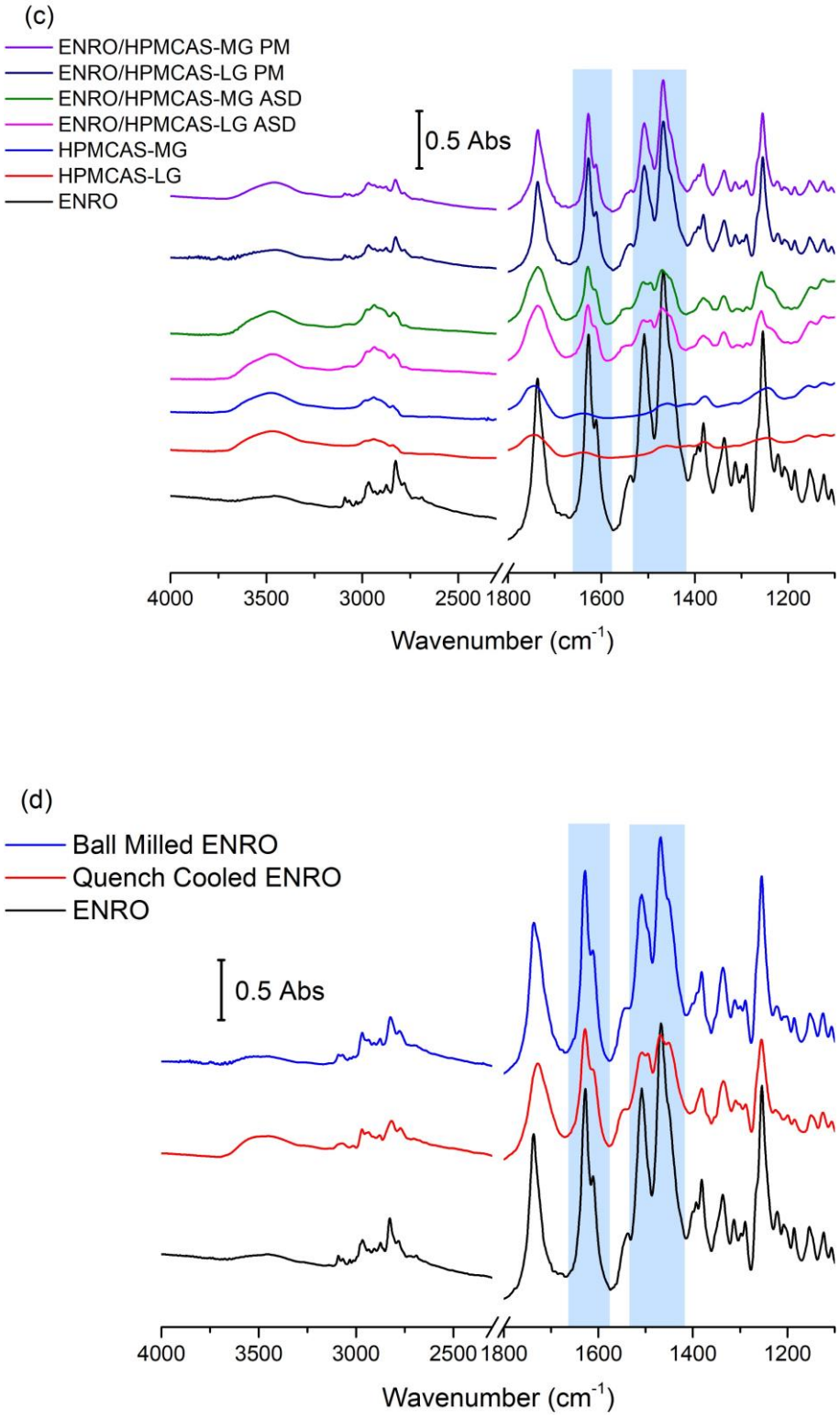

Figure 6.3. FTIR analysis of ENRO ASDs and PMs containing (a) Eudragit L100 and Eudragit L100-55 40% (w/w) (b) Carbopol 40% (w/w) and (c) HPMCAS-LG and HPMCAS-

MG 60% (w/w). (d) FTIR analysis of ball milled, quench cooled and crystalline ENRO. The areas of the spectra that undergo significant changes upon amorphization are highlighted in blue.

The main differences between the spectra of ENRO and the ASDs may be seen in the 1650–1450 cm^{-1} region. The relevant peaks are highlighted in **Figure 6.3**. In the case of crystalline ENRO, the carbonyl stretch of its ketone group appears as a sharp, strongly absorbing peak at 1628 cm^{-1}. The medium intensity shoulder at 1611 cm^{-1} may be assigned to C=C stretching vibrations of the drug's aromatic ring. While these peaks are not significantly shifted in the spectra of the ASDs, differences in their relative absorbance were observed. In crystalline ENRO the absorbance of the ketone peak is approximately 1.8 times greater than that of the aromatic peak. This ratio decreases to 1.5–1.7 for each of the ASDs. However, a similar decrease in the relative absorbance of these peaks was also seen with quench cooled ENRO, and is therefore likely due to changes in the interactions of these groups upon amorphization.

The peaks at 1508 and 1469 cm^{-1} in the spectrum of ENRO may be attributed to C=C stretching of the aromatic ring, and C-C stretching of the drug's piperazine group, respectively.[265] The shape of these peaks was altered notably in the ASDs, and the presence of multiple overlapping peaks became evident. In order to separate the individual peaks in this region, and to quantify their relative absorbance, deconvolution of the spectra, with Gaussian peak fitting, was carried out. The resulting spectra are shown in **Figure A.5.2**. Deconvolution allowed the detection of a further peak at approximately 1453 cm^{-1} in the spectrum of ENRO, which may be tentatively assigned to the C-H bending vibrations of the ethyl group. This peak is also present in the spectra of ball milled and quench cooled ENRO, and all of the ASDs, along with an additional peak at approximately 1494 cm^{-1}. Although a slight broadening is visible at this wavenumber in the spectrum of crystalline ENRO, it is not as distinct as with the other samples. Clear differences in the relative absorbance of these peaks may also be seen between the pure drug and ASDs. For instance, in crystalline ENRO the area of the peak at 1508 cm^{-1} is approximately two times smaller than the combined area of the peaks at 1469–1453 cm^{-1}. While a similar ratio was obtained with the equivalent peaks in ball milled ENRO, with the quench cooled form of the drug it decreased to 1.9. With the ASDs on the other hand, this ratio decreased further to 1.3–1.55. Similarly, in the spectra of

crystalline and ball milled ENRO the absorbance of the peak at 1469 cm^{-1} is clearly greater than that at 1453 cm^{-1}. In contrast, in each of the ASDs, as well as quench cooled ENRO, the maximum absorbance of these peaks did not differ greatly. Similar changes in this region were seen in the spectra of the amorphous enrofloxacin succinate salts, as well as the partially crystalline ENRO/PVA solid dispersion, whereas the less disordered ENRO/PVP more closely resembled the crystalline ENRO starting material (**Figure A.5.3** and **Figure A.5.4**).

As previously mentioned, the N3 tertiary amine of ENRO may be protonated in these ASDs, forming ionic bonds with the carboxylate groups of the polymers. If this is the case, the main differences in the FTIR spectra of the ASDs compared to the starting materials or PMs can be attributed to the change in ionization state of the drug, and the presence of an additional $^{+}$N-H bond. Unfortunately, the $^{+}$N-H stretch is difficult to assign with certainty, as it will produce a weak band in the 3000–2600 cm^{-1} region that possibly overlaps with others, such as that of the C-H stretch of the neighbouring aliphatic group.[265] Similarly, the $^{+}$N-H bend of a tertiary amine salt generally appears as a very weak band in the 1610–1500 cm^{-1} region,[266] and therefore is likely to be obscured by more intense peaks in the spectra of the ASDs. However, as described above, a number of differences in the 1450–1550 cm^{-1} region of the spectra of ENRO and the ASDs were observed. Therefore, it is possible that the presence of a peak corresponding to the $^{+}$N-H bend contributed to the variations in this area of the spectra. In addition, as the peaks in this region correspond to groups surrounding the terminal amino group of ENRO, it is likely that they would be altered upon the protonation of N3.

The theory that ENRO is protonated in these ASDs is supported by the FTIR analysis of ENRO salts conducted by Karanam et al.[129] In the spectra of each of the salts containing an acidic counterion, a decrease in the absorbance of the peak around 1469 cm^{-1} relative to that at 1508 cm^{-1} can be seen, in common with the ENRO ASDs. Single crystal X-ray diffraction confirmed that the N3 of the drug is protonated in these salts, and forms an ionic bond with the carboxylate groups of the acids. Therefore, it is likely that ENRO is in the same cationic state in these ASDs, and interacts with the acidic groups of the polymers to form amorphous salts.

6.3.3 Thermal Analysis

The conventional DSC thermograms of ENRO and the ASDs are shown in **Figure 6.4**. The melting point onset of crystalline ENRO, as well as the ball milled and quench cooled drug, was approximately 225 ^{o}C. Its lower melting point in comparison to CIP (approximately 272 ^{o}C) can be explained by the less extensive intermolecular bonds in ENRO. In contrast to the pure drug, the thermograms of the ENRO ASDs were missing a clear melting point. Similarly, the ASDs did not show distinct crystallization exotherms during DSC analysis, although the small, broad peaks visible at approximately 157 ^{o}C and 148 ^{o}C in the thermograms of ENRO/HPMCAS-LG and ENRO/HPMCAS-MG, respectively, may be due to some crystallization. The indistinct nature of the thermograms can be attributed to the amorphous nature of these formulations, and their stability upon heating.[267] In contrast, ball milled and quench cooled ENRO had clear crystallization peaks at approximately 73 ^{o}C and 106 ^{o}C respectively, confirming their lower resistance to crystallization. The particularly low crystallization temperature of ball milled ENRO is to be expected, as the residual crystallinity present in this sample would enable crystal growth to occur more quickly upon heating.

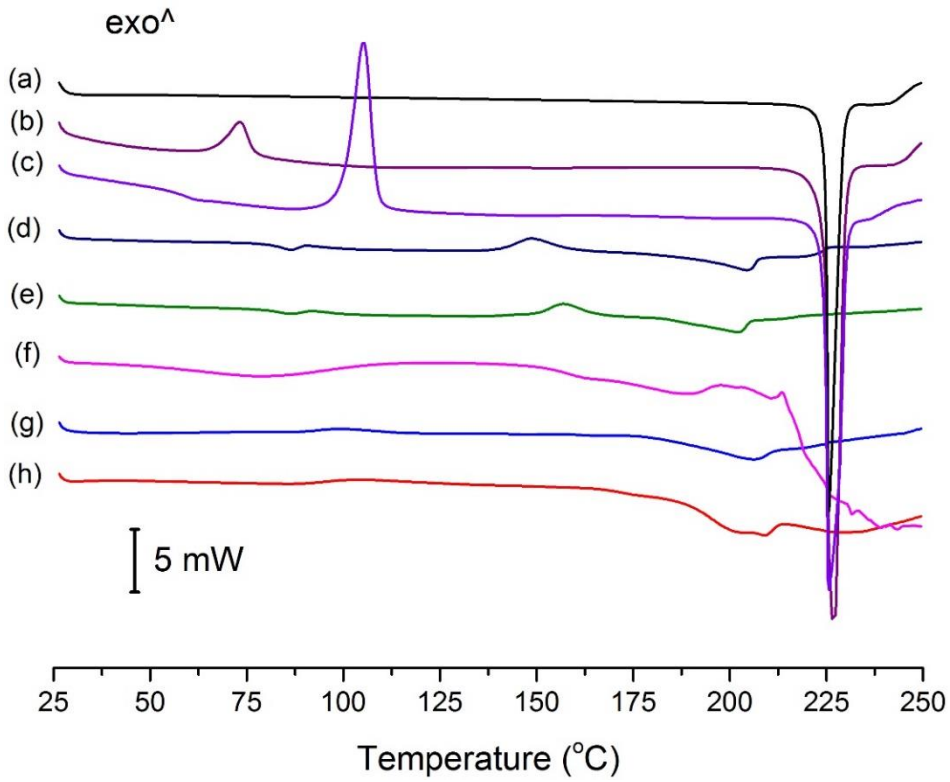

Figure 6.4. DSC thermograms of (a) crystalline ENRO (b) ball milled ENRO (c) quench cooled ENRO (d) ENRO/HPMCAS-MG (e) ENRO/HPMCAS-LG (f) ENRO/Carbopol (g) ENRO/Eudragit L100-55 and (h) ENRO/Eudragit L100. The thermograms of the ASDs are those obtained from the second heating cycle, following initial heating to 65 °C to allow for water evaporation.

The T_g of quench cooled ENRO was detected at 58.9 °C, which is significantly lower than that of CIP (86.7 °C). Again, this may be attributed to the weaker intermolecular interactions present in ENRO. As a distinct T_g could not be found for all of the ENRO ASDs using conventional DSC, they were therefore analyzed by MTDSC. The resultant T_g's are listed in **Table 6.1**. In each case, a single T_g was detected. This suggests that the drug is miscible with each of these polymers, and that they form a single homogeneous phase.[41] Due to its low amorphous content and high crystallization rate, no T_g could be determined for ball milled ENRO with either DSC technique.

The G-T equation was used to calculate the expected T_g's of the ASDs, given their weight percentage of drug and polymer. Similar to CIP, the experimental T_g's of the ASDs

containing Eudragit L100, Eudragit L100-55 and Carbopol were substantially higher than the theoretically derived values (**Table 6.1)**. Such large positive deviations from the predicted T_g's indicates that strong interactions exist between the components, and is particularly indicative of salt formation.[62] Also in common with CIP, a much smaller divergence was observed between the experimental and G-T T_g's of the HPMCAS-containing ASDs, which differed by only a few degrees. This suggests that these polymers are fully miscible with ENRO, but do not form specific interactions with the drug.[60] Alternatively, the heteromolecular drug-polymer interactions may be of a similar strength to the homomolecular interactions present in the individual raw materials.[53] Both drugs appear to be unable to interact with HPMCAS to the same extent as the other polymers, perhaps due to its bulkier structure and lower carboxylic acid content.

Table 6.1. Glass Transition Temperatures of ENRO and ENRO ASDs

Sample	Experimental T_g (°C)	G-T T_g (°C)
ENRO	58.9	N/A
ENRO/Eudragit L100	109.9 ± 1.6	82.5
ENRO/Eudragit L100-55	103.2 ± 0.2	74.0
ENRO/Carbopol	155.6 ± 0.2	71.4
ENRO/HPMCAS-LG	86.8 ± 0.4	85.6
ENRO/HPMCAS-MG	83.3 ± 0.4	85.9

The amorphous ENRO succinate salts have much lower T_g's than the ASDs, of only 50.0 ± 0.7 °C and 55.0 ± 0.5 °C for the 1:1 and 2:1 salts, respectively. This was soon followed by crystallization during DSC analysis, with a peak at 86.9 ± 0.2 °C for the 1:1 salt, and at 89.7 ± 0.2 °C for the 2:1 salt. A second, much broader exotherm was also visible in the thermograms of both salts at approximately 123 and 127 °C, respectively (**Figure A.5.5**). This is similar to the double exothermic peaks that were observed in the thermogram of the amorphous CS 2:1 salt, as described in Chapter 4, and may be due to the presence of residual crystal nuclei in the samples.[103] With each salt, the same crystal phases were identified by PXRD after both crystallization events, however an increase in their crystallinity was observed. The PXRD pattern of the 1:1 salt was found to match that of the enrofloxacin

hemisuccinate salt, while that of the 2:1 salt consisted of a combination of enrofloxacin hemisuccinate and anhydrous ENRO.[129] This suggests that ENRO may not have formed a separate salt when milled with succinic acid in a 2:1 ratio, but instead formed the enrofloxacin hemisuccinate salt, with excess drug present in the amorphous form. This is in contrast to CIP, which when milled with succinic acid in the same ratio forms the succinate salt, consisting of two drug molecules interacting with a single succinic acid molecule.[125]

The low glass transition and crystallization temperatures of the ENRO/succinic acid salts indicate that they have high molecular mobility and poor stability. Indeed, during storage at 2–5 ºC, the salts began to crystallize after approximately 2 months. In contrast, the polymeric ASDs remained fully X-ray amorphous under the same storage conditions for at least 16 months (longer term stability studies have not been carried out). Therefore, the remainder of this study will focus on the more stable polymeric ASDs.

As described in Chapter 2, the conversion of zwitterionic CIP to the unionized form upon melting was visualized as a small endothermic peak in the HSDSC thermogram of the drug, just prior to the melting endotherm. However, this low energy event was only visible when CIP was heated at 500 ºC/min. HSDSC analysis was therefore carried out on crystalline ENRO in order to determine if it also undergoes proton transfer at high temperatures, in this case from the unionized form to the zwitterion. Even when heated at the maximum heating rate of 500 ºC/min, the drug did not show any evidence of solid state transformation (**Figure A.5.6**). As described in Chapter 2, the transformation of CIP from the zwitterionic to the unionized form was more obvious with cryomilled CIP, and could be clearly detected with a heating rate of 10 ºC/min. HSDSC was therefore also carried out on quench cooled ENRO. However, like the pure drug, no transition could be detected with this disordered sample, even when heated at 500 ºC/min.

While crystalline ENRO is pale yellow, quench cooled ENRO is a golden color, and when heated to 250 ºC the drug becomes dark orange/rusty. CIP also turns from off-white to a yellow color prior to melting, however when heated past its melting point it becomes brown due to substantial degradation. From the TGA curves obtained with ENRO and the ASDs (**Figure 6.5**), crystalline and ball milled ENRO do not appear to undergo substantial thermal

degradation, decreasing in mass by only 3.4% over the course of the TGA study. CIP on the other hand is much more prone to thermal degradation, with a total mass loss of 12.8% and 17.3% being obtained with the crystalline and cryomilled forms of the drug, respectively, as mentioned in Chapter 2. An initial mass loss was observed below 70 °C with all of the ENRO ASDs due to water evaporation. The amorphous samples also degraded to a greater degree than the pure drug, in particular the Carbopol ASD. This is most likely due to their polymer content, as the polymers undergo significant thermal degradation themselves at high temperatures (**Figure A.5.7**).

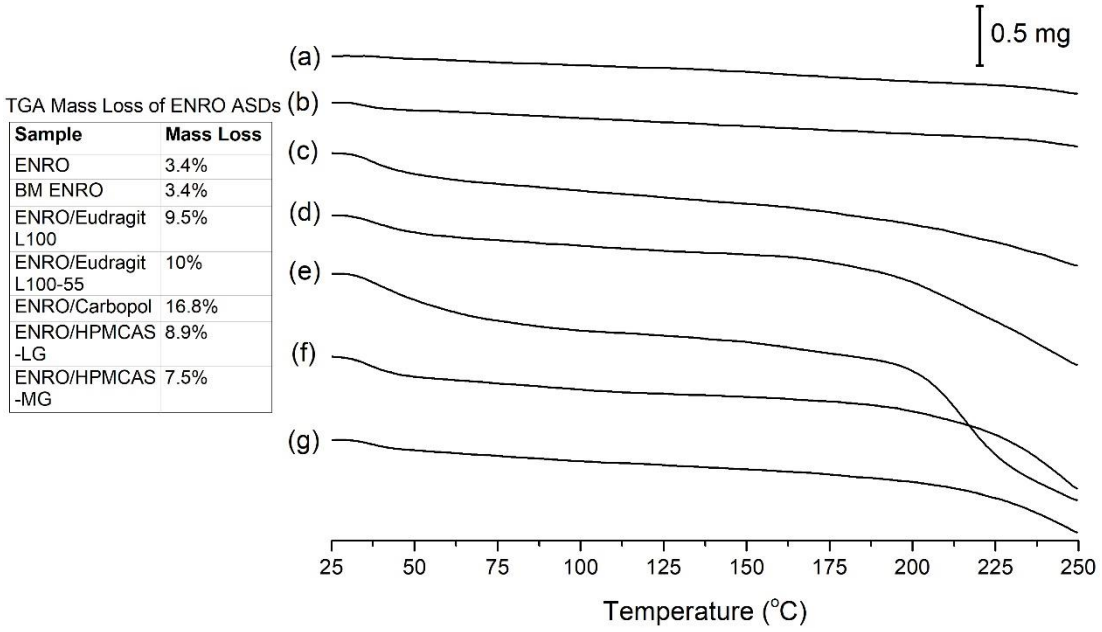

Figure 6.5. TGA analysis of (a) crystalline ENRO (b) ball milled ENRO (c) ENRO/Eudragit L100 (d) ENRO/Eudragit L100-55 (e) ENRO/Carbopol (f) ENRO/HPMCAS-LG and (g) ENRO/HPMCAS-MG.

6.3.4 Water Sorption Studies

The stability of the ASDs when exposed to various humidity levels was examined by DVS. At the end of the sorption cycle, at 90% RH, ENRO absorbed only 0.13% (w/w) water. This increased to 2.9% for the ball milled drug, due to the increase in disordered material (**Figure 6.6a**). CIP also absorbed low levels of water during DVS analysis, increasing in mass by

only 0.6 % (w/w).[125] PXRD analysis of the drugs at the end of the sorption studies revealed that the solid state of both ENRO and CIP was unchanged, with PXRD patterns matching those of the starting materials (**Figure 6.7**).[125] In contrast to the crystalline drug, the ENRO ASDs were far more hygroscopic, absorbing 16–19% of their mass in water. Very similar levels of water uptake were observed with the equivalent CIP ASDs. The higher hygroscopicity of the amorphous formulations can be explained by the random orientation of their molecules. This leads to a larger free volume, and enables the penetration of water into the samples.[42] In addition, polymers are often more hygroscopic than the amorphous form of a drug, which increases the tendency of an ASD to take up moisture.[48]

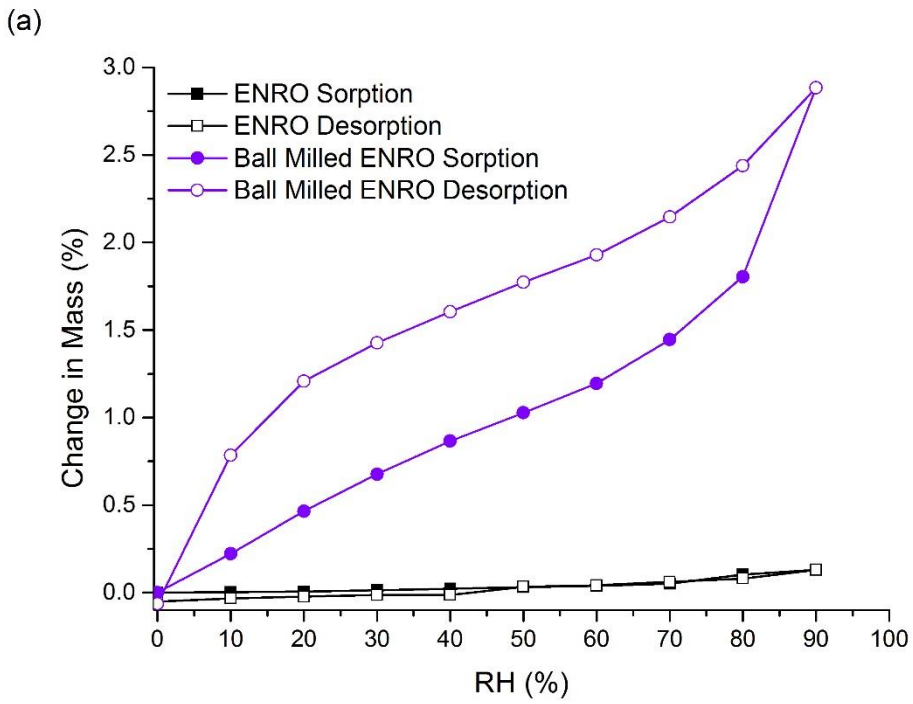

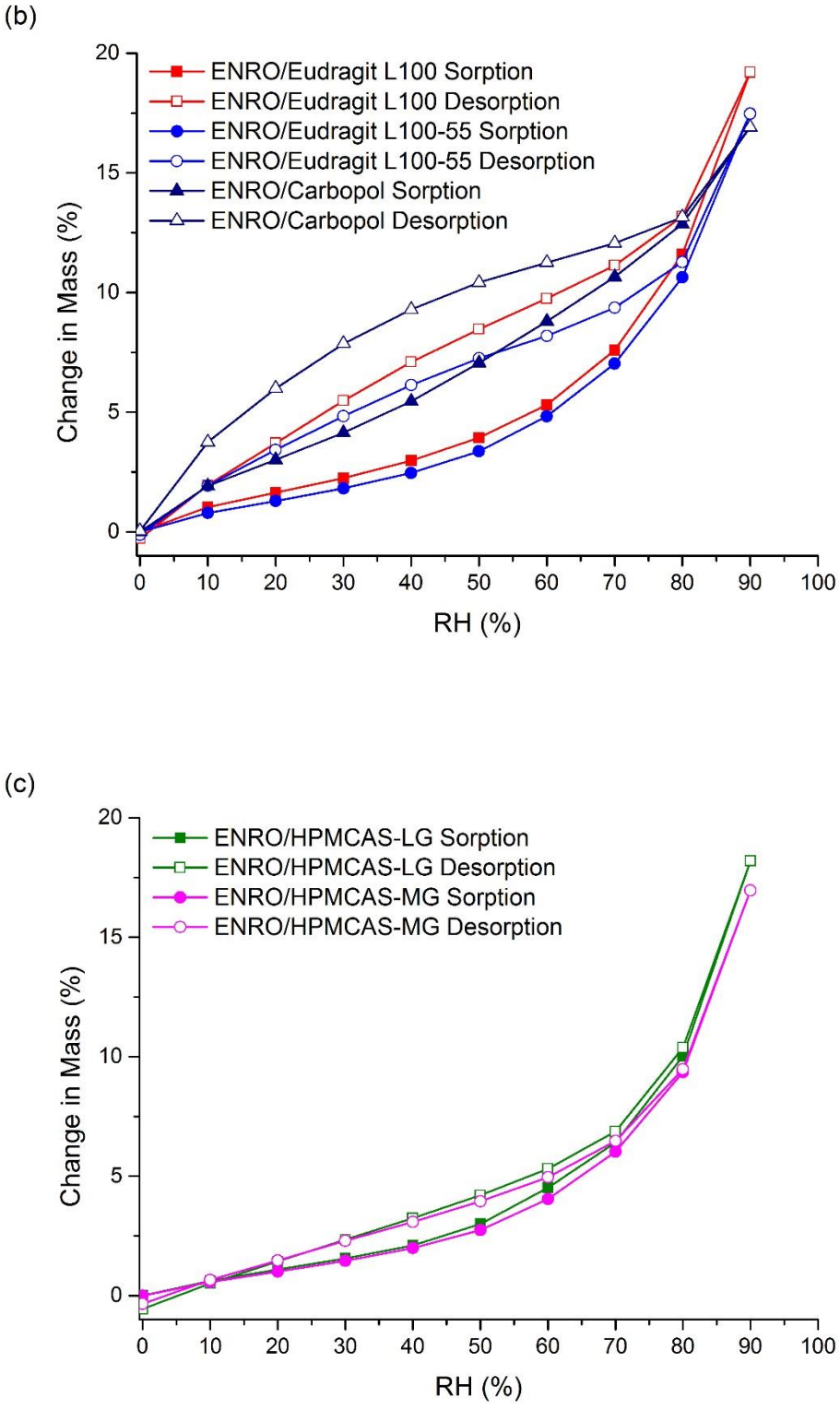

Figure 6.6. DVS analysis of (a) crystalline and ball milled ENRO (b) ENRO ASDs containing 40% (w/w) Eudragit L100, Eudragit L100-55 and Carbopol and (c) ENRO ASDs containing 60% (w/w) HPMCAS-LG and HPMCAS-MG.

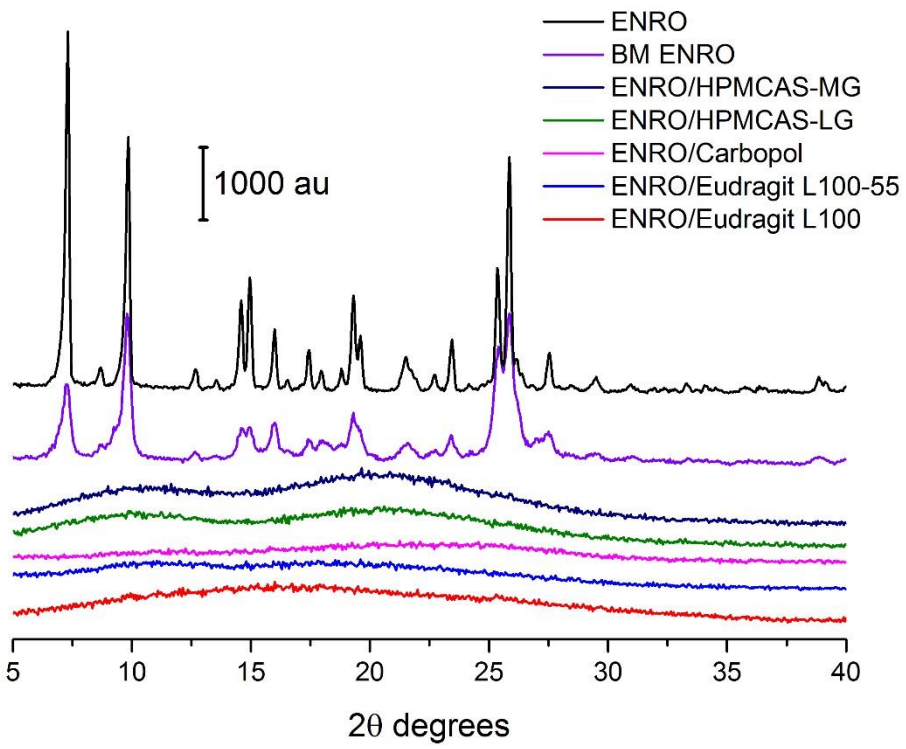

Figure 6.7. PXRD analysis of ENRO and ENRO ASDs following DVS studies.

As can be seen in **Figure 6.6b**, the isotherms obtained with the ASDs containing Eudragit L100, Eudragit L100-55 and Carbopol were very similar in shape, with significant hysteresis. Hysteresis is commonly encountered with amorphous or porous solids, as water can absorb into the interior of the material.[257] If water diffuses into the sample bulk more quickly than it can return to the surface, then, at the same RH level, a greater amount of moisture will be present during desorption than sorption, resulting in the appearance of hysteresis. This may occur with polymers that swell upon water exposure, as this increases the area available for water absorption. During desorption, such polymers will dehydrate and shrink, potentially blocking the sites of moisture absorption, and preventing the loss of water from these areas until a lower RH level is reached.[268]

Unlike the other ASDs, the isotherms of both ENRO/HPMCAS ASDs were convex in shape with a small amount of hysteresis, suggesting that water was mainly adsorbed to the outer surfaces of these samples (**Figure 6.6c**). Therefore, the water uptake behavior of the ENRO ASDs differs depending on the polymer used. This was further examined by fitting the sorption and desorption data to the Young-Nelson equations. According to the Young-

Nelson model, water can be taken up by a sample in three different ways: adsorbed as a monomolecular layer, adsorbed as a multilayer, or absorbed into the interior of the solid.[262] The parameters calculated using the Young-Nelson equations are listed in **Table A.5.1**, and the isotherms obtained using this approach are shown in **Figure 6.8** and **Figure A.5.8**. The corresponding CIP ASDs were also examined for comparison (**Figure A.5.9**).

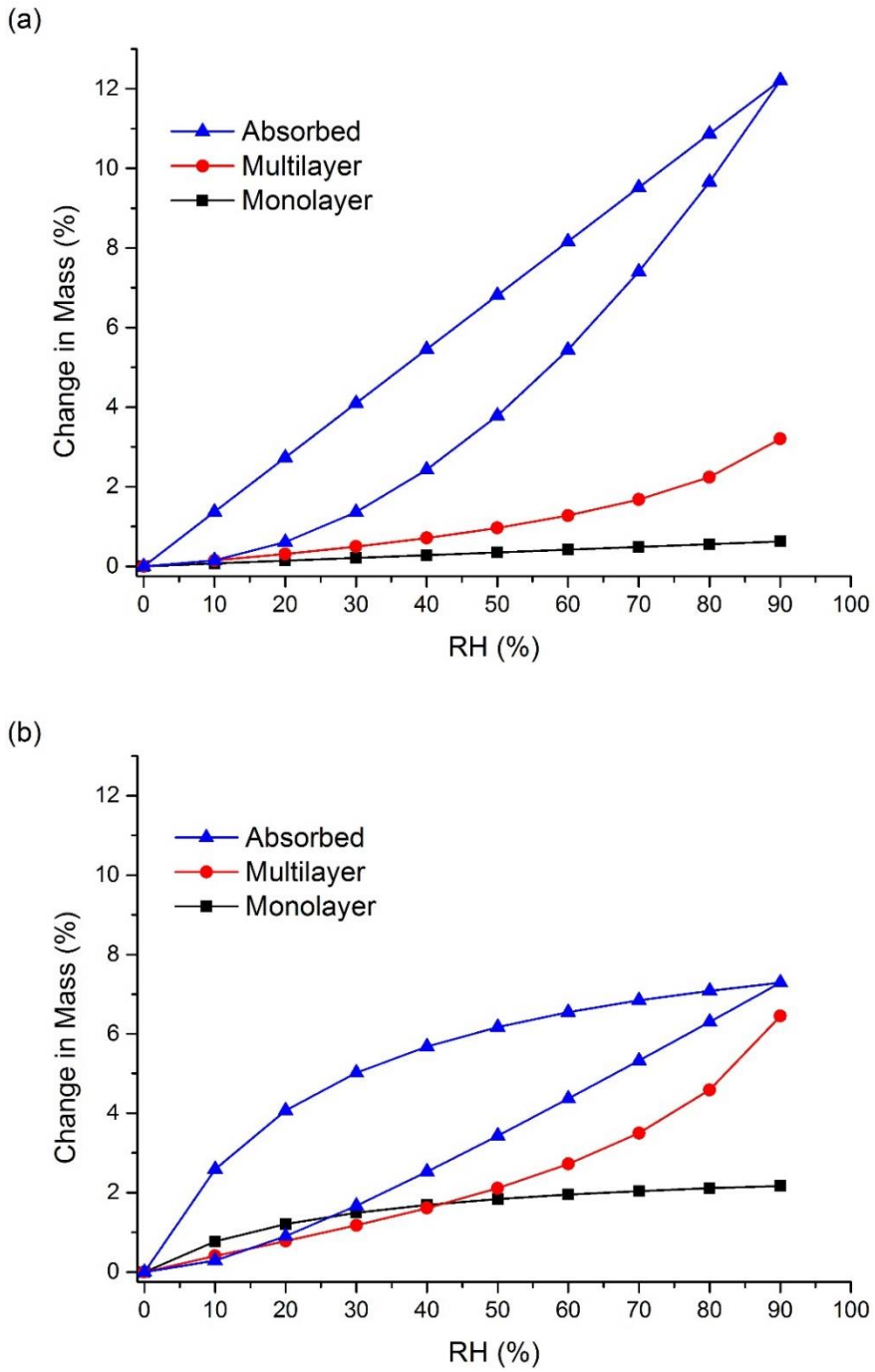

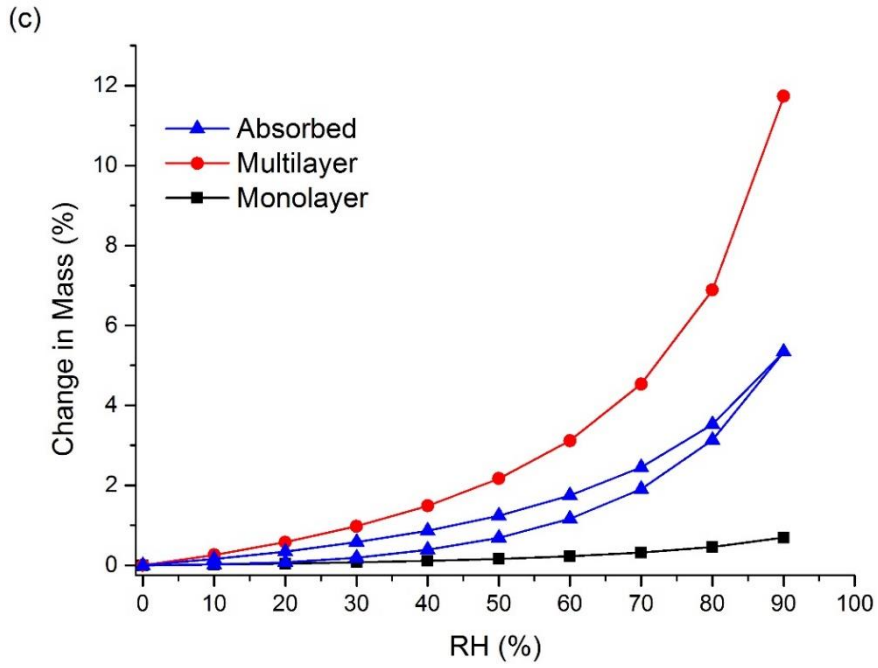

Figure 6.8. Water distribution patterns according to the Young-Nelson model in ENRO ASDs containing (a) Eudragit L100 40% (w/w) (b) Carbopol 40% (w/w) and (c) HPMCAS-LG 60% (w/w).

As predicted from the DVS isotherms, the major water uptake mechanism of the ENRO ASDs containing Eudragit L100, Carbopol and Eudragit L100-55 was water absorption (**Figure 6.8a**, **6.8b** and **Figure A.5.8a**). The small degree of absorption that occurred with the ENRO/HPMCAS ASDs confirms that they are somewhat porous, but less so than the other ASDs, as suggested by the minor hysteresis in their DVS isotherms. Unlike the other samples, the majority of water taken up by the ENRO/HPMCAS ASDs was bound to their exterior surfaces as a multilayer. Multilayer formation begins at low RH levels, and appears to occur simultaneously with monolayer adsorption (**Figure 6.8c** and **Figure A.5.8b**). In contrast, the major water uptake mechanism for the CIP ASDs containing HPMCAS was absorption (**Figure A.5.9**). This suggests that the CIP/HPMCAS ASDs are more porous than the corresponding ENRO ASDs, or the polymers may be capable of swelling to a greater degree in the former formulations. As with the ENRO ASDs, water is primarily absorbed into the interior of the CIP ASDs containing Eudragit L100, Eudragit L100-55 and Carbopol. However, the water distribution patterns obtained with the ENRO and CIP ASDs containing Carbopol differed somewhat from those containing Eudragit, due to more extensive

monolayer adsorption. This may be due to the presence of more hydrophilic groups that can interact with water molecules on the surface of the Carbopol ASDs.[263]

With both sets of ASDs, the highest value of the Young-Nelson equilibrium constant E was obtained with the samples containing HPMCAS-LG, followed by HPMCAS-MG (**Table A.5.1**). However, this constant was more than 10 times larger for the ENRO/HPMCAS samples than the equivalent CIP ASDs. This indicates that water molecules form stronger and more extensive interactions with the surface of these samples,[269] which would explain why water appears to be mainly adsorbed to the surface of these ASDs in a multilayer.

The value of the correlation coefficient, r, was ≥ 0.98 for all of the ASDs, showing that there was a good fit between the experimental and estimated values of the different parameters (**Table A.5.1**). Therefore, application of the Young-Nelson model is a suitable approach for comparing the water uptake of these samples.

The permeation of water molecules into the interior of an amorphous solid can increase its free volume, resulting in a decrease in T_g.[256] Water sorption is also known to increase the molecular mobility and thus crystallization rate of amorphous substances, and to decrease the crystallization onset temperature.[42,49] However, despite the plasticizing effects of sorbed water, all five of the ENRO ASDs remained fully X-ray amorphous following DVS analysis (**Figure 6.7**). This was also the case for the corresponding CIP polymeric ASDs described in Chapter 3. The high stability of these ASDs may be due to stabilizing drug-polymer interactions, the presence of which was suggested by the results of FTIR and DSC analysis. As previously discussed, polymers are also known to have anti-plasticizing effects and to reduce the molecular mobility of amorphous formulations, while steric hindrance from the polymer chains can prevent the nucleation and crystal growth of drug molecules.[52,56]

6.3.5 Solubility and Dissolution Studies

Due to issues with clumping and viscosity, solubility studies could not be carried out accurately on the ASDs containing Eudragit L100-55 and Carbopol, and these samples were therefore excluded from further studies. The superior solubility of the remaining ASDs in

FaSSIF in comparison to crystalline ENRO is clear from **Figure 6.9a**. With the pure drug, a peak in concentration was seen at 30–60 sec, which then quickly fell to a constant level of approximately 0.7 mg/ml. A steep initial increase in drug concentration was also seen with the ASDs containing HPMCAS-LG and HPMCAS-MG, which peaked after 5 and 2 min, respectively. While this supersaturation then fell after 10–15 min, the concentration was still significantly higher than that obtained with crystalline ENRO. This solubility enhancement was sustained for the remainder of the study, with final concentrations of 12.2 mg/ml and 5.6 mg/ml being obtained with ENRO/HPMCAS-LG and ENRO/HPMCAS-MG, respectively. In contrast to the other samples, a more gradual increase in drug concentration was seen with ENRO/Eudragit L100, followed by a plateau after 20 min. This sample was also less soluble than those containing HPMCAS, reaching a concentration of 4.6 mg/ml after 2 hours.

The dissolution behavior observed with these ASDs is similar to that described by the "spring" and "parachute" model discussed previously.[76] The high energy of amorphous solids and their lack of a crystal lattice enables such rapid drug dissolution and supersaturation to occur, while the polymers present in ASDs can inhibit or delay the precipitation of dissolved drug.[76] Although the concentration obtained with the ENRO/HPMCAS ASDs did decrease somewhat over the course of the study, the polymers present in these ASDs most likely prevented extensive crystallization of the drug in solution, enabling supersaturation to be maintained for at least 2 hours. By avoiding the rapid generation of supersaturation, less nucleation and crystallization would be expected to occur with the ENRO/Eudragit L100 ASD. This was confirmed by PXRD analysis of the excess solid recovered at the end of the solubility studies. In each case enrofloxacin hexahydrate[129] was detected; however, with ENRO/Eudragit L100 the sample was far less crystalline (**Figure A.5.10**).

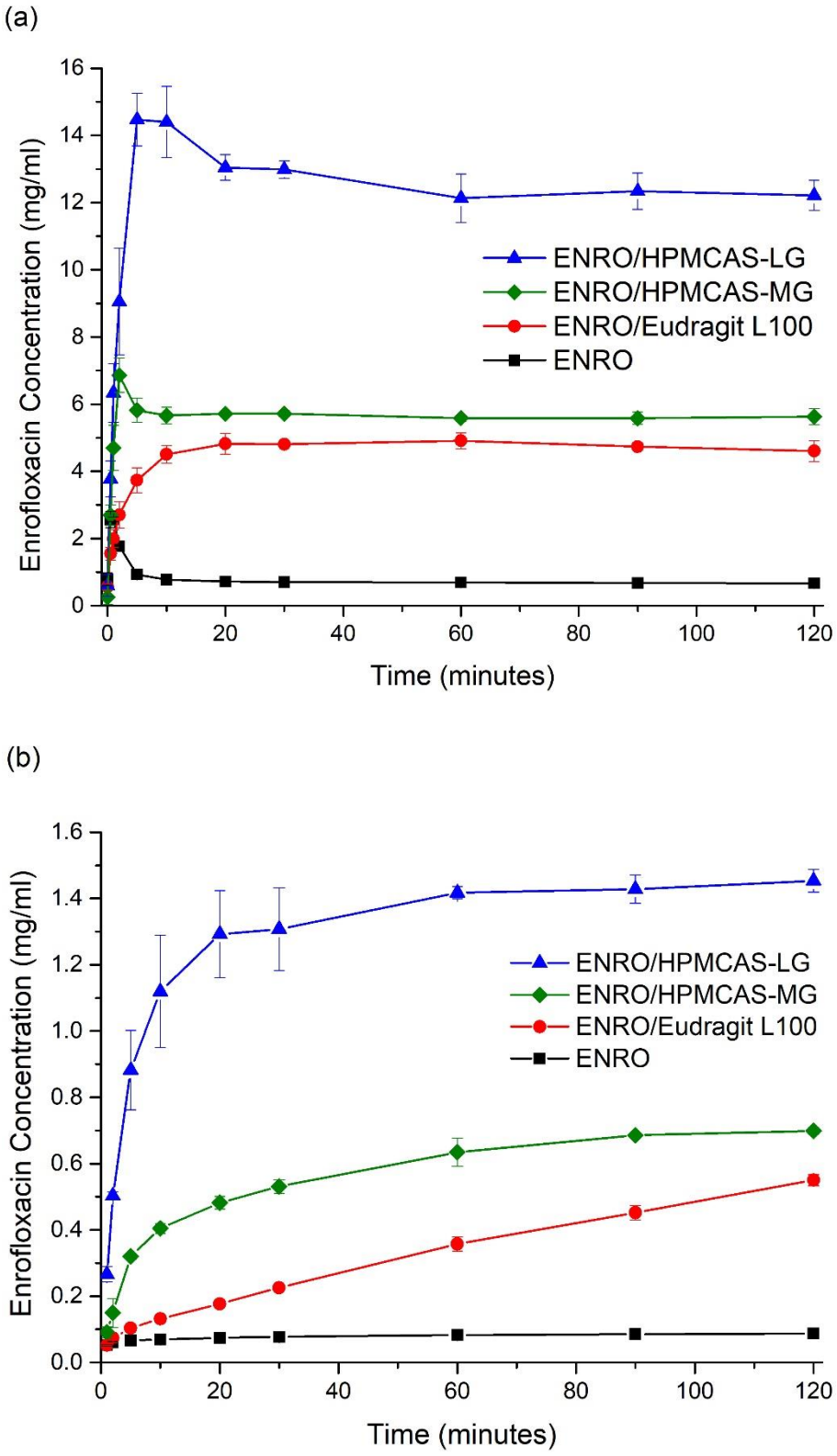

Figure 6.9. (a) Solubility and (b) dissolution studies in FaSSIF at 37 ºC. The average of three experiments is plotted, ± the standard deviation.

Similarly enhanced concentrations were obtained with the ENRO ASDs in dissolution studies in comparison to crystalline ENRO. After 2 hours, the highest concentration was achieved with ENRO/HPMCAS-LG, at 1.45 ± 0.03 mg/ml, followed by ENRO/HPMCAS-MG (0.70 ± 0.01 mg/ml) and ENRO/Eudragit L100 (0.55 ± 0.02 mg/ml). Crystalline ENRO on the other hand only attained 0.09 ± 0.00 mg/ml over the course of the study (**Figure 6.9b**). Apart from concentration, the ASDs also differed in the shape of their dissolution profiles. With ENRO/HPMCAS-LG, the drug concentration increased quite rapidly at the start of the study and then remained fairly constant for the remainder. While a similar profile was obtained with ENRO/HPMCAS-MG, the initial drug release was more gradual than with the LG grade of polymer. As was the case in the solubility study, the final concentration obtained with ENRO/HPMCAS-MG was approximately half that of ENRO/HPMCAS-LG. However, ASDs containing different grades of HPMCAS are known to demonstrate different rates and extents of drug release, due to differences in their succinoyl and acetyl content.[197] This may affect the pH of the diffusion layer surrounding the ASD particles, or the strength of drug-polymer interactions.

In contrast to the other ASDs, a steady, linear increase in drug concentration was observed with ENRO/Eudragit L100 during dissolution studies. As no levelling off occurred during the study, it is possible that the drug concentration would continue to rise during longer term studies, similar to an extended release formulation. The gradual dissolution of ENRO from this ASD may be due to strong drug-polymer interactions, which could delay the dissociation and dissolution of the drug.[200] Such interactions would also explain the higher than predicted T_g of this formulation, and the absence of crystallization during DSC analysis, unlike the ASDs containing HPMCAS. Alternatively, this polymer may be less soluble than HPMCAS, which would reduce the diffusion of water into the ASD and thus its dissolution rate. The CIP/Eudragit L100 ASD also resulted in lower drug release during solubility studies compared to CIP/HPMCAS-LG and CIP/HPMCAS-MG, likely for the same reasons.

Visible differences in the behavior of the ENRO ASD powders were also evident during dissolution studies. Both ENRO/Eudragit L100 and ENRO/HPMCAS-MG formed clumps when added to the dissolution vessels. While these eventually dissolved in the case of ENRO/HPMCAS-MG, with ENRO/Eudragit L100 they remained largely intact for the

duration of the study. This would have hindered the release of the drug and reduced the surface area exposed to the dissolution medium. In contrast, no clumping was observed with ENRO/HPMCAS-LG, which enabled faster dissolution and higher concentrations of ENRO to be achieved.

From the results of this study and those described in Chapter 3, it can be concluded that ENRO is more soluble than CIP in FaSSIF. CIP was found to have a solubility of only 0.14 mg/ml in this medium, which is five times lower than that of ENRO. Higher drug concentrations were also obtained with the ENRO ASDs than the equivalent CIP ASDs. These results are in agreement with those of Blokhina et al, who found ENRO to be the more soluble of the two fluoroquinolones in pH 7.4 phosphate buffer.[132] As previously mentioned, the greater solubility of ENRO may be explained by its weaker crystal lattice, which would facilitate the release of drug molecules into solution.

6.3.6 Bacterial Studies

The minimum inhibitory concentrations (MICs) and minimum bactericidal concentrations (MBCs) of ENRO and the ASDs are listed in **Table 6.2**. Values that differ significantly from those of ENRO are shown in bold. As previously mentioned, if the ratio of MBC to MIC is ≤ 4, this indicates that a drug is bactericidal,[214] which was the case for ENRO and the ASDs in all species of bacteria in this study. A MIC of $\leq$ 0.5 µg/mL may be considered as susceptible to ENRO, while $\geq$ 2 µg/mL indicates bacterial resistance, and 1 µg/mL is intermediate.[270] Therefore, from the results of this study it can be concluded that *E. coli, S. aureus* and *K. pneumoniae* are susceptible to ENRO, while *P.aeruginosa* is not. As was the case with CIP, *E. coli* was found to be the most susceptible of these bacteria to ENRO, having a MIC of 0.004–0.0016 µg/ml. Quite low MIC levels were also obtained in *K. pneumoniae* (0.032–0.125 µg/ml), followed by *S. aureus* (MIC 0.125–0.25 µg/ml). In contrast, much higher MIC and MBC values of 4–8 µg/ml were obtained with *P. aeruginosa*. However, the outer membrane of this bacteria is known to be far less permeable than that of *E. coli,* while fluoroquinolones are also believed to be substrates for an active efflux system within *P.*

aeruginosa.[271] In each case, the MIC values obtained for ENRO in these four species agree well with those reported previously.[270]

As can be seen from **Table 6.2**, the formulation of ENRO as an ASD did not significantly affect its antibacterial activity in any species of bacteria, while the MIC and MBC obtained with ENRO/HPMCAS-MG was significantly lower in *E. coli* and *K. pneumoniae* than the pure drug. These results are similar to those obtained with the CIP ASDs of Chapter 3, whereby the MIC and MBC of CIP/HPMCAS-MG was significantly lower than crystalline CIP in all four of these species, while the MIC of CIP/HPMCAS-LG was also significantly reduced in *E. coli,* and its MBC was lower in both *E. coli* and *S. aureus*. These ASDs were also found to increase the passive transmembrane permeability of CIP. Therefore, it is possible that the formulation of ENRO as an ASD with HPMCAS-MG also improved its permeability, enabling more of the drug to be transported through the bacterial cell membranes via passive diffusion.

Table 6.2. Minimum Inhibitory Concentration and Minimum Bactericidal Concentration of Enrofloxacin and ASDs in Various Bacteria[a]

Sample	***S. aureus***	***E. coli***	***P. aeruginosa***	***K. pneumoniae***
Minimum Inhibitory Concentration (μg/ml)				
ENRO	0.25	0.016	4	0.125
ENRO/Eudragit L100	0.125-0.25	0.008-0.016	4	0.063-0.125
ENRO/HPMCAS-LG	0.125-0.25	0.008-0.016	4-8	0.063-0.125
ENRO/HPMCAS-MG	0.125	**0.004-0.008**	4	**0.032-0.063**
Minimum Bactericidal Concentration (μg/ml)				
ENRO	0.25	0.032	4	0.25
ENRO/Eudragit L100	0.25	0.016	8	0.125
ENRO/HPMCAS-LG	0.125	0.016	8	0.125
ENRO/HPMCAS-MG	0.125	**0.008**	4	**0.063**

[a]The values shown in bold differ significantly from those of pure crystalline ENRO.

6.4 Conclusions

In this study ball milling was successfully used to produce several ASDs of ENRO. Despite its extra ethyl group, ENRO behaved very similarly to CIP in terms of polymer compatibility, with each drug only forming fully X-ray amorphous ASDs with acidic polymers. FTIR analysis indicated that the N3 tertiary amine of ENRO may be protonated in these ASDs, forming an ionic bond with the carboxylate groups of the polymers. The relatively high T_g's of the ASDs and their resistance to crystallization during DSC analysis reinforces the suggestion that strong interactions exist between the components. In contrast to the polymeric samples, amorphous ENRO/succinic acid salts possessed very low stability, and therefore were not suitable for further study. Although the ASDs were hygroscopic, they remained fully X-ray amorphous during water sorption studies, due to the stabilizing effects of the polymers. The ASDs also generated significantly higher drug concentrations than crystalline ENRO during solubility and dissolution testing, and these levels were sustained for the duration of the studies. As the prolongation of supersaturation is believed to increase drug absorption, the in vivo absorption of these formulations is likely to be superior to that of the pure drug. In addition, the antimicrobial activity of ENRO was not decreased by ASD formation, while it was improved by ENRO/HPMCAS-MG in *E. coli* and *S. aureus*. This study has therefore demonstrated that the formulation of ENRO as a polymeric ASD can improve a number of the drug's biopharmaceutical properties.

Chapter 7: General Discussion and Conclusions

7.1 General Discussion and Conclusions

As previously mentioned, the primary aim of this project was to prepare various amorphous formulations of CIP, and thereby improve the physicochemical and biopharmaceutical properties of the drug. Some of the more specific goals of the project were to find a method of amorphizing CIP, to discover which polymers or small organic molecules make suitable stabilizers for CIP ASDs, to produce ASDs of the closely related drug ENRO, to examine the stability of the successful formulations, and to establish whether they can improve the solubility of CIP without affecting its permeability. From the material covered in the previous chapters it can be seen that all of these objectives were achieved, at least to some degree. While this project may be of most interest to other researchers working with CIP, it also serves as an example of the steps that may be taken to amorphize a drug with poor glass-forming ability.

Although the main focus of this project was on multicomponent CIP systems, it was also important to gain a greater understanding of the drug itself. Therefore, Chapter 2 was dedicated to filling some of the gaps in the literature concerning CIP. The crystal structures of unionized and zwitterionic CIP have been described by Mahapatra et al[138] and Fabbiani et al,[139] respectively, and it is well known that CIP equilibrates between both ionization states in aqueous solutions.[112] However, until now, no study has examined the ability of anhydrous CIP to transform from one form to the other in the solid state. Although Mahapatra et al observed the PXRD pattern of CIP change to that of the unionized form at 250 ^{o}C, the authors misinterpreted the data.[138] They believed that the drug existed as a hydrate below this temperature, whereas the PXRD pattern actually matched that of anhydrous zwitterionic CIP. Their study served as a starting point for the investigation of proton transfer described in Chapter 2, which confirmed that zwitterionic CIP converts to the unionized form just prior to melting. Chapter 2 also contains a comprehensive comparison of the molecular properties of zwitterionic and unionized CIP, which enables greater understanding of the behavior of this drug. For example, the more extensive intermolecular interactions, greater packing energy and lower reactivity of the zwitterion confirmed that it is the more stable of the two structures. This explains why CIP usually exists in this form in the solid state, and why the drug is so difficult to amorphize.

It has been claimed that the amorphization of pure CIP is not possible via milling, melt quenching or spray drying,[125] and the inadequacy of the former methods was confirmed by this project. Although quench cooling did produce the amorphous form of the drug, it also resulted in its partial decomposition, and was therefore only useful for reference purposes. In contrast, this study disproved the belief that spray drying could not be used to amorphize CIP. However, as mentioned in Chapter 2, a large volume of dilute solution was required to produce a few milligrams of amorphous CIP via spray drying, due to the poor solubility of the drug. As the yield was so low, this was a time consuming and inefficient process. For this reason, the experiments described in later chapters that required a large quantity of sample, such as solubility studies, were carried out on crystalline CIP rather than the amorphous spray dried form of the drug.

In order to improve the stability and solubility of an amorphous drug, it can be formulated as an ASD. This requires the selection of suitable excipients, and Chapters 3–6 explored some of the possible stabilizers that may be used with CIP and ENRO. It was discovered that fully X-ray amorphous solid dispersions were only produced with compounds with which the drugs could form a salt. In all other cases a semi-crystalline product was obtained. All of the successful additives had the common feature of containing a carboxylic acid group, which formed an ionic bond with the protonated piperazine amino group of the drugs. With each ASD, proton transfer from the stabilizer to the carboxylate group of the drug was identified by FTIR. This transfer could also be observed visually, as all of the amorphous composite formulations became dark yellow or orange in color following milling. In contrast, the semi-crystalline solid dispersions were either off-white or pale yellow, due to a small degree of proton transfer. As mentioned in Chapter 2, CIP also becomes yellow upon conversion to the unionized form; however, it is far less vibrant in color than the ASDs.

From the results of this project it can be concluded that the ability of a compound to form an ASD with CIP or ENRO depends not only on the functional groups of the co-former, but also on the proportion of each ingredient included in the formulation, as well as the method of preparation. For example, as discussed in Chapter 3, longer milling times, lower temperatures and a larger percentage of polymer were required to amorphize a mixture of CIP and HPMCAS, compared to Carbopol, Eudragit L100 or Eudragit L100-55. The fact

that semi-crystalline solid dispersions were obtained with neutral polymers such as PVP and PVA for all attempted combinations of polymer content and milling conditions, indicates that the one uncompromising factor needed to form an ASD with these fluoroquinolones is the presence of a carboxylic acid in the co-former. However, this does not always guarantee success. For instance, as mentioned in Chapter 4, when CIP, succinic acid and PVP were ball milled without any pre-milling, a semi-crystalline product was obtained, with PXRD peaks largely matching those of zwitterionic CIP. In this case the polymer appears to have prevented the formation of ionic interactions between the drug and acid. Some of the amino acids studied in Chapter 5 were also unable to fully amorphize CIP, despite the fact that they all contain α-carboxylate groups. Therefore, other features of the molecules influenced their ability to interact to a sufficient degree with CIP, perhaps related to their size, shape and pK_a. However, further studies will be required to determine what these important molecular properties are.

While the ASDs prepared in this project are very similar in terms of drug-co-former interactions, many of their solid state and pharmaceutical properties differ, in particular their stability, solubility and permeability. When comparing the physical stability of the amorphous samples, the binary polymeric ASDs of Chapter 3 and 6 appear to be superior. The thermograms of these ASDs lacked clear crystallization peaks, indicating that they have good thermal stability. These samples were also found to remain X-ray amorphous following DVS analysis, although they sorbed large quantities of water due to the hygroscopicity of the polymers. In contrast, all of the samples described in Chapter 4 and 5, which contain small molecules as stabilizers, crystallized during DSC and water sorption studies. Despite the presence of 20–60% (w/w) polymer in the ternary ASDs, the CS 1:1 and CS 2:1 salts still underwent crystallization during these processes. However, these ASDs, as well as those containing the amino acids, remained X-ray amorphous when stored for at least 10 months under dry conditions at RT. Equivalent studies were not carried out with the binary polymeric ASDs, however it can be assumed that they would also remain amorphous under the same conditions. In contrast, the polymer-free amorphous CIP succinate salts crystallized during this study after only 1–2 months, indicating that the amino acids are capable of stabilizing CIP for longer periods than succinic acid. Similarly, the T_g's of the amino acid ASDs were also far higher than those of CS 1:1 and CS 2:1 (equal to 86.7 ^oC and 69.3 ^oC, respectively).

Although the addition of polymer increased the T_g's of the latter samples, only the ASD containing 60% (w/w) PVP had a T_g above 100 ^oC, whereas this was the case with all four of the amino acid ASDs. The binary polymeric CIP ASDs also had T_g's above 100 ^oC, with CIP/Eudragit L100 having the highest, at 154.1 ^oC.

The greater stability of the binary polymeric ASDs may be attributed to the fact that the polymers are amorphous themselves, with high T_g's and molecular weights. This enables them to delay or prevent the crystallization of an amorphous drug in a mixture by reducing the molecular mobility of the system and providing steric hindrance, as previously discussed. In contrast, succinic acid and the amino acids are poor glass-forming, low molecular weight, crystalline molecules, with very low T_g's. They are therefore prone to crystallization themselves, which would reduce their ability to stabilize an amorphous drug compared to the polymers.

All of the ASDs prepared in this study displayed superior solubility compared to the pure crystalline drugs, and this enhancement was sustained for at least 2 hours. However, when ranking the CIP ASDs by solubility, it is clear that the most soluble preparations are those containing the most acidic counterions, i.e. succinic acid, aspartic acid and glutamic acid. While a comparable CIP concentration was obtained with these ASDs in FaSSIF, the ASDs containing the latter acids offered a greater solubility advantage in water and FaSSGF. In FaSSGF in particular, the CIP/ASP and CIP/GLU ASDs achieved very high concentrations of 240 mg/ml and 120 mg/ml, respectively, at the end of the study, whereas the CIP succinate ASDs reached 39–57 mg/ml in this medium. Based on the results of this study and that of Olivera et al,[121] the amino acid and CIP succinate ASDs are likely to have a similar solubility to the commercially available salt, CIP HCl, in water, whereas their solubility in FaSSIF should be significantly higher. Although the ASDs containing CYS, ARG or a polymer were also significantly more soluble than the pure drug in water and FaSSIF, this increase was far more modest than that offered by the other ASDs, with concentrations of less than 2 mg/ml being achieved, compared to 29–48 mg/ml for the ASDs containing the more acidic counterions. In addition, as described in Chapter 3, a higher drug concentration was obtained with crystalline CIP in FaSSGF than with the binary polymeric ASDs. While the solubility

of the drug increases at low pH due to its ionization, the reduced solubility of the polymers in this medium most likely hindered the release of the drug from these ASDs.

The results of this project corroborate the studies of Miller et al, Dahan et al and Beig et al[30–32] discussed in Chapter 1, which found a negative association between solubility and permeability for a number of formulation types. The CIP/ASP, CIP/GLU and CIP succinate ASDs, which had the highest solubility, were also significantly less permeable than pure crystalline CIP, as was CIP HCl. This may be due to an increase in the proportion of drug bearing a net positive charge, which would reduce its lipophilicity. In contrast, the other ASDs that were tested either had no effect on the permeability of CIP or slightly increased it. Therefore, ASDs that have a more moderate effect on solubility, such as those analyzed in Chapter 3 and 6, may result in greater oral bioavailability overall. However, in order to determine unequivocally whether this is the case, in vivo studies would be required.

As discussed in Chapter 6, the CIP and ENRO ASDs behaved quite similarly in most regards, however the small difference in their chemical structures did result in some variation in their solid state properties. A summary of these differences is given in **Table 7.1**. For instance, HPMCAS appeared to form ASDs more easily with ENRO than CIP, as this process was successful when conducted for 4 hours at RT with the former drug, whereas low temperatures of 2–5 ^{o}C and an additional 2 hours of milling were required for the latter. Clearly, the presence of an ethyl substituent on the N3 of the piperazine group did not hinder the ability of the drug to interact with these polymers. The T_g's of the ENRO ASDs were 23–44 ^{o}C lower than the equivalent CIP ASDs; however, a similar divergence exists between the T_g's of the pure drugs (58.9 ^{o}C vs. 86.7 ^{o}C for ENRO and CIP, respectively). Therefore, although ENRO may form ASDs more readily than CIP, these are likely to have a lower physical stability. This was indeed found to be the case for the amorphous succinate salts. When ENRO was milled with succinic acid in a 1:1 or 2:1 ratio, an X-ray amorphous formulation was obtained after only 1 hour of ball milling. However, these salts were very unstable, and began to crystallize after approximately 2 months when stored at 2–5 ^{o}C. In contrast, 6 hours of milling was required to amorphize the CS 1:1 and 2:1 salts, but they then remained amorphous for approximately 6 months under the same storage conditions. While all of the polymeric ENRO and CIP ASDs have remained stable when stored in the fridge for at least

16 months, as well as during DVS analysis, no long-term studies comparing the stability of the ENRO and CIP ASDs at higher temperatures have been carried out.

Table 7.1. Comparison of Solid State and Pharmaceutical Properties of CIP and ENRO

Property	**ENRO**	**CIP**
Crystalline Anhydrous Drugs		
Ionization state	Unionized	Zwitterionic
Melting point	225 °C	272 °C
T_g	58.9 °C	86.7 °C
TGA mass loss	3.4%	12.8%
FaSSIF solubility	0.67 mg/ml	0.14 mg/ml
ASDs		
Amorphization conditions:		
Eudragit L100, Eudragit L100-55 and Carbopol	40% (w/w) polymer BM x 4 hours at RT	40% (w/w) polymer BM x 4 hours at RT
HPMCAS	60% (w/w) polymer BM x 4 hours at RT	60% (w/w) polymer BM x 6 hours at 2–5 °C
Succinic acid	1 hour at RT	6 hours at RT
Primary water uptake mechanism	Absorption (Eudragit L100, Eudragit L100-55 and Carbopol), multilayer adsorption (HPMCAS)	Absorption

The biopharmaceutical properties of CIP and ENRO, and the corresponding ASDs, would be expected to vary somewhat due to differences in the structure and lipophilicity of the APIs. This was found to be the case in this study in relation to the solubility, dissolution and antibacterial activity of the samples. ENRO has a solubility of 0.67 mg/ml in FaSSIF, compared to 0.14 mg/ml for CIP. The final drug concentrations achieved with the ENRO ASDs in solubility studies were also approximately 2.4–9.4 times greater than those containing CIP, perhaps due to weaker intermolecular interactions within the former samples. Although their solubility differed, similar profiles were obtained with both sets of ASDs during dissolution studies. The ASDs containing Eudragit L100 both formed slowly dissolving clumps when added to the dissolution vessel, resulting in a gradual increase in

drug concentration. The strong drug-polymer interactions present in these ASDs, as indicated by their particularly high T_g's, may have also contributed to the slow release of the drug. The ENRO and CIP ASDs containing HPMCAS on the other hand dispersed more readily in FaSSIF. With all four of these samples, the drug concentration increased quite rapidly within the first 20 min of the study and then began to level off.

The CIP and ENRO ASDs also behaved similarly in bacterial studies, in that they did not decrease the antimicrobial activity of the drug, while those containing HPMCAS-MG demonstrated a significant improvement. As discussed in Chapter 3, this may be due to an increase in the permeability of these samples. However, differences in the MIC and MBC values of the drugs were seen. While ENRO and CIP, and the equivalent ASDs, showed similar MIC values in *K. pneumoniae*, lower MIC values were obtained with ENRO in *E. coli* and *S. aureus*, whereas CIP was found to be the more potent antibiotic in *P. aeruginosa*. Differences in the susceptibility of bacteria to different fluoroquinolones may be due to differences in the affinity of the drugs for the target enzymes, outer membrane porins, or efflux pumps.[272] Due to its greater lipophilicity, ENRO would be expected to be taken up by bacteria via the passive transmembrane diffusion route more readily than CIP, which would account for its greater activity in *E. coli* and *S. aureus*. As the DNA gyrase of different species of bacteria is not expected to differ significantly in terms of fluoroquinolone affinity,[119] the greater potency of CIP in *P. aeruginosa* compared to ENRO is unlikely to be due to greater binding to the target enzyme. Instead, it may be due to increased uptake of the more hydrophilic CIP molecules via water-filled porins in the outer membrane of *P. aeruginosa*. In addition, more hydrophobic fluoroquinolones such as ENRO have been found to have a higher affinity for bacterial efflux pumps than CIP,[272] which would reduce the concentration of the drug in the cytoplasm of *P. aeruginosa* cells.

Based on the available literature concerning ASDs, the samples prepared in this project are somewhat unusual. In addition to containing drugs that are poor glass-formers, the ASDs examined in Chapter 3 and 6 are examples of amorphous polymeric salts, of which there are few examples in the literature. Although studies by Weuts et al,[61] Song et al[87] and Maniruzzaman et al[192] involve the production of amorphous drug-polymer salts, they are exceptions to the norm. The majority of ASDs described in the literature are stabilized by

nonionic interactions between the components, such as hydrogen bonds, and do not involve proton transfer between the drug and polymer. The polymer/salt formulations discussed in Chapter 4 are also quite unusual. While a number of ternary ASDs containing a drug plus two polymers or two small molecules have been reported in the literature,[145,227,273] few consist of a salt dispersed in a polymer, with the exception of those prepared by Patel et al[218] and Telang et al.[274] Similarly, in the majority of published studies concerning drug/amino acid ASDs, the components were found to interact via hydrogen bonds or π-π interactions.[243] A number of amorphous amino acid salts have also been produced by various researchers, however in each case an ionic interaction was formed between an acidic drug and the basic amino acids arginine, lysine or histidine.[62,86] No examples of amorphous salt formation between basic drugs and the α-carboxylate of amino acids could be found, making the CIP/amino acid ASDs of Chapter 5 relatively unique. Considering the fact that a recent screening study by Kasten et al concluded that ASP, GLU and CYS are poor co-formers for ASDs, whereas ARG is only suitable for acidic drugs,[236] the work outlined in Chapter 5 contributes to the literature surrounding this subcategory of ASD, as it contradicts these findings.

As with any research project, there were limitations to the work described in this thesis, in particular due to equipment and time restrictions. For instance, as the detection limit of PXRD for crystalline content is about 1–5% (w/w),[275] it is not possible to say with absolute certainty that the amorphous samples produced in this project were 100% amorphous. Therefore, in each case they were described as "X-ray amorphous" to take account of the possibility that they may have contained a small amount of residual crystallinity. As previously discussed, this is more likely to be true for the ball milled ASDs, and the presence of two crystallization peaks in the DSC thermograms of a few of the samples indicated that they may in fact contain a small amount of crystal nuclei.[26] Similarly, it is possible that some of the ASDs had small areas of inhomogeneity. As discussed in Chapter 1, separated amorphous domains of less than approximately 30 nm will not be detected by DSC, and such formulations will appear as homogeneous, single-phase systems.[65] In order to determine whether an X-ray amorphous material is truly amorphous, or if an ASD is phase separated, more complex techniques are required. SSNMR and PXRD with pair distribution function analysis have been recommended for this purpose.[65] SSNMR analysis is also a very useful

method for determining the nature of drug-stabilizer interactions present in an ASD. While SSNMR confirmed the amorphous state of the ASDs described in Chapter 5, as well as the nature of the drug-amino acid interactions, it was unfortunately not possible to carry out this analysis on all of the samples in this project due to the unavailability of the instrument. However, as PXRD, DSC and FTIR are used to characterize amorphous solids in the vast majority of published studies, they were therefore deemed sufficient for the purposes of this project.

In conclusion, the primary aim of this project was achieved with the production of a number of amorphous formulations of CIP. Due to the lack of comprehensive studies examining CIP or ENRO ASDs, this work is a substantial addition to the body of knowledge concerning the amorphous form of these drugs. While all of the ASDs significantly increased the solubility of CIP, the polymeric ASDs of Chapter 3 and 6 offered a more favorable solubility-permeability balance, and were also more stable than the amorphous salts of Chapter 4 and 5. The amorphous CIP succinate salts and corresponding polymer/salt ASDs appear to be the least stable of all of the ASDs produced in this study, and also had the lowest effective permeability. Considering the fact that the crystalline CS 1:1 and CS 2:1 salts prepared by Paluch et al are reported to have an aqueous solubility in water very similar to that of these ASDs (~ 30 mg/ml),[125] there does not seem to be any benefit in amorphizing these salts, and therefore no further studies shall be conducted on these ASDs. The binary polymeric ASDs are perhaps the most promising of the amorphous formulations produced in this project, and should be the subject of further research. However, the particularly high solubility and T_g's of the ASDs containing ASP and GLU may help to offset their lower stability and permeability, and therefore further studies with these samples may also be warranted.

7.2 Main Findings

- The production of pure amorphous CIP was achieved for the first time by spray drying a solution of the drug in water.
- Zwitterionic CIP undergoes intramolecular proton transfer and converts to the unionized form when heated to its melting point. This transformation was visualized using HSDSC.

- Fully X-ray amorphous ASDs were produced by ball milling CIP with acidic polymers, whereas neutral polymers were unsuccessful in this regard. In each ASD the positively charged secondary amino group of the drug was found to interact with the carboxylate groups of the polymers. Therefore, they may be considered as amorphous polymeric drug salts.
- The binary CIP ASDs had higher than expected T_g's, were stable when exposed to high humidity, and significantly improved the solubility of CIP.
- The CIP/HPMCAS ASDs increased the effective permeability of the drug as well as its antibacterial efficacy, whereas CIP/Eudragit L100 had no significant effect on these properties.
- ASDs consisting of the amorphous CIP/succinic acid 1:1 or 2:1 salt dispersed in various quantities of PVP or Soluplus were produced by spray drying and ball milling. The results of DSC and IGC analysis indicated that these salts and polymers are miscible.
- The ternary ASDs had higher T_g's and crystallization temperatures than the corresponding amorphous succinate salts, and displayed greater resistance to crystallization during long-term stability studies.
- All of the ternary ASDs significantly enhanced the solubility of CIP, in particular those containing CS 1:1. However, the ASDs did not offer any additional benefit over the amorphous succinate salts in terms of solubility.
- The addition of polymer did not improve the stability of the CS 1:1 or 2:1 salts during water sorption studies, nor did it affect their permeability.
- The amorphous succinate salts were significantly less permeable than pure crystalline CIP. This is most likely due to ionization of the drug.
- The milling of CIP with ASP, GLU, CYS and ARG resulted in fully X-ray amorphous solid dispersions. An ionic interaction between the positively charged piperazine amino group of CIP and the negatively charged α-carboxylate groups of the amino acids was detected by FTIR and SSNMR.
- The amino acid ASDs demonstrated high T_g's and crystallization temperatures, and remained X-ray amorphous for at least 10 months when stored under dry conditions at RT. However, they all crystallized during DVS and solubility studies.

- The enhanced solubility of the amino acid ASDs is related to the pH effect of the counterion. However, the fact that each ASD was more soluble than the corresponding PM proves that the disordered state of the drug had a significant positive effect on its solubility.
- Although the chemical structure, ionization state and intermolecular interactions of crystalline ENRO differ from those of CIP, the drugs behaved very similarly in terms of ASD formation and drug-polymer interactions.
- The T_g's of ENRO and its ASDs were significantly lower than those of CIP, however the samples remained X-ray amorphous during DVS analysis.
- Higher concentrations were obtained with the ENRO ASDs in solubility and dissolution studies relative to the pure drug. The solubility of ENRO in FaSSIF was also higher than that of CIP.
- Like CIP, the antimicrobial efficacy of ENRO was not decreased by ASD formation, while it was improved further by ENRO/HPMCAS-MG in *E. coli* and *S. aureus*.

7.3 Future Work

As previously discussed, PAMPA is not the most representative model of the human intestinal barrier. However, as the main aim of the permeability studies performed in this project was to determine whether ASD formation affected the permeability of CIP, PAMPA was suitable for this comparative analysis. In order to obtain a more accurate quantitative estimate of the permeability of the drug and ASDs, permeability studies should be conducted with more representative models. Human colon adenocarcinoma (Caco-2) cell culture studies are often used in early stage drug development, as they take account of both passive and active transport. However, there are a number of limitations to this method. In particular, the permeability of many drugs is underestimated by Caco-2 assays due to the less permeable tight junctions, lower surface area, and altered transporter expression of the cell monolayer compared to the intestinal epithelium.[276] In vivo animal studies, such as rat in situ perfusion assays, should more closely mimic the environment in the human GIT. Therefore, it would be interesting to see if the results of such studies are in line with those obtained by PAMPA for the samples analyzed in this project.

Further investigations into the amino acid ASDs could also be carried out. As discussed in Chapter 5, CIP appears to be more likely to form amorphous salts with amino acids of higher molecular weights, with more complex side chains, and lower α-carboxylate pK_a values. In order to strengthen this theory, CIP should be milled with other amino acids. A screening study by Kasten et al found non-polar amino acids to be successful co-formers for most drugs.[236] Therefore, future attempts to amorphize CIP could involve the amino acids isoleucine, leucine, methionine, phenylalanine, tryptophan or valine.

In relation to the CIP/amino acid samples, it would also be useful to develop a method of producing good quality crystals of the pure salts. This would allow single crystal X-ray analysis to be conducted, and thus the accurate determination of the interactions present between the drug and amino acids. It would also provide a definite PXRD pattern of the salts, to which those of the corresponding crystallized ASDs could be compared. As described in Chapter 5, all attempts to crystallize the CIP aspartate and glutamate salts thus far appear to have resulted in a mixture of phases. Although these salts were reportedly produced by ElShaer et al, their XRD analysis was unfortunately not published.[230] The authors used freeze drying to prepare these salts, and it may be worthwhile to explore this technique in subsequent studies.

A comparatively small amount of research was performed on ENRO in this project. The work of Chapter 6 could be continued with further analysis of the ENRO ASDs, such as permeability and long-term and/or accelerated stability studies. In order to confirm the nature of the drug-polymer interactions in the ASDs, SSNMR analysis would be useful. It would also be interesting to determine whether ENRO forms ASDs with the same amino acids as CIP, and if the components interact in the same manner.

Finally, the formulations produced in this project were very simple, consisting of only 2–3 ingredients in powder form. The development of more complex formulations may improve the biopharmaceutical properties of the ASDs further. For example, the addition of a surfactant can increase the solubility and stability of polymeric solid dispersions.[75] It would also be compelling to manufacture oral solid dosage forms, such as tablets or capsules, from

the most promising ASDs. Their bioavailability could then be compared to commercial CIP HCl tablets to discern if they offer any benefit over what is already on the market.

References

(1) Food and Drug Administration Center for Drug Evaluation and Research (CDER). *Guidance for Industry: Waiver of In Vivo Bioavailability and Bioequivalence Studies for Immediate-Release Solid Oral Dosage Forms Based on a Biopharmaceutics Classification System*; 2015.

(2) Amidon, G. L.; Lennernäs, H.; Shah, V. P.; Crison, J. R. A Theoretical Basis for a Biopharmaceutic Drug Classification: The Correlation of in Vitro Drug Product Dissolution and in Vivo Bioavailability. *Pharm. Res.* **1995**, *12*, 413–420.

(3) Butler, J. M.; Dressman, J. B. The Developability Classification System: Application of Biopharmaceutics Concepts to Formulation Development. *J. Pharm. Sci.* **2010**, *99*, 4940–4954.

(4) US Food and Drug Administration. The Biopharmaceutics Classification System (BCS) Guidance http://www.fda.gov/AboutFDA/CentersOffices/OfficeofMedicalProductsandTobacco/CDER/ucm128219.htm (accessed Feb 15, 2017).

(5) Ku, M. S.; Dulin, W. A Biopharmaceutical Classification-Based Right-First-Time Formulation Approach to Reduce Human Pharmacokinetic Variability and Project Cycle Time from First-In-Human to Clinical Proof-Of-Concept. *Pharm. Dev. Technol.* **2012**, *17*, 285–302.

(6) Smith, B. T. Solubility and Dissolution. In *Physical Pharmacy*; Pharmaceutical Press: Londan, 2016.

(7) Takano, R.; Takata, N.; Saito, R.; Furumoto, K.; Higo, S.; Hayashi, Y.; Machida, M.; Aso, Y.; Yamashita, S. Quantitative Analysis of the Effect of Supersaturation on in Vivo Drug Absorption. *Mol. Pharm.* **2010**, *7*, 1431–1440.

(8) Bevernage, J.; Brouwers, J.; Annaert, P.; Augustijns, P. Drug Precipitation-Permeation Interplay: Supersaturation in an Absorptive Environment. *Eur. J. Pharm. Biopharm.* **2012**, *82*, 424–428.

(9) Mosharraf, M.; Nyström, C. The Effect of Particle Size and Shape on the Surface Specific Dissolution Rate of Microsized Practically Insoluble Drugs. *Int. J. Pharm.* **1995**, *122*, 35–47.

(10) Noyes, A. A.; Whitney, W. R. The Rate of Solution of Solid Substances in Their Own Solutions. *J. Am. Chem. Soc.* **1897**, *19*, 930–934.

(11) Hörter, D.; Dressman, J. . Influence of Physicochemical Properties on Dissolution of Drugs in the Gastrointestinal Tract. *Adv. Drug Deliv. Rev.* **1997**, *25*, 3–14.

(12) Fagerholm, U. The Role of Permeability in Drug ADME/PK, Interactions and Toxicity, and the Permeability-Based Classification System (PCS). In *Burger's Medicinal Chemistry and Drug Discovery*; John Wiley & Sons, Inc.: Hoboken, NJ, USA, 2010; p. 367.

(13) Balimane, P. V; Han, Y.-H.; Chong, S. Current Industrial Practices of Assessing Permeability and P-Glycoprotein Interaction. *AAPS J.* **2006**, *8*, E1-13.

(14) Sugano, K.; Kansy, M.; Artursson, P.; Avdeef, A.; Bendels, S.; Di, L.; Ecker, G. F.; Faller, B.; Fischer, H.; Gerebtzoff, G.; et al. Coexistence of Passive and Carrier-Mediated Processes in Drug Transport. *Nat. Rev. drug Discov.* **2010**, *9*, 597–614.

(15) Avdeef, A. *Absorption and Drug Development: Solubility, Permeability, and Charge State*; John Wiley & Sons, Inc.: New Jersey, 2003.

(16) Lennernäs, H. Human Intestinal Permeability. *J. Pharm. Sci.* **1998**, *87*, 403–410.

(17) Schmidt, D.; Lynch, J. *MultiScreen Filter Plates for PAMPA - Evaluation of the Reproducibility of Parallel Artificial Membrane Permeation Assays (PAMPA)*; Massachusetts, 2003.

(18) Stegemann, S.; Leveiller, F.; Franchi, D.; de Jong, H.; Lindén, H. When Poor Solubility Becomes an Issue: From Early Stage to Proof of Concept. *Eur. J. Pharm. Sci.* **2007**, *31*, 249–261.

(19) Kawabata, Y.; Wada, K.; Nakatani, M.; Yamada, S.; Onoue, S. Formulation Design for Poorly Water-Soluble Drugs Based on Biopharmaceutics Classification System: Basic Approaches and Practical Applications. *Int. J. Pharm.* **2011**, *420*, 1–10.

(20) Bergström, C. A. S.; Wassvik, C. M.; Johansson, K.; Hubatsch, I. Poorly Soluble Marketed Drugs Display Solvation Limited Solubility. *J. Med. Chem.* **2007**, *50*, 5858–5862.

(21) Wassvik, C. M.; Holmén, A. G.; Draheim, R.; Artursson, P.; Bergström, C. A. S. Molecular Characteristics for Solid-State Limited Solubility. *J. Med. Chem.* **2008**, *51*, 3035–3039.

(22) Lipinski, C. A.; Lombardo, F.; Dominy, B. W.; Feeney, P. J. Experimental and Computational Approaches to Estimate Solubility and Permeability in Drug Discovery and Development Settings. *Adv. Drug Deliv. Rev.* **1997**, *23*, 3–25.

(23) Zaki, N. M.; Artursson, P.; Bergström, C. A. S. A Modified Physiological BCS for Prediction of Intestinal Absorption in Drug Discovery. *Mol. Pharm.* **2010**, *7*, 1478–1487.

(24) Williams, H. D.; Trevaskis, N. L.; Charman, S. A.; Shanker, R. M.; Charman, W. N.; Pouton, C. W.; Porter, C. J. H. Strategies to Address Low Drug Solubility in Discovery and Development. *Pharmacol. Rev.* **2013**, *65*, 315–499.

(25) Rasenack, N.; Hartenhauer, H.; Müller, B. W. Microcrystals for Dissolution Rate Enhancement of Poorly Water-Soluble Drugs. *Int. J. Pharm.* **2003**, *254*, 137–145.

(26) Trasi, N. S.; Byrn, S. R. Mechanically Induced Amorphization of Drugs: A Study of the Thermal Behavior of Cryomilled Compounds. *AAPS PharmSciTech* **2012**, *13*, 772–784.

(27) Huang, L.-F.; Tong, W.-Q. Impact of Solid State Properties on Developability Assessment of Drug Candidates. *Adv. Drug Deliv. Rev.* **2004**, *56*, 321–334.

(28) Serajuddin, A. T. M. Salt Formation to Improve Drug Solubility. *Adv. Drug Deliv. Rev.* **2007**, *59*, 603–616.

(29) Dahan, A.; Miller, J. M. The Solubility-Permeability Interplay and Its Implications in Formulation Design and Development for Poorly Soluble Drugs. *AAPS J.* **2012**, *14*, 244–251.

(30) Dahan, A.; Miller, J. M.; Hoffman, A.; Amidon, G. E.; Amidon, G. L. The Solubility-Permeability Interplay in Using Cyclodextrins as Pharmaceutical Solubilizers: Mechanistic Modeling and Application to Progesterone. *J. Pharm. Sci.* **2010**, *99*, 2739–2749.

(31) Miller, J. M.; Beig, A.; Carr, R. A.; Spence, J. K.; Dahan, A. A Win-Win Solution in Oral Delivery of Lipophilic Drugs: Supersaturation via Amorphous Solid Dispersions Increases Apparent Solubility without Sacrifice of Intestinal Membrane Permeability. *Mol. Pharm.* **2012**, *9*, 2009–2016.

(32) Beig, A.; Miller, J. M.; Lindley, D.; Carr, R. A.; Zocharski, P.; Agbaria, R.; Dahan, A. Head-to-Head Comparison of Different Solubility-Enabling Formulations of

Etoposide and Their Consequent Solubility-Permeability Interplay. *J. Pharm. Sci.* **2015**, *104*, 2941–2947.

(33) Bevernage, J.; Brouwers, J.; Brewster, M. E.; Augustijns, P. Evaluation of Gastrointestinal Drug Supersaturation and Precipitation: Strategies and Issues. *Int. J. Pharm.* **2013**, *453*, 25–35.

(34) Yu, L. Amorphous Pharmaceutical Solids: Preparation, Characterization and Stabilization. *Adv. Drug Deliv. Rev.* **2001**, *48*, 27–42.

(35) Hancock, B. C. Disordered Drug Delivery: Destiny, Dynamics and the Deborah Number. *J. Pharm. Pharmacol.* **2002**, *54*, 737–746.

(36) Nara, S. On the Relationship between Specific Volume and Crystallinity of Starch. *Starch/Stärke* **1979**, *31*, 73–75.

(37) Brough, C.; Williams, R. O. Amorphous Solid Dispersions and Nano-Crystal Technologies for Poorly Water-Soluble Drug Delivery. *Int. J. Pharm.* **2013**, *453*, 157–166.

(38) Shah, N.; Sandhu, H.; Choi, D. S.; Chokshi, H.; Malick, A. W. *Amorphous Solid Dispersions: Theory and Practice*; 1st ed.; Springer: London, 2014.

(39) Hancock, B. C.; Zografi, G. Characteristics and Significance of the Amorphous State in Pharmaceutical Systems. *J. Pharm. Sci.* **1997**, *86*, 1–12.

(40) Crowley, K. J.; Zografi, G. Water Vapor Absorption into Amorphous Hydrophobic Drug/poly(vinylpyrrolidone) Dispersions. *J. Pharm. Sci.* **2002**, *91*, 2150–2165.

(41) Brostow, W.; Chiu, R.; Kalogeras, I. M.; Vassilikou-Dova, A. Prediction of Glass Transition Temperatures: Binary Blends and Copolymers. *Mater. Lett.* **2008**, *62*, 3152–3155.

(42) Andronis, V.; Yoshioka, M.; Zografi, G. Effects of Sorbed Water on the Crystallization of Indomethacin from the Amorphous State. *J. Pharm. Sci.* **1997**, *86*, 346–351.

(43) Yoshioka, M.; Hancock, B. C.; Zografi, G. Crystallization of Indomethacin from the Amorphous State below and above Its Glass Transition Temperature. *J. Pharm. Sci.* **1994**, *83*, 1700–1705.

(44) Hancock, B. C.; Shamblin, S. L.; Zografi, G. Molecular Mobility of Amorphous Pharmaceutical Solids below Their Glass Transition Temperatures. *Pharm. Res.* **1995**,

12, 799–806.

(45) Ilevbare, G. A.; Liu, H.; Edgar, K. J.; Taylor, L. S. Maintaining Supersaturation in Aqueous Drug Solutions: Impact of Different Polymers on Induction Times. *Cryst. Growth Des.* **2013**, *13*, 740–751.

(46) Zhou, D.; Zhang, G. G. Z.; Law, D.; Grant, D. J. W.; Schmitt, E. A. Thermodynamics, Molecular Mobility and Crystallization Kinetics of Amorphous Griseofulvin. *Mol. Pharm.* **2008**, *5*, 927–936.

(47) Hancock, B. C.; Zografi, G. The Use of Solution Theories for Predicting Water Vapor Absorption by Amorphous Pharmaceutical Solids: A Test of the Flory-Huggins and Vrentas Models. *Pharm. Res.* **1993**, *10*, 1262–1267.

(48) Marsac, P. J.; Konno, H.; Rumondor, A. C. F.; Taylor, L. S. Recrystallization of Nifedipine and Felodipine from Amorphous Molecular Level Solid Dispersions Containing Poly(vinylpyrrolidone) and Sorbed Water. *Pharm. Res.* **2008**, *25*, 647–656.

(49) Aso, Y.; Yoshioka, S.; Zhang, J.; Zografi, G. Effect of Water on the Molecular Mobility of Sucrose and Poly(vinylpyrrolidone) in a Colyophilized Formulation as Measured by (13)C-NMR Relaxation Time. *Chem. Pharm. Bull. (Tokyo).* **2002**, *50*, 822–826.

(50) Teja, S.; Patil, S.; Shete, G.; Patel, S.; Bansal, A. Drug-Excipient Behavior in Polymeric Amorphous Solid Dispersions. *J. Excipients Food Chem.* **2013**, *4*, 70–94.

(51) Baghel, S.; Cathcart, H.; O'Reilly, N. J. Polymeric Amorphous Solid Dispersions: A Review of Amorphization, Crystallization, Stabilization, Solid-State Characterization, and Aqueous Solubilization of Biopharmaceutical Classification System Class II Drugs. *J. Pharm. Sci.* **2016**, *105*, 2527–2544.

(52) Yang, J.; Grey, K.; Doney, J. An Improved Kinetics Approach to Describe the Physical Stability of Amorphous Solid Dispersions. *Int. J. Pharm.* **2010**, *384*, 24–31.

(53) Konno, H.; Taylor, L. S. Influence of Different Polymers on the Crystallization Tendency of Molecularly Dispersed Amorphous Felodipine. *J. Pharm. Sci.* **2006**, *95*, 2692–2705.

(54) Yang, Z.; Nollenberger, K.; Albers, J.; Qi, S. Molecular Implications of Drug-Polymer Solubility in Understanding the Destabilization of Solid Dispersions by Milling. *Mol.*

Pharm. **2014**, *11*, 2453–2465.

(55) Shamblin, S. L.; Zografi, G. The Effects of Absorbed Water on the Properties of Amorphous Mixtures Containing Sucrose. *Pharm. Res.* **1999**, *16*, 1119–1124.

(56) Knapik, J.; Wojnarowska, Z.; Grzybowska, K.; Tajber, L.; Mesallati, H.; Paluch, K. J.; Paluch, M. Molecular Dynamics and Physical Stability of Amorphous Nimesulide Drug and Its Binary Drug–polymer Systems. *Mol. Pharm.* **2016**, *13*, 1937–1946.

(57) Khougaz, K.; Clas, S. Crystallization Inhibition in Solid Dispersions of MK-0591 and Poly(vinylpyrrolidone) Polymers. *J. Pharm. Sci.* **2000**, *89*, 1325–1334.

(58) Rumondor, A. C. F.; Ivanisevic, I.; Bates, S.; Alonzo, D. E.; Taylor, L. S. Evaluation of Drug-Polymer Miscibility in Amorphous Solid Dispersion Systems. *Pharm. Res.* **2009**, *26*, 2523–2534.

(59) Gordon, M.; Taylor, J. S. Ideal Copolymers and the Second-Order Transitions of Synthetic Rubbers. I. Non-Crystalline Copolymers. *J. Appl. Chem.* **1952**, *2*, 493–500.

(60) van Drooge, D. J.; Hinrichs, W. L. J.; Visser, M. R.; Frijlink, H. W. Characterization of the Molecular Distribution of Drugs in Glassy Solid Dispersions at the Nano-Meter Scale, Using Differential Scanning Calorimetry and Gravimetric Water Vapour Sorption Techniques. *Int. J. Pharm.* **2006**, *310*, 220–229.

(61) Weuts, I.; Kempen, D.; Verreck, G.; Peeters, J.; Brewster, M.; Blaton, N.; Van den Mooter, G. Salt Formation in Solid Dispersions Consisting of Polyacrylic Acid as a Carrier and Three Basic Model Compounds Resulting in Very High Glass Transition Temperatures and Constant Dissolution Properties upon Storage. *Eur. J. Pharm. Sci.* **2005**, *25*, 387–393.

(62) Jensen, K. T.; Löbmann, K.; Rades, T.; Grohganz, H. Improving Co-Amorphous Drug Formulations by the Addition of the Highly Water Soluble Amino Acid, Proline. *Pharmaceutics* **2014**, *6*, 416–435.

(63) Zhang, G. G. Z.; Zhou, D. Amorphous Drugs and Solid Dispersions. In *Developing solid oral dosage forms: pharmaceutical theory & practice*; Qiu, Y.; Chen, Y.; Zhang, G. G. Z.; Liu, L.; Porter, W. R., Eds.; Academic Press: New York, 2009.

(64) Lu, Q.; Zografi, G. Phase Behavior of Binary and Ternary Amorphous Mixtures Containing Indomethacin, Citric Acid, and PVP. *Pharm. Res.* **1998**, *15*, 1202–1206.

(65) Newman, A.; Engers, D.; Bates, S.; Ivanisevic, I.; Kelly, R. C.; Zografi, G.

Characterization of Amorphous API:Polymer Mixtures Using X-Ray Powder Diffraction. *J. Pharm. Sci.* **2008**, *97*, 4840–4856.

(66) Aso, Y.; Yoshioka, S.; Miyazaki, T.; Kawanishi, T.; Tanaka, K.; Kitamura, S.; Takakura, A.; Hayashi, T.; Muranushi, N. Miscibility of Nifedipine and Hydrophilic Polymers as Measured by (1)H-NMR Spin-Lattice Relaxation. *Chem. Pharm. Bull. (Tokyo).* **2007**, *55*, 1227–1231.

(67) Calahan, J. L.; Azali, S. C.; Munson, E. J.; Nagapudi, K. Investigation of Phase Mixing in Amorphous Solid Dispersions of AMG 517 in HPMC-AS Using DSC, Solid-State NMR, and Solution Calorimetry. *Mol. Pharm.* **2015**, *12*, 4115–4123.

(68) Pajula, K.; Taskinen, M.; Lehto, V.-P.; Ketolainen, J.; Korhonen, O. Predicting the Formation and Stability of Amorphous Small Molecule Binary Mixtures from Computationally Determined Flory-Huggins Interaction Parameter and Phase Diagram. *Mol. Pharm.* **2010**, *7*, 795–804.

(69) Hansen, C. M. *Hansen Solubility Parameters: A User's Handbook*; 2nd ed.; CRC Press: Boca Raton, 2007; Vol. 2.

(70) Thakral, S.; Thakral, N. K. Prediction of Drug-Polymer Miscibility through the Use of Solubility Parameter Based Flory-Huggins Interaction Parameter and the Experimental Validation: PEG as Model Polymer. *J. Pharm. Sci.* **2013**, *102*, 2254–2263.

(71) Greenhalgh, D. J.; Williams, A. C.; Timmins, P.; York, P. Solubility Parameters as Predictors of Miscibility in Solid Dispersions. *J. Pharm. Sci.* **1999**, *88*, 1182–1190.

(72) Kitak, T.; Dumičić, A.; Planinšek, O.; Šibanc, R.; Srčič, S. Determination of Solubility Parameters of Ibuprofen and Ibuprofen Lysinate. *Molecules* **2015**, *20*, 21549–21568.

(73) Vasconcelos, T.; Costa, P. Development of a Rapid Dissolving Ibuprofen Solid Dispersion. *PSWC–Pharmaceutical Sci. World Conf.* **2007**, *DD-W-103*.

(74) Chokshi, R. J.; Zia, H.; Sandhu, H. K.; Shah, N. H.; Malick, W. A. Improving the Dissolution Rate of Poorly Water Soluble Drug by Solid Dispersion and Solid Solution: Pros and Cons. *Drug Deliv.* **2007**, *14*, 33–45.

(75) Vasconcelos, T.; Sarmento, B.; Costa, P. Solid Dispersions as Strategy to Improve Oral Bioavailability of Poor Water Soluble Drugs. *Drug Discov. Today* **2007**, *12*, 1068–1075.

(76) Guzmán, H. R.; Tawa, M.; Zhang, Z.; Ratanabanangkoon, P.; Shaw, P.; Gardner, C. R.; Chen, H.; Moreau, J.-P.; Almarsson, O.; Remenar, J. F. Combined Use of Crystalline Salt Forms and Precipitation Inhibitors to Improve Oral Absorption of Celecoxib from Solid Oral Formulations. *J. Pharm. Sci.* **2007**, *96*, 2686–2702.

(77) Somasundaran, P.; Krishnakumar, S. Adsorption of Surfactants and Polymers at the Solid-Liquid Interface. *Colloids Surfaces A Physicochem. Eng. Asp.* **1997**, *123–124*, 491–513.

(78) Ilevbare, G. A.; Liu, H.; Edgar, K. J.; Taylor, L. S. Understanding Polymer Properties Important for Crystal Growth Inhibition—Impact of Chemically Diverse Polymers on Solution Crystal Growth of Ritonavir. *Cryst. Growth Des.* **2012**, *12*, 3133–3143.

(79) Ilevbare, G. A.; Liu, H.; Edgar, K. J.; Taylor, L. S. Inhibition of Solution Crystal Growth of Ritonavir by Cellulose Polymers – Factors Influencing Polymer Effectiveness. *CrystEngComm* **2012**, *14*, 6503–6514.

(80) Schram, C. J.; Beaudoin, S. P.; Taylor, L. S. Impact of Polymer Conformation on the Crystal Growth Inhibition of a Poorly Water-Soluble Drug in Aqueous Solution. *Langmuir* **2015**, *31*, 171–179.

(81) Chen, Y.; Liu, C.; Chen, Z.; Su, C.; Hageman, M.; Hussain, M.; Haskell, R.; Stefanski, K.; Feng, Q. Drug-Polymer-Water Interaction and Its Implication to the Dissolution Performance of Amorphous Solid Dispersions. *Mol. Pharm.* **2015**, *12*, 576–589.

(82) Ueda, K.; Higashi, K.; Yamamoto, K.; Moribe, K. Equilibrium State at Supersaturated Drug Concentration Achieved by Hydroxypropyl Methylcellulose Acetate Succinate: Molecular Characterization Using (1)H NMR Technique. *Mol. Pharm.* **2015**.

(83) Sun, D. D.; Lee, P. I. Probing the Mechanisms of Drug Release from Amorphous Solid Dispersions in Medium-Soluble and Medium-Insoluble Carriers. *J. Control. Release* **2015**, *211*, 85–93.

(84) Sun, D. D.; Lee, P. I. Evolution of Supersaturation of Amorphous Pharmaceuticals: The Effect of Rate of Supersaturation Generation. *Mol. Pharm.* **2013**, *10*, 4330–4346.

(85) Bowker, M.; Stahl, P. Preparation of Water-Soluble Compounds through Salt Formation. In *The Practice of Medicinal Chemistry*; Academic Press: London, 2008; pp. 749–765.

(86) Jensen, K. T.; Blaabjerg, L. I.; Lenz, E.; Bohr, A.; Grohganz, H.; Kleinebudde, P.;

Rades, T.; Löbmann, K. Preparation and Characterization of Spray-Dried Co-Amorphous Drug-Amino Acid Salts. *J. Pharm. Pharmacol.* **2016**, *68*, 615–624.

(87) Song, Y.; Yang, X.; Chen, X.; Nie, H.; Byrn, S.; Lubach, J. W. Investigation of Drug–Excipient Interactions in Lapatinib Amorphous Solid Dispersions Using Solid-State NMR Spectroscopy. *Mol. Pharm.* **2015**, *12*, 857–866.

(88) Karmwar, P.; Graeser, K.; Gordon, K. C.; Strachan, C. J.; Rades, T. Investigation of Properties and Recrystallisation Behaviour of Amorphous Indomethacin Samples Prepared by Different Methods. *Int. J. Pharm.* **2011**, *417*, 94–100.

(89) Shah, B.; Kakumanu, V. K.; Bansal, A. K. Analytical Techniques for Quantification of Amorphous/crystalline Phases in Pharmaceutical Solids. *J. Pharm. Sci.* **2006**, *95*, 1641–1665.

(90) Feng, T.; Pinal, R.; Carvajal, M. T. Process Induced Disorder in Crystalline Materials: Differentiating Defective Crystals from the Amorphous Form of Griseofulvin. *J. Pharm. Sci.* **2008**, *97*, 3207–3221.

(91) Surana, R.; Pyne, A.; Suryanarayanan, R. Effect of Preparation Method on Physical Properties of Amorphous Trehalose. *Pharm. Res.* **2004**, *21*, 1167–1176.

(92) Patterson, J. E.; James, M. B.; Forster, A. H.; Lancaster, R. W.; Butler, J. M.; Rades, T. Preparation of Glass Solutions of Three Poorly Water Soluble Drugs by Spray Drying, Melt Extrusion and Ball Milling. *Int. J. Pharm.* **2007**, *336*, 22–34.

(93) Balaz, P. High-Energy Milling. In *Mechanochemistry in nanoscience and minerals engineering*; Springer-Verlag Berlin Heidelberg: Košice, 2008.

(94) Boldyreva, E. Mechanochemistry of Inorganic and Organic Systems: What Is Similar, What Is Different? *Chem. Soc. Rev.* **2013**, *42*, 7719.

(95) Willart, J. F.; Descamps, M. Solid State Amorphization of Pharmaceuticals. *Mol. Pharm.* **2008**, *5*, 905–920.

(96) Crowley, K. J.; Zografi, G. Cryogenic Grinding of Indomethacin Polymorphs and Solvates: Assessment of Amorphous Phase Formation and Amorphous Phase Physical Stability. *J. Pharm. Sci.* **2002**, *91*, 492–507.

(97) Descamps, M.; Willart, J. F.; Dudognon, E.; Caron, V. Transformation of Pharmaceutical Compounds upon Milling and Comilling: The Role of T(g). *J. Pharm. Sci.* **2007**, *96*, 1398–1407.

(98) De Gusseme, A.; Neves, C.; Willart, J. F.; Rameau, A.; Descamps, M. Ordering and Disordering of Molecular Solids upon Mechanical Milling: The Case of Fananserine. *J. Pharm. Sci.* **2008**, *97*, 5000–5012.

(99) Macfhionnghaile, P.; Hu, Y.; Gniado, K.; Curran, S.; Mcardle, P.; Erxleben, A. Effects of Ball-Milling and Cryomilling on Sulfamerazine Polymorphs: A Quantitative Study. *J. Pharm. Sci.* **2014**, *103*, 1766–1778.

(100) Mah, P. T.; Laaksonen, T.; Rades, T.; Aaltonen, J.; Peltonen, L.; Strachan, C. J. Unravelling the Relationship between Degree of Disorder and the Dissolution Behavior of Milled Glibenclamide. *Mol. Pharm.* **2014**, *11*, 234–242.

(101) Ke, P.; Hasegawa, S.; Al-Obaidi, H.; Buckton, G. Investigation of Preparation Methods on Surface/bulk Structural Relaxation and Glass Fragility of Amorphous Solid Dispersions. *Int. J. Pharm.* **2012**, *422*, 170–178.

(102) Caron, V.; Tajber, L.; Corrigan, O. I.; Healy, A. M. A Comparison of Spray Drying and Milling in the Production of Amorphous Dispersions of Sulfathiazole/polyvinylpyrrolidone and Sulfadimidine/polyvinylpyrrolidone. *Mol. Pharm.* **2011**, *8*, 532–542.

(103) Trasi, N. S.; Boerrigter, S. X. M.; Byrn, S. R. Investigation of the Milling-Induced Thermal Behavior of Crystalline and Amorphous Griseofulvin. *Pharm. Res.* **2010**, *27*, 1377–1389.

(104) Paudel, A.; Worku, Z. A.; Meeus, J.; Guns, S.; Van den Mooter, G. Manufacturing of Solid Dispersions of Poorly Water Soluble Drugs by Spray Drying: Formulation and Process Considerations. *Int. J. Pharm.* **2013**, *453*, 253–284.

(105) Vasconcelos, T.; Marques, S.; das Neves, J.; Sarmento, B. Amorphous Solid Dispersions: Rational Selection of a Manufacturing Process. *Adv. Drug Deliv. Rev.* **2016**, *100*, 85–101.

(106) Mahmah, O.; Tabbakh, R.; Kelly, A.; Paradkar, A. A Comparative Study of the Effect of Spray Drying and Hot-Melt Extrusion on the Properties of Amorphous Solid Dispersions Containing Felodipine. *J. Pharm. Pharmacol.* **2014**, *66*, 275–284.

(107) Hawkey, P. M. Mechanisms of Quinolone Action and Microbial Response. *J. Antimicrob. Chemother.* **2003**, *51 Suppl 1*, 29–35.

(108) Chen, C. R.; Malik, M.; Snyder, M.; Drlica, K. DNA Gyrase and Topoisomerase IV

on the Bacterial Chromosome: Quinolone-Induced DNA Cleavage. *J. Mol. Biol.* **1996**, *258*, 627–637.

(109) Bermejo, M.; Avdeef, A.; Ruiz, A.; Nalda, R.; Ruell, J. A.; Tsinman, O.; González, I.; Fernández, C.; Sánchez, G.; Garrigues, T. M.; et al. PAMPA--a Drug Absorption in Vitro Model 7. Comparing Rat in Situ, Caco-2, and PAMPA Permeability of Fluoroquinolones. *Eur. J. Pharm. Sci.* **2004**, *21*, 429–441.

(110) Sun, J.; Sakai, S.; Tauchi, Y.; Deguchi, Y.; Chen, J.; Zhang, R.; Morimoto, K. Determination of Lipophilicity of Two Quinolone Antibacterials, Ciprofloxacin and Grepafloxacin, in the Protonation Equilibrium. *Eur. J. Pharm. Biopharm.* **2002**, *54*, 51–58.

(111) Mudie, D. M.; Murray, K.; Hoad, C. L.; Pritchard, S. E.; Garnett, M. C.; Amidon, G. L.; Gowland, P. A.; Spiller, R. C.; Amidon, G. E.; Marciani, L. Quantification of Gastrointestinal Liquid Volumes and Distribution Following a 240 mL Dose of Water in the Fasted State. *Mol. Pharm.* **2014**, *11*, 3039–3047.

(112) Breda, S. A.; Jimenez-Kairuz, A. F.; Manzo, R. H.; Olivera, M. E. Solubility Behavior and Biopharmaceutical Classification of Novel High-Solubility Ciprofloxacin and Norfloxacin Pharmaceutical Derivatives. *Int. J. Pharm.* **2009**, *371*, 106–113.

(113) Tehler, U.; Fagerberg, J. H.; Svensson, R.; Larhed, M.; Artursson, P.; Bergström, C. A. S. Optimizing Solubility and Permeability of a Biopharmaceutics Classification System (BCS) Class 4 Antibiotic Drug Using Lipophilic Fragments Disturbing the Crystal Lattice. *J. Med. Chem.* **2013**, *56*, 2690–2694.

(114) Hann, M. M.; Keserü, G. M. Finding the Sweet Spot: The Role of Nature and Nurture in Medicinal Chemistry. *Nat. Rev. Drug Discov.* **2012**, *11*, 355–365.

(115) Takács-Novák, K.; Józan, M.; Szász, G. Lipophilicity of Amphoteric Molecules Expressed by the True Partition Coefficient. *Int. J. Pharm.* **1995**, *113*, 47–55.

(116) Pagliara, A.; Carrupt, P.-A.; Caron, G.; Gaillard, P.; Testa, B. Lipophilicity Profiles of Ampholytes. *Chem. Rev.* **1997**, *97*, 3385–3400.

(117) Cramariuc, O.; Rog, T.; Javanainen, M.; Monticelli, L.; Polishchuk, A. V; Vattulainen, I. Mechanism for Translocation of Fluoroquinolones across Lipid Membranes. *Biochim. Biophys. Acta* **2012**, *1818*, 2563–2571.

(118) Tam, K. Y.; Avdeef, A.; Tsinman, O.; Sun, N. The Permeation of Amphoteric Drugs

through Artificial Membranes--an in Combo Absorption Model Based on Paracellular and Transmembrane Permeability. *J. Med. Chem.* **2010**, *53*, 392–401.

(119) Nikaido, H.; David Thanassi, An. G. Penetration of Lipophilic Agents with Multiple Protonation Sites into Bacterial Cells: Tetracyclines and Fluoroquinolones as Examples. *Antimicrob. Agents Chemother.* **1993**, *37*, 1393–1399.

(120) Nurchi, V. M.; Crisponi, G.; Lachowicz, J. I.; Zoroddu, M. A.; Peana, M.; Medici, S.; Veclani, D.; Tolazzi, M.; Melchior, A. Fluoroquinolones: A Micro-Species Equilibrium in the Protonation of Amphoteric Compounds. *Eur. J. Pharm. Sci.* **2016**, *93*, 380–391.

(121) Olivera, M. E.; Manzo, R. H.; Junginger, H. E.; Midha, K. K.; Shah, V. P.; Stavchansky, S.; Dressman, J. B.; Barends, D. M. Biowaiver Monographs for Immediate Release Solid Oral Dosage Forms: Ciprofloxacin Hydrochloride. *J. Pharm. Sci.* **2011**, *100*, 22–33.

(122) Plaisance, K. I.; Drusano, G. L.; Forrest, A.; Bustamante, C. I.; Standiford, H. C. Effect of Dose Size on Bioavailability of Ciprofloxacin. *Antimicrob. Agents Chemother.* **1987**, *31*, 956–958.

(123) Florindo, C.; Costa, A.; Matos, C.; Nunes, S. L.; Matias, A. N.; Duarte, C. M. M.; Rebelo, L. P. N.; Branco, L. C.; Marrucho, I. M. Novel Organic Salts Based on Fluoroquinolone Drugs: Synthesis, Bioavailability and Toxicological Profiles. *Int. J. Pharm.* **2014**, *469*, 179–189.

(124) Reddy, J. S.; Ganesh, S. V.; Nagalapalli, R.; Dandela, R.; Solomon, K. A.; Kumar, K. A.; Goud, N. R.; Nangia, A. Fluoroquinolone Salts with Carboxylic Acids. *J. Pharm. Sci.* **2011**, *100*, 3160–3176.

(125) Paluch, K. J.; McCabe, T.; Müller-Bunz, H.; Corrigan, O. I.; Healy, A. M.; Tajber, L. Formation and Physicochemical Properties of Crystalline and Amorphous Salts with Different Stoichiometries Formed between Ciprofloxacin and Succinic Acid. *Mol. Pharm.* **2013**, *10*, 3640–3654.

(126) Surov, A. O.; Manin, A. N.; Voronin, A. P.; Drozd, K. V; Simagina, A. A.; Churakov, A. V; Perlovich, G. L. Pharmaceutical Salts of Ciprofloxacin with Dicarboxylic Acids. *Eur. J. Pharm. Sci.* **2015**, *77*, 112–121.

(127) Cheow, W. S.; Hadinoto, K. Self-Assembled Amorphous Drug-Polyelectrolyte

Nanoparticle Complex with Enhanced Dissolution Rate and Saturation Solubility. *J. Colloid Interface Sci.* **2012**, *367*, 518–526.

(128) Osman, R.; Kan, P. L.; Awad, G.; Mortada, N.; El-Shamy, A.-E.; Alpar, O. Spray Dried Inhalable Ciprofloxacin Powder with Improved Aerosolisation and Antimicrobial Activity. *Int. J. Pharm.* **2013**, *449*, 44–58.

(129) Karanam, M.; Choudhury, A. R. Structural Landscape of Pure Enrofloxacin and Its Novel Salts: Enhanced Solubility for Better Pharmaceutical Applicability. *Cryst. Growth Des.* **2013**, *13*, 1626–1637.

(130) Escribano, E.; Calpena, A. C.; Garrigues, T. M.; Freixas, J.; Domenech, J.; Moreno, J. Structure-Absorption Relationships of a Series of 6-Fluoroquinolones. *Antimicrob. Agents Chemother.* **1997**, *41*, 1996–2000.

(131) Lizondo, M.; Pons, M.; Gallardo, M.; Estelrich, J. Physicochemical Properties of Enrofloxacin. *J. Pharm. Biomed. Anal.* **1997**, *15*, 1845–1849.

(132) Blokhina, S. V.; Sharapova, A. V.; Ol'khovich, M. V.; Volkova, T. V.; Perlovich, G. L. Solubility, Lipophilicity and Membrane Permeability of Some Fluoroquinolone Antimicrobials. *Eur. J. Pharm. Sci.* **2016**, *93*, 29–37.

(133) Giguère, S.; Dowling, P. M. Fluoroquinolones. In *Antimicrobial Therapy in Veterinary Medicine*; Giguère, S.; Prescott, J. F.; Dowling, P. M., Eds.; Ames, Iowa, US, 2013.

(134) Appelbaum, P. C.; Hunter, P. A. The Fluoroquinolone Antibacterials: Past, Present and Future Perspectives. *Int. J. Antimicrob. Agents* **2000**, *16*, 5–15.

(135) Sanders, C. C.; Sanders, W. E.; Goering, R. V. Overview of Preclinical Studies with Ciprofloxacin. *Am. J. Med.* **1987**, *82*, 2–11.

(136) Grüneberg, R. N.; Felmingham, D.; O'Hare, M. D.; Robbins, M. J.; Perry, K.; Wall, R. A.; Ridgway, G. L. The Comparative in-Vitro Activity of Ofloxacin. *J. Antimicrob. Chemother.* **1988**, *22 Suppl C*, 9–19.

(137) Gay, J. D.; DeYoung, D. R.; Roberts, G. D. In Vitro Activities of Norfloxacin and Ciprofloxacin against Mycobacterium Tuberculosis, M. Avium Complex, M. Chelonei, M. Fortuitum, and M. Kansasii. *Antimicrob. Agents Chemother.* **1984**, *26*, 94–96.

(138) Mahapatra, S.; Venugopala, K. N.; Guru Row, T. N. A Device to Crystallize Organic

Solids: Structure of Ciprofloxacin, Midazolam, and Ofloxacin as Targets. *Cryst. Growth Des.* **2010**, *10*, 1866–1870.

(139) Fabbiani, F. P. A.; Dittrich, B.; Florence, A. J.; Gelbrich, T.; Hursthouse, M. B.; Kuhs, W. F.; Shankland, N.; Sowa, H. Crystal Structures with a Challenge: High-Pressure Crystallisation of Ciprofloxacin Sodium Salts and Their Recovery to Ambient Pressure. *CrystEngComm* **2009**, *11*, 1396–1406.

(140) Webb, M. S.; Boman, N. L.; Wiseman, D. J.; Saxon, D.; Sutton, K.; Wong, K. F.; Logan, P.; Hope, M. J. Antibacterial Efficacy against an In Vivo Salmonella Typhimurium Infection Model and Pharmacokinetics of a Liposomal Ciprofloxacin Formulation. *Antimicrob. Agents Chemother.* **1998**, *42*, 45–52.

(141) Caco, A.; Varanda, F.; Pratas de Melo, M.; Dias, A.; Dohrn, R.; Marrucho, I. Solubility of Antibiotics in Different Solvents. Part II. Non-Hydrochloride Forms of Tetracycline and Ciprofloxacin. *Ind. Eng. Chem. Res.* **2008**, *47*, 8083–8089.

(142) Zhang, C.-L.; Zhao, F.; Wang, Y. Thermodynamics of the Solubility of Ciprofloxacin in Methanol, Ethanol, 1-Propanol, Acetone, and Chloroform from 293.15 to 333.15K. *J. Mol. Liq.* **2010**, *156*, 191–193.

(143) British Pharmacopoeia Commission. British Pharmacopoeia. In *Volume I & II*; The Stationery Office: London, 2016.

(144) Hancock, B. C.; Parks, M. What Is the True Solubility Advantage for Amorphous Pharmaceuticals? *Pharm. Res.* **2000**, *17*, 397–404.

(145) Al-Obaidi, H.; Buckton, G. Evaluation of Griseofulvin Binary and Ternary Solid Dispersions with HPMCAS. *AAPS PharmSciTech* **2009**, *10*, 1172–1177.

(146) Šuštar, B.; Bukovec, N.; Bukovec, P. Polymorphism and Stability of Norfloxacin, (1-Ethyl-6-Fluoro-1,4-Dihydro-4-Oxo-7-(1-Piperazinil)-3-Quinolinocarboxylic Acid. *J. Therm. Anal.* **1993**, *40*, 475–481.

(147) Barbas, R.; Prohens, R.; Puigjaner, C. A New Polymorph of Norfloxacin. *J. Therm. Anal. Calorim.* **2007**, *89*, 687–692.

(148) Duan, J.; Vogt, F. G.; Li, X.; Hayes, D.; Mansour, H. M. Design, Characterization, and Aerosolization of Organic Solution Advanced Spray-Dried Moxifloxacin and Ofloxacin Dipalmitoylphosphatidylcholine (DPPC) Microparticulate/nanoparticulate Powders for Pulmonary Inhalation Aerosol Delivery. *Int. J. Nanomedicine* **2013**, *8*,

3489–3505.

(149) Jie, Y.; Xin, H. Stable Levofloxacin Hydrochloride Compound. CN102351881 A, 2012.

(150) Hong, C. Y.; Kim, Y. K.; Chang, J. H.; Kim, S. H.; Choi, H.; Nam, D. H.; Kim, Y. Z.; Kwak, J. H. Novel Fluoroquinolone Antibacterial Agents Containing Oxime-Substituted (Aminomethyl)pyrrolidines: Synthesis and Antibacterial Activity of 7-(4-(Aminomethyl)-3-(Methoxyimino)pyrrolidin-1-Yl)-1-Cyclopropyl-6-Fluoro- 4-Oxo-1,4-dihydro[1,8]naphthyridine-3-C. *J. Med. Chem.* **1997**, *40*, 3584–3593.

(151) Spek, A. Single-Crystal Structure Validation with the Program PLATON. *J. Appl. Crystallogr.* **2003**, *36*, 7–13.

(152) Wolff, S.; Grimwood, D.; McKinnon, J.; Turner, M.; Jayatilaka, D.; Spackman, M. CrystalExplorer (Version 3.1), University of Western Australia, 2012.

(153) Macrae, C. F.; Edgington, P. R.; McCabe, P.; Pidcock, E.; Shields, G. P.; Taylor, R.; Towler, M.; van de Streek, J. Mercury : Visualization and Analysis of Crystal Structures. *J. Appl. Crystallogr.* **2006**, *39*, 453–457.

(154) Frisch, M.; Trucks, G.; Schlegel, H.; Scuseria, G.; Robb, M.; Cheeseman, J.; Montgomery, J.; Vreven, T, J.; Kudin, K.; Burant, J.; et al. *Gaussian 03, Revision C.02*; Gaussian, Inc., Wallingford CT, 2004.

(155) Koopmans, T. Über Die Zuordnung von Wellenfunktionen Und Eigenwerten Zu Den Einzelnen Elektronen Eines Atoms. *Physica* **1934**, *1*, 104–113.

(156) Pandey, J.; Prajapati, P.; Shimpi, M. R.; Tandon, P.; Velaga, S. P.; Srivastava, A.; Sinha, K.; Khan, E.; Shukla, A.; Srivastava, A.; et al. Studies of Molecular Structure, Hydrogen Bonding and Chemical Activity of a Nitrofurantoin- L -Proline Cocrystal: A Combined Spectroscopic and Quantum Chemical Approach. *RSC Adv.* **2016**, *6*, 74135–74154.

(157) Klopman, G. Chemical Reactivity and the Concept of Charge- and Frontier-Controlled Reactions. *J. Am. Chem. Soc.* **1968**, *90*, 223–234.

(158) Mafra, L.; Santos, S. M.; Siegel, R.; Alves, I.; Paz, F. A. A.; Dudenko, D.; Spiess, H. W. Packing Interactions in Hydrated and Anhydrous Forms of the Antibiotic Ciprofloxacin: A Solid-State NMR, X-Ray Diffraction, and Computer Simulation Study. *J. Am. Chem. Soc.* **2012**, *134*, 71–4.

(159) Martin, A. D.; Britton, J.; Easun, T. L.; Blake, A. J.; Lewis, W.; Schröder, M. Hirshfeld Surface Investigation of Structure-Directing Interactions within Dipicolinic Acid Derivatives. *Cryst. Growth Des.* **2015**, *15*, 1697–1706.

(160) Sheth, A. R.; Lubach, J. W.; Munson, E. J.; Muller, F. X.; Grant, D. J. W. Mechanochromism of Piroxicam Accompanied by Intermolecular Proton Transfer Probed by Spectroscopic Methods and Solid-Phase Changes. *J. Am. Chem. Soc.* **2005**, *127*, 6641–6651.

(161) Ho, R.; Naderi, M.; Heng, J. Y. Y.; Williams, D. R.; Thielmann, F.; Bouza, P.; Keith, A. R.; Thiele, G.; Burnett, D. J. Effect of Milling on Particle Shape and Surface Energy Heterogeneity of Needle-Shaped Crystals. *Pharm. Res.* **2012**, *29*, 2806–2816.

(162) Modi, S. R.; Dantuluri, A. K. R.; Perumalla, S. R.; Sun, C. C.; Bansal, A. K. Effect of Crystal Habit on Intrinsic Dissolution Behavior of Celecoxib due to Differential Wettability. *Cryst. Growth Des.* **2014**, *14*, 5283–5292.

(163) Sun, C. C.; Kiang, Y.-H. On the Identification of Slip Planes in Organic Crystals Based on Attachment Energy Calculation. *J. Pharm. Sci.* **2008**, *97*, 3456–3461.

(164) Gaisford, S.; Buanz, A. B. M. Pharmaceutical Physical Form Characterisation with Fast (>200 °C min−1) DSC Heating Rates. *J. Therm. Anal. Calorim.* **2011**, *106*, 221–226.

(165) Dorofeev, V. L. The Betainelike Structure and Infrared Spectra of Drugs of the Fluoroquinolone Group. *Pharm. Chem. J.* **2004**, *38*, 698–702.

(166) Turel, I.; Bukovec, P.; Quirós, M. Crystal Structure of Ciprofloxacin Hexahydrate and Its Characterization. *Int. J. Pharm.* **1997**, *152*, 59–65.

(167) Heinz, A.; Strachan, C. J.; Gordon, K. C.; Rades, T. Analysis of Solid-State Transformations of Pharmaceutical Compounds Using Vibrational Spectroscopy. *J. Pharm. Pharmacol.* **2009**, *61*, 971–988.

(168) Parojčić, J.; Stojković, A.; Tajber, L.; Grbić, S.; Paluch, K. J.; Djurić, Z.; Corrigan, O. I. Biopharmaceutical Characterization of Ciprofloxacin HCl-Ferrous Sulfate Interaction. *J. Pharm. Sci.* **2011**, *100*, 5174–5184.

(169) Turel, I.; Bukovec, P. Comparison of the Thermal Stability of Ciprofloxacin and Its Compounds. *Thermochim. Acta* **1996**, *287*, 311–318.

(170) Cassel, B.; Packer, R. Modulated temperature DSC and the DSC 8500: a step up in

performance. http://www.perkinelmer.com/CMSResources/Images/44-74834TCH_DSCandDSC8500.pdf (accessed Sep 1, 2015).

(171) Thomas, L. C. Use of Multiple Heating Rate DSC and Modulated Temperature DSC to Detect and Analyze Temperature-Time-Dependent Transitions in Materials. *Am. Lab.* **2001**, *33*.

(172) Vektariene, A.; Vektaris, G.; Svoboda, J. A Theoretical Approach to the Nucleophilic Behavior of Benzofused thieno[3,2-B]furans Using DFT and HF Based Reactivity Descriptors. *Arch. Org. Chem.* **2009**, 311–329.

(173) Wales, C.; Thomas, L. H.; Wilson, C. C. Tautomerisation and Polymorphism in Molecular Complexes of Piroxicam with Mono-Substituted Benzoic Acids. *CrystEngComm* **2012**, *14*, 7264–7274.

(174) Vippagunta, S. R.; Brittain, H. G.; Grant, D. J. W. Crystalline Solids. *Adv. Drug Deliv. Rev.* **2001**, *48*, 3–26.

(175) Hu, T.-C.; Wang, S.-L.; Chen, T.-F.; Lin, S.-Y. Hydration-Induced Proton Transfer in the Solid State of Norfloxacin. *J. Pharm. Sci.* **2002**, *91*, 1351–1357.

(176) Kakkar, R.; Katoch, V. AM1 Study of Proton-Transfer Reactions of Barbituric Acid. *Int. J. Quantum Chem.* **1999**, *74*, 327–336.

(177) Florence, A. T.; Attwood, D. *Physicochemical Principles of Pharmacy*; 5th ed.; Pharmaceutical Press: Cornwall, 2011.

(178) Yeon, K. .; Kim, J. H.; Choi, K. E.; Kim, D. H.; Lee, K. H. Salts of a Quinolone-Carboxylic Acid. U.S. Patent US5484785 A, 1996.

(179) Willis, C. R.; Banker, G. S. Polymer–drug Interacted Systems in the Physicochemical Design of Pharmaceutical Dosage Forms I. Drug Salts with PVM/MA and with a PVM/MA Hemi-Ester. *J. Pharm. Sci.* **1968**, *57*, 1598–1603.

(180) Huang, Y.; Dai, W.-G. Fundamental Aspects of Solid Dispersion Technology for Poorly Soluble Drugs. *Acta Pharm. Sin. B* **2014**, *4*, 18–25.

(181) Evonik Industries. EUDRAGIT® L 100 http://eudragit.evonik.com/product/eudragit/en/products-services/eudragit-products/enteric-formulations/l-100/Pages/default.aspx (accessed Feb 18, 2015).

(182) Evonik Industries. EUDRAGIT® L 100-55 http://eudragit.evonik.com/product/eudragit/en/products-services/eudragit-

products/enteric-formulations/l-100-55/pages/default.aspx.

(183) Ashland. AquaSolve hydroxypropylmethylcellulose acetate succinate http://www.ashland.com/Ashland/Static/Documents/ASI/PC_12624_AquaSolve_AS_Handbook.pdf (accessed Feb 11, 2015).

(184) Evonik Industries. EUDRAGIT® L 100 and EUDRAGIT® S 100 http://eudragit.evonik.com/sites/lists/HN/ProductSpecifications/TI-EUDRAGIT-L-100-S-100-EN.pdf (accessed Jan 11, 2016).

(185) Evonik Industries. EUDRAGIT® L 100-55 http://eudragit.evonik.com/sites/lists/HN/ProductSpecifications/TI-EUDRAGIT-L-100-55-EN.pdf (accessed Jan 11, 2016).

(186) Xiang, T.-X.; Anderson, B. D. Molecular Dynamics Simulation of Amorphous Hydroxypropyl-Methylcellulose Acetate Succinate (HPMCAS): Polymer Model Development, Water Distribution, and Plasticization. *Mol. Pharm.* **2014**, *11*, 2400–2411.

(187) Merck Millipore. *Lipid-PAMPA with the MultiScreen® Filter Plates*; Billerica, MA, 2004.

(188) Wohnsland, F.; Faller, B. High-Throughput Permeability pH Profile and High-Throughput Alkane/water Log P with Artificial Membranes. *J. Med. Chem.* **2001**, *44*, 923–930.

(189) Umerska, A.; Cassisa, V.; Matougui, N.; Joly-Guillou, M.-L.; Eveillard, M.; Saulnier, P. Antibacterial Action of Lipid Nanocapsules Containing Fatty Acids or Monoglycerides as Co-Surfactants. *Eur. J. Pharm. Biopharm.* **2016**, *108*, 100–110.

(190) Lubrizol. *Pharmaceutical Bulletin 23: Bioadhesion*; Wickliffe, Ohio, 2011.

(191) Huang, K.-S.; Britton, D.; Margaret, L.; C. Etter, T.; Byrn, S. R. A Novel Class of Phenol–pyridine Co-Crystals for Second Harmonic Generation. *J. Mater. Chem.* **1997**, *7*, 713–720.

(192) Maniruzzaman, M.; Morgan, D. J.; Mendham, A. P.; Pang, J.; Snowden, M. J.; Douroumis, D. Drug-Polymer Intermolecular Interactions in Hot-Melt Extruded Solid Dispersions. *Int. J. Pharm.* **2013**, *443*, 199–208.

(193) Borbas, E.; Sinko, B.; Tsinman, O.; Tsinman, K.; Kiserdei, E.; Demuth, B.; Balogh, A.; Bodak, B.; Domokos, A.; Dargo, G.; et al. Investigation and Mathematical

Description of the Real Driving Force of Passive Transport of Drug Molecules from Supersaturated Solutions. *Mol. Pharm.* **2016**, *13*, 3816–26.

(194) Tong, P.; Taylor, L. S.; Zografi, G. Influence of Alkali Metal Counterions on the Glass Transition Temperature of Amorphous Indomethacin Salts. *Pharm. Res.* **2002**, *19*, 649–654.

(195) Chawla, G.; Bansal, A. K. A Comparative Assessment of Solubility Advantage from Glassy and Crystalline Forms of a Water-Insoluble Drug. *Eur. J. Pharm. Sci.* **2007**, *32*, 45–57.

(196) biorelevant.com. FaSSIF, FeSSIF & FaSSGF contain bile salts and phospholipids http://biorelevant.com/fassif-fessif-fassgf-powder/contains-bile-salts-phospholipids/ (accessed Feb 18, 2015).

(197) Tanno, F.; Nishiyama, Y.; Kokubo, H.; Obara, S. Evaluation of Hypromellose Acetate Succinate (HPMCAS) as a Carrier in Solid Dispersions. *Drug Dev. Ind. Pharm.* **2004**, *30*, 9–17.

(198) Li, X.; Zhi, F.; Hu, Y. Investigation of Excipient and Processing on Solid Phase Transformation and Dissolution of Ciprofloxacin. *Int. J. Pharm.* **2007**, *328*, 177–182.

(199) Kramer, S. F.; Flynn, G. L. Solubility of Organic Hydrochlorides. *J. Pharm. Sci.* **1972**, *61*, 1896–1904.

(200) Van den Mooter, G.; Wuyts, M.; Blaton, N.; Busson, R.; Grobet, P.; Augustijns, P.; Kinget, R. Physical Stabilisation of Amorphous Ketoconazole in Solid Dispersions with Polyvinylpyrrolidone K25. *Eur. J. Pharm. Sci.* **2001**, *12*, 261–269.

(201) Fortuna, A.; Alves, G.; Soares-da-Silva, P.; Falcão, A. Optimization of a Parallel Artificial Membrane Permeability Assay for the Fast and Simultaneous Prediction of Human Intestinal Absorption and Plasma Protein Binding of Drug Candidates: Application to Dibenz[b,f]azepine-5-Carboxamide Derivatives. *J. Pharm. Sci.* **2012**, *101*, 530–540.

(202) Harder, S.; Fuhr, U.; Beermann, D.; Staib, A. H. Ciprofloxacin Absorption in Different Regions of the Human Gastrointestinal Tract. Investigations with the Hf-Capsule. *Br. J. Clin. Pharmacol.* **1990**, *30*, 35–39.

(203) Said, H. M.; Blair, J. A.; Lucas, M. L.; Hilburn, M. E. Intestinal Surface Acid Microclimate in Vitro and in Vivo in the Rat. *J. Lab. Clin. Med.* **1986**, *107*, 420–424.

(204) Sugano, K. Permeability of a Drug. In *Biopharmaceutics modeling and simulations: theory, practice, methods, and applications*; John Wiley & Sons: New Jersey, 2012; p. 170.

(205) Friesen, D. T.; Shanker, R.; Crew, M.; Smithey, D. T.; Curatolo, W. J.; Nightingale, J. A. S. Hydroxypropyl Methylcellulose Acetate Succinate-Based Spray-Dried Dispersions: An Overview. *Mol. Pharm.* **2008**, *5*, 1003–1019.

(206) Markovic, B. D.; Vladimirov, S. M.; Cudina, O. A.; Odovic, J. V; Karljikovic-Rajic, K. D. A PAMPA Assay as Fast Predictive Model of Passive Human Skin Permeability of New Synthesized Corticosteroid C-21 Esters. *Molecules* **2012**, *17*, 480–491.

(207) Rodríguez-Ibáñez, M.; Sánchez-Castaño, G.; Montalar-Montero, M.; Garrigues, T. M.; Bermejo, M.; Merino, V. Mathematical Modelling of in Situ and in Vitro Efflux of Ciprofloxacin and Grepafloxacin. *Int. J. Pharm.* **2006**, *307*, 33–41.

(208) Maeda, T.; Takahashi, K.; Ohtsu, N.; Oguma, T.; Ohnishi, T.; Atsumi, R.; Tamai, I. Identification of Influx Transporter for the Quinolone Antibacterial Agent Levofloxacin. *Mol. Pharm.* **2007**, *4*, 85–94.

(209) Merino, G.; Alvarez, A. I.; Pulido, M. M.; Molina, A. J.; Schinkel, A. H.; Prieto, J. G. Breast Cancer Resistance Protein (BCRP/ABCG2) Transports Fluoroquinolone Antibiotics and Affects Their Oral Availability, Pharmacokinetics, and Milk Secretion. *Drug Metab. Dispos.* **2006**, *34*, 690–695.

(210) Barry, A. L.; Fass, R. J.; Anhalt, J. P.; Neu, H. C.; Thornsberry, C.; Tilton, R. C.; Painter, B. G.; Washington, J. A. 2nd. Ciprofloxacin Disk Susceptibility Tests: Interpretive Zone Size Standards for 5-Microgram Disks. *J. Clin. Microbiol.* **1985**, *21*, 880–883.

(211) Barry, A. L.; Jones, R. N.; Thornsberry, C.; Ayers, L. W.; Gerlach, E. H.; Sommers6, A. H. M. Antibacterial Activities of Ciprofloxacin, Norfloxacin, Oxolinic Acid, Cinoxacin, and Nalidixic Acid. *Antimicrob. Agents Chemother.* **1984**, *25*, 633–637.

(212) Standiford, H. C.; Drusano, G. L.; Forrest, A.; Tatem, B.; Plaisance3, K. Bactericidal Activity of Ciprofloxacin Compared with that of Cefotaxime in Normal Volunteers. *Antimicrob. Agents Chemother.* **1987**, *31*, 1177–1182.

(213) Well, M.; Naber, K. G.; Kinzig-Schippers, M.; Sörgel, F. Urinary Bactericidal Activity and Pharmacokinetics of Enoxacin versus Norfloxacin and Ciprofloxacin in

Healthy Volunteers after a Single Oral Dose. *Int. J. Antimicrob. Agents* **1998**, *10*, 31–38.

(214) Pankey, G. A.; Sabath, L. D. Clinical Relevance of Bacteriostatic versus Bactericidal Mechanisms of Action in the Treatment of Gram-Positive Bacterial Infections. *Clin. Infect. Dis.* **2004**, *38*, 864–870.

(215) Zhang, G.; Zhang, L.; Yang, D.; Zhang, N.; He, L.; Du, G.; Lu, Y. Salt Screening and Characterization of Ciprofloxacin. *Acta Crystallogr. Sect. B Struct. Sci. Cryst. Eng. Mater.* **2016**, *72*, 20–28.

(216) Cheong, H.-A.; Choi, H.-K. Enhanced Percutaneous Absorption of Piroxicam via Salt Formation with Ethanolamines. *Pharm. Res.* **2002**, *19*, 1375–1380.

(217) Berge, S. M.; Bighley, L. D.; Monkhouse, D. C. Pharmaceutical Salts. *J. Pharm. Sci.* **1977**, *66*, 1–19.

(218) Patel, J. R.; Carlton, R. A.; Yuniatine, F.; Needham, T. E.; Wu, L.; Vogt, F. G. Preparation and Structural Characterization of Amorphous Spray-Dried Dispersions of Tenoxicam with Enhanced Dissolution. *J. Pharm. Sci.* **2012**, *101*, 641–663.

(219) Caron, V.; Hu, Y.; Tajber, L.; Erxleben, A.; Corrigan, O. I.; McArdle, P.; Healy, A. M. Amorphous Solid Dispersions of sulfonamide/Soluplus® and sulfonamide/PVP Prepared by Ball Milling. *AAPS PharmSciTech* **2013**, *14*, 464–474.

(220) Chen, Y.; Wang, S.; Wang, S.; Liu, C.; Su, C.; Hageman, M.; Hussain, M.; Haskell, R.; Stefanski, K.; Qian, F. Initial Drug Dissolution from Amorphous Solid Dispersions Controlled by Polymer Dissolution and Drug-Polymer Interaction. *Pharm. Res.* **2016**, *33*, 2445–2458.

(221) Shalaev, E. Y.; Gatlin, L. A. The Impact of Buffer on Solid-State Properties and Stability of Freeze-Dried Dosage Forms. In *Formulation and process development strategies for manufacturing biopharmaceuticals*; Jameel, F.; Hershenson, S., Eds.; John Wiley & Sons, Inc.: New Jersey, 2010; p. 508.

(222) Knopp, M. M.; Tajber, L.; Tian, Y.; Olesen, N. E.; Jones, D. S.; Kozyra, A.; Löbmann, K.; Paluch, K.; Brennan, C. M.; Holm, R.; et al. Comparative Study of Different Methods for the Prediction of Drug-Polymer Solubility. *Mol. Pharm.* **2015**, *12*, 3408–3419.

(223) Djuris, J.; Nikolakakis, I.; Ibric, S.; Djuric, Z.; Kachrimanis, K. Preparation of

carbamazepine–Soluplus® Solid Dispersions by Hot-Melt Extrusion, and Prediction of Drug–polymer Miscibility by Thermodynamic Model Fitting. *Eur. J. Pharm. Biopharm.* **2013**, *84*, 228–237.

(224) Barham, A. S.; Tewes, F.; Healy, A. M. Moisture Diffusion and Permeability Characteristics of Hydroxypropylmethylcellulose and Hard Gelatin Capsules. *Int. J. Pharm.* **2015**, *478*, 796–803.

(225) Hughey, J. R.; Keen, J. M.; Miller, D. A.; Kolter, K.; Langley, N.; McGinity, J. W. The Use of Inorganic Salts to Improve the Dissolution Characteristics of Tablets Containing Soluplus®-Based Solid Dispersions. *Eur. J. Pharm. Sci.* **2013**, *48*, 758–766.

(226) Tilborg, A.; Norberg, B.; Wouters, J. Pharmaceutical Salts and Cocrystals Involving Amino Acids: A Brief Structural Overview of the State-of-Art. *Eur. J. Med. Chem.* **2014**, *74*, 411–426.

(227) Löbmann, K.; Grohganz, H.; Laitinen, R.; Strachan, C.; Rades, T. Amino Acids as Co-Amorphous Stabilizers for Poorly Water Soluble Drugs--Part 1: Preparation, Stability and Dissolution Enhancement. *Eur. J. Pharm. Biopharm.* **2013**, *85*, 873–881.

(228) Laitinen, R.; Loebmann, K.; Grohganz, H.; Strachan, C.; Rades, T. Amino Acids as Co-Amorphous Excipients for Simvastatin and Glibenclamide: Physical Properties and Stability. *Mol. Pharm.* **2014**, *11*, 2381–2389.

(229) Jensen, K. T.; Larsen, F. H.; Löbmann, K.; Rades, T.; Grohganz, H. Influence of Variation in Molar Ratio on Co-Amorphous Drug-Amino Acid Systems. *Eur. J. Pharm. Biopharm.* **2016**, *107*, 32–39.

(230) ElShaer, A.; Ouyang, D.; Hanson, P.; Mohammed, A. R. Preparation and Evaluation of Amino Acid Based Salt Forms of Model Zwitterionic Drug Ciprofloxacin. *Pharm. Drug Deliv. Res.* **2013**, *2*, 1–10.

(231) Heikkinen, A. T.; DeClerck, L.; Löbmann, K.; Grohganz, H.; Rades, T.; Laitinen, R. Dissolution Properties of Co-Amorphous Drug-Amino Acid Formulations in Buffer and Biorelevant Media. *Pharmazie* **2015**, *70*, 452–457.

(232) Morcombe, C. R.; Zilm, K. W. Chemical Shift Referencing in MAS Solid State NMR. *J. Magn. Reson.* **2003**, *162*, 479–486.

(233) Fung, B. M.; Khitrin, A. K.; Ermolaev, K. An Improved Broadband Decoupling

Sequence for Liquid Crystals and Solids. *J. Magn. Reson.* **2000**, *142*, 97–101.

(234) Mattern, M.; Winter, G.; Kohnert, U.; Lee, G. Formulation of Proteins in Vacuum-Dried Glasses. II. Process and Storage Stability in Sugar-Free Amino Acid Systems. *Pharm. Dev. Technol.* **1999**, *4*, 199–208.

(235) Chieng, N.; Aaltonen, J.; Saville, D.; Rades, T. Physical Characterization and Stability of Amorphous Indomethacin and Ranitidine Hydrochloride Binary Systems Prepared by Mechanical Activation. *Eur. J. Pharm. Biopharm.* **2009**, *71*, 47–54.

(236) Kasten, G.; Grohganz, H.; Rades, T.; Löbmann, K. Development of a Screening Method for Co-Amorphous Formulations of Drugs and Amino Acids. *Eur. J. Pharm. Sci.* **2016**, *95*, 28–35.

(237) Berg, J. M.; Tymoczko, J. L.; Stryer, L. Appendix: Acid-Base Concepts. In *Biochemistry*; W H Freeman: New York, 2002.

(238) Wolpert, M.; Hellwig, P. Infrared Spectra and Molar Absorption Coefficients of the 20 Alpha Amino Acids in Aqueous Solutions in the Spectral Range from 1800 to 500 Cm-1. *Spectrochim. Acta. A. Mol. Biomol. Spectrosc.* **2006**, *64*, 987–1001.

(239) Socrates, G. *Infrared and Raman Characteristic Group Frequencies: Tables and Charts*; 3rd ed.; John Wiley & Sons: West Sussex, 2004.

(240) Lambert, J. B.; Shurvell, H. F.; Cooks, R. G. Infrared and Raman Spectroscopy. In *Introduction to organic spectroscopy*; Macmillan: New York, 1987.

(241) Im, S.; Jang, S.-W.; Lee, S.; Lee, Y.; Kim, B. Arginine Zwitterion Is More Stable than the Canonical Form When Solvated by a Water Molecule. *J. Phys. Chem. A* **2008**, *112*, 9767–9770.

(242) Barth, A. The Infrared Absorption of Amino Acid Side Chains. *Prog. Biophys. Mol. Biol.* **2000**, *74*, 141–173.

(243) Löbmann, K.; Laitinen, R.; Strachan, C.; Rades, T.; Grohganz, H. Amino Acids as Co-Amorphous Stabilizers for Poorly Water-Soluble Drugs--Part 2: Molecular Interactions. *Eur. J. Pharm. Biopharm.* **2013**, *85*, 882–888.

(244) Wang, Y.; Wilson, D.; Harbison, G. S. Solid-State NMR and the Crystallization of Aspartic and Glutamic Acids. *Cryst. Growth Des.* **2016**, *16*, 625–631.

(245) Abraham, A.; Mihaliuk, E.; Kumar, B.; Legleiter, J.; Gullion, T. Solid-State NMR Study of Cysteine on Gold Nanoparticles. *J. Phys. Chem. C* **2010**, *114*, 18109–18114.

(246) Guilbaud, J.-B.; Baker, H.; Clark, B. C.; Meehan, E.; Khimyak, Y. Z. Effect of Encapsulating Arginine Containing Molecules on PLGA: A Solid-State NMR Study. *J. Pharm. Sci.* **2010**, *99*, 2697–2710.

(247) Lubach, J. W.; Xu, D.; Segmuller, B. E.; Munson, E. J. Investigation of the Effects of Pharmaceutical Processing upon Solid-State NMR Relaxation Times and Implications to Solid-State Formulation Stability. *J. Pharm. Sci.* **2007**, *96*, 777–787.

(248) Gunnam, A.; Suresh, K.; Ganduri, R.; Nangia, A. Crystal Engineering of a Zwitterionic Drug to Neutral Cocrystals: A General Solution for Floxacins. *Chem. Commun.* **2016**, *52*, 12610–12613.

(249) Romañuk, C. B.; Manzo, R. H.; Linck, Y. G.; Chattah, A. K.; Monti, G. A.; Olivera, M. E. Characterization of the Solubility and Solid-State Properties of Saccharin Salts of Fluoroquinolones. *J. Pharm. Sci.* **2009**, *98*, 3788–3801.

(250) Izutsu, K.-I.; Fujimaki, Y.; Kuwabara, A.; Aoyagi, N. Effect of Counterions on the Physical Properties of L-Arginine in Frozen Solutions and Freeze-Dried Solids. *Int. J. Pharm.* **2005**, *301*, 161–169.

(251) AlHusban, F.; Perrie, Y.; Mohammed, A. R. Formulation and Characterisation of Lyophilised Rapid Disintegrating Tablets Using Amino Acids as Matrix Forming Agents. *Eur. J. Pharm. Biopharm.* **2010**, *75*, 254–262.

(252) Suzuki, T.; Franks, F. Solid–liquid Phase Transitions and Amorphous States in Ternary Sucrose–glycine–water Systems. *J. Chem. Soc., Faraday Trans.* **1993**, *89*, 3283–3288.

(253) Hua, T.-C.; Liu, B.-L.; Zhang, H. Amino-Acid Type Protective Agents. In *Freeze-Drying of Pharmaceutical and Food Products*; Woodhead Publishing Limited: Cambridge, UK, 2010; p. 176.

(254) Gabbott, P.; Clarke, P.; Mann, T.; Royall, P.; Shergill, S. A high-sensitivity, sigh-speed DSC technique: measurement of amorphous lactose http://www.perkinelmer.com/CMSResources/Images/44-157513APP_Measurement_Amorphous_Lactose_High-Sensitivity_High-Speed_DSC_Technique_010058_01.pdf (accessed Aug 13, 2015).

(255) Galcera, J.; Molins, E. Effect of the Counterion on the Solubility of Isostructural Pharmaceutical Lamotrigine Salts. *Cryst. Growth Des.* **2009**, *9*, 327–334.

(256) Zografi, G. States of Water Associated with Solids. *Drug Dev. Ind. Pharm.* **1988**, *14*, 1905–1926.

(257) Sheokand, S.; Modi, S. R.; Bansal, A. K. Dynamic Vapor Sorption as a Tool for Characterization and Quantification of Amorphous Content in Predominantly Crystalline Materials. *J. Pharm. Sci.* **2014**, *103*, 3364–3376.

(258) Powell, D. W. Barrier Function of Epithelia. *Am. J. Physiol.* **1981**, *241*, G275-88.

(259) Chun, M.-K.; Choi, H.-K. Preparation and Characterization of Enrofloxacin/carbopol Complex in Aqueous Solution. *Arch. Pharm. Res.* **2004**, *27*, 670–675.

(260) Lubrizol. *Pharmaceutical Polymers Typical Properties and Specifications*; Cleveland, Ohio, 2013.

(261) LookChem. Enrofloxacin http://www.lookchem.com/Enrofloxacin/ (accessed Oct 28, 2016).

(262) Young, J.; Nelson, G. Theory of Hysteresis between Sorption and Desorption. Isotherms in Biological Materials. *Trans. Am. Soc. Agric. Biol. Eng.* **1967**, *10*, 260–263.

(263) Bravo-Osuna, I.; Ferrero, C.; Jiménez-Castellanos, M. R. Water Sorption-Desorption Behaviour of Methyl Methacrylate-Starch Copolymers: Effect of Hydrophobic Graft and Drying Method. *Eur. J. Pharm. Biopharm.* **2005**, *59*, 537–548.

(264) Löbmann, K.; Laitinen, R.; Grohganz, H.; Strachan, C.; Rades, T.; Gordon, K. C. A Theoretical and Spectroscopic Study of Co-Amorphous Naproxen and Indomethacin. *Int. J. Pharm.* **2013**, *453*, 80–87.

(265) Gunasekaran, S.; Anita, B. Spectral Investigation and Normal Coordinate Analysis of Piperazine. *Indian J. Pure Appl. Phys.* **2008**, *46*, 833–838.

(266) Sahil, K.; Prashant, B.; Akanksha, M.; Premjeet, S.; Devashish, R. Interpretation of Infra Red Spectra. *Int. J. Pharm. Chem. Sci.* **2012**, *1*, 174–200.

(267) Mahlin, D.; Bergström, C. A. S. Early Drug Development Predictions of Glass-Forming Ability and Physical Stability of Drugs. *Eur. J. Pharm. Sci.* **2013**, *49*, 323–332.

(268) Saripella, K. K.; Mallipeddi, R.; Neau, S. H. Crospovidone Interactions with Water. II. Dynamic Vapor Sorption Analysis of the Effect of Polyplasdone Particle Size on Its Uptake and Distribution of Water. *Int. J. Pharm.* **2014**, *475*, 174–180.

(269) Miao, P.; Naderi, M.; Acharya, M.; Burnett, D.; Williams, D.; Ng, T. H.; Song, J. Characterisation of Wheat Straw for Bio-fuel Application http://www.surfacemeasurementsystems.com/wp-content/uploads/2014/05/App57-Biomass3.pdf (accessed Jan 25, 2017).

(270) Bayer HealthCare LLC Animal Health Division. Baytril® - enrofloxacin injection, solution https://dailymed.nlm.nih.gov/dailymed/drugInfo.cfm?setid=7deb5c76-90c2-471c-9e68-bcc088af5cac (accessed Jun 4, 2017).

(271) Hancock, R. E. Resistance Mechanisms in Pseudomonas Aeruginosa and Other Nonfermentative Gram-Negative Bacteria. *Clin. Infect. Dis.* **1998**, *27*, S93-9.

(272) Huguet, A.; Pensec, J.; Soumet, C. Resistance in Escherichia Coli : Variable Contribution of Efflux Pumps with Respect to Different Fluoroquinolones. *J. Appl. Microbiol.* **2013**, *114*, 1294–1299.

(273) Prasad, D.; Chauhan, H.; Atef, E. Amorphous Stabilization and Dissolution Enhancement of Amorphous Ternary Solid Dispersions: Combination of Polymers Showing Drug-Polymer Interaction for Synergistic Effects. *J. Pharm. Sci.* **2014**, *103*, 3511–3523.

(274) Telang, C.; Mujumdar, S.; Mathew, M. Improved Physical Stability of Amorphous State through Acid Base Interactions. *J. Pharm. Sci.* **2009**, *98*, 2149–2159.

(275) Vogt, F. G. Solid-State Characterization of Amorphous Dispersions. In *Pharmaceutical amorphous solid dispersions*; Newman, A., Ed.; John Wiley & Sons, Inc.: New Jersey, 2015.

(276) Artursson, P.; Palm, K.; Luthman, K. Caco-2 Monolayers in Experimental and Theoretical Predictions of Drug Transport. *Adv. Drug Deliv. Rev.* **1996**, *22*, 67–84.

Appendices

Appendix 1

Table A.1.1. Hydrogen Bonding Geometry of Unionized and Zwitterionic CIP[a]

Unionized CIP				
Donor --- H…Acceptor	D - H	H…A	D…A	D - H...A
O2 ---H2...O3	0.82	1.79	2.548(7)	154
N3 ---H3...N3	0.86	2.29	3.076(9)	153
C10 ---H10...O1	0.93	2.48	2.814(9)	102
C14 ---H14A...F1	0.97	2.15	2.842(8)	127
C14 ---H14B...O1	0.97	2.56	3.252(10)	128
C16 ---H16A...O1	0.97	2.52	3.486(9)	175
C17 ---H17B...O2	0.97	2.48	3.451(9)	175
Zwitterionic CIP				
Donor --- H…Acceptor	D - H	H…A	D…A	D - H...A
N3 ---H3A...O1	0.856(9)	2.186(9)	3.010(4)	161.4(9)
N3 ---H3B...O2	0.870(9)	1.713(10)	2.541(6)	158.1(10)
C5 ---H5...O3	0.953(10)	2.580(10)	3.450(4)	152.0(8)
C15 ---H15A...O2	0.991(10)	2.503(10)	3.410(5)	152.1(7)
C15 ---H15A...O3	0.991(10)	2.516(10)	3.285(4)	134.3(7)
C14 ---H14A...F1	0.990(10)	2.196(10)	2.883(4)	125.2(7)

[a]Calculated using PLATON software. The molecular structures of both forms of CIP, with atom labels, are presented in **Figure 2.1**.

Intermolecular interactions and packing arrangements in the crystal structures of unionized and zwitterionic CIP, calculated using unified pair-potentials (UNI) force-field calculations, as implemented in Mercury CSD 3.5.1, are shown below:

(a) Unionized CIP

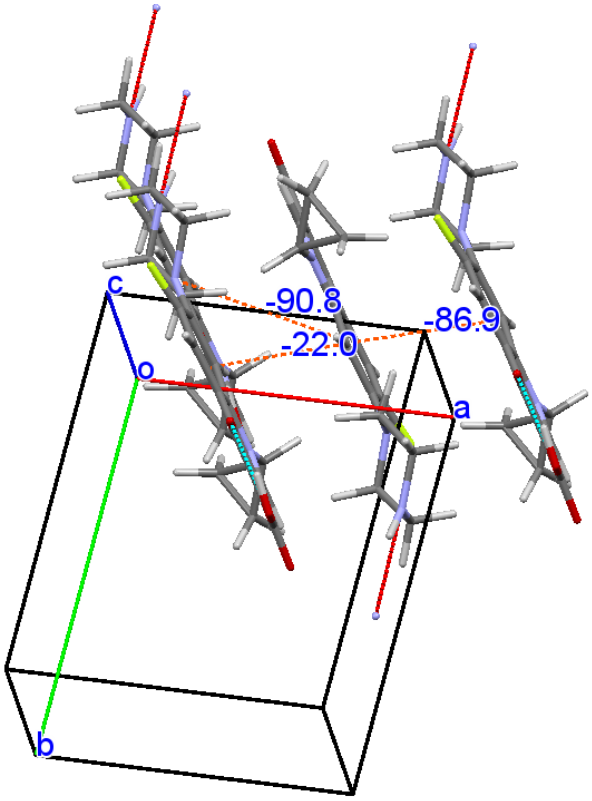

Calculated intermolecular potentials:

mol1	mol2	distance	energy (kJ/mol)
0	1	6.17013	-90.8467
0	2	4.68753	-86.9062
0	3	6.87957	-22.0323

Hydrogen normalization: On

Packing energy:

PE = -126.53 kJ/mol 40 interactions
PE = -129.32 kJ/mol 120 interactions
PE = -129.64 kJ/mol 160 interactions
PE = -129.74 kJ/mol 180 interactions
PE = -129.78 kJ/mol 190 interactions
PE = -129.82 kJ/mol 200 interactions

Potential = A*exp(-Br) - Cr(-6)

Unified (UNI) pair-potential parameters:

atom1	code1	atom2	code2	A	B	C
F1	6	F1	6	170916.4	4.22	564.8
F1	6	O1	17	182706.1	3.98	868.3
F1	6	O2	18	182706.1	3.98	868.3
F1	6	N1	23	249858.9	3.93	1277.9
F1	6	N3	19	249858.9	3.93	1277.9
F1	6	C1	3	196600.9	3.84	1168.8
F1	6	H2AA	26	64257.8	4.11	248.4
F1	6	H5AA	1	64257.8	4.11	248.4
F1	6	H3AA	27	64257.8	4.11	248.4
O1	17	O1	17	195309.1	3.74	1335
O1	17	O2	18	195309.1	3.74	1335
O1	17	N1	23	268571	3.86	1523
O1	17	N3	19	268571	3.86	1523
O1	17	C1	3	393086.8	3.74	2682
O1	17	H2AA	26	26416400	8.75	857.7
O1	17	H5AA	1	295432.3	4.82	439.3
O1	17	H3AA	27	15095080	7.78	995.8
O2	18	O2	18	195309	3.74	1335
O2	18	N1	23	268571	3.86	1523
O2	18	N3	19	268571	3.86	1523
O2	18	C1	3	393086.8	3.74	2682
O2	18	H2AA	26	295432	4.82	439.3
O2	18	H5AA	1	295432.3	4.82	439.3
O2	18	H3AA	27	18868790	7.78	1246.8
N1	23	N1	23	365263	3.65	2891
N1	23	N3	19	365263.2	3.65	2891
N1	23	C1	3	491494	3.86	2791
N1	23	H2AA	26	23867340	7.78	1577
N1	23	H5AA	1	228279	4.52	502.1
N1	23	H3AA	27	30190070	7.78	1992
N3	19	N3	19	365263.2	3.65	2891
N3	19	C1	3	491494	3.86	2791
N3	19	H2AA	26	23867340	7.78	1577.4
N3	19	H5AA	1	228279	4.52	502.1
N3	19	H3AA	27	228279	4.52	502.1
C1	3	C1	3	226145.2	3.47	2418
C1	3	H2AA	26	120792.1	4.1	472.8
C1	3	H5AA	1	120792.1	4.1	472.8

C1	3	H3AA	27	120792.1	4.1	472.8
H2AA	26	H2AA	26	24158	4.01	109.2
H2AA	26	H5AA	1	24158	4.01	109.2
H2AA	26	H3AA	27	24158	4.01	109.2
H5AA	1	H5AA	1	24158	4.01	109.2
H5AA	1	H3AA	27	24158	4.01	109.2
H3AA	27	H3AA	27	24158	4.01	109.2

(b) Zwitterionic CIP

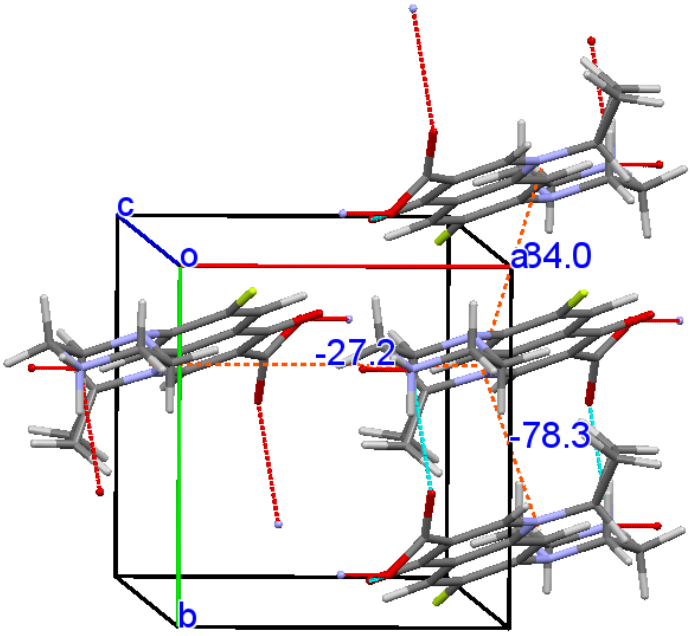

Calculated intermolecular potentials:

mol1	mol2	distance	energy (kJ/mol)
0	1	4.87307	-83.9764
0	2	4.51027	-78.2713
0	3	7.9606	-27.2428

Hydrogen normalization: On

Packing energy:

PE = -165.88 kJ/mol 40 interactions
PE = -168.94 kJ/mol 120 interactions
PE = -169.27 kJ/mol 160 interactions
PE = -169.36 kJ/mol 180 interactions
PE = -169.40 kJ/mol 190 interactions
PE = -169.44 kJ/mol 200 interactions

Potential = A*exp(-Br) - Cr(-6)

Unified (UNI) pair-potential parameters:

atom1	code1	atom2	code2	A	B	C
F1	6	F1	6	170916.4	4.22	564.8
F1	6	O1	17	182706.1	3.98	868.3
F1	6	N1	23	249858.9	3.93	1277.9
F1	6	N3	4	249858.9	3.93	1277.9
F1	6	C1	3	196600.9	3.84	1168.8
F1	6	H11	1	64257.8	4.11	248.4
F1	6	H311	28	64257.8	4.11	248.4
O1	17	O1	17	195309.1	3.74	1335
O1	17	N1	23	268571	3.86	1523
O1	17	N3	4	268571	3.86	1523
O1	17	C1	3	393086.8	3.74	2682
O1	17	H11	1	295432.3	4.82	439.3
O1	17	H311	28	15095080	7.78	995.8
N1	23	N1	23	365263	3.65	2891
N1	23	N3	4	365263.2	3.65	2891
N1	23	C1	3	491494	3.86	2791
N1	23	H11	1	228279	4.52	502.1
N1	23	H311	28	7547602	7.37	690.4
N3	4	N3	4	365263.2	3.65	2891
N3	4	C1	3	491494	3.86	2791
N3	4	H11	1	228279	4.52	502.1
N3	4	H311	28	7547602	7.37	690.4
C1	3	C1	3	226145.2	3.47	2418
C1	3	H11	1	120792.1	4.1	472.8
C1	3	H311	28	120792.1	4.1	472.8
H11	1	H11	1	24158	4.01	109.2
H11	1	H311	28	24158	4.01	109.2
H311	28	H311	28	24158	4.01	109.2

Appendix 2

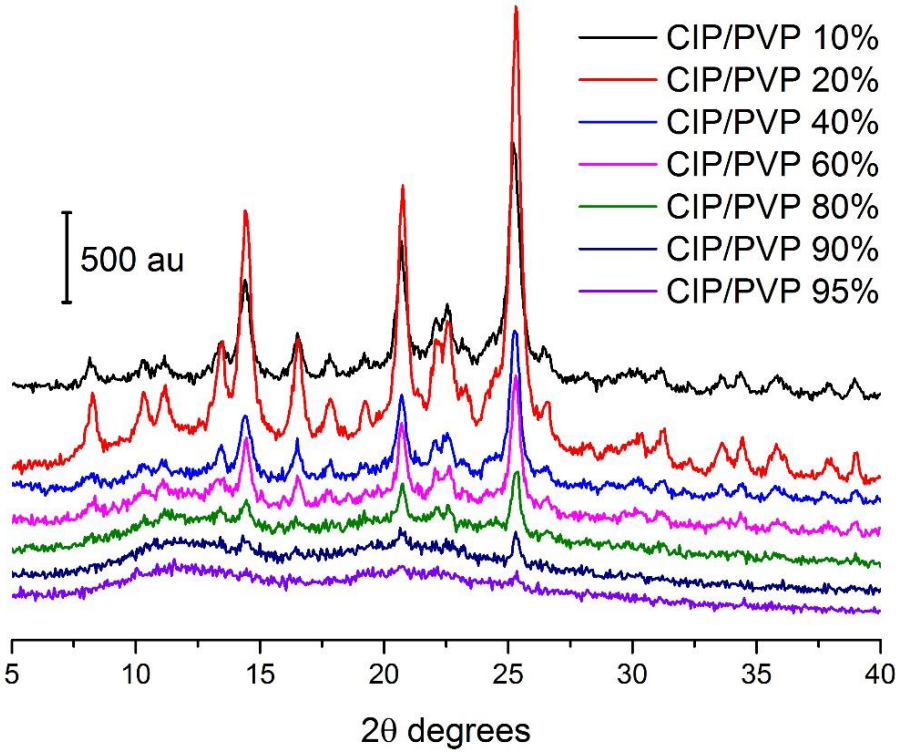

Figure A.2.1. PXRD analysis of partially crystalline CIP solid dispersions containing various (w/w) concentrations of PVP.

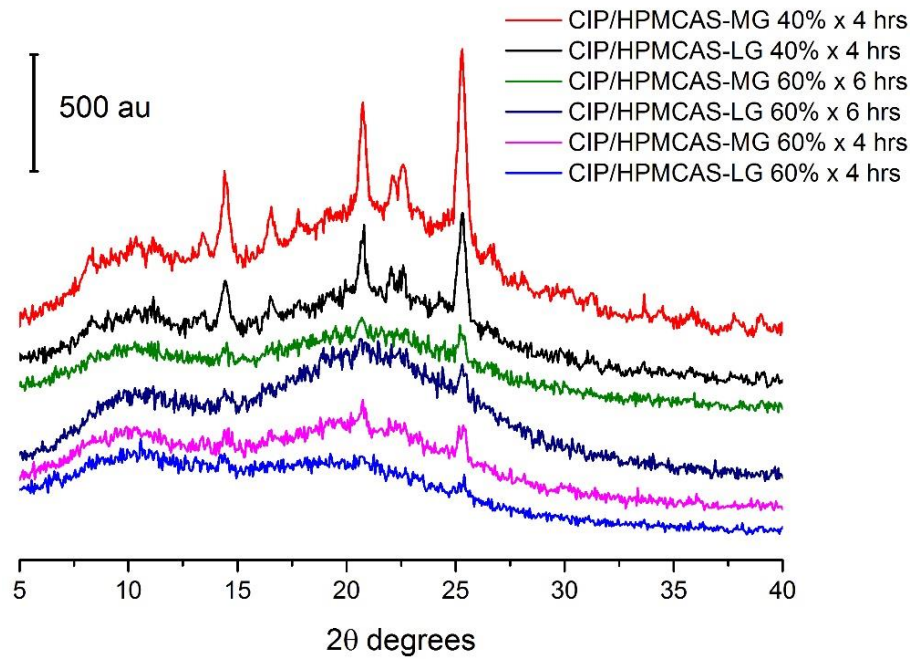

Figure A.2.2. PXRD analysis of solid dispersions formed by milling CIP with 40–60% (w/w) HPMCAS-LG and HPMCAS-MG for 4 or 6 hours at RT.

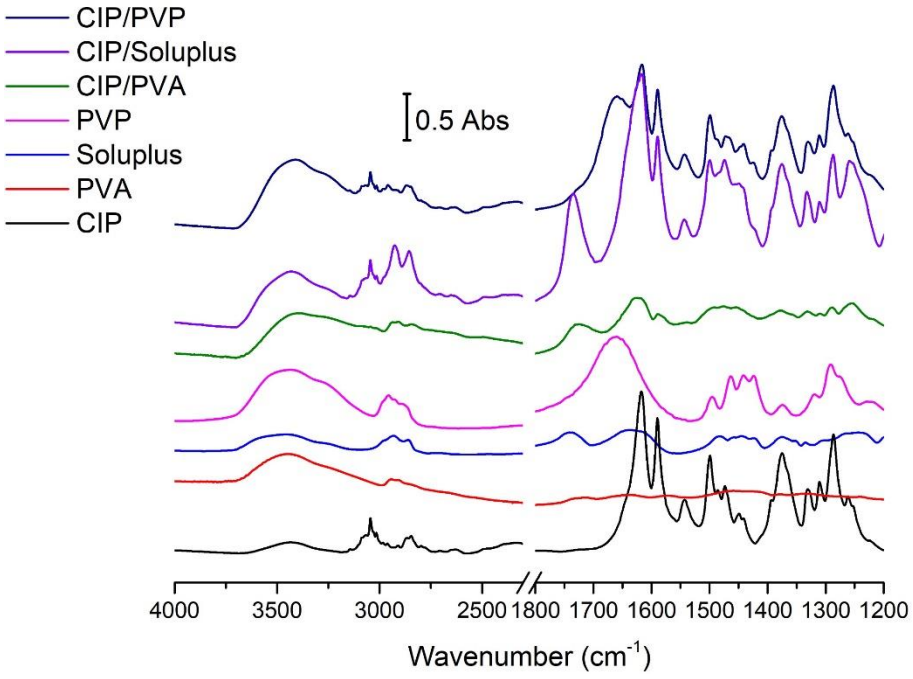

Figure A.2.3. FTIR analysis of partially crystalline solid dispersions formed by milling CIP with 40% (w/w) PVP, Soluplus or PVA.

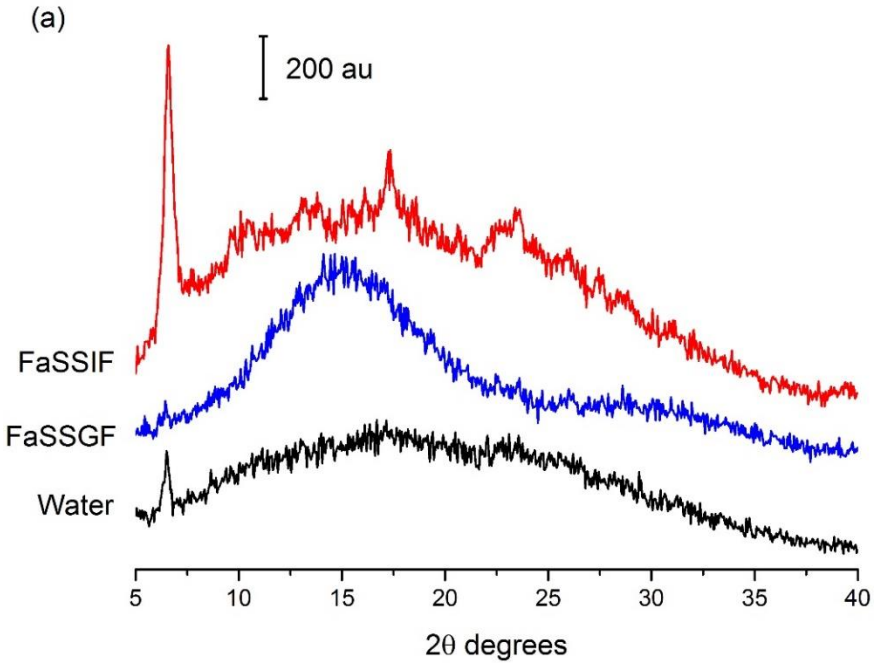
(a)
200 au
FaSSIF
FaSSGF
Water
5
10
15
20
25
30
35
40
2θ degrees

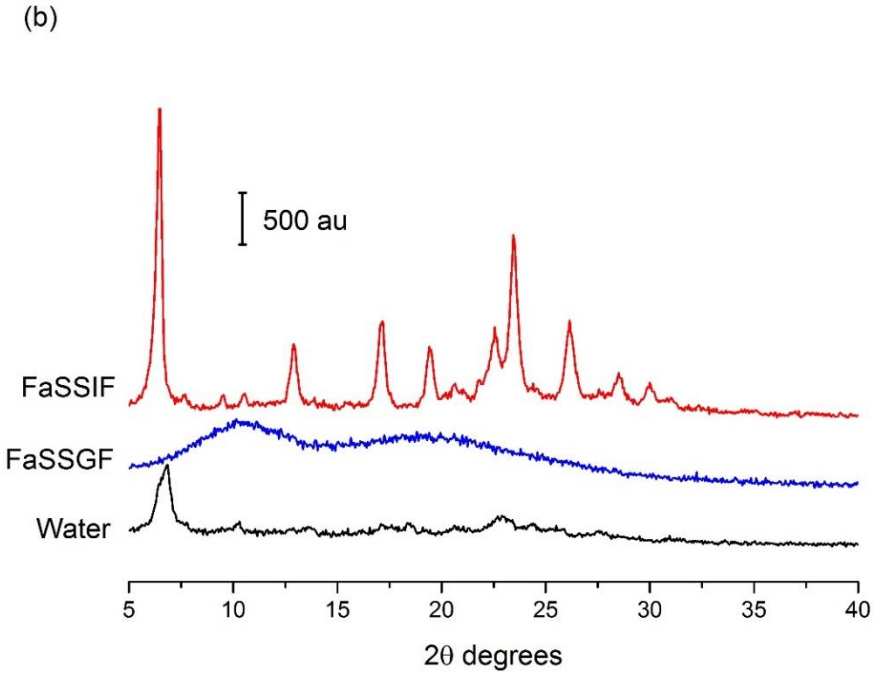
(b)
500 au
FaSSIF
FaSSGF
Water
5
10
15
20
25
30
35
40
2θ degrees

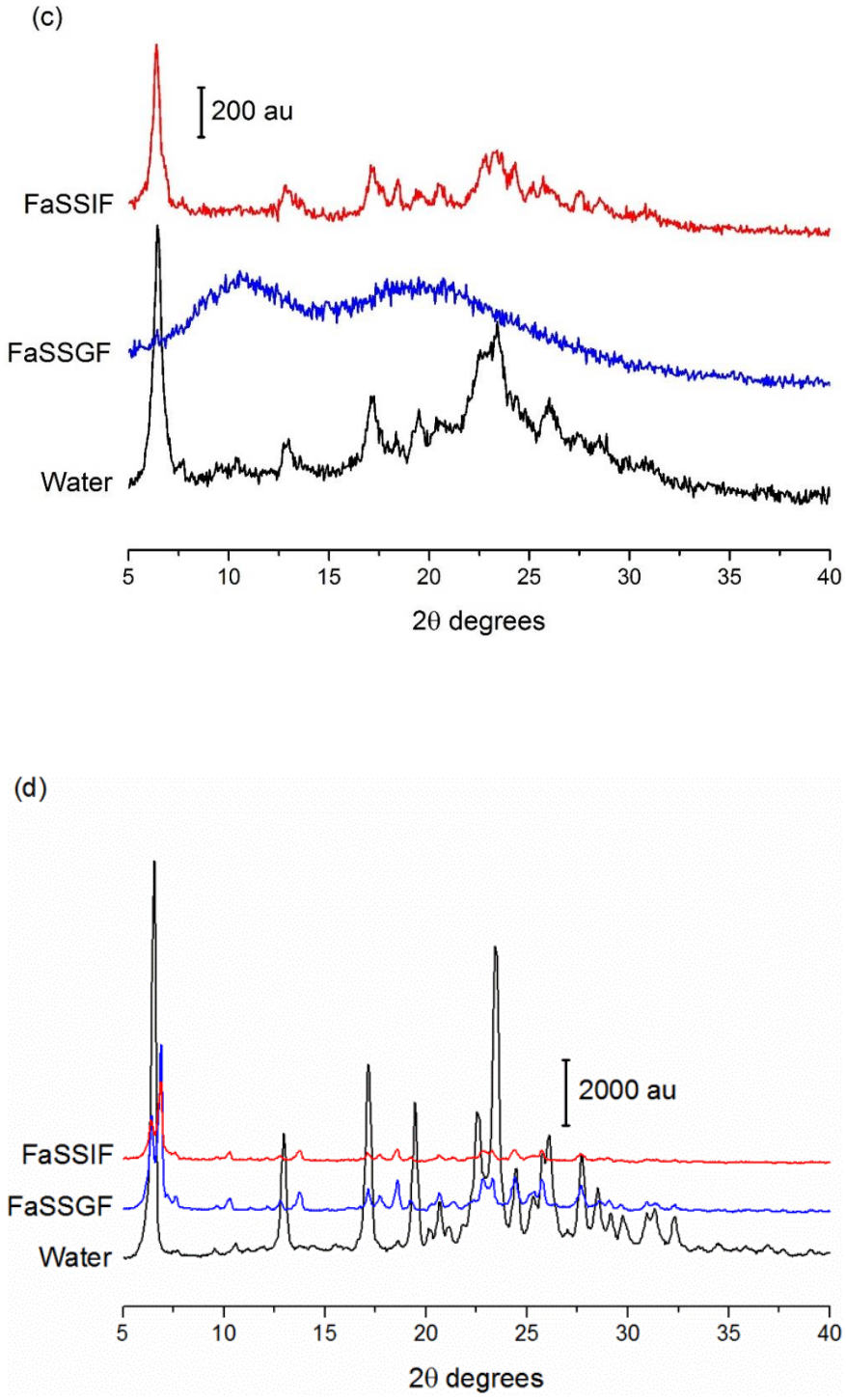

Figure A.2.4. PXRD analysis following solubility studies of (a) CIP/Eudragit L100 (b) CIP/HPMCAS-LG (c) CIP/HPMCAS-MG and (d) CIP.

Appendix 3

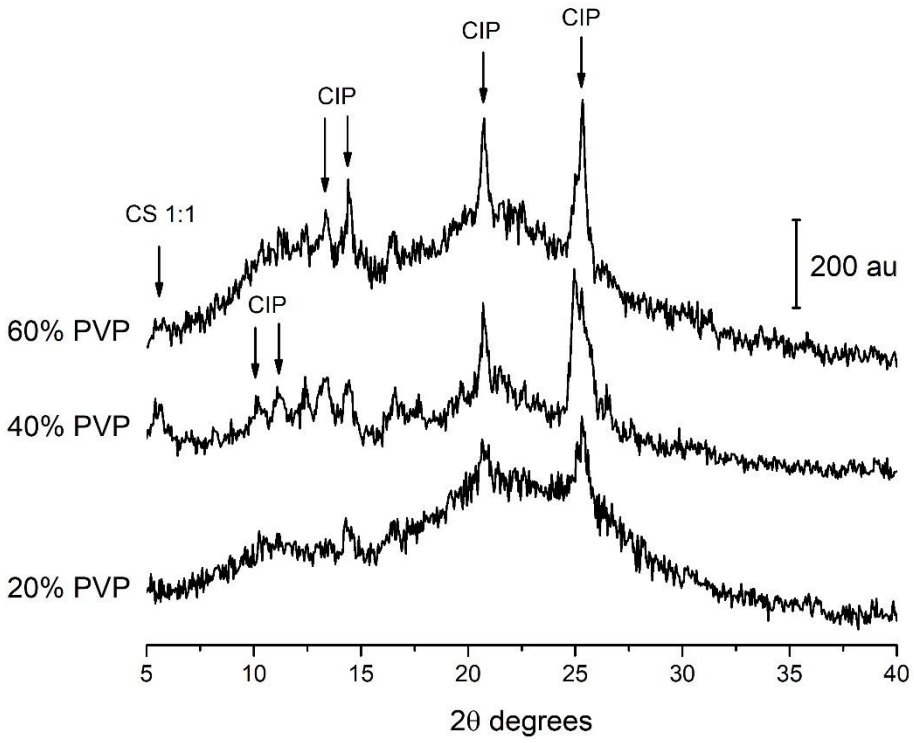

Figure A.3.1. PXRD analysis of CIP and succinic acid 1:1 plus 20–60% (w/w) PVP milled for 4 hours, without pre-milling. The arrows identify the most prominent peaks, corresponding to CIP and the CS 1:1 salt.

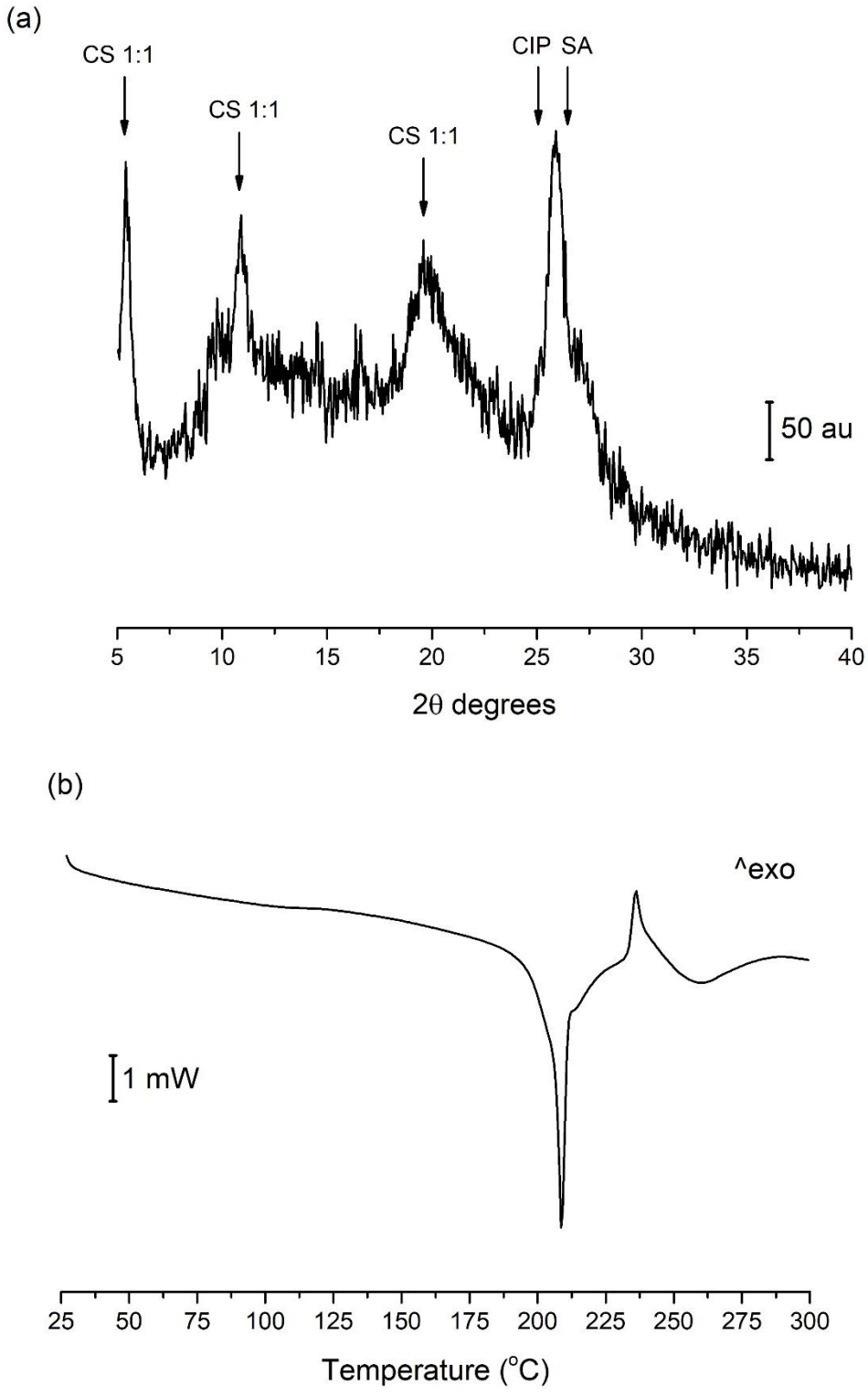

Figure A.3.2. (a) PXRD analysis of SDD CS 1:1/40% Soluplus. The arrows identify the most prominent peaks, corresponding to CS 1:1, CIP and succinic acid (SA). (b) DSC analysis of SDD CS 1:1/40% Soluplus.

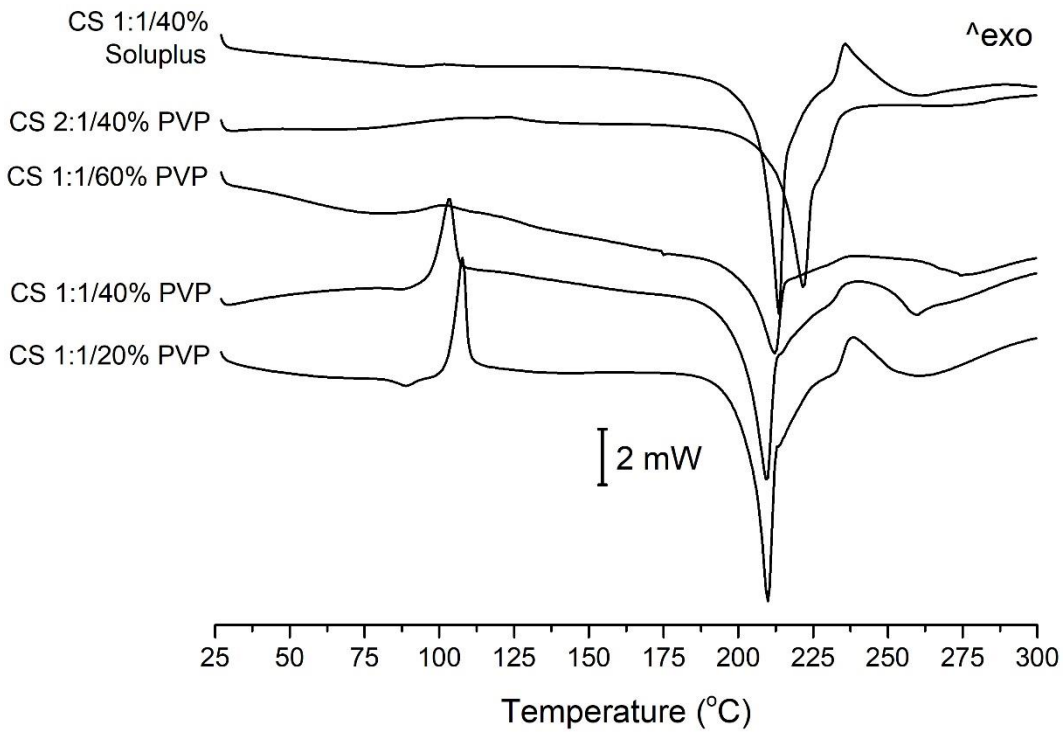

Figure A.3.3. DSC analysis of PMs containing the CS 1:1 or CS 2:1 amorphous salt plus PVP or Soluplus.

Table A.3.1. Thermal Properties of CS 1:1 and CS 2:1 Amorphous Salt/Polymer Physical Mixtures

Sample	**T_g (°C)**	**Crystallization onset (°C)**	**Crystallization peak (°C)**
CS 1:1/20% PVP	86.0 ± 0.1	103.4 ± 0.1	107.6 ± 0.2
CS 1:1/40% PVP	83.7 ± 0.5	97.7 ± 0.2	104.9 ± 2.1
CS 1:1/60% PVP	N.D.	94.3 ± 0.7	101.4 ± 0.2
CS 2:1/40% PVP	N.D.	114.9 ± 0.4	121.8 ± 0.1
CS 1:1/40% Soluplus	N.D.	95.2 ± 0.4	101.9 ± 0.2

Table A.3.2. pH of Solutions at the End of Solubility Studies

Sample	Media	pH	Sample	Media	pH
CIP	Water	6.34 ± 0.12	CS 1:1	Water	4.64 ± 0.01
	FaSSIF	6.57 ± 0.02		FaSSIF	4.69 ± 0.02
	FaSSGF	4.71 ± 0.06		FaSSGF	4.07 ± 0.09
CS 2:1	Water	4.69 ± 0.02	SDD CS 1:1/20 % PVP	Water	4.61 ± 0.06
	FaSSIF	4.86 ± 0.04		FaSSIF	4.73 ± 0.01
	FaSSGF	4.69 ± 0.10		FaSSGF	4.10 ± 0.02
SDD CS 1:1/40 % PVP	Water	4.74 ± 0.01	SDD CS 1:1/60 % PVP	Water	4.57 ± 0.08
	FaSSIF	4.76 ± 0.01		FaSSIF	4.72 ± 0.03
	FaSSGF	4.15 ± 0.04		FaSSGF	4.27 ± 0.02
BM CS 1:1/40 % PVP	Water	4.59 ± 0.01	BM CS 2:1/40 % PVP	Water	5.36 ± 0.01
	FaSSIF	4.69 ± 0.00		FaSSIF	6.04 ± 0.03
	FaSSGF	4.13 ± 0.04		FaSSGF	4.89 ± 0.02

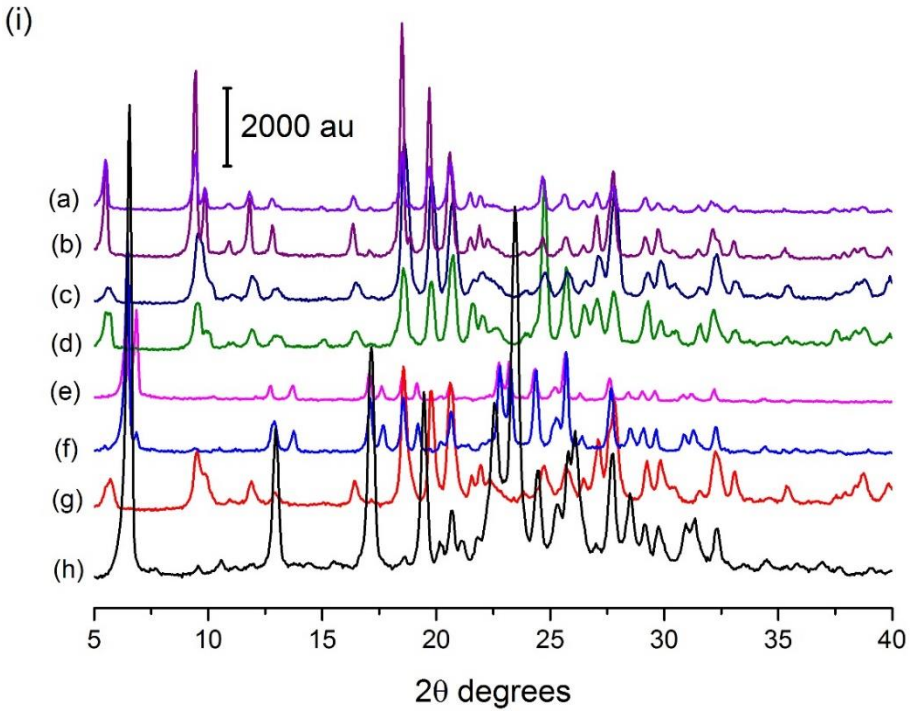

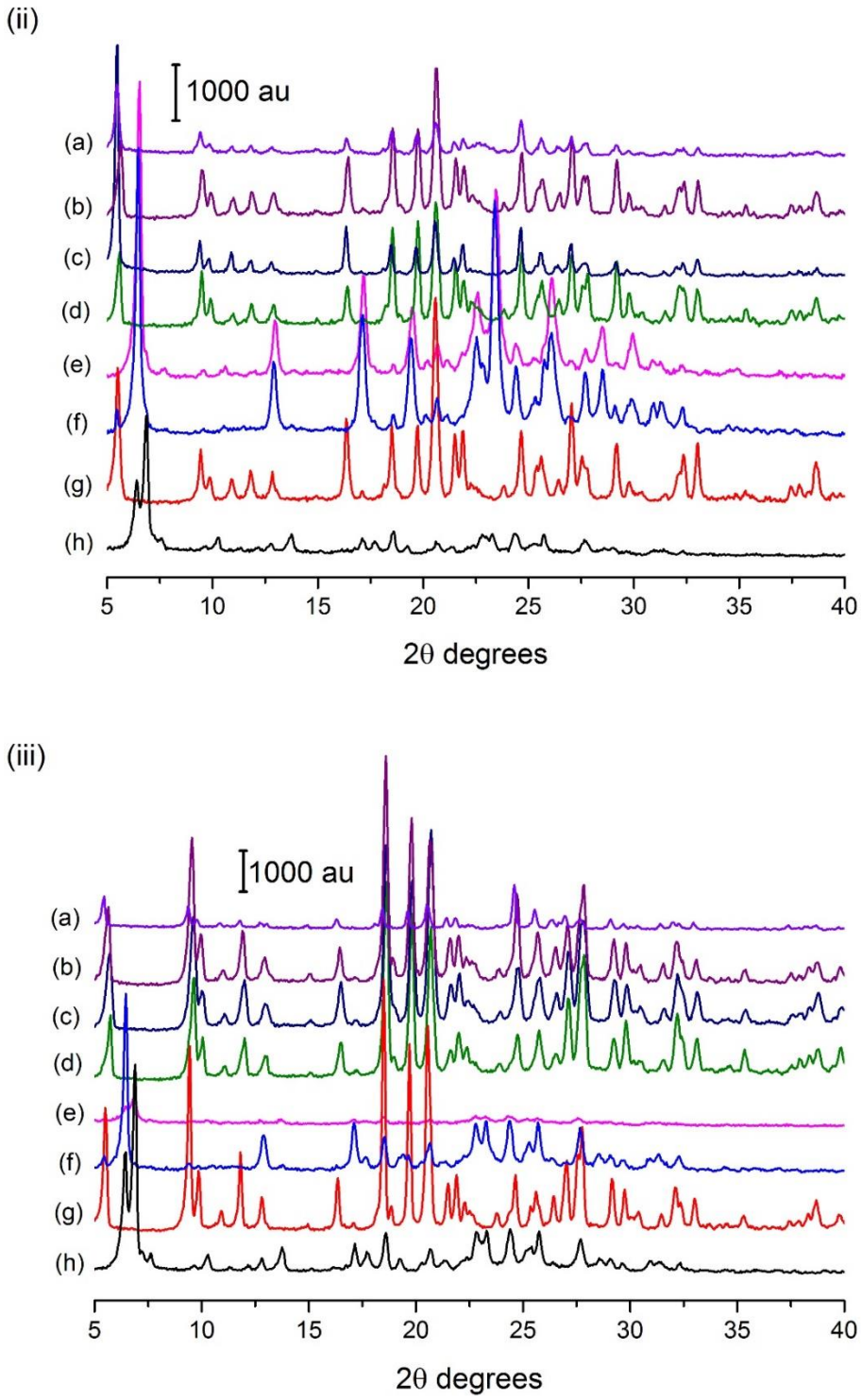

Figure A.3.4. PXRD analysis following solubility studies in (i) water (ii) FaSSIF and (iii) FaSSGF: (a) SDD CS 1:1/60% PVP (b) SDD CS 1:1/40% PVP (c) SDD CS 1:1/20% PVP (d) BM CS 1:1/40% PVP (e) BM CS 2:1/40% PVP (f) CS 2:1 (g) CS 1:1 and (h) CIP.

Appendix 4

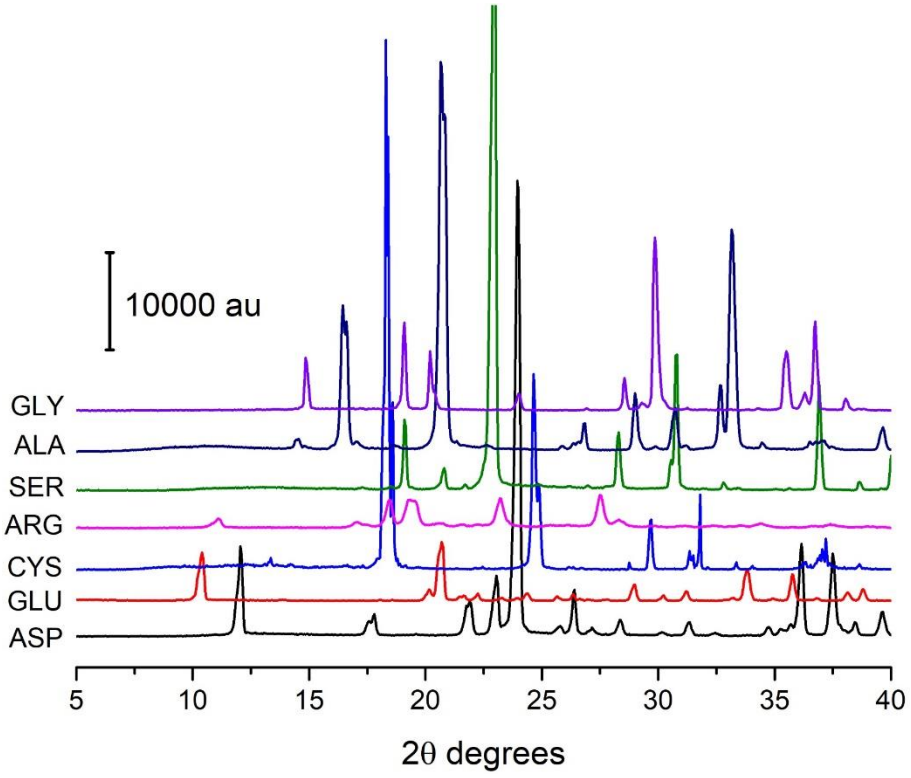

Figure A.4.1. PXRD analysis of crystalline amino acids.

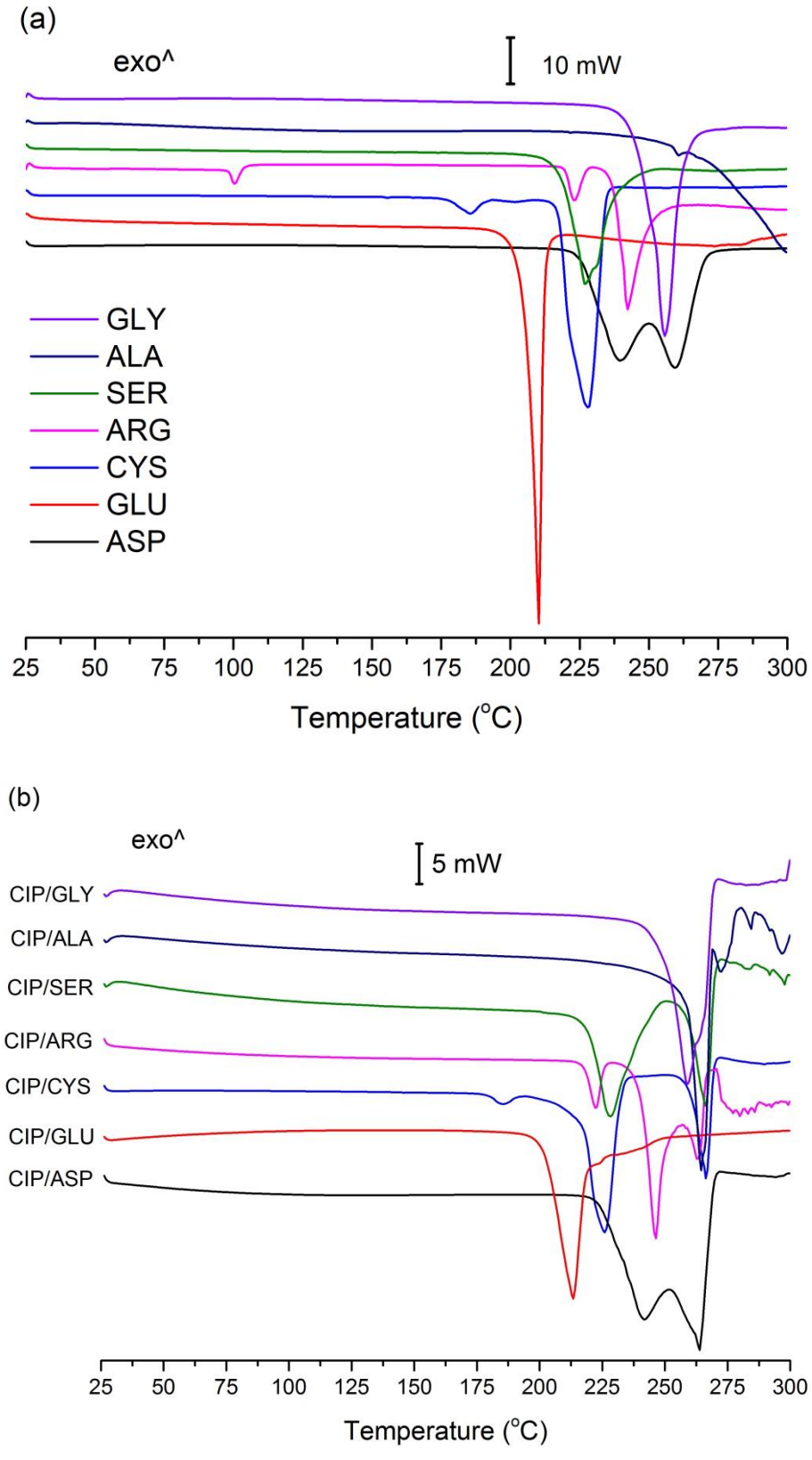

Figure A.4.2. DSC analysis of (a) crystalline amino acids and (b) CIP/amino acid PMs.

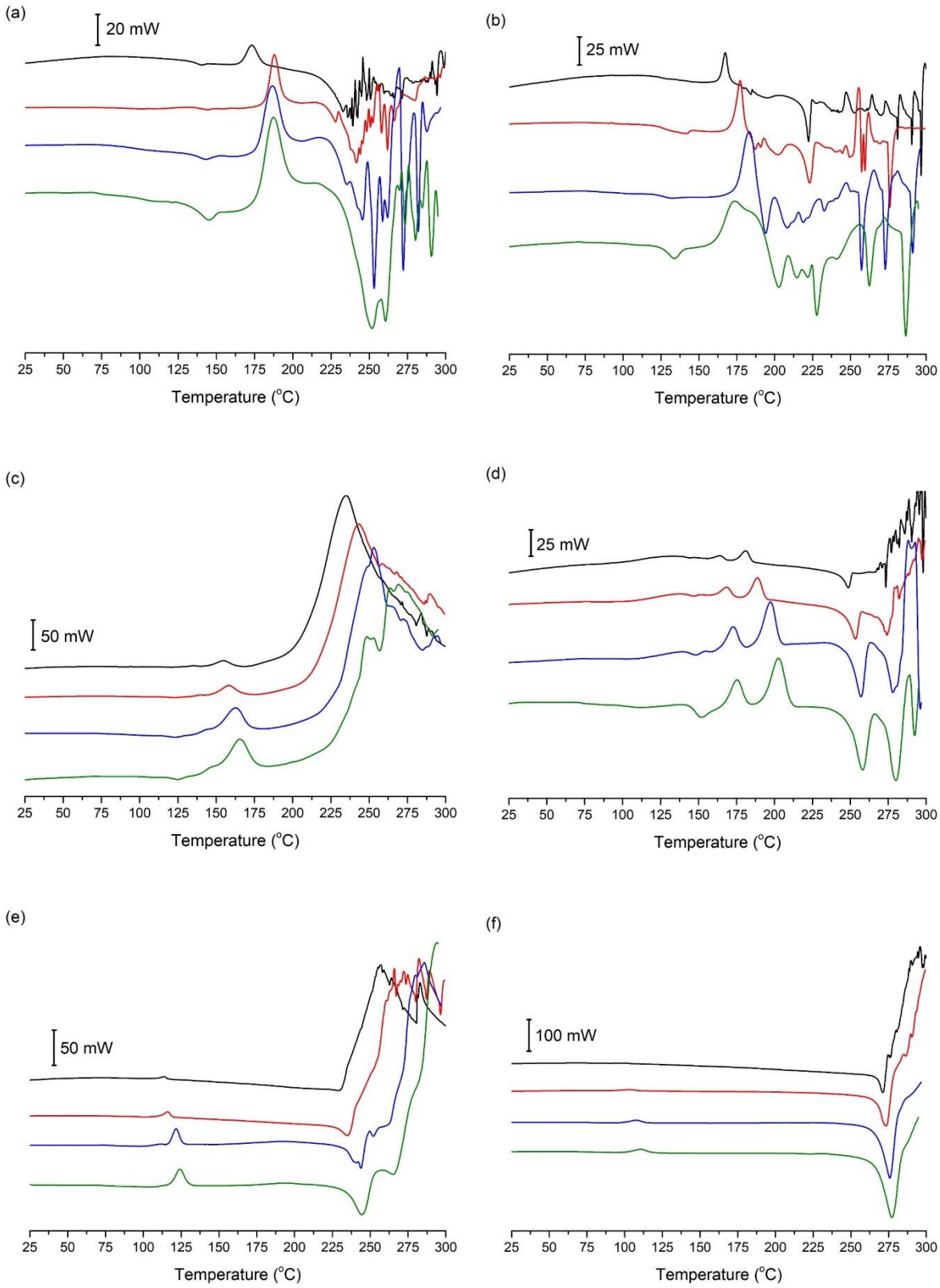
(a)
20 mW
25 50 75 100 125 150 175 200 225 250 275 300
Temperature (°C)
(b)
25 mW
25 50 75 100 125 150 175 200 225 250 275 300
Temperature (°C)
(c)
50 mW
25 50 75 100 125 150 175 200 225 250 275 300
Temperature (°C)
(d)
25 mW
25 50 75 100 125 150 175 200 225 250 275 300
Temperature (°C)
(e)
50 mW
25 50 75 100 125 150 175 200 225 250 275 300
Temperature (°C)
(f)
100 mW
25 50 75 100 125 150 175 200 225 250 275 300
Temperature (°C)

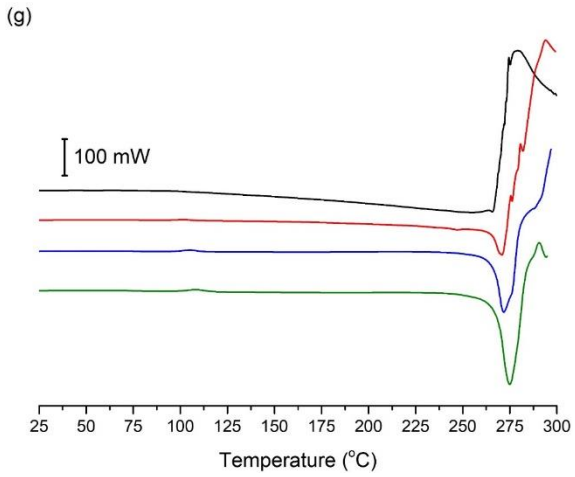

Figure A.4.3. HSDSC analysis of CIP/amino acid ASDs and SDs heated at different rates: (a) CIP/ASP (b) CIP/GLU (c) CIP/CYS (d) CIP/ARG (e) CIP/SER (f) CIP/ALA and (g) CIP/GLY. Black: 50 ºC/min; red: 100 ºC/min; blue: 200 ºC/min; and green: 300 ºC/min.

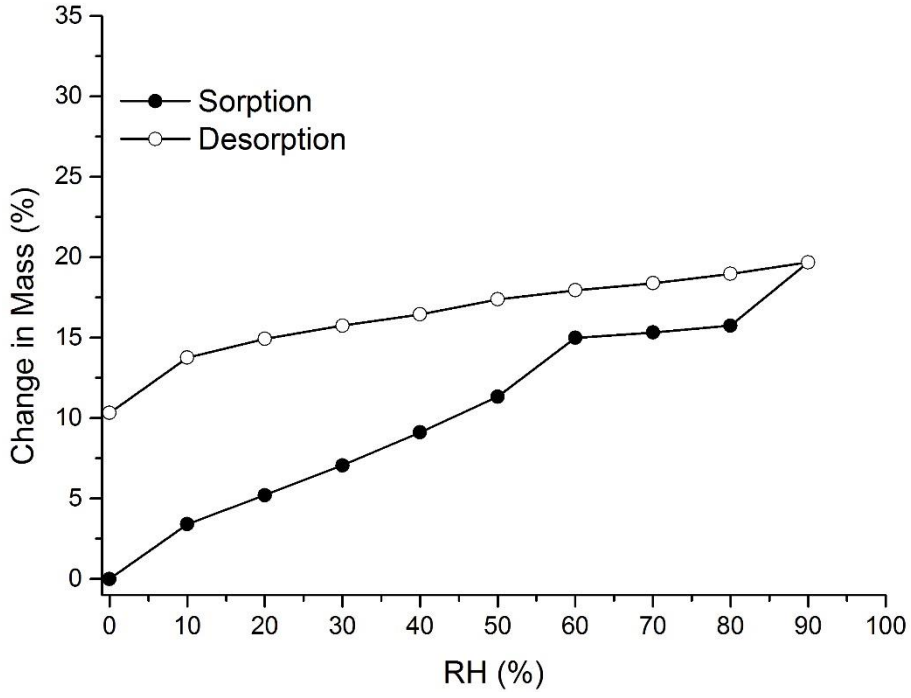

Figure A.4.4. DVS isotherm of the CIP/ARG ASD analyzed with six hour maximum equilibration time.

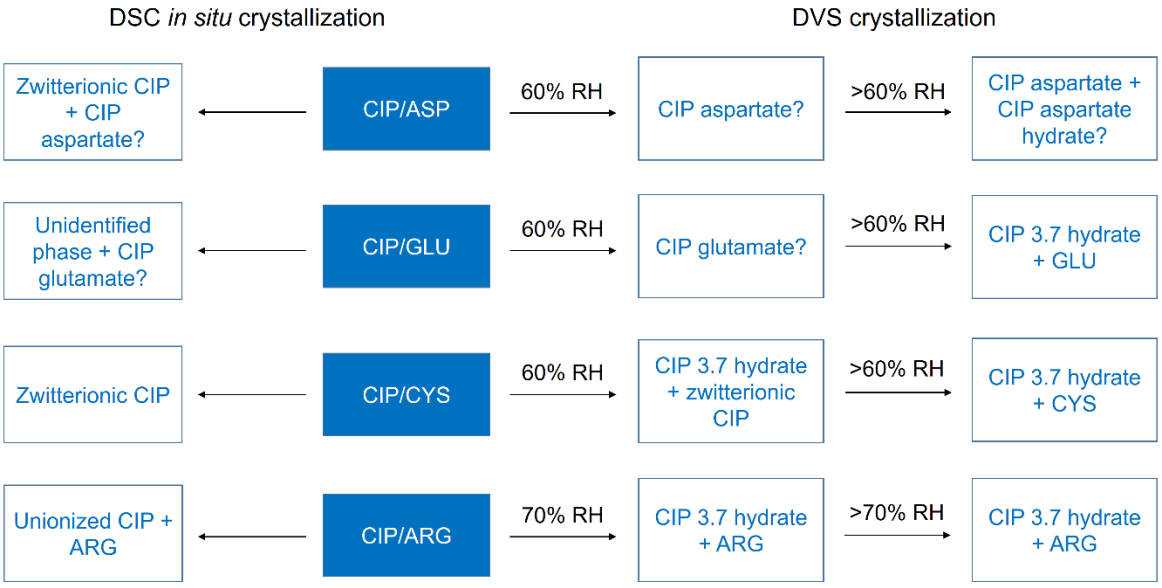

Fig. A.4.5. Summary of major phases present following crystallization of CIP/amino acid ASDs during DSC and DVS analysis.

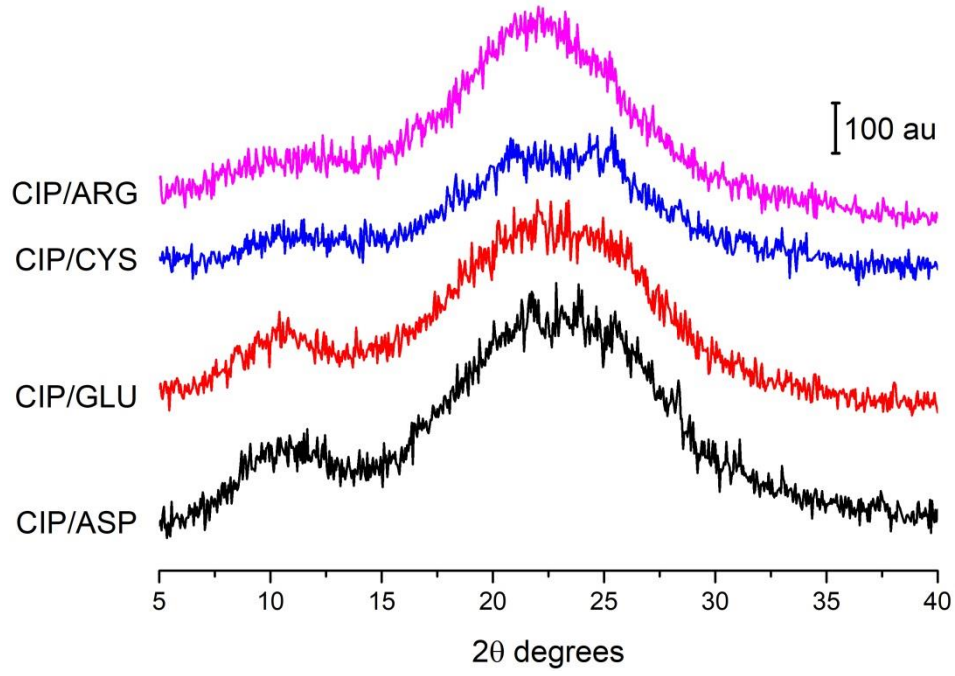

Figure A.4.6. PXRD analysis of CIP/amino acid ASDs following 12 months of storage at RT.

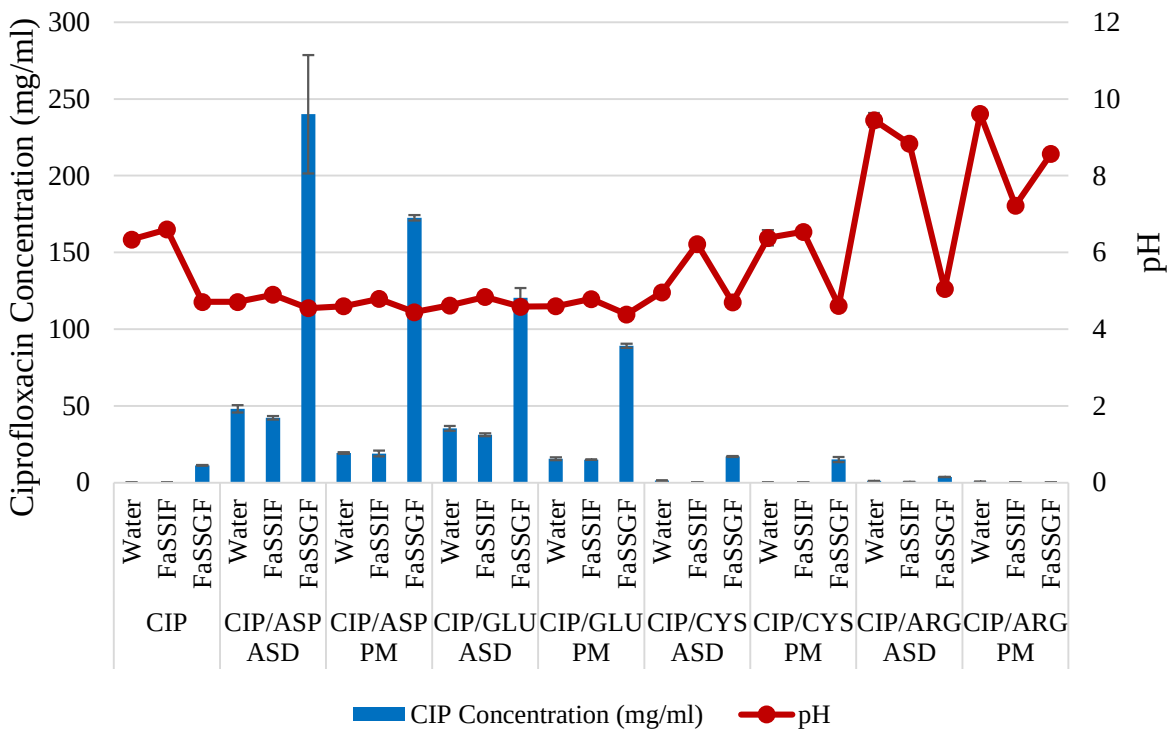

Figure A.4.7. Concentration and pH of solutions at end of solubility studies with CIP/amino acid ASDs and PMs.

(a)

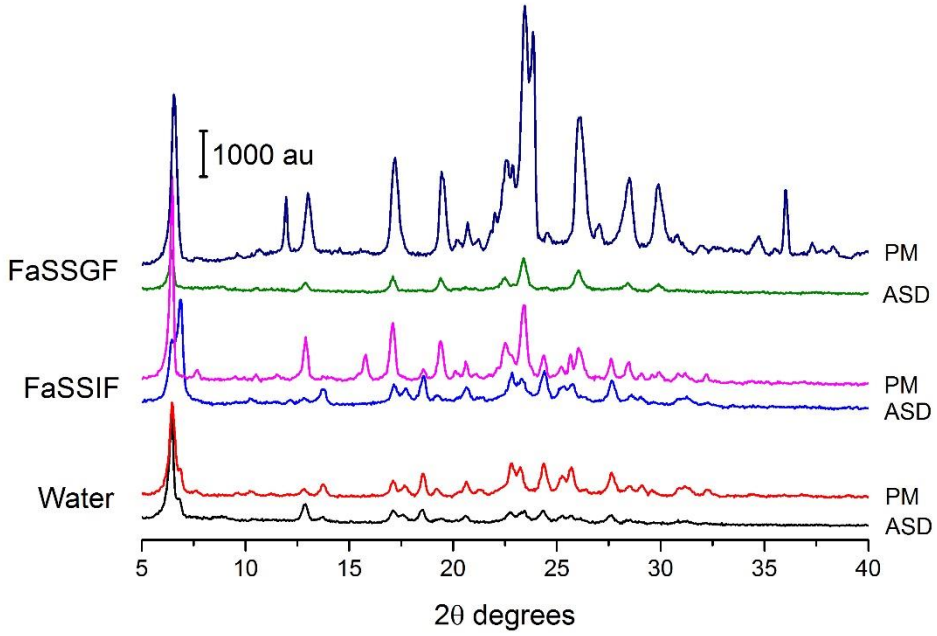
1000 au
FaSSGF
PM
ASD
FaSSIF
PM
ASD
Water
PM
ASD
5
10
15
20
25
30
35
40
2θ degrees

(b)

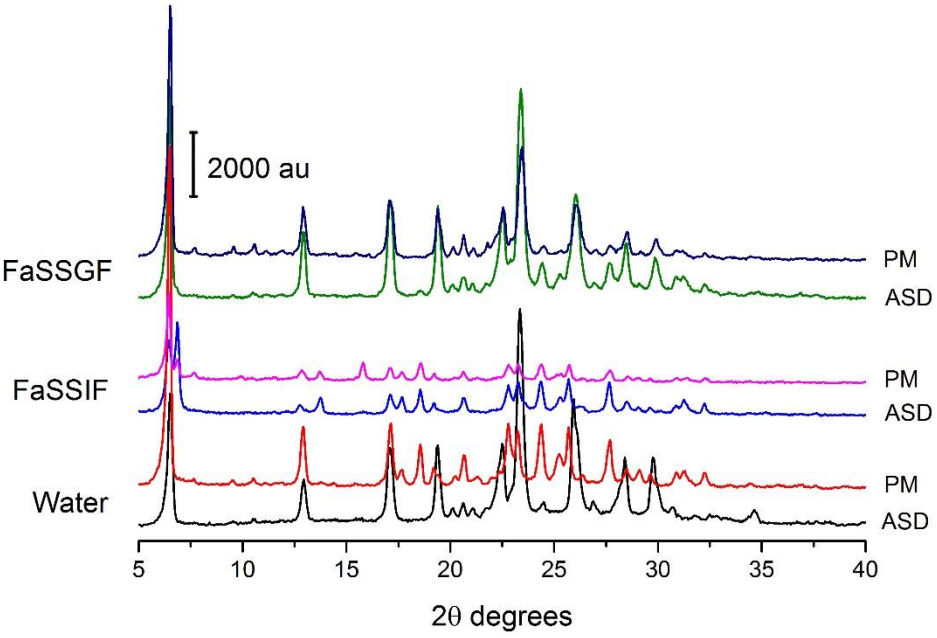
2000 au
FaSSGF
PM
ASD
FaSSIF
PM
ASD
Water
PM
ASD
5
10
15
20
25
30
35
40
2θ degrees

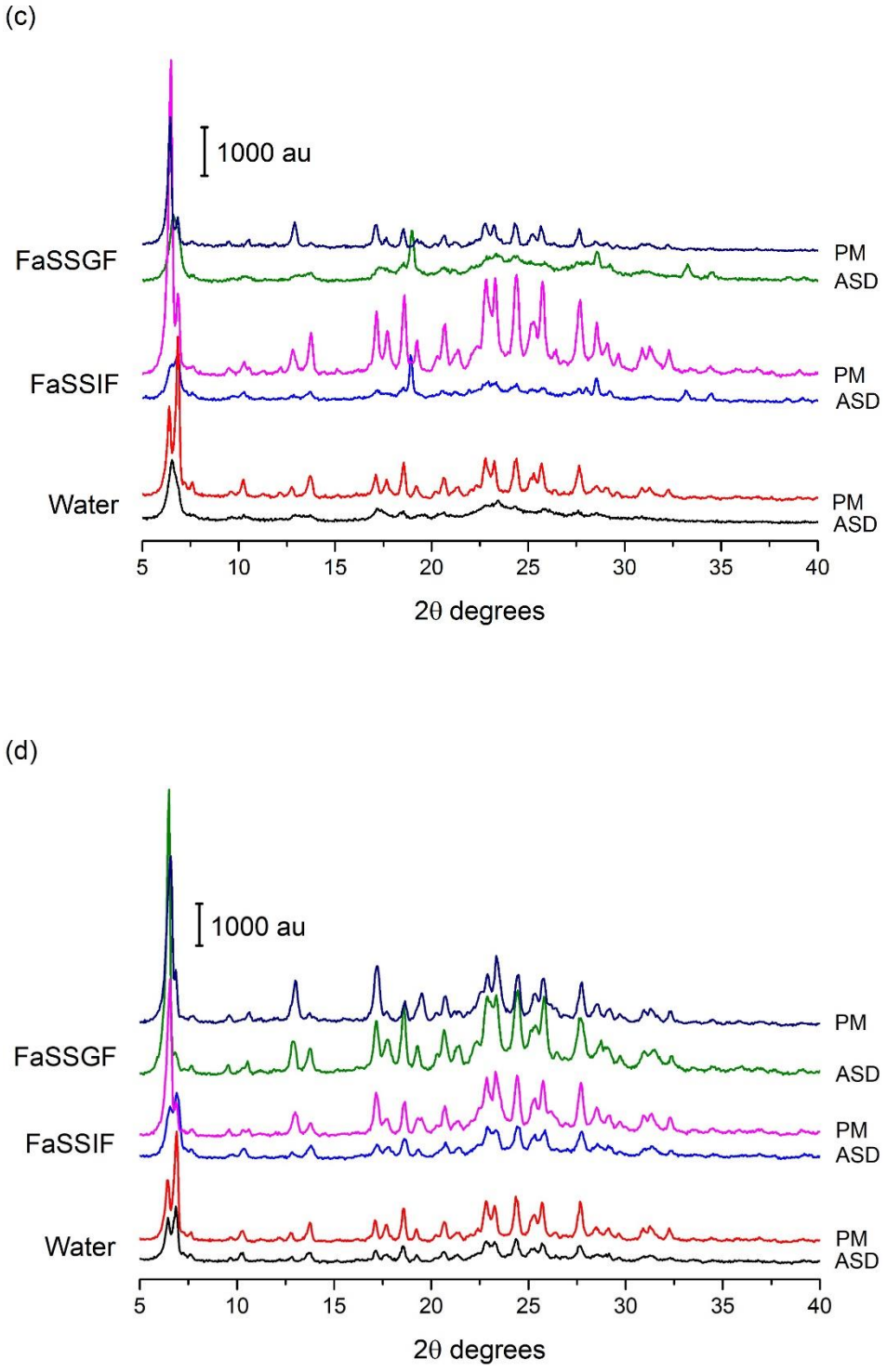

Figure A.4.8. PXRD analysis following solubility studies of (a) CIP/ASP (b) CIP/GLU (c) CIP/CYS and (d) CIP/ARG.

Appendix 5

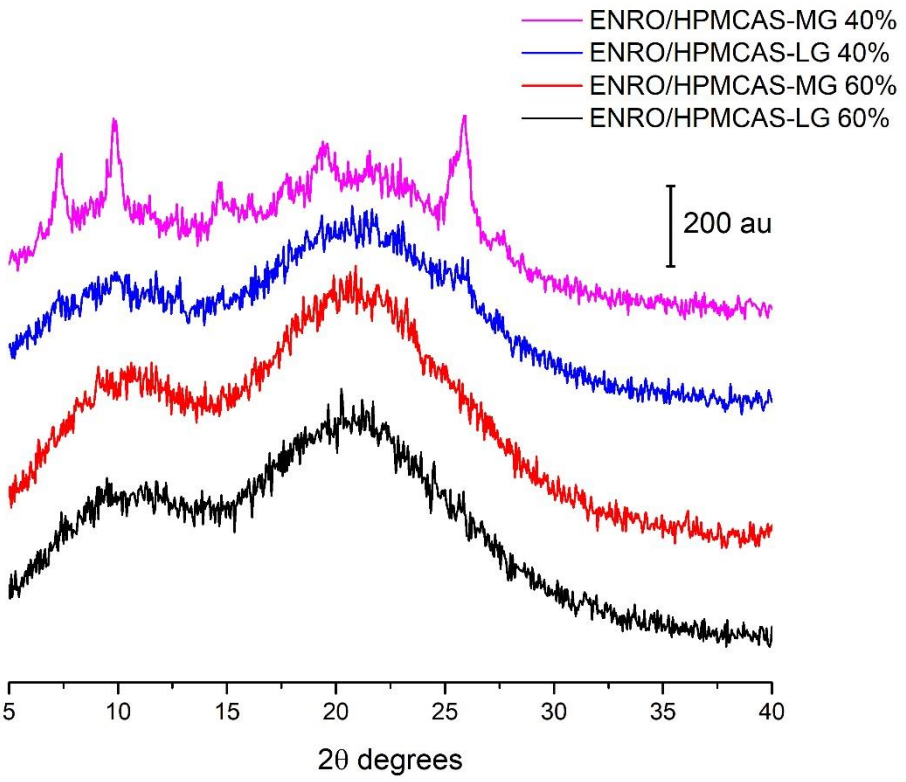

Figure A.5.1. PXRD analysis of solid dispersions formed by milling ENRO with 40–60% (w/w) HPMCAS-LG and HPMCAS-MG for 4 hours at room temperature.

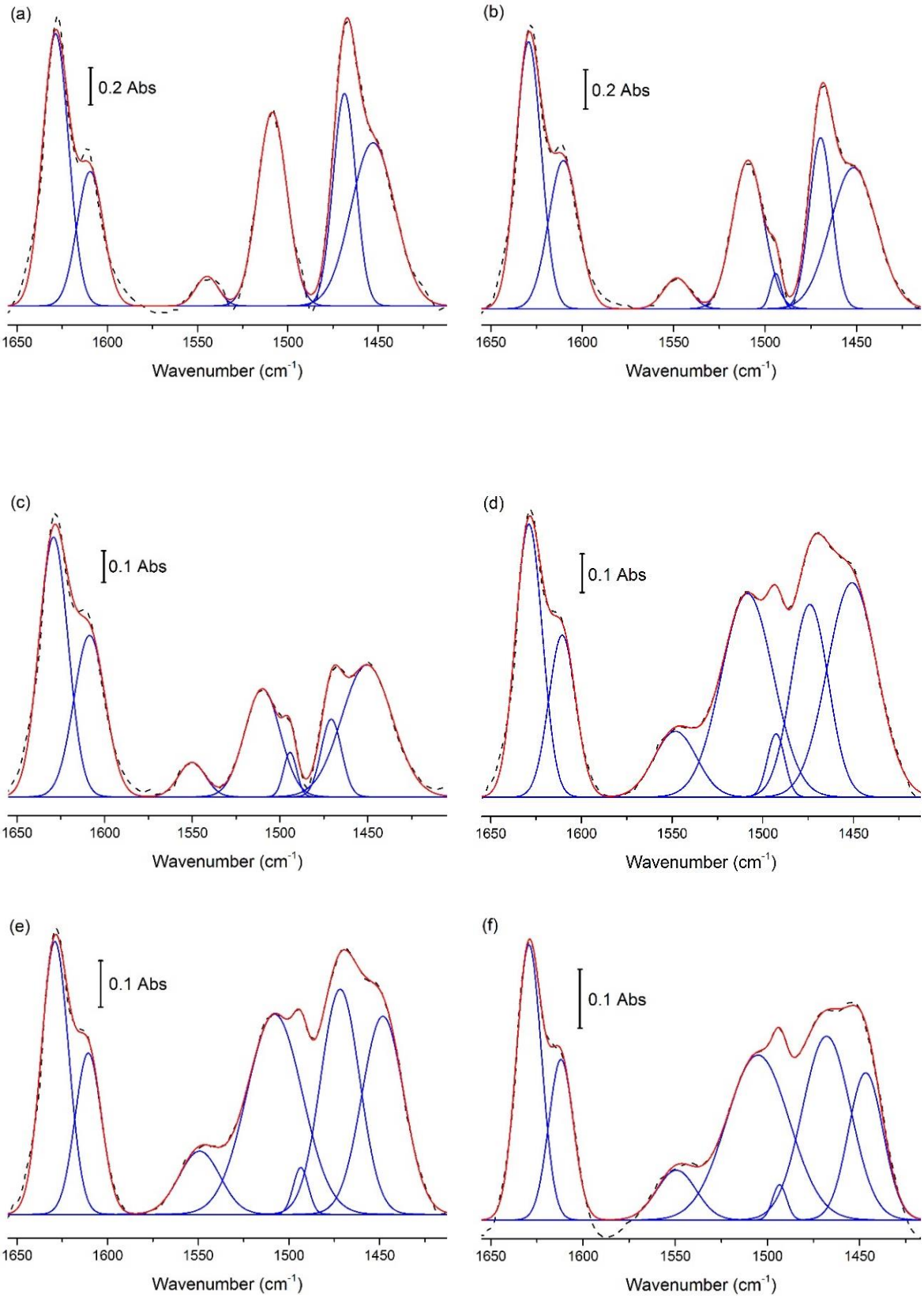
(a)
0.2 Abs
1650
1600
1550
1500
1450
Wavenumber (cm-1)
(b)
0.2 Abs
1650
1600
1550
1500
1450
Wavenumber (cm-1)
(c)
0.1 Abs
1650
1600
1550
1500
1450
Wavenumber (cm-1)
(d)
0.1 Abs
1650
1600
1550
1500
1450
Wavenumber (cm-1)
(e)
0.1 Abs
1650
1600
1550
1500
1450
Wavenumber (cm-1)
(f)
0.1 Abs
1650
1600
1550
1500
1450
Wavenumber (cm-1)

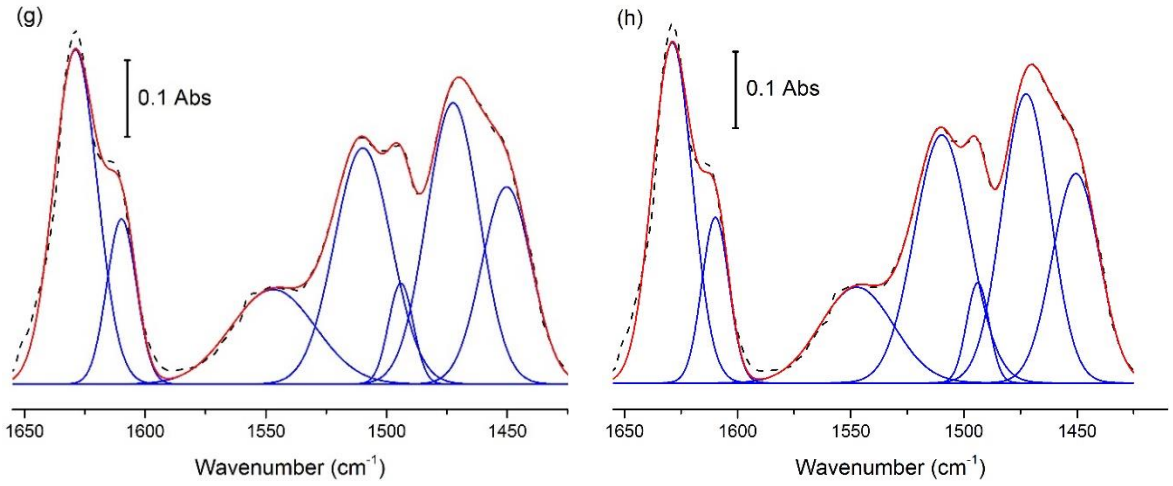

Figure A.5.2. FTIR peak deconvolution of (a) crystalline ENRO (b) ball milled ENRO (c) quench cooled ENRO (d) ENRO/Eudragit L100 (e) ENRO/Eudragit L100-55 (f) ENRO/Carbopol (g) ENRO/HPMCAS-LG and (h) ENRO/HPMCAS-MG. Dotted black line: recorded spectrum; solid blue lines: deconvoluted individual Gauss peaks; and solid red line: sum of the component peaks.

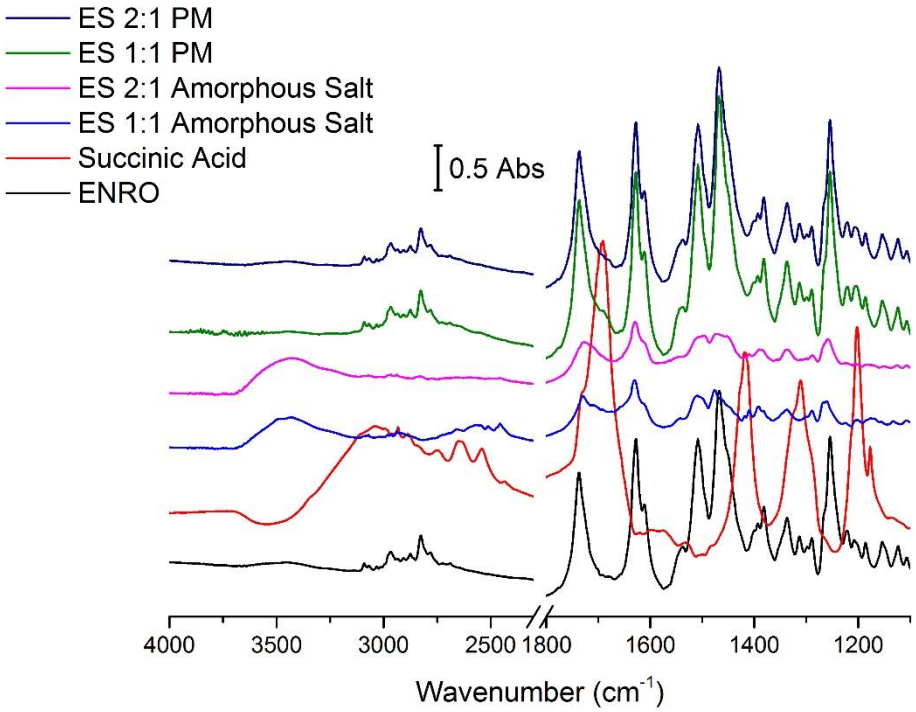

Figure A.5.3. FTIR analysis of ENRO/succinic acid (ES) 1:1 and 2:1 amorphous salts and PMs.

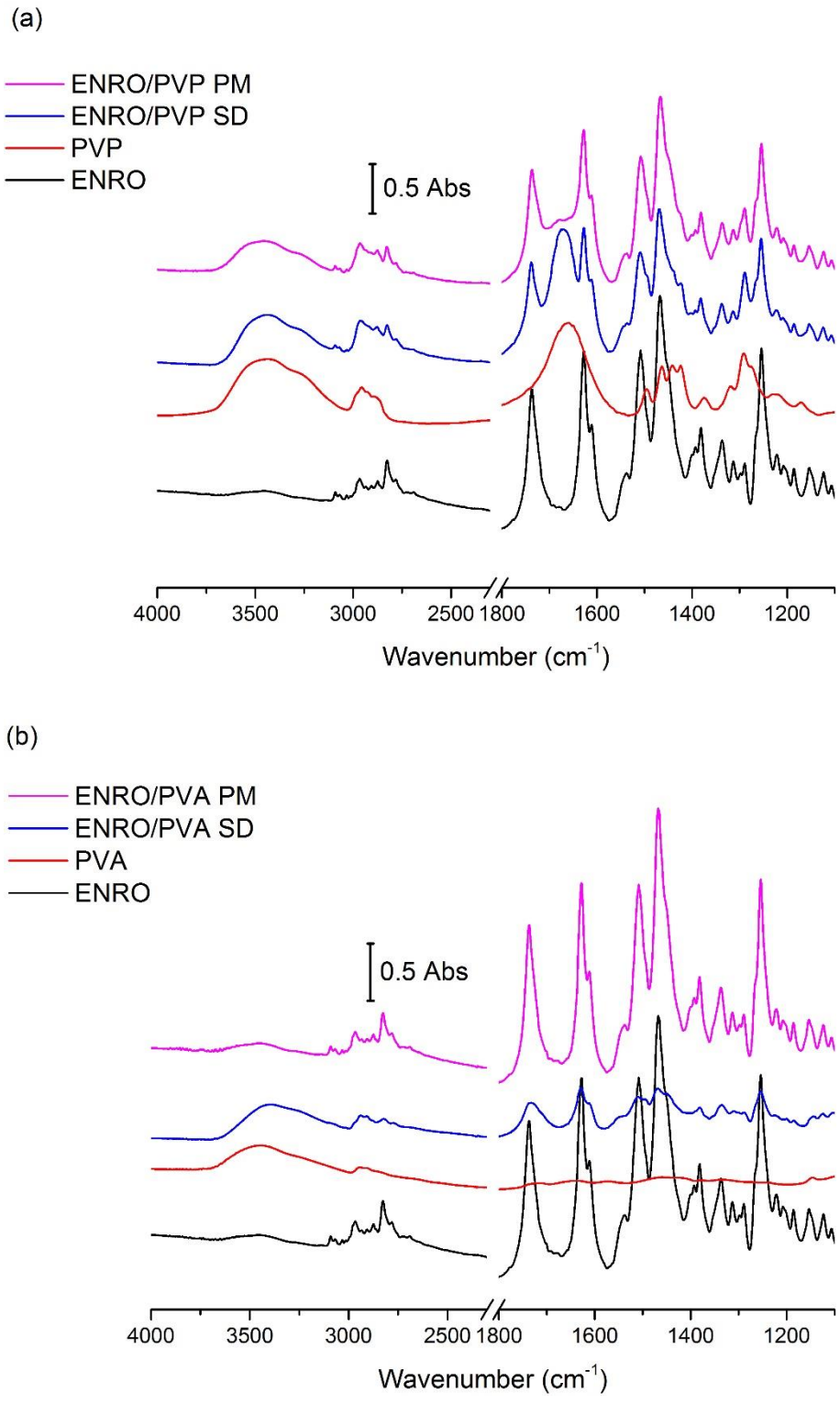

Figure A.5.4. FTIR spectra of ENRO semi-crystalline solid dispersions (SD) and PMs containing (a) 50% (w/w) PVP and (b) 40% (w/w) PVA.

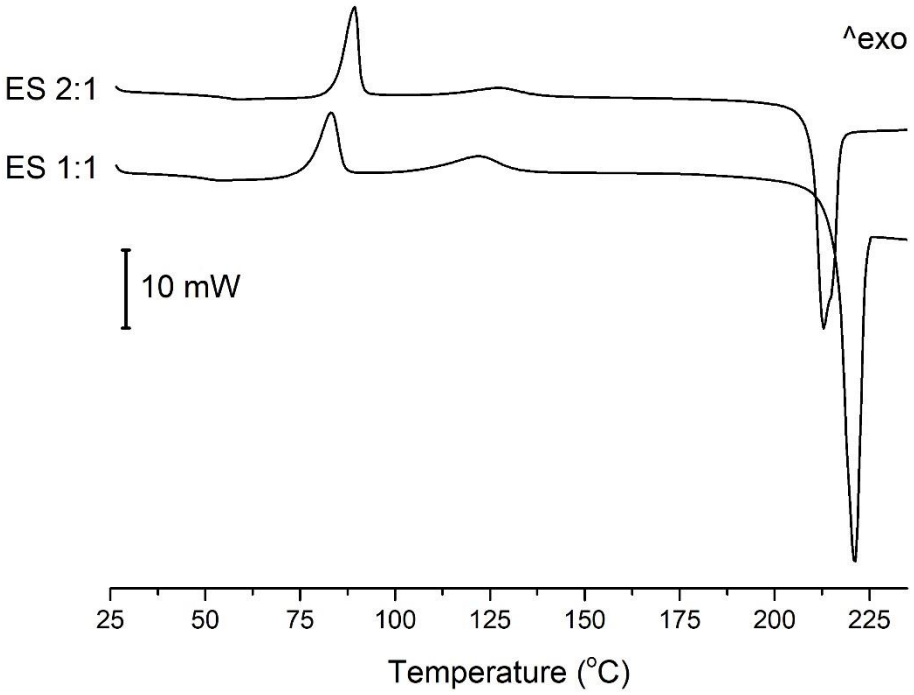

Figure A.5.5. DSC analysis of ENRO/succinic acid 1:1 and 2:1 amorphous salts.

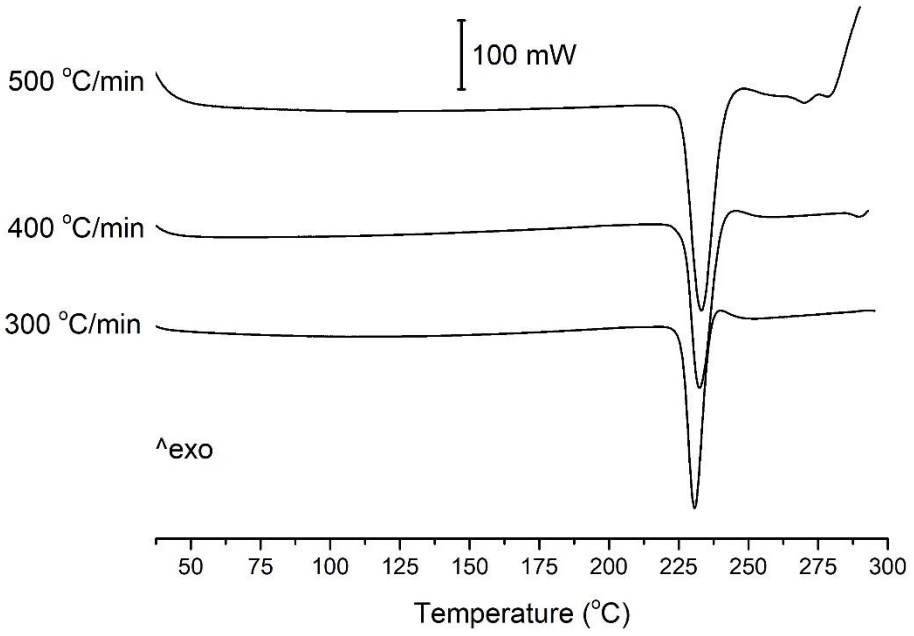

Figure A.5.6. HSDSC analysis of crystalline ENRO using various heating rates.

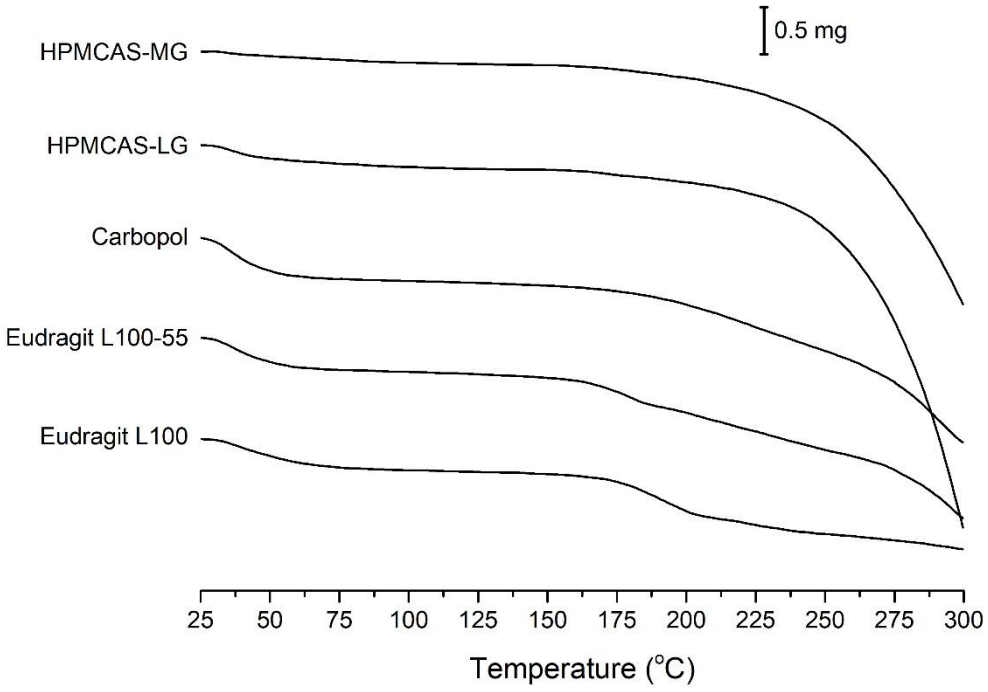

Figure A.5.7. TGA analysis of polymer starting materials.

Table A.5.1. Parameters Estimated from Young-Nelson Model for the ENRO and CIP ASDs

ASD	A[a]	B[b]	E[c]	r[d]
ENRO/Eudragit L100	0.007	0.151	0.990	0.981
ENRO/Eudragit L100-55	0.009	0.117	0.990	0.978
ENRO/Carbopol	0.022	0.083	0.209	0.998
ENRO/HPMCAS-LG	0.012	0.101	6.330	0.991
ENRO/HPMCAS-MG	0.011	0.100	6.281	0.989
CIP/Eudragit L100	0.009	0.160	0.471	0.997
CIP/Eudragit L100-55	0.017	0.115	0.447	0.991
CIP/Carbopol	0.019	0.094	0.203	0.999
CIP/HPMCAS-LG	0.014	0.105	0.597	0.995
CIP/HPMCAS-MG	0.011	0.117	0.507	0.996

[a]A: fraction of adsorbed water; [b]B: fraction of absorbed water; [c]E: equilibrium constant; and [d]r: correlation coefficient.

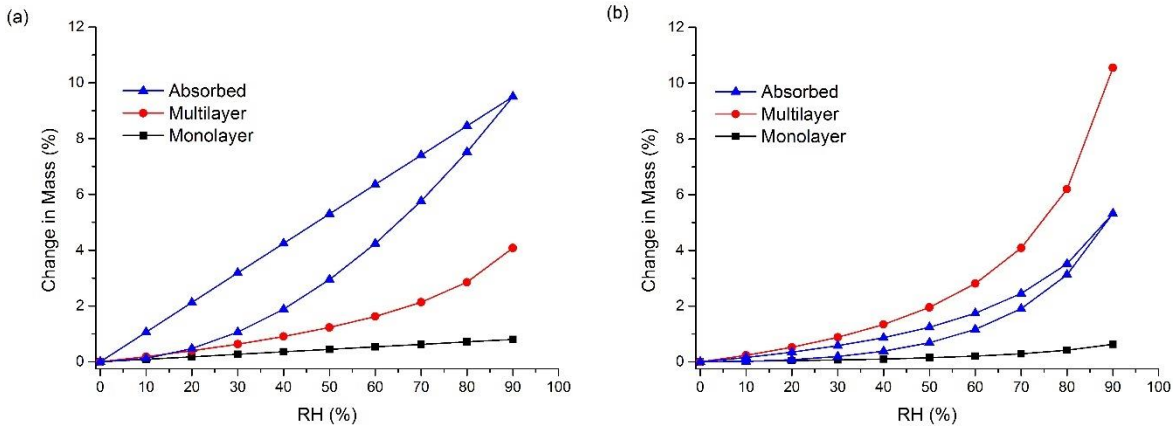

Figure A.5.8. Water distribution patterns according to the Young-Nelson model in ENRO ASDs containing (a) Eudragit L100-55 40% (w/w) and (b) HPMCAS-MG 60% (w/w).

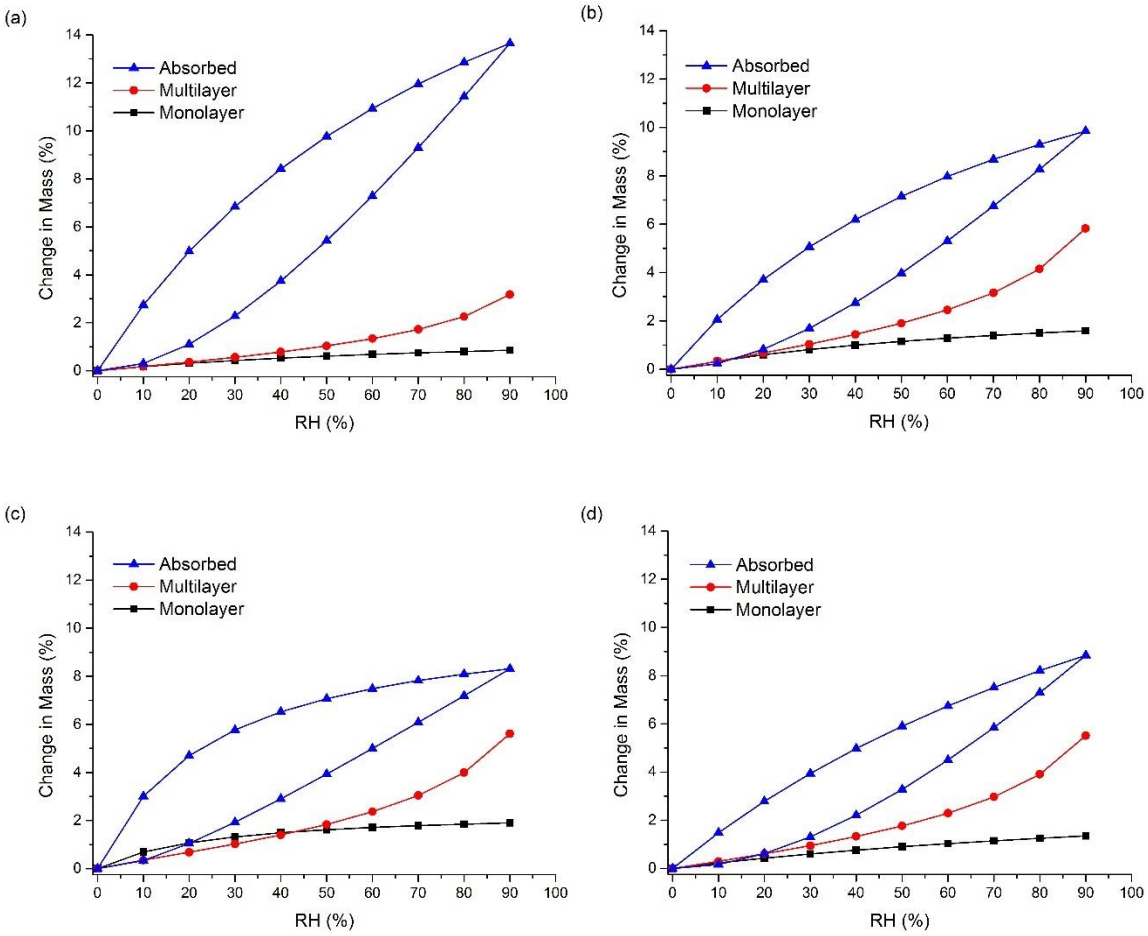

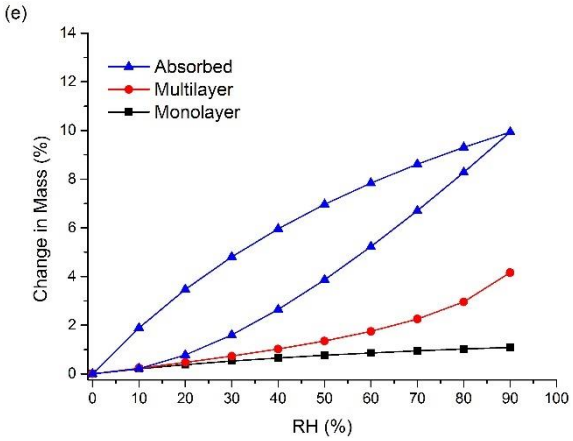

Figure A.5.9. Water distribution patterns according to the Young-Nelson model in CIP ASDs containing (a) Eudragit L100 40% (w/w) (b) Eudragit L100-55 40% (w/w) (c) Carbopol 40% (w/w) (d) HPMCAS-LG 60% (w/w) and (e) HPMCAS-MG 60% (w/w).

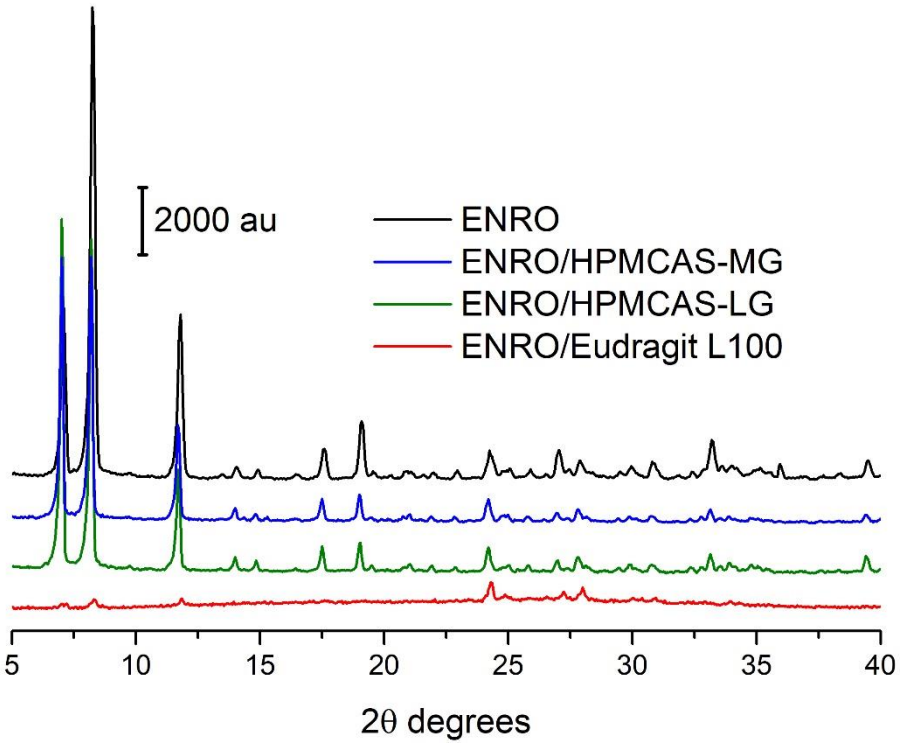

Figure A.5.10. PXRD analysis following solubility studies of ENRO and ENRO ASDs in FaSSIF.